DRUGS AND THE PHARMACEUTICAL SCIENCES VOLUME 192

SECOND EDITION

Polymorphism in Pharmaceutical Solids

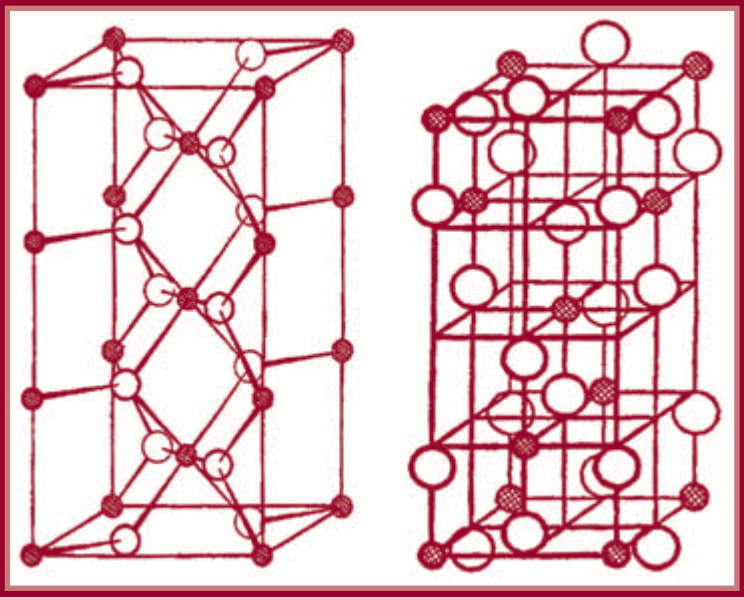

edited by

Harry G. Brittain

informa
healthcare

Polymorphism in Pharmaceutical Solids

DRUGS AND THE PHARMACEUTICAL SCIENCES
A Series of Textbooks and Monographs

Executive Editor

James Swarbrick
PharmaceuTech, Inc.
Pinehurst, North Carolina

Advisory Board

Larry L. Augsburger
University of Maryland
Baltimore, Maryland

Jennifer B. Dressman
University of Frankfurt Institute of
Pharmaceutical Technology
Frankfurt, Germany

Anthony J. Hickey
University of North Carolina
School of Pharmacy
Chapel Hill, North Carolina

Ajaz Hussain
Sandoz
Princeton, New Jersey

Joseph W. Polli
GlaxoSmithKline
Research Triangle Park
North Carolina

Stephen G. Schulman
University of Florida
Gainesville, Florida

Yuichi Sugiyama
University of Tokyo, Tokyo, Japan

Geoffrey T. Tucker
University of Sheffield
Royal Hallamshire Hospital
Sheffield, United Kingdom

Harry G. Brittain
Center for Pharmaceutical Physics
Milford, New Jersey

Robert Gurny
Universite de Geneve
Geneve, Switzerland

Jeffrey A. Hughes
University of Florida College
of Pharmacy
Gainesville, Florida

Vincent H. L. Lee
US FDA Center for Drug
Evaluation and Research
Los Angeles, California

Kinam Park
Purdue University
West Lafayette, Indiana

Jerome P. Skelly
Alexandria, Virginia

Elizabeth M. Topp
University of Kansas
Lawrence, Kansas

Peter York
University of Bradford
School of Pharmacy
Bradford, United Kingdom

For information on volumes 1–149 in the *Drugs and the Pharmaceutical Science* Series, please visit www.informahealthcare.com

150. Laboratory Auditing for Quality and Regulatory Compliance, *Donald Singer, Raluca-loana Stefan, and Jacobus van Staden*
151. Active Pharmaceutical Ingredients: Development, Manufacturing, and Regulation, *edited by Stanley Nusim*
152. Preclinical Drug Development, *edited by Mark C. Rogge and David R. Taft*
153. Pharmaceutical Stress Testing: Predicting Drug Degradation, *edited by Steven W. Baertschi*
154. Handbook of Pharmaceutical Granulation Technology: Second Edition, *edited by Dilip M. Parikh*
155. Percutaneous Absorption: Drugs–Cosmetics–Mechanisms–Methodology, Fourth Edition, *edited by Robert L. Bronaugh and Howard I. Maibach*
156. Pharmacogenomics: Second Edition, *edited by Werner Kalow, Urs A. Meyer, and Rachel F. Tyndale*
157. Pharmaceutical Process Scale-Up, Second Edition, *edited by Michael Levin*
158. Microencapsulation: Methods and Industrial Applications, Second Edition, *edited by Simon Benita*
159. Nanoparticle Technology for Drug Delivery, *edited by Ram B. Gupta and Uday B. Kompella*
160. Spectroscopy of Pharmaceutical Solids, *edited by Harry G. Brittain*
161. Dose Optimization in Drug Development, *edited by Rajesh Krishna*
162. Herbal Supplements-Drug Interactions: Scientific and Regulatory Perspectives, *edited by Y. W. Francis Lam, Shiew-Mei Huang, and Stephen D. Hall*
163. Pharmaceutical Photostability and Stabilization Technology, *edited by Joseph T. Piechocki and Karl Thoma*
164. Environmental Monitoring for Cleanrooms and Controlled Environments, *edited by Anne Marie Dixon*
165. Pharmaceutical Product Development: In Vitro-In Vivo Correlation, *edited by Dakshina Murthy Chilukuri, Gangadhar Sunkara, and David Young*
166. Nanoparticulate Drug Delivery Systems, *edited by Deepak Thassu, Michel Deleers, and Yashwant Pathak*
167. Endotoxins: Pyrogens, LAL Testing and Depyrogenation, Third Edition, *edited by Kevin L. Williams*
168. Good Laboratory Practice Regulations, Fourth Edition, *edited by Anne Sandy Weinberg*
169. Good Manufacturing Practices for Pharmaceuticals, Sixth Edition, *edited by Joseph D. Nally*
170. Oral-Lipid Based Formulations: Enhancing the Bioavailability of Poorly Water-soluble Drugs, *edited by David J. Hauss*
171. Handbook of Bioequivalence Testing, *edited by Sarfaraz K. Niazi*
172. Advanced Drug Formulation Design to Optimize Therapeutic Outcomes, *edited by Robert O. Williams III, David R. Taft, and Jason T. McConville*
173. Clean-in-Place for Biopharmaceutical Processes, *edited by Dale A. Seiberling*
174. Filtration and Purification in the Biopharmaceutical Industry, Second Edition, *edited by Maik W. Jornitz and Theodore H. Meltzer*
175. Protein Formulation and Delivery, Second Edition, *edited by Eugene J. McNally and Jayne E. Hastedt*
176. Aqueous Polymeric Coatings for Pharmaceutical Dosage Forms, Third Edition, *edited by James McGinity and Linda A. Felton*
177. Dermal Absorption and Toxicity Assessment, Second Edition, *edited by Michael S. Roberts and Kenneth A. Walters*
178. Preformulation Solid Dosage Form Development, *edited by Moji C. Adeyeye and Harry G. Brittain*
179. Drug-Drug Interactions, Second Edition, *edited by A. David Rodrigues*

180. Generic Drug Product Development: Bioequivalence Issues, *edited by Isadore Kanfer and Leon Shargel*
181. Pharmaceutical Pre-Approval Inspections: A Guide to Regulatory Success, Second Edition, *edited by Martin D. Hynes III*
182. Pharmaceutical Project Management, Second Edition, *edited by Anthony Kennedy*
183. Modified Release Drug Delivery Technology, Second Edition, Volume 1, *edited by Michael J. Rathbone, Jonathan Hadgraft, Michael S. Roberts, and Majella E. Lane*
184. Modified-Release Drug Delivery Technology, Second Edition, Volume 2, *edited by Michael J. Rathbone, Jonathan Hadgraft, Michael S. Roberts, and Majella E. Lane*
185. The Pharmaceutical Regulatory Process, Second Edition, *edited by Ira R. Berry and Robert P. Martin*
186. Handbook of Drug Metabolism, Second Edition, *edited by Paul G. Pearson and Larry C. Wienkers*
187. Preclinical Drug Development, Second Edition, *edited by Mark Rogge and David R. Taft*
188. Modern Pharmaceutics, Fifth Edition, Volume 1: Basic Principles and Systems, *edited by Alexander T. Florence and Jurgen Siepmann*
189. Modern Pharmaceutics, Fifth Edition, Volume 2: Applications and Advances, *edited by Alexander T. Florence and Jurgen Siepmann*
190. New Drug Approval Process, Fifth Edition: Global Challenges and Solutions, *edited by Richard A. Guarino*
191. Drug Delivery Nanoparticulate Formulation and Characterization, *edited by Yashwant Pathak and Deepak Thassu*
192. Polymorphism in Pharmaceutical Solids, Second Edition, *edited by Harry G. Brittain*

SECOND EDITION

Polymorphism in Pharmaceutical Solids

edited by
Harry G. Brittain
Center for Pharmaceutical Physics
Milford, New Jersey, USA

informa
healthcare
New York London

Informa Healthcare USA, Inc.
52 Vanderbilt Avenue
New York, NY 10017

© 2009 by Informa Healthcare USA, Inc.
Informa Healthcare is an Informa business

No claim to original U.S. Government works
Printed in the United States of America on acid-free paper
10 9 8 7 6 5 4 3 2 1

International Standard Book Number-10: 1-4200-7321-4 (Hardcover)
International Standard Book Number-13: 978-1-4200-7321-8 (Hardcover)

This book contains information obtained from authentic and highly regarded sources. Reprinted material is quoted with permission, and sources are indicated. A wide variety of references are listed. Reasonable efforts have been made to publish reliable data and information, but the author and the publisher cannot assume responsibility for the validity of all materials or for the consequence of their use.

No part of this book may be reprinted, reproduced, transmitted, or utilized in any form by any electronic, mechanical, or other means, now known or hereafter invented, including photocopying, microfilming, and recording, or in any information storage or retrieval system, without written permission from the publishers.

For permission to photocopy or use material electronically from this work, please access www.copyright.com (http://www.copyright.com/) or contact the Copyright Clearance Center, Inc. (CCC) 222 Rosewood Drive, Danvers, MA 01923, 978-750-8400. CCC is a not-for-profit organization that provides licenses and registration for a variety of users. For organizations that have been granted a photocopy license by the CCC, a separate system of payment has been arranged.

Trademark Notice: Product or corporate names may be trademarks or registered trademarks, and are used only for identification and explanation without intent to infringe.

Library of Congress Cataloging-in-Publication Data

Polymorphism in pharmaceutical solids / edited by Harry G. Brittain. — 2nd ed.
p. ; cm. — (Drugs and the pharmaceutical sciences ; v. 192)
Rev. ed. of: Polymorphism in pharmaceutical solids / edited by Harry G. Brittain. 1999.
Includes bibliographical references and index.
ISBN-13: 978-1-4200-7321-8 (hb : alk. paper)
ISBN-10: 1-4200-7321-4 (hb : alk. paper) 1. Solid dosage forms. 2. Polymorphism (Crystallography) 3. Solvation. 4. Hydration. I. Brittain, H. G. II. Polymorphism in pharmaceutical solids. III. Series: Drugs and the pharmaceutical sciences ; v. 192.
[DNLM: 1. Chemistry, Pharmaceutical. 2. Crystallization. 3. Molecular Structure. W1 DR893B v.192 2009 / QV 744 P7833 2009]
RS201.S57P64 2009
615′.19—dc22

2009015389

For Corporate Sales and Reprint Permissions call 212-520-2700 or write to: Sales Department, 52 Vanderbilt Avenue, 16th floor, New York, NY 10017.

Visit the Informa Web site at
www.informa.com

and the Informa Healthcare Web site at
www.informahealthcare.com

Preface

It is now just about 10 years since the publication of the first edition of *Polymorphism in Pharmaceutical Solids*, which certainly received a positive reaction from workers in drug development. Since then, Joel Bernstein and Rolf Hilfiker have published their books on polymorphic phenomena, and the field has continued to expand both in the number of works published and also in the depth of their coverage. Some things have not changed, however, and the effects of crystal structure on the solid-state properties of a given system remains of paramount importance. As I stated in the preface to the first edition, the heat capacity, conductivity, volume, density, viscosity, surface tension, diffusivity, crystal hardness, crystal shape and color, refractive index, electrolytic conductivity, melting or sublimation properties, latent heat of fusion, heat of solution, solubility, dissolution rate, enthalpy of transitions, phase diagrams, stability, hygroscopicity, and rates of reactions are all strongly influenced by the nature of the crystal structure.

The content of the present edition of *Polymorphism in Pharmaceutical Solids* has expanded to reflect the larger scope of topics having interest to development scientists. The book is now divided into six main sections, the first dealing with thermodynamic and theoretical issues. Within this initial section, one will find updated chapters from the first edition, "Theory and Principles of Polymorphic Systems" and "Application of the Phase Rule to the Characterization of Polymorphic and Solvatomorphic Systems." Reflecting the growing trend in predictive science, a new chapter entitled "Computational Methodologies: Toward Crystal Structure and Polymorph Prediction" is now featured in this section.

The second section of the new edition features preparative methods for polymorphs and solvatomorphs, and the single chapter of the first edition has been split into two chapters entitled "Classical Methods of Preparation of Polymorphs and Alternative Solid Forms" and "Approaches to High-Throughput Physical Form Screening and Discovery." In the next section, one will find chapters relating to the structural properties of polymorphs and solvatomorphs, updating the chapters from the first edition, "Structural Aspects of Polymorphism" and "Structural Aspects of Solvatomorphic Systems." With greater interest developing about the advantageous properties of co-crystal systems, it was appropriate to expand the structural section to include a new chapter entitled "Pharmaceutical Co-crystals: A New Opportunity in Pharmaceutical Science for a Long-Known but Little-Studied Class of Compounds."

In the first edition, topics related to the characterization methods for polymorphs and solvatomorphs were covered in two chapters, but the growth in the field that has taken place in the past 10 years required far greater coverage of these

areas. Hence, the four chapters of the next section are entitled, "Thermoanalytical and Crystallographic Methods," "Vibrational Spectroscopy," "Solid-State Nuclear Magnetic Resonance Spectroscopy," and "Effects of Polymorphism and Solid-State Solvation on Solubility and Dissolution Rate." The chapter on solubility and dissolution is especially poignant, as it retains timeless and consequential contributions written by the late Professor David Grant for the analogous chapter in the first edition.

In the first edition, the phase interconversion of polymorphs and solvatomorphs was covered only from a processing viewpoint, but in the present edition, this important topic is now covered in two chapters, "Solid-State Phase Transformations" and "Effects of Pharmaceutical Processing on the Solid Form of Drug and Excipient Materials."

As in the first edition, the last section contains chapters that have been grouped together as special topics. The chapter "Structural Aspects of Molecular Dissymmetry" concerns structural variations that can arise from the existence of molecular dissymmetry, manifested primarily in marked differences in solid-state properties between solids composed of racemates relative to solids composed of separated enantiomers. Finally, as the amorphous state represents one polymorphic form potentially available to all compounds, this extremely important field is covered in great depth in a chapter entitled "Amorphous Solids."

Even though the scope of the second edition of *Polymorphism in Pharmaceutical Solids* is substantially increased relative to that of the first edition, there is simply no way that all developments in the field could have been covered in depth in a single volume. Beginning with a survey of papers published during 2004, I am writing annual reviews of polymorphism and solvatomorphism that attempt to summarize the state of the field during a given calendar year. Interested readers can easily find these in the literature.

In the present edition of *Polymorphism in Pharmaceutical Solids*, I have once again tried to bring together a single volume that contains a comprehensive view of the principles, practical concerns, and consequences of the existence of polymorphism and solvatomorphism. As with the previous edition, I hope that the new chapters will continue to suggest approaches that will stimulate work and encourage additional growth in this area of solid-state pharmaceutics.

Harry G. Brittain

Contents

Preface . . . vii
Contributors . . . xi

PART I THERMODYNAMIC AND THEORETICAL ISSUES

1. Theory and Principles of Polymorphic Systems *1*
Harry G. Brittain

2. Application of the Phase Rule to the Characterization of Polymorphic and Solvatomorphic Systems *24*
Harry G. Brittain

3. Computational Methodologies: Toward Crystal Structure and Polymorph Prediction *52*
Sarah (Sally) L. Price

PART II PREPARATIVE METHODS FOR POLYMORPHS AND SOLVATOMORPHS

4. Classical Methods of Preparation of Polymorphs and Alternative Solid Forms *76*
Peter W. Cains

5. Approaches to High-Throughput Physical Form Screening and Discovery *139*
Alastair J. Florence

PART III STRUCTURAL PROPERTIES OF POLYMORPHS AND SOLVATOMORPHS

6. Structural Aspects of Polymorphism *185*
Harry G. Brittain, Stephen R. Byrn, and Eunhee Lee

7. Structural Aspects of Solvatomorphic Systems *233*
Harry G. Brittain, Kenneth R. Morris, and Stephan X. M. Boerrigter

8. Pharmaceutical Co-crystals: A New Opportunity in Pharmaceutical Science for a Long-Known but Little-Studied Class of Compounds *282*
Kapildev K. Arora and Michael J. Zaworotko

PART IV CHARACTERIZATION METHODS FOR POLYMORPHS AND SOLVATOMORPHS

9. Thermoanalytical and Crystallographic Methods *318*
Sisir Bhattacharya, Harry G. Brittain, and Raj Suryanarayanan

10. Vibrational Spectroscopy *347*
Harry G. Brittain

11. Solid-State Nuclear Magnetic Resonance Spectroscopy *381*
Patrick A. Tishmack

12. Effects of Polymorphism and Solid-State Solvation on Solubility and Dissolution Rate *436*
Harry G. Brittain, David J. R. Grant, and Paul B. Myrdal

PART V INTERCONVERSION OF POLYMORPHS AND SOLVATOMORPHS

13. Solid-State Phase Transformations *481*
Harry G. Brittain

14. Effects of Pharmaceutical Processing on the Solid Form of Drug and Excipient Materials *510*
Peter L. D. Wildfong

PART VI SPECIAL TOPICS RELATED TO POLYMORPHISM AND SOLVATOMORPHISM

15. Structural Aspects of Molecular Dissymmetry *560*
Harry G. Brittain

16. Amorphous Solids *587*
Lynne S. Taylor and Sheri L. Shamblin

Index . . . 631

Contributors

Kapildev K. Arora Department of Chemistry, University of South Florida, Tampa, Florida, U.S.A.

Sisir Bhattacharya* Department of Pharmaceutics, University of Minnesota, Minneapolis, Minnesota, U.S.A.

Stephan X. M. Boerrigter SSCI, an Aptuit Company, West Lafayette, Indiana, U.S.A.

Harry G. Brittain Center for Pharmaceutical Physics, Milford, New Jersey, U.S.A.

Stephen R. Byrn Department of Industrial and Physical Pharmacy, Purdue University, West Lafayette, Indiana, U.S.A.

Peter W. Cains Avantium Technologies BV, Amsterdam, The Netherlands

Alastair J. Florence Solid-State Research Group, Strathclyde Institute of Pharmacy and Biomedical Sciences, University of Strathclyde, Glasgow, U.K.

David J. R. Grant College of Pharmacy, University of Minnesota, Minneapolis, Minnesota, U.S.A.

Eunhee Lee Department of Industrial and Physical Pharmacy, Purdue University, West Lafayette, Indiana, U.S.A.

Kenneth R. Morris College of Pharmacy, University of Hawaii at Hilo, Hilo, Hawaii, U.S.A.

Paul B. Myrdal College of Pharmacy, University of Arizona, Tucson, Arizona, U.S.A.

Sarah (Sally) L. Price Department of Chemistry, University College London, London, U.K.

Sheri L. Shamblin Pfizer Global Research and Development, Pfizer, Inc., Groton, Connecticut, U.S.A.

Raj Suryanarayanan Department of Pharmaceutics, University of Minnesota, Minneapolis, Minnesota, U.S.A.

Lynne S. Taylor Department of Industrial and Physical Pharmacy, School of Pharmacy and Pharmaceutical Sciences, Purdue University, West Lafayette, Indiana, U.S.A.

Patrick A. Tishmack SSCI, an Aptuit Company, West Lafayette, Indiana, U.S.A.

Peter L. D. Wildfong Duquesne University, Pittsburgh, Pennsylvania, U.S.A.

Michael J. Zaworotko Department of Chemistry, University of South Florida, Tampa, Florida, U.S.A.

**Current affiliation*: Forest Laboratories, Inc., Commack, New York, U.S.A.

1 Theory and Principles of Polymorphic Systems

Harry G. Brittain
Center for Pharmaceutical Physics, Milford, New Jersey, U.S.A.

INTRODUCTION

With the discovery by Bragg that one could use the angular dependence of scattering of X rays from a crystalline solid to determine the structure of that solid (1), structural science has played a large role in the fields of chemistry and physics. Very early in the 19th century, it had become known that many compounds were capable of exhibiting the phenomenon of *dimorphism*, and could be crystallized into solids having different melting points and crystal habits. For example, the α- and β-forms of potassium ethyl sulfate were found to exhibit different solubilities and eutectic temperatures in their phase diagram (2). The existence of a thermally induced phase transition between the anhydrous and monohydrate forms of 5-nitrosalicylic acid was deduced from the temperature dependence of its solubility (3).

As the techniques of structure elucidation grew in their sophistication, the crystallographic basis of dimorphism became firmly established. The X-ray crystallographic technique enabled workers to determine the dimensions and angles associated with the fundamental building blocks of crystals, namely, the unit cell. At the same time it also became recognized that crystalline solids were not limited to one or two crystal forms, and that many solids were capable of being isolated in multitudes of crystalline forms.

During the very first series of studies using single-crystal X-ray crystallography to determine the structures of organic molecules, Robertson reported the structure of resorcinol (1,3-dihydroxybenzene) (4). This crystalline material corresponded to that ordinarily obtained at room temperature, and was later termed the α-form. Shortly thereafter, it was found that the α-form underwent a transformation into a denser crystalline modification (denoted as the β-form) when heated to about 74°C, and that the structure of this newer form was completely different (5). A summary of the unit cell parameters reported for both forms is provided in Table 1. The α-form features a relative open architecture that is maintained by a spiraling array of hydrogen bonding that ascends through the various planes of the crystal. The effect of the thermally induced phase transformation is to collapse the open arrangement of the α-form by a more compact and parallel arrangement of the molecules in the β-form. This structural change causes an increase in crystal density on passing from the α-form (1.278 g/cm^3) to the β-form (1.327 g/cm^3).

The term *polymorphism* has come to denote those crystal systems for which a substance can exist in structures characterized by different unit cells, but where each of the forms consists of exactly the same elemental composition. For a long time, the term *pseudopolymorphism* was used to denote other crystal variations where the crystal structure of the substance is defined by still other unit cells where these unit cells differ in their elemental composition through the inclusion of one or more

TABLE 1 Summary of the Unit Cell Parameters Associated with the two Polymorphs of Resorcinol (4,5)

Polymorphic form	α-form	β-form
Crystal class	Orthorhombic	Orthorhombic
Space group	P*na*	P*na*
Number of molecules per unit cell	$Z = 4$	$Z = 4$
Unit cell axis lengths	a =10.53 Å	a = 7.91 Å
	b = 9.53 Å	b = 12.57 Å
	c = 5.66 Å	c = 5.50 Å
Unit cell angles	$\alpha = 90°$	$\alpha = 90°$
	$\beta = 90°$	$\beta = 90°$
	$\gamma = 90°$	$\gamma = 90°$

molecules of solvent, and more recently this term has become replaced by the term *solvatomorphism*. The crystallographic origins and consequences of polymorphism and solvatomorphism have been the focus of several monographs and reviews (6–12), recent annual reviews (13–15), and will be discussed in great detail in one of the later chapters in this book.

The existence of different crystal structures of the various polymorphs of a substance often causes these solids to exhibit a variety of different physical properties, many of which are listed in Table 2. Because of differences in the dimensions, shape, symmetry, capacity (number of molecules), and void volumes of their unit cells, the different polymorphs of a given substance have different physical properties arising from differences in molecular packing. Such properties include molecular volume, molar volume (i.e., molecular volume multiplied by Avogadro's number), density, refractive index along a given crystal axis, thermal conductivity, electrical conductivity, and hygroscopicity. Differences in melting points of the various polymorphs arise from differences of the cooperative interactions of the molecules in the solid state compared with the liquid state. Also observed are differences in spectroscopic properties, kinetic properties, and some surface properties. Differences in packing properties and in the energetics of the intermolecular interactions (i.e., thermodynamic properties) among polymorphs give rise to differences in mechanical properties.

These differences in physical properties among the crystal forms of a polymorphic system have become extremely interesting to pharmaceutical scientists because their manifestation can sometimes lead to observable differences that have implications for processing, formulation, and drug availability (16–21). For such situations, the regulatory concerns can often become critically important, and can determine the path of development for a given drug substance (22). Consequently, an entire field of characterization techniques for the evaluation of pharmaceutical solids has arisen, and its degree of sophistication continues to grow (23–29).

Once the phase space of a substance has been determined, and the scope of possible polymorphic or solvatomorphic forms is established, it becomes critical to determine the boundaries of stability for the different forms and how they might be interconverted. At the very least, one must determine which crystal form is the most stable state, because unless mitigating circumstances dictate otherwise, that form would be the one to be chosen for continued development.

TABLE 2 Physical Properties that Differ Among Crystal Forms of a Polymorphic System

Packing properties	Molar volume and density
	Refractive index
	Conductivity: electrical and thermal
	Hygroscopicity
Thermodynamic properties	Melting and sublimation temperatures
	Internal or structural energy
	Enthalpy
	Heat capacity
	Entropy
	Free Energy and Chemical Potential
	Thermodynamic Activity
	Vapor Pressure
	Solubility
Spectroscopic properties	Electronic state transitions
	Vibrational state transitions
	Nuclear spin state transitions
Kinetic properties	Dissolution rate
	Rates of solid-state reactions
	Stability
Surface properties	Surface free energy
	Interfacial tensions
	Crystal habit
Mechanical properties	Hardness
	Tensile strength
	Compactibility, tabletting
	Handling, flow, and blending

THERMODYNAMICS OF POLYMORPHIC SYSTEMS

Before a discussion of the thermodynamics associated with systems capable of being crystallized in more than one form can be undertaken, a number of fundamental principles regarding the interactions that can take place in solid systems must be set out. In such discussions, one often uses thermodynamics to treat an *ideal* system, which may be taken as approximating some type of limiting condition. Real systems are often difficult to treat, but ideal systems are useful in that their boundaries can be used to deduce simple laws that are often sufficiently accurate to be practically useful. The following discussion has been distilled from several standard texts on thermodynamics and chemical equilibrium (30–34).

Systems are said to possess *energy*, and interacting systems exhibit simultaneous changes in observable properties that are accompanied by changes in energy. The energy of a system therefore implies the power to interact but also is a description of the results of interaction in terms of changed properties. To the thermodynamic scientist, these properties are usually descriptions in which the system exchanges energy with some standard system, although the properties can also be defined with respect to another member of the system. The changes of interest most pertinent to the present discussion involve changes in *potential* energy, or energy stored in a system as a result of how it came into that state. For example, the transformation of a substance from one physical phase to another involves the transfer of energy in the form of heat. Only changes or differences in energy are empirically measurable, because the

absolute energy of a system depends critically on the standard from which that energy might be measured.

Properties are identified as being *extensive* (dependent on the quantity of mass present) or *intensive* (independent of the amount of mass present), and the latter properties express a quality of the system rather than a quantity of something. For example, one may measure the amount of heat required to vaporize one gram of water, but dividing that amount of heat by that amount of water yields an intensive property that defines the substance called water. For every type of energy, there is a property whose difference between two systems determines whether energy will be exchanged and over which direction that energy will flow. Temperature, for example, is a measure of the intensity of heat in a system, and the value of this property with respect to the temperature of another system determines how much heat will flow and which system will be the donor of that heat.

It is concluded that the relative intensities of the various forms of energy in different systems determine whether interactions of exchanges of energy can take place between them. For a series of systems isolated from the universe, energy must flow until total equality in all forms of energy is attained. Consequently, to define a system one must be able to state the intensities of all significant forms of energy contained within that system. When this situation has been reached, the intensities of these energies existing within the system are grouped together in a class of properties denoted as *conditions*.

The conditions of a system can be controlled by manipulating the surroundings of the system. For example, unless a system is contained in a closed vessel, the pressure of ordinary chemical and physical transformations is fixed as the same as atmospheric pressure by virtue of the interaction of the system with open surroundings. As will be seen in the next chapter dealing with the Phase Rule, this stipulation results in reduced degrees of freedom and a limitation on the number of equilibria available to a system. In partly isolated systems, one may vary conditions by the deliberate introduction of one type of energy in order to observe the consequences of that addition in a linear manner.

In numerous experiments, it has been demonstrated that although energy can be converted from one form to another, it cannot be created or destroyed. This finding is the basis for the law of conservation of energy, which in turn, is the basis for the *first law of thermodynamics*: "The total energy of a system and its surroundings must remain constant, although it may be changed from one form to another." The energy of a system is seen to depend upon its pressure, volume, temperature, mass, and composition, with these five quantities being related by the *equation of state* for the system. Therefore, it is possible to assign a definite amount of energy to any given state of a system, which is determined only by the state itself and not by its previous history. If E_A represents the energy of the state A, and E_B is the energy of the state B, then the change in energy that accompanies the transformation of the system from A to B is independent of the path taken, and is given by:

$$\Delta E = E_B - E_A \tag{1}$$

The *internal energy* of the system, E, is a function of pressure, volume, and temperature, and includes all forms of energy other than those resulting from the position of the system in space. The actual magnitude of the internal energy is usually not known, but because thermodynamics is concerned primarily with changes in energy, the actual value of the internal energy is not significant.

When a system changes from one state to another, it may perform some type of external work, the magnitude of which is represented by w. If the work is done by the system, then w is positive, but if work is not done in the system, then w is negative. In addition, the system may absorb or evolve an amount of heat equal to q during the change, and q will always be positive if the system absorbs heat. According to the first law of thermodynamics, in order for the total energy of the system and surroundings to remain unchanged during the transition, it follows that the change in energy (ΔE) must be exactly equivalent to the heat q absorbed from the surroundings less the energy w lost to the surroundings in the from of external work:

$$\Delta E = q - w \tag{2}$$

For non-electrical thermodynamic processes that take place at constant pressure, the work term in equation (2) can be replaced by an expansion term, where P is the constant external pressure and ΔV is the increase of volume. If the amount of heat absorbed at constant pressure is represented as q_P, then with a slight rearrangement, one obtains:

$$q_P = \Delta E + P\Delta V \tag{3}$$

Because P and V are thermodynamic properties of the system, and because E depends only on the state of the system and not on its previous history, it follows that the quantity ($E + PV$) is also dependent only the state of the system. This latter quantity is called the *enthalpy* (H) of the system:

$$H = E + PV \tag{4}$$

At constant pressure:

$$\Delta H = \Delta E + P\Delta V \tag{5}$$

Comparison of equations (3) and (5) indicates that the increase ΔH in the enthalpy of the system at constant pressure equals the heat absorbed under these conditions.

Thermochemistry deals with the changes in heat of a system that accompany chemical or physical transformations where reactants transition into products. Because different substances have different amounts of internal energy in the form of chemical energy, the total energy of the products of a reaction will differ from the total energy of the reactants. As a result, the reaction will be accompanied either by the liberation or consumption of heat. An *exothermic* reaction is one where heat is produced as a product of the reaction, while an *endothermic* reaction is one where hear is consumed as a reactant in the reaction.

If a system transformation is run under constant atmospheric pressure, then the amount of heat absorbed is identified as the *enthalpy of reaction*, and this quantity represents the difference in the enthalpies of the reaction products and the reactants. For example, the combustion of solid elemental graphite with gaseous elemental oxygen at 25°C (i.e., 298 K) to yield gaseous carbon dioxide is endothermic:

$$C_{(S)} + O_{2\,(G)} \rightarrow CO_{2\,(G)} \tag{6}$$

and the enthalpy of combustion equals –94.05 kcal/mol. It is generally postulated that elements are in their standard states (i.e., the stable forms at ambient conditions), and

therefore their respective enthalpies are set to zero. Because equation (6) depicts the formation of CO_2 from its constituent elements, the enthalpy of that reaction is termed the enthalpy of formation for CO_2.

When the reaction under consideration involves a phase change, then the change in enthalpy is indicative of that reaction. For example, the *enthalpy of vaporization* of a substance is defined as the amount of heat required at constant pressure to vaporize one mole of that substance. One may determine the difference in enthalpy between two polymorphic forms of a compound by applying Hess's Law of constant heat summation, if the enthalpies of combustion for the two forms are known. The enthalpy of combustion for the reaction of diamond with oxygen equals –94.50 kcal/mol, and therefore the enthalpy of transition accompanying the conversion of diamond into graphite equals –0.45 kcal/mol.

Although the majority of chemical reactions that are exothermic in character will spontaneously go to completion under ordinary conditions, a number of reactions are known to require the absorption of heat and are still spontaneous. For example, the dissolution of most salts is endothermic, and yet their dissolution proceeds spontaneously as long as the equilibrium solubility is not exceeded. This simple observation demonstrates that enthalpy considerations are not sufficient to determine the spontaneity of a reaction, and that the definition of another parameter is required.

This additional state function is known as the *entropy* of the system, and has been given the symbol, S. One often encounters the explanation that entropy is a measure of disorder in a system, and that a spontaneous reaction is accompanied by an increase in entropy. Although apart from statistical mechanics it is difficult to define entropy, it is easier to define changes in entropy. Even though it is clear that spontaneous reactions are irreversible in nature, one can still break down the overall irreversible process into a series of infinitely small processes, each one of which is reversible in nature. The increase in entropy, dS, that accompanies an infinitesimal change equals the heat absorbed when the change is carried out in a reversible manner divided by the absolute temperature, T:

$$dS = \delta(q_{REV})/T \tag{7}$$

Because $\delta(q_{REV})$ has a definite value for a reversible, isothermal change, one can integrate equation (7) between the temperature limits of the initial and final states to obtain the entropy change for the process, ΔS.

It has proven expeditious to define other functions where the entropy is part of the determinant of spontaneity, one of these being:

$$A = E - TS \tag{8}$$

where the *work function*, A, equals the maximum amount of work obtainable when a system undergoes a change under reversible conditions. More useful to pharmaceutics and issues of polymorphism is the *free energy*:

$$G = H - TS \tag{9}$$

It is not difficult to show that combination of equations (4), (8), and (9) yields the relation:

$$G = A + PV \tag{10}$$

When a system undergoes a transformation, that change takes place at constant temperature and then the free energy of the transition is given by:

$$\Delta G = \Delta H - T\Delta S \tag{11}$$

If the transformation is also conducted at constant pressure, then equation (5) can be substituted into equation (11) to yield:

$$\Delta G = \Delta E + P\Delta V - T\Delta S \tag{12}$$

Figure 1 shows the energy relationships for a hypothetical system where the enthalpy and the entropy of the system increase with increasing absolute temperature. According to the Third Law of Thermodynamics, the entropy of a perfect, pure crystalline solid is zero at absolute zero, enabling one to set the zero-point entropy of the system. The $(T \cdot S)$ product is seen to increase more rapidly with increasing temperature than does the enthalpy, and therefore the free energy will decrease with increasing temperature. This decrease also corresponds to the fact that the slope $(\delta G/\delta T)$, of the plot of G against T is negative according to the equation:

$$(\delta G/\delta T)_P = -S \tag{13}$$

Each polymorphic form of a substance will yield an energy diagram similar to that of Figure 1, and because each polymorph has its own distinctive crystal lattice, it is to be anticipated that the values of enthalpy, entropy, and free energy at a given temperature would be different among the various polymorphs. In discussions of the relative stability of polymorphs and the driving force for polymorphic transformations at constant temperature and pressure, the difference in free energy between the forms is the decisive factor, with the form exhibiting the lowest free energy being the most stable.

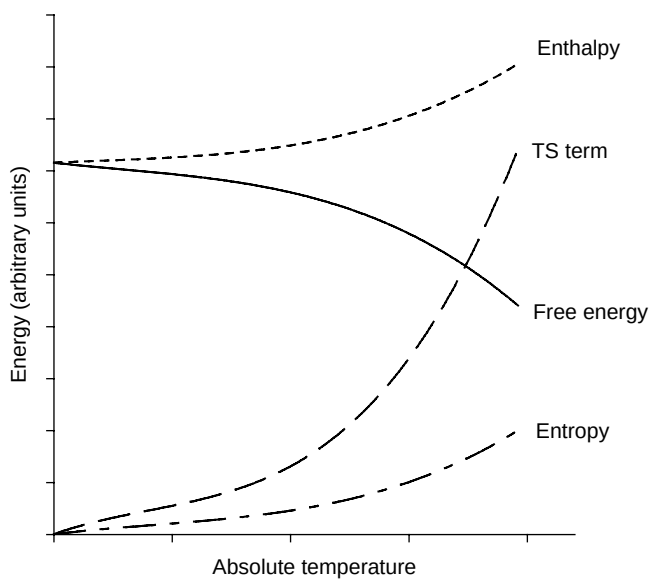

FIGURE 1 Temperature dependence of various thermodynamic functions.

Figure 2 shows the temperature dependence of the enthalpy and free energy for two different polymorphs, identified as Form-1 and Form-2. Because the temperature dependence of the free energies of the forms differs, at some temperature the respective curves cross and the two forms become isoenergetic. If the intersection point is determined under ambient conditions, the temperature is referred to as the *ordinary transition point* (T_{TR}). The fact that the free energies of the two polymorphs are equal implies that Form-1 and Form-2 are in equilibrium at that temperature.

Figure 2 shows Form-2 having an enthalpy that is higher than that of Form-1, so that the difference in enthalpies has the order $H_2 > H_1$ (i.e., ΔH is positive and the transition is endothermic in nature). Because at the transition temperature the difference in free energies of the forms equals zero, it follows that the difference in entropies will have the order $S_2 > S_1$. Equating the free energies of the two forms leads to the useful relation:

$$\Delta H_{TR} = T_{TR}\Delta S_{TR} \tag{14}$$

where $\Delta H_{TR} = H_2 - H_1$ and $\Delta S_{TR} = S_2 - S_1$ at the transition point. Through the use of differential scanning calorimetry, one may measure the enthalpy of the transition, and therefore calculate the entropy of the transition as long as the transition point is accurately determined. For this measurement to be accurate, the rate of temperature increase must be slow enough to allow Form-1 to completely transform into Form-2 over a span of a few degrees so as to achieve reversible conditions as closely as possible.

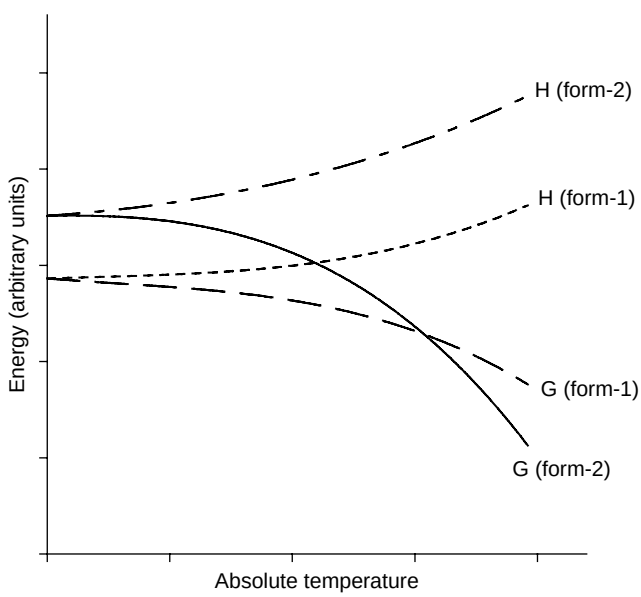

FIGURE 2 Temperature dependence of the enthalpy (*H*) and free energy (*G*) for two polymorphic crystal forms.

Figure 2 also shows that below the transition temperature, Form-1 has the lower free energy (i.e., $G_2 > G_1$), and therefore is more stable within that temperature range. On the other hand, above the transition temperature, Form-2 now has the lower free energy and is therefore more stable (i.e., $G_2 < G_1$). One concludes that under defined conditions of temperature and pressure, only one polymorph can be stable, and that all other polymorphs must be unstable. It is important to note that thermodynamics speaks to the relative energies and stabilities of polymorphs, but as will be discussed shortly, has nothing to say regarding the rates of these phase transformations. Diamond is thermodynamically unstable with respect to graphite, but the kinetics associated with that phase change are so infinitesimally slow that one refers to diamond as a metastable phase.

Equation (10) applies to the ideal systems discussed thus far, and differentiating both sides of the equation yields:

$$dG = dA + PdV + VdP \tag{15}$$

But dA is the maximum work of the expansion and must therefore be numerically equal to $-P$dV, so equation (15) reduces to:

$$dG = VdP \tag{16}$$

In order to integrate equation (16), one requires an equation of state defining V in terms of P. For one mole of an ideal gas, the law is simply:

$$V = nRT/P \tag{17}$$

where n is the number of moles of gas and R is the gas constant. Substitution of equation (17) into (16) and integrating yields:

$$\Delta G = G_2 - G_1 = RT \ln(P_2/P_1) \tag{18}$$

Equation (18) applies to any change of state or isothermal transfer of a substance from a region in which it has a vapor pressure P_1 to another region where its vapor pressure is P_2.

Practically all substances do not behave as ideal gases, so the concept of *fugacity* has been developed for real materials. One way to understand fugacity is to see it as the tendency manifested by a substance to leave the phase where it exists and pass into every other phase to which it has access. Because for an ideal gas, the partial pressure equals the fugacity, it is clear that equation (18) is a limiting instance of a more general equation. One may therefore substitute the fugacities (f_i) of the substance in each phase for the partial pressures to obtain:

$$\Delta G = RT \ln(f_2/f_1) \tag{19}$$

As is typically the case for thermodynamics, it is useful to define the fugacity of a substance with respect to the fugacity of some standard state, which can be taken as f^0. The ratio of the fugacity of a substance to that of the substance in the standard state has been termed the *activity* (a):

$$a = f/f^0 \tag{20}$$

so that:

$$G - G^0 = RT \ln(a) \tag{21}$$

As long as the reference state used to define G^0 and f^0 is the same, the quantities may be used interchangeably, so it follows that:

$$\Delta G = G_2 - G_1 = RT \ln(a_2/a_1) \tag{22}$$

The tendency of any one substance to be transferred from one phase or state to another at the same temperature depends on the properties of that substance, on the states involved, and on the temperature in question. However, neither the fugacity nor the activity are dependent upon the path or mechanism of transfer. At any specified temperature, these quantities can be considered to be governed by a property of the substance in the separate states. For many purposes, they are satisfactorily measured by the free energy of transfer or difference in molal free energy between the states. The molal free energy in any individual phase therefore comprises a measure of the escaping tendency of the substance in that phase relative to a standard state.

For dilute solutions, the activity is approximately proportional to the solubility, s, in any given solvent. One can then write an expression approximating the free energy difference between two polymorphic forms in terms of their respective equilibrium solubilities, or:

$$\Delta G \sim RT \ln(s_2/s_1) \tag{23}$$

If the dissolution of the polymorphic forms is conducted under transport-controlled sink conditions and under conditions of constant hydrodynamic flow, then the dissolution rate per unit surface area, J, is proportional to the solubility according to the Noyes–Whitney equation. One then can write another approximation for the free energy difference of two polymorphs as:

$$\Delta G \sim RT \ln(J_2/J_1) \tag{24}$$

Because the most stable polymorph under defined conditions of temperature and pressure has the lowest free energy content, it must therefore have the lowest values of fugacity, vapor pressure, thermodynamic activity, and solubility, and dissolution rate per unit surface area in any solvent.

ENANTIOTROPY AND MONOTROPY

In the preceding section, the general thermodynamics associated with systems was discussed, and methods were developed for determining the degree of spontaneity of a potential change were outlined. Implicit to the discussion was the understanding that the thermodynamic relations applied to systems undergoing reversible changes. In real crystals, however, a multitude of complicating factors introduce a degree of irreproducibility into the thermodynamic relations, thus limiting the scope of exact calculations in the understanding of real systems (35). Consequently, a number of more empirical concepts and rules have been developed to deal with actual polymorphic systems.

As described above, it is possible for polymorphic crystal forms to exhibit an ordinary transition point where one form can reversibly transform into another. Obviously, the temperature of this transition point must be less than the melting point of either polymorph or else the system would pass into the liquid state and no phase transition could be detected. For such systems, one polymorph will be

characterized by a definite range of conditions under which it will be the most stable phase, and the other form will be characterized by a different range of conditions under which it is the most stable phase. Polymorphic systems of this type are said to exhibit *enantiotropy*, and the two polymorphs are said to be enantiotropes of each other.

The free energy relationships between two enantiotropic polymorphs is illustrated in Figure 3, where now the enthalpy and free energy curves of the liquid (molten) state have been added. In the figure, Form-1 is shown as having a lower free energy content over the lower temperature range, while Form-2 is shown to have a lower free energy over a higher temperature range. For such an enantiotropic system, a reversible transition between forms can be observed at the transition temperature where the free energy curves cross and the forms are isoenergetic. The existence of enantiotropism in the system is indicated by the fact that the free energy curve for the liquid phase intersects the free energy curves for both polymorphs at a temperature that is higher than the temperature of the transition point.

Other systems exist where only one polymorph is stable at all temperatures below the melting point. As a result, all other polymorphs have no region of stability anywhere on a pressure–temperature diagram, and must be unstable with respect to the stable form. Polymorphic systems of this type are said to exhibit *monotropy*, and the two polymorphs are said to be monotropes of each other. The polymorph having the lowest free energy curve and solubility at any given temperature will necessarily be the most thermodynamically stable form.

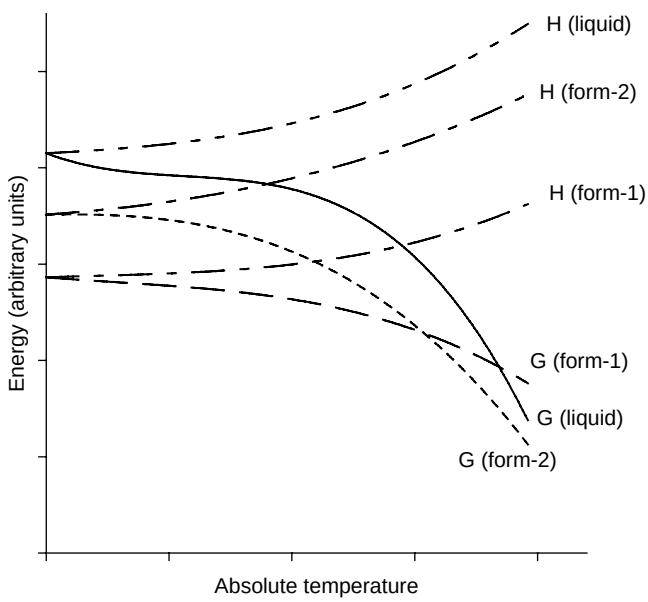

FIGURE 3 Temperature dependence of the enthalpy (*H*) and free energy (*G*) for two enantiotropic polymorphic crystal forms and their liquid (molten) state.

The free energy relationships between two monotropic polymorphs is illustrated in Figure 4, including the enthalpy and free energy curves of the liquid (molten) state. In this figure, Form-1 is shown as always having a lower free energy content over the entire accessible temperature range, and Form-2 has a higher free energy over the same temperature range. The free energy curve of the liquid state crosses the free energy curves of both polymorphs at temperatures less than that of the transition point, and hence, there can be no temperature at which the two polymorphs would exhibit a reversible phase transition. For a monotropic system the free energy curves do not cross, so no reversible transition can be observed below the melting point.

The isolation of polymorphs that form an enantiotropic system requires careful control over the isolation conditions. For enantiotropic materials, one can always identify a set of conditions where one polymorph or the other is the most thermodynamically stable form, and if crystallization is performed under those conditions one can usually obtain the desired form. Owing to its superior stability under all accessible temperature and pressure conditions, the isolation of the most stable polymorph in a monotropic system can usually be achieved without great difficulty. Isolation of the less stable form, however, requires a kinetic trapping of the system under conditions where the polymorph is characterized as being metastable at best.

A number of rules have been developed that serve to aid in the elucidation of the relative order of stability of polymorphs, and to facilitate determination of the existence of enantiotropism or monotropism in a polymorphic system (36–41). Although a summary of these many thermodynamic rules is provided in Table 3, it should be noted that the most useful and generally applicable rules are the Heat of Fusion rule and the Heat of Transition rule.

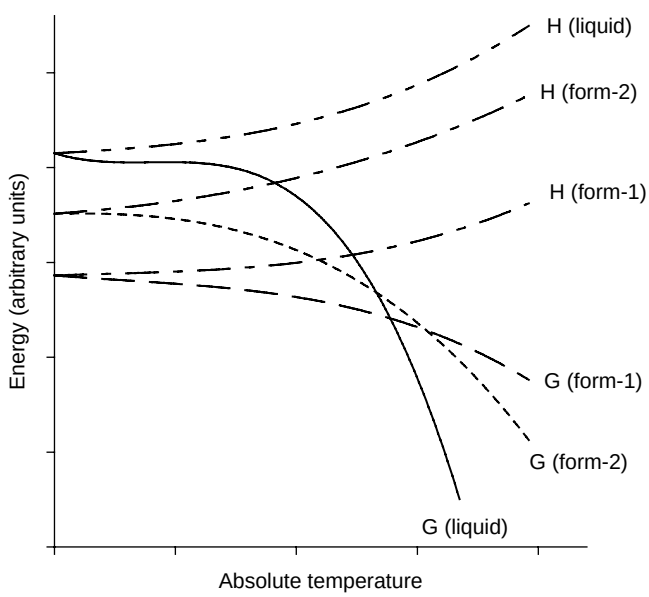

FIGURE 4 Temperature dependence of the enthalpy (*H*) and free energy (*G*) for two monotropic polymorphic crystal forms and their liquid (molten) state.

TABLE 3 Empirically Based Rules for Assigning the Nature of Phase Relationships in Polymorphic Systems[a]

Rule	Enantiotropic system	Monotropic system
Fundamental definition	Form-1 is the most stable polymorphic form at temperatures below the transition point, while Form-2 is the most stable polymorphic form at temperatures above the transition point	Form-1 is the stable polymorph at all temperatures below that of the melting point
Heat of fusion	The enthalpy of fusion of Form-1 is less than the enthalpy of fusion of Form-2	The enthalpy of fusion of Form-1 is more than the enthalpy of fusion of Form-2
Heat of transition	The phase transition of Form-2 to Form-1 is endothermic	The phase transition of Form-2 to Form-1 is exothermic
Entropy of fusion	The melting points of both Form-1 and Form-2 is less than the temperature of the transition point	The melting point of the most stable polymorph is higher than the temperature of the transition point
Phase transformation reversibility	The phase transformation at the transition point is reversible	The phase transformation of Form-2 into Form-1 is irreversible
Solubility	Form-1 is the most soluble polymorphic form at temperatures below the transition point, while Form-2 is the most soluble polymorphic form at temperatures above the transition point	Form-1 is the most soluble polymorph at all temperatures below that of the melting point
Density	The density of Form-1 is less than the density of Form-2	The density of Form-1 is more than the density of Form-2

[a]In the table, the convention where Form-1 has a higher melting point relative to that of Form-2 has been used.

The *Heat of Transition Rule* states that, if the transition between polymorphic forms is endothermic in nature, then the two forms are related by enantiotropy. Conversely, if the phase transformation is exothermic, then the two polymorphic forms are related by monotropy. Burger and Ramberger based this rule on the fact that because ΔH and ΔS are ordinarily positive for a spontaneous reaction, the enthalpy curves will not intersect and the free energy curves can intersect only once (36). In favorable circumstances, the sign and magnitude of the enthalpy change can be determined using differential scanning calorimetry (DSC).

When the enthalpy of transition cannot be measured by DSC, the *Heat of Fusion Rule* should be applied next. This rule states that if the higher melting polymorph has the lower enthalpy of fusion, then the two forms are enantiotropes. Conversely, if the higher melting polymorph has the higher enthalpy of fusion, then the two forms are monotropes. Burger and Ramberger have pointed out that the difference between the enthalpies of fusion of a polymorphic pair does not

exactly equal the enthalpy of transition, and have provided an improvement to the difference in enthalpies of fusion based on the difference in heat capacities of the two forms (36).

The *Entropy of Fusion Rule* states that if the polymorph having the higher melting point has a lower entropy of fusion, then the two forms are related by enantiotropy (38). One may calculate the entropy of fusion (ΔS_F) from the enthalpy of fusion (ΔH_F) measured for a reversible phase transformation taking place as the transition point (T_{TR}) by applying equation (7) to the melting process:

$$\Delta S_F = \Delta H_F / T_{TR} \tag{25}$$

Equation (25) cannot properly be applied to the calculation of ΔS_F for a monotropic system, because monotropy is fundamentally irreversible in nature. However, if the form having the higher melting point had a higher entropy of fusion, then the two polymorphic forms would be related by monotropy. Yu has developed a method for inferring thermodynamic stability relationships from melting data, calculating the free energy difference and the temperature slope of ΔG between two polymorphs (40).

The *Solubility Rule* proceeds directly from equation (23), which relates the free energy difference between two polymorphic forms to the solubility ratio of these. Because the solubility of a solid phase is directly determined by its free energy, it follows that if one polymorph is the most soluble form at temperatures below the transition point, and the other form is the most soluble form at temperatures above the transition point, then the two polymorphs must be enantiotropes. Conversely, if one polymorph is the most soluble form at all temperatures below that of the melting point of either form, then the two polymorphs must be monotropes.

The *Density Rule* is probably the least reliable of the Burger and Ramberger rules (36), and states that the polymorph having the highest true density will be the more stable crystal form. The basis for this rule is the assumption that the most stable polymorphic form would have the most efficient crystal packing, and hence, the greatest amount of lattice energy. A number of exceptions have been observed to the density rule, among them the instance of resorcinol that was discussed earlier (4,5).

As an example of how the thermodynamic rules are used, consider the enantiotropically related system constituted by the two non-solvated polymorphs of auranofin (i.e., 5-triethylphosphine-gold-2,3,4,6-tetra-*o*-acetyl-1-thio—*D*-glyucopyranoside) (42). Form-A was found to melt at 112°C, with the enthalpy of fusion being determined as 9.04 kcal/mol. Form-B was found to melt at 116°C, and its enthalpy of fusion was found to be 5.84 kcal/mol. According to the heat of fusion rule, because the higher melting form has the lower heat of fusion, the two polymorphs must be enantiotropically related and the difference in fusion enthalpies was calculated to be 3.20 kcal/mol. Using solution calorimetry, the enthalpy of solution for Form-A in 95% ethanol was found to be 12.42 kcal/mol, whereas the enthalpy of solution for Form-B in the same solvent system was found to be 9.52 kcal/mol. In dimethylformamide, the enthalpy of solution of Form-A was found to be 5.57 kcal/mol, whereas the enthalpy of solution for Form-B was found to be 2.72 kcal/mol. Thus, the enthalpy difference between the two forms was found to be 2.90 kcal/mol in 95% ethanol and 2.85 kcal/mol in dimethylformamide. The equilibrium solubility of Form-A in 25% aqueous polyethylene glycol 200 was found to be 0.65 mg/mL, whereas the equilibrium solubility of Form-B in the same

solvent system was found to be 1.30 mg/mL. The enantiotropic nature of the auranofin system is demonstrated that at room temperature Form-A is the most stable, whereas at elevated temperatures Form-B is the most stable.

NUCLEATION AND CRYSTAL GROWTH

Among the various methods one may use to prepare different polymorphs are crystallization from liquid solutions of various pure and mixed solvents, crystallization from the molten liquid state, suspension of less-soluble substances in pure and mixed solvents, thermal treatment of crystallized substances, exposure of solids to various relative humidities, sublimation, and crystallization from supercritical fluids. Typically, the first experiments performed in a preformulation study entail the attempted crystallization of polymorphic solids from solutions using various solvents and various temperature regimes (43,44). In these experiments, initially supersaturated solutions are prepared, and then the supersaturation is discharged by either slow or rapid cooling of the solution, evaporation of the solvent, addition of an anti-solvent to induce precipitation, chemical reaction between two or more soluble species, or variation of pH to produce a less soluble acid or base.

The crystallization process begins with the aggregation of molecules into clusters, and the continued addition of molecules to the clusters eventually results in the formation of tiny crystallites (45–48). The *critical nucleus* is obtained when the clusters of molecules have the smallest size capable of independent existence in the supersaturated phase, with these particles existing in a reversible state where they have an equal probability of growing into larger crystals or dissolving back in the solution phase. These critical nuclei are too small to be observed directly, and their structure is not known. Mullin has stated that the structure of a critical nucleus could be anything from a diffuse agglomeration of molecules to a miniature crystal that is perfect in form (46).

The typical theory of nucleation is based on the theory developed for the condensation of vapor into a liquid that has been extended to crystallization from the molten state. The formation of a liquid droplet or a solid particle in a homogeneous fluid requires the performance of work to obtain the end product. The total amount of work required to form a crystal nucleus, W_{TOT}, equals the amount of work required to form the surface (W_S) plus the amount of work needed to form the bulk of the particle (W_V):

$$W_{TOT} = W_S + W_V \tag{26}$$

Using the geometrical equations known for spherical particles, it can be shown that total work of equation (26) equals:

$$W_{TOT} = \tfrac{4}{3}\pi\sigma r^2 \tag{27}$$

where r is the radius of the particle and σ is the surface energy of the particle per unit area.

The increase in vapor pressure resulting from the decrease in size of a droplet can be estimated from the Gibbs–Thompson equation:

$$\ln(P_R/P^*) = \frac{2M\sigma}{RT\rho r} \tag{28}$$

where P_R is the vapor pressure over a droplet of radius r, P^* is the equilibrium vapor pressure of the liquid, M is the molecular weight, ρ is the liquid density, T is the absolute temperature, and R is the universal gas constant.

For solid particles, the pressure terms of equation (28) can be replaced by concentration equivalents. However, the ratio of the concentration of a particle having a radius equal to r (C_R) to the equilibrium solubility (C^*) is a measure of the degree of supersaturation (D) in the system:

$$D = C_R / C^* \tag{29}$$

In that case, equation (28) can be written as:

$$\ln(D) = \frac{2M\sigma}{RT\rho r} \tag{30}$$

or more usefully as:

$$r = \frac{2M\sigma}{RT\rho \ln(D)} \tag{31}$$

Substitution of equation (31) into equation (27) yields the important relationship:

$$W_{TOT} = \frac{16\pi M^2 \sigma^3}{3[RT\rho \ln(D)]^2} \tag{32}$$

According to equation (32), a saturated solution cannot spontaneously nucleate, because $\ln(D) = 0$, and the work required for nucleation would be infinite. The equation also indicates that any supersaturated solution can undergo spontaneously nucleation as long as a sufficient amount of energy is supplied to the system. Nucleation may be primary (not requiring pre-existing crystals of the crystallizing substance) or secondary (nucleation is induced by pre-existing crystals of the substance). Primary nucleation may be homogeneous (the nuclei of the crystallizing substance arise spontaneously in the medium), or heterogeneous (the nuclei comprise foreign solid matter, such as particulate contaminants, dust particles, or the walls of the container.

The change in free energy associated with the process of nucleation (ΔG_{TOT}) from a homogeneous solution is given by:

$$\Delta G_{TOT} = \Delta G_S + \Delta G_V \tag{33}$$

where ΔG_S is the excess free energy between the surface of the particle and the bulk of the particle, whereas ΔG_V is the excess free energy between a very large particle having $r = \infty$ and the solution in solution. ΔG_S is a positive quantity known as the surface excess free energy, ΔG_V is a negative quantity known as the volume excess free energy, and both quantities are functions of the radius of the particle.

Because the ΔG_S and ΔG_V terms contribute opposing contributions to the total free energy change as the radius of the nucleus increases, the free energy passes through a maximum (ΔG_{CRIT}) at a particle radius equal to the radius (r_{CRIT}) of the critical nucleus. This behavior has been illustrated in Figure 5, and the free energy of the critical nucleus can be calculated as:

$$\Delta G_{CRIT} = 4\pi\sigma r_{CRIT}{}^{2}/_{3} \tag{34}$$

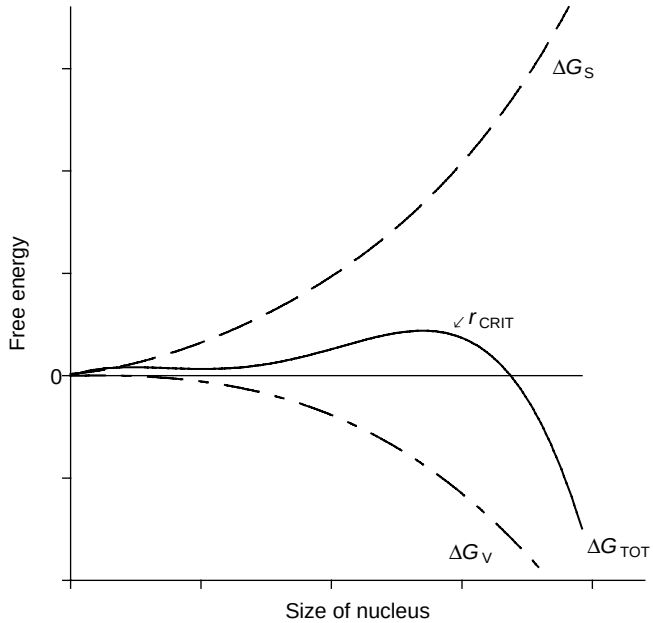

FIGURE 5 Dependence of the surface excess free energy (ΔG_S) and the volume excess free energy (ΔG_V), illustrating the existence of a critical nucleus having a diameter equal to r_{CRIT}.

Spontaneous nucleation is therefore seen to be governed by the algebraic opposition of a volume term that favors the accretion of additional molecules from the supersaturated medium and a surface term that favors the dissolution of the molecular aggregates that would otherwise form nuclei (45–48). The molecules of the crystallizing substance tend to aggregate in the supersaturated medium under the influence of the volume term that tends to reduce the Gibbs free energy of the system.

For a substance capable of existing in two or more polymorphic forms, each polymorph would have its own characteristic ΔG_{TOT} as determined by its particular ΔG_V and ΔG_S properties, as well as its own characteristic value of r_{CRIT} and ΔG_{CRIT}. Within the limits imposed by their characteristic curves, the aggregates or embryos of the various polymorphs would compete for molecules in their relative attempts to grow into crystallites so that their free energies could decrease. Depending on the characteristics of the free energy curves and the properties of the solution, it is to be anticipated that the aggregate for which the critical activation energy is the lowest will form the first nucleus, and continued deposition of molecules on that nucleus would eventually yield the crystallization of that particular polymorph.

In order to form crystals from the nuclei, molecules of the crystallizing substance attach onto the nuclei until the crystallization medium is no longer supersaturated and the equilibrium solubility of the substance is reached. The small but definite increase of solubility with decreasing particle size for microscopic solid particles predicted by equation (30) does, however, account for the increase in the average particle size when crystals of various sizes are allowed to age in constant

with a saturated solution. This phenomenon, known as *Ostwald ripening*, occurs because a smaller particle, having a higher solubility, will dissolve in the unsaturated solution that is saturated with respect to a larger particle of lower solubility. Conversely, a larger particle having a lower solubility will grow in the supersaturated solution that is actually saturated with respect to a smaller particle of higher solubility. Larger particles will therefore grow at the expense of smaller particles and the concentration of the "saturated" solution will decrease asymptotically.

Because the most easily nucleated polymorph is the one whose critical nuclei are the easiest to form (i.e., they have the most favorable free energy characteristics), one frequently finds that a phase transformation accompanies an Ostwald ripening process. As the science of crystallization developed during the 19th century and workers learned that compounds could be obtained in more than one solid state form, a number of cases were documented where a metastable form of a compound crystallized first and subsequently transformed into a more stable form. These findings led Ostwald to propose his *Law of Stages*, which stated that a supersaturated state does not spontaneously transform directly into that phase that is the most stable of the possible states, but instead, transforms into the phase that is next more stable than itself (49). In thermodynamic terms, the crystal form most likely to be initially crystallized would be the one whose free energy was closest to the free energy of the dissolved state.

Stranski and Totomanov provided an explanation for this phenomenon developed in terms of the kinetics of transformation (50). In this model, the determining factors are the relative rates of nucleation and crystal growth for the stable and metastable forms. The differences between the various parameters may be such that at the working temperature, the rate of nucleation is greater for the metastable product. This situation would cause the metastable phase to preferentially nucleate. In another scenario, the rates of nucleation may be more or less the same for the two forms, but if the metastable phase has a higher rate of growth, then this form would eventually predominate in the isolated product.

One may also encounter the situation where nucleation of the stable form may have taken place to a small extent along with the nucleation and growth of the metastable form. Because the stable form would necessarily have a lower solubility, a process of solution-mediated phase transformation is set up where over time the metastable phase transforms into the stable phase. For the situation where no nuclei of the stable phase were formed, then for a phase transformation to occur nuclei of the stable form would have to be created. The most likely situation for formation of these nuclei would be that they would not be generated within the bulk solution, but would instead be formed on the surfaces of the metastable crystals.

One typically identifies those situations where two crystal forms are obtained in an isolated product as *concomitant crystallization*, the products as *concomitant polymorphs*, and the thermodynamics and kinetics of the phenomenon have been discussed in detail (51). For example, two orthorhombic polymorphs of 1-deoxy-α-D-tagatose have been crystallized from a mixed methanol/ethyl acetate solvent system (52). Form-II was obtained as hexagonal places after allowing the mother liquor to stand for 16 hours, while Form-I crystallized as needles from the same solution after 72 hours. The two polymorphic forms were collected in approximately equal amounts from the crystallizing solution, and the single-crystal structures of these forms indicated that the polymorphism was derived from differences in hydrogen-bonding patterns.

Probably the best way to avoid the generation of concomitant polymorphs is through the introduction of seed crystals into a slightly supersaturated solution. As long as the seed crystals do not undergo a solution-mediated phase transformation of their own, the supersaturation in the crystallization medium is then discharged through growth onto the seeds. The implementation of this process requires knowledge of the temperature dependence of the equilibrium solubility and the spontaneous nucleation curve, and seeding is conducted in the concentration region between these boundaries (i.e., the *metastable zone*). The techniques for seeding a desirable polymorphic form during crystallization have been discussed in detail (46–48,53).

Another possibility where one may obtain stable or metastable crystal forms is where nucleation and subsequent crystal growth takes place on foreign surfaces, a process known as *epitaxial crystallization*. When surfaces, foreign nuclei, or appropriate seed crystals are present in a solution, these may favor the formation of a different form when the surfaces of the epitaxial agents present interfaces for which the structure closely matches the structure that would exist in a crystal of the new form (54,55). For example, Form-III of anthranilic acid was obtained by crystallization on glass coated with trimethoxysilane, Form-II was obtained when the crystallization took place on glass coated with chloro-triisobutlysilane, and a mixture of Form-II and Form-III was obtained if the crystallization was conducted on uncoated glass (56). It was concluded that the availability of hydrogen-bonding functionality at the nucleation surface played an important role in the polymorphic selectivity.

The various phenomena discussed in the preceding paragraphs amply demonstrate that one must exercise a considerable degree of control over the nucleation process and succeeding crystal growth processes if one seeks to obtain phase-pure materials. The crystal nucleation process has been discussed in detail (57), as has been the significance of controlling crystallization mechanisms and kinetics (58). These phenomena have also been critically examined with a view toward polymorph selection, and the crystal engineering that would be desirable in obtaining bulk drug substances having appropriate structures (59).

DISAPPEARING AND REAPPEARING POLYMORPHS

Over the years, stories have accumulated that summarize the failed attempts to reproduce previously reported crystallization products. When observed, the phenomenon is simultaneously frustrating and infuriating because modern physical science is often judged on the basis of its reproducibility. Dunitz and Bernstein addressed systems where a particular crystal form could not be obtained despite heroic efforts, concluding that control over nucleation and crystal growth processes was required (60). Crystallographers and preformulation scientists recognize the role of seeding in initiating nucleation, and many consider the disappearance of a metastable form to be a local and temporary phenomenon. These authors concluded that, "once a particular polymorph has been obtained, it is always possible to obtain it again; it is only a matter of finding the right experimental conditions."

In a subsequent work, Bernstein and Henck returned to the subject of transient polymorphs, examining this time certain systems where polymorphs had become elusive after a new polymorphic form was isolated (61). Through studies of the benzocaine:picric acid, *p*′-methylchalcone, benzophenone, and N-(N′-methylanilino) phthalimide systems, hot-stage microscopy was demonstrated to be of great use in the design of further experimentation that would yield the elusive polymorph.

The monoclinic polymorph of paracetamol (i.e., acetaminophen) is a commercially important form of the drug substance, despite its unsuitability in direct compression formulations. An orthorhombic crystal form of the drug substance had been characterized (62), but this polymorph could not be reproduced by several groups even though they followed the reported method of isolation. Eventually the experimental difficulties were overcome and a scalable process was reported that yielded the orthorhombic form in sufficient quantities for its characterization and formulation (63). The key to the successful process came through the use of appropriate seeding techniques to suppress the nucleation of the unwanted monoclinic polymorph, and rapid isolation of the product at low temperatures to suppress any phase transformation.

One example where a metastable polymorph was replaced by a more stable crystal form is that of meso-xylitol. In the early 1940s, two polymorphs of xylitol were described, with one being a metastable, hygroscopic, monoclinic form, melting at 61–61.5°C (64) and the other a stable orthorhombic form melting at 93–94.5°C (65). After a sample of the orthorhombic form was introduced into a laboratory in which the monoclinic polymorph had been prepared, the metastable spontaneously transformed into the stable form on exposure to the ambient environment. As part of a structural study of the orthorhombic polymorph, it was noted that "Attempts to obtain the lower melting monoclinic form from alcoholic solutions either at room temperature or close to 0°C have hitherto been unsuccessful. We invariably grow the orthorhombic crystals. It is interesting to note that although xylitol was first prepared as a syrup in 1891 there was no report of crystallization until 50 years later, when it was the metastable hygroscopic form that was prepared first. Having now obtained the stable form, it is difficult to recover the metastable crystals" (66).

The existence of two new polymorphic forms of 3-aminobenzenesulfonic acid (orthorhombic needles and monoclinic plates) have been reported, one of which had not been previously known (67). Form-I was suggested to be a disappearing polymorph, and the serendipitous discovery of Form-III resulted from the attempt to use tailor-made additives in order to re-obtain Form I. Although the attempt to prepare Form-I did not succeed, the study demonstrated the necessity to explore the polymorphic phase space as fully as possible even in simple systems.

A metastable form of benzamide was identified by Liebig and Woehler in 1832, but the structure of this unstable modification was determined much later (68). During reproductions of the historical experiments, rapid phase transformation was observed of the metastable form to the stable form, with the phase transformation being complete within 800 seconds. Ultimately, a high-resolution powder diffraction pattern of the metastable form was obtained by performing the crystallization in a sealed capillary, and subtracting the diffraction peaks of the stable form. Detailed evaluation of the structures of the stable and metastable polymorphs indicated that the phase transformation involved little structural rearrangement, and this fact was deduced as contributing to the difficulty of preparing phase-pure metastable crystals.

Three concomitant polymorphs of 1,3-bis(*m*-nitrophenyl)urea were reported in 1899 as yellow prisms (the α-form), white needles (the β-form), and yellow tablets (the γ-form), and a more detailed investigation of the system has been conducted (69). During work designed to prepare the γ-form, a new δ-form (that had the same color and habit as the β-form) and a monohydrate form were discovered, and the analysis suggested that the monohydrate was actually the reported γ-form.

It was also observed that despite the existence of considerable conformational differences in the molecules constituting the various crystal forms, the small degree of difference in the solid-state ^{13}C-NMR spectra of these forms indicated the existence of comparable environments for the NMR-active nuclei.

In their review, Dunitz and Bernstein pointed out that their examples of disappearing polymorphs involved molecules capable of adopting different conformations (60). These molecules would possess significant degrees of conformational freedom and molecular configurations that would facilitate the existence of equilibrium amounts of the different conformations in the solution, and solid-state effects would dictate which of these could be best able to build up into a crystal. It was noted that the rate of formation of nuclei of a stable polymorph could be significantly reduced by a low concentration of the required conformer, whereas another conformer might be incorporated in the nuclei of a metastable polymorph, which then underwent rapid growth. The phase interconversions accessible to systems of these types must be considered in the context of their enantiotropic or monotropic character, and therefore correctly designed preformulation studies of pharmaceutical compounds should resolve these kinetic and thermodynamic issues.

REFERENCES

1. Bragg WH, Bragg WL. X-Rays and Crystal Structure. London: G. Bell and Sons, Ltd., 1918.
2. Hammick DL, Mullaly JM. The dimorphism of potassium ethyl sulfate. J Chem Soc London 1921: 1802–6.
3. Chattaway FD, Curjel WRC. The crystalline forms of 5-nitrosalicylic acid and of related compounds. J Chem Soc London 1926: 3210–15.
4. Robertson JM. The structure of resorcinol: A quantitative X-ray investigation. Proc Royal Soc London 1936; A157: 79–99.
5. Robertson JM, Ubbelohde AR. A New Form of Resorcinol. I. Structure Determination by X-Rays. Proc Royal Soc London 1938; A167: 122–35.
6. McCrone WC. Polymorphism, chapter 8 in Physics and Chemistry of the Organic Solid State, volume II. In: Fox D, Labes MM, Weissberger A, eds. New York: Interscience Pub, 1965: 725–67.
7. Verna AR, Krishna P. Polymorphism and Polytypism in Crystals. New York: John Wiley & Sons, 1966.
8. Byrn SR, Pfeiffer RR, Stowell JG. Solid State Chemistry of Drugs, 2nd edn. West Lafayette: SSCI Inc., 1999.
9. Brittain HG. Polymorphism in Pharmaceutical Solids. New York: Marcel Dekker, 1999.
10. Vippagunta SR, Brittain HG, Grant DJW. Crystalline solids. Adv Drug Del Rev 2001; 48: 3–26.
11. Bernstein J. Polymorphism in Molecular Crystals. Oxford: Clarendon Press, 2002.
12. Hilfiker R. Polymorphism in the Pharmaceutical Industry. Weinheim: Wiley-VCH, 2006.
13. Brittain HG. Polymorphism and solvatomorphism 2004, Chapter 8 in Profiles of Drug Substances, Excipients, and Related Methodology, volume 32. In: Brittain HG, ed. Amsterdam: Elsevier Academic Press, 2005: 263–83.
14. Brittain HG. Polymorphism and solvatomorphism 2005. J Pharm Sci 2007; 96: 705–28.
15. (a) Brittain HG. Polymorphism and solvatomorphism 2006. J Pharm Sci 2008; 97: 3611–36. (b) Brittan HG. Polymorphism and solvatomorphism 2007. J Pharm Sci 2008; 98: 1617–42.
16. Haleblian JK, McCrone WC. Pharmaceutical applications of polymorphism. J Pharm Sci 1969; 58: 911–29.
17. Haleblian JK. Characterization of habits and crystalline modification of solids and their pharmaceutical applications. J Pharm Sci 1975; 64: 1269–88.

18. Bernstein J. Conformational Polymorphism, in Organic Solid State Chemistry. In: Desiraju GR, ed. Amsterdam: Elsevier, 1987: 471–518.
19. Morris KR, Rodriguez-Hornado N. Hydrates, in Encyclopedia of Pharmaceutical Technology, volume 7. In: Swarbrick J, Boylan J, eds. New York: Marcel Dekker, 1993: 393–440.
20. Byrn SR, Pfeiffer RR, Stephenson G, Grant DJW, Gleason WB. Solid-state pharmaceutical chemistry. Chem Mat 1994; 6: 1148–58.
21. Brittain HG. Effects of mechanical processing on phase composition. J Pharm Sci 2002; 91: 1573–80.
22. Byrn SR, Pfeiffer RR, Ganey M, Hoiberg C, Poochikian G. Pharmaceutical solids: a strategic approach to regulatory considerations. Pharm Res 1995; 12: 945–54.
23. Brittain HG, Bogdanowich SJ, Bugay DE, et al. Physical Characterization of Pharmaceutical Solids. Pharm Res 1991; 8: 963–73.
24. Bugay DE. Solid-state nuclear magnetic resonance spectroscopy: theory and pharmaceutical applications. Pharm Res 1993; 10: 317–27.
25. Threlfall TL. Analysis of organic polymorphs. Analyst 1995; 120: 2435–60.
26. Brittain HG. Spectral methods for the characterization of polymorphs and solvates. J Pharm Sci 1997; 86: 405–12.
27. Brittain HG. Solid-state analysis, Chapter 3, in the Handbook of Pharmaceutical Analysis. In: Ahuja S, Scypinski S, eds. New York: Marcel Dekker, 2001: 57–84.
28. Brittain HG, Medek A. Polymorphic and solvatomorphic impurities, chapter 3 in Handbook of Isolation and Characterization of Impurities in Pharmaceuticals. In: Ahuja S, Alsante KM, eds. Academic Press, 2003: 39–73.
29. Brittain HG. Spectroscopy of Pharmaceutical Solids. New York: Taylor and Francis, 2006.
30. Lewis GN, Randall M. Thermodynamics and the Free Energy of Chemical Substances. New York: McGraw-Hill Book Co, 1923.
31. Denbigh K. The Principles of Chemical Equilibrium. Cambridge: University Press, 1955.
32. Klotz IM. Chemical Thermodynamics. New York: W.A. Benjamin, 1964.
33. Vanderslice JT, Schamp HW, Mason EA. Thermodynamics. Englewood Cliffs: Prentice-Hall, 1966.
34. Sonntag RE, van Wylen GJ. Introduction to Thermodynamics: classical and statistical. New York: John Wiley & Sons, 1971.
35. Westrum EF, McCullough JP. Thermodynamics of crystals, chapter 1 in Physics and Chemistry of the Organic Solid State, volume I. In: Fox D, Labes MM, Weissberger A, eds. New York: Interscience Pub, 1963: 1–178.
36. Burger A, Ramberger R. On the polymorphism of pharmaceuticals and other molecular crystals: I, Mikrochim. Acta [Wien] 1979; II: 259–71.
37. Burger A, Ramberger R. On the polymorphism of pharmaceuticals and other molecular crystals: II, Mikrochim. Acta [Wien] 1979; II: 273–316.
38. Burger A. Thermodynamic and other aspects of the polymorphism of drugs. Pharm Int 1982: 158–63.
39. Giron D. Thermal analysis and calorimetric methods in the characterization of polymorphs and solvates. Thermochim Acta 1995; 248: 1–59.
40. Yu L. Inferring thermodynamic stability relationship of polymorphs from melting data. J Pharm Sci 1995; 84: 966–74.
41. Grunenberg A, Henck J-O, Siesler HW. Theoretical derivation and practical application of energy/temperature diagrams as an instrument in preformulation studies of polymorphic drug substances. Int J Pharm 1996; 129: 147–58.
42. Lindenbaum S, Rattie ES, Zuber GE, Miller ME, Ravin LJ. Polymorphism of auranofin. Int J Pharm 1985; 26: 123–32.
43. Newman AW, Stahly GP. Form selection of pharmaceutical compounds, chapter 1 in Handbook of Pharmaceutical Analysis. In: Ohannesian L, Streeter AJ, eds. New York: Marcel Dekker, 2001: 1–57.

44. Brittain HG. Preparation and identification of polymorphs and solvatomorphs, Chapter 3.3, in Preformulation in Solid Dosage Form Development. In: Adeyeye MC, Brittain HG, eds. New York: Informa Healthcare Press, 2008: 185–228.
45. Strickland-Constable RF. Kinetics and Mechanism of Crystallization. London: Academic Press, 1968: 74–129.
46. Mullin JW. Crystallization, 2nd edn. London: Butterworth & Co, 1972: 136–200.
47. Mersmann A. Crystallization Technology Handbook, 2nd edn. New York: Marcel Dekker, 2001: 45–79.
48. Myerson AS. Handbook of Industrial Crystallization, 2nd edn. Boston: Butterworth Heinemann, 2002: 33–65.
49. Ostwald W. Z Phys Chem 1897; 22: 289–330.
50. Stranski IN, Totomanov D. Z Phys Chem 1933; A163: 399.
51. Bernstein J, Davey RJ, Henck J-O. Concomitant polymorphs. Angew Chem Int Ed 1999; 38: 3441–61.
52. Jones NA, Jenkinson SF, Soengas R, et al. The concomitant crystallization of two polymorphs of 1-deoxy-α-D-tagatose. Acta Cryst 2007; C63: o7–o10.
53. Beckmann W. Seeding the desired polymorph: background, possibilities, limitations and case studies. Org Process Res Dev 2000; 4: 372–83.
54. Carter PW, Ward MD. Topographically directed nucleation of organic crystals on molecular single-crystal substrates. J Am Chem Soc 1993; 115: 11521–35.
55. Bonafede SJ, Ward MD. Selective nucleation and growth of an organic polymorph by ledge-directed epitaxy on a molecular crystal substrate. J Am Chem Soc 1995; 117: 7853–61.
56. Carter PW, Ward MD. Directing polymorph selectivity during nucleation of anthranilic acid on molecular substrates. J Am Chem Soc 1994; 116: 769–70.
57. Weissbuch I, Lahav M, Leiserowitz L. Toward stereochemical control, monitoring, and understanding of crystal nucleation. Cryst Growth Design 2003; 3: 125–50.
58. Rodriguez-Hornedo N, Murphy D. Significance of controlling crystallization mechanisms and kinetics in pharmaceutical systems. J Pharm Sci 1999; 88: 651–60.
59. Blagden N, Davey RJ. Polymorph selection: challenges for the future. Cryst Growth Design 2003; 3: 873–85.
60. Dunitz JD, Bernstein J. Disappearing polymorphs. Acc Chem Res 1995; 28: 193–200.
61. Bernstein J, Henck J-O. Disappearing and reappearing polymorphs – an anathema to crystal engineering. Cryst Engineer 1998; 1: 119–28.
62. Haisa M, Kashino S, Maeda H. The orthorhombic form of p-hydroxyacetanilide. Acta Cryst 1974; B30: 2510–12.
63. Nichols G, Frampton CS. Physicochemical characterization of the orthorhombic polymorph of paracetamol crystallized from solution. J Pharm Sci 1998; 87: 684–93.
64. Wolfrom ML, Kohn EJ. Crystalline xylitol. J Am Chem Soc 1942; 64: 1739.
65. Carson JF, Waisbrot SW, Jones FT. A new form of crystalline xylitol. J Am Chem Soc 1943; 65: 1777–8.
66. Weissbuch I, Zbaida D, Addadi L, Leiserowitz L, Lahav M. Design of polymeric inhibitors for the control of crystal polymorphism. Induced enantiomeric resolution at racemic histidine by crystallization at 25°C. J Am Chem Soc 1987; 109: 1869–71.
67. Rubin-Preminger JM, Bernstein J. 3-Aminobenzenesulfonic acid: a disappearing polymorph. Cryst Growth Design 2005; 5: 1343–9.
68. Blagden N, Davey R, Dent G, et al. Woehler and Liebig revisited: a small molecule reveals its secrets – the crystal structure of the unstable polymorph of benzamide solved after 173 years. Cryst Growth Design 2005; 5: 2218–24.
69. Rafilovich M, Bernstein J, Harris RK, et al. Groth's original concomitant polymorphs revisited. Cryst Growth Design 2005; 5: 2197–209.Theory and Principles of Polymorphic Systems

the same time Desiraju defined crystal engineering as "the understanding of intermolecular interactions in the context of crystal packing and in the utilization of such understanding in the design of new solids with desired physical and chemical properties" (11). Crystal engineering has now matured into a widely accepted paradigm for the preparation or supramolecular synthesis of new compounds. A salient feature of crystal engineered structures is that they are designed from first principles using the concepts of supramolecular chemistry and self-assembly (16,70–73).

A crystal engineering experiment typically involves CSD surveys followed by experimental work to prepare and characterize new compounds that are sustained by molecular recognition events or *supramolecular synthons* (5). A detailed understanding of the supramolecular chemistry of the functional groups present in a given molecule is a prerequisite for designing a co-crystal because it facilitates selection of appropriate co-crystal formers. However, when multiple functional groups are present in a molecule, the CSD rarely contains enough information to address the hierarchy of the possible supramolecular synthons. Furthermore, the role of solvent in nucleation of crystals and co-crystals remains poorly understood, and solvent can play a critical role in obtaining a particular co-crystal. However, the hierarchy of the supramolecular synthons that can occur for common functional groups such as carboxylic acids, amides, and alcohols with emphasis upon *supramolecular heterosynthons*, that is, non-covalent bonds between different but complementary functional groups (29,47,67b,e,f,74) is becoming better defined. Furthermore, it is becoming evident that such interactions are key to implementing a design strategy for co-crystals in which a target molecule forms co-crystals with a series of co-crystal formers that are carefully selected for their ability to form supramolecular heterosynthons with the target molecule.

How Are Co-crystals Prepared?

Synthesis of a co-crystal from solution might be thought of as counter-intuitive because crystallization is such an efficient and effective method of purification. However, if different molecules with complementary functional groups result in hydrogen bonds that are energetically more favorable than those between like molecules of either component, then co-crystals are likely to be thermodynamically (although not necessarily kinetically) favored. Supramolecular heterosynthons that seem to favor formation of co-crystals are exemplified by carboxylic acid–pyridine (29a,67b,e,75), carboxylic acid–amide (67g,76), and alcohol–pyridine (67f,77) (Fig. 5).

Single crystals involving these supramolecular heterosynthons are commonly discovered via slow evaporation from a solution containing stoichiometric amounts

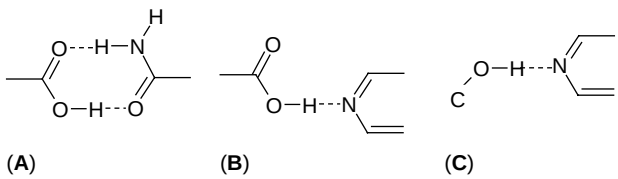

FIGURE 5 (**A**) Acid–amide, (**B**) acid–pyridine, and (**C**) alcohol–pyridine supramolecular heterosynthons.

of the components (co-crystal formers); however, sublimation, growth from the melt, slurrying, and grinding of two or more solid co-crystal formers in a ballmill are also suitable methodologies. Indeed, dry grinding was used as far back as the 19th century (40,56), and the recently developed technique of solvent-drop grinding, addition of a small amount of suitable solvent to the ground mixture to accelerate co-crystallization, appears to be a particularly fruitful methodology (41–44). The crystal form that is obtained is typically (45,74a), but not always, (4a) independent of the synthetic methodology. However, that co-crystals can often be prepared in a facile one-step manner using "green chemistry" approaches (78) does not mean that their synthesis and isolation is routine:

- As mentioned above, a detailed understanding of the supramolecular chemistry of the functional groups present in a given molecule is a prerequisite for designing a co-crystal because it facilitates selection of appropriate co-crystal formers. However, when multiple functional groups are present in a molecule the CSD rarely contains enough information to address the hierarchy of the multiple possible supramolecular synthons.
- Mismatched solubility between the components of a co-crystal can preclude their generation from solution if the co-crystal formers are present in a stoichiometric ratio.
- The role of solvent in nucleation of crystals and co-crystals remains poorly understood, and choice of solvent can be crucial in obtaining a particular co-crystal.

Why are Co-crystals Broadly Relevant?

Co-crystals are attractive to solid-state chemists because they offer opportunities to modify the composition of matter and the chemical and/or physical properties of a molecular species without the need to make or break covalent bonds. Thus far, there are several notable applications for co-crystals, all of which have direct or indirect relevance to pharmaceuticals:

- *Non-covalent derivatization* (79,80) was coined in the context of modifying the stability of Polaroid film (80,81). In this particular context, reduced solubility of a co-crystal reduced solubility and diffusion of an active ingredient. The net effect was greater stability and shelf life. Such a situation could be relevant to drug formulation, especially transdermal formulations, but has not to our knowledge yet been applied as such.
- *Solid-state synthesis*. Crystal engineering was first implemented in the context of photodimerization in the solid-state (9), and there are multiple examples of co-crystal formers having been used as templates to control the orientation of photoreactive molecules (Fig. 6) (67d,77c). Such a situation affords a level of control that cannot be achieved in the absence of the co-crystal former or in solution, and can lead to 100% yield and no waste. Co-crystals in which both co-crystal formers are reactants have also been exploited for solid-state synthesis. Etter et al. reported the first example of such a reaction in 1989 (82), a nucleophilic substitution reaction, and more recently, Cheney et al. have reported co-crystal controlled solid-state synthesis of imides, C^3S^3, via condensation of amines and acid anhydrides (83).
- *Chiral resolution.* Whereas spontaneous resolution of racemic mixtures into racemic conglomerates, "Pasteur crystallization," represents one of the best

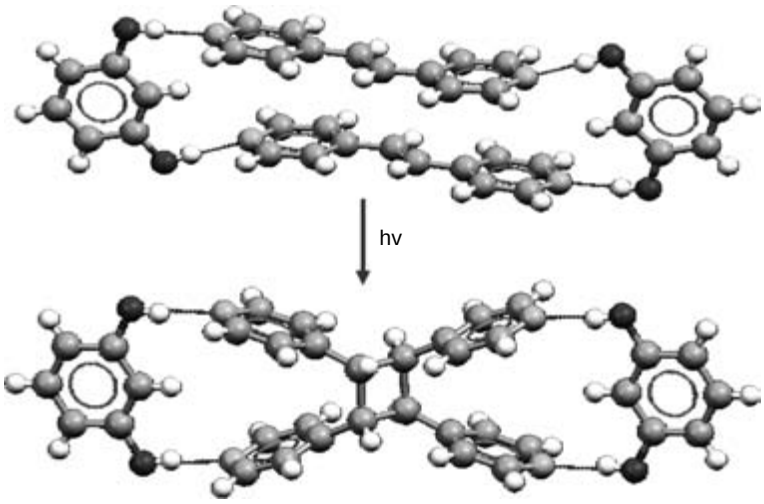

FIGURE 6 The co-crystal controlled (2+2) photodimerization of a resorcinol co-crystal of a substituted olefin.

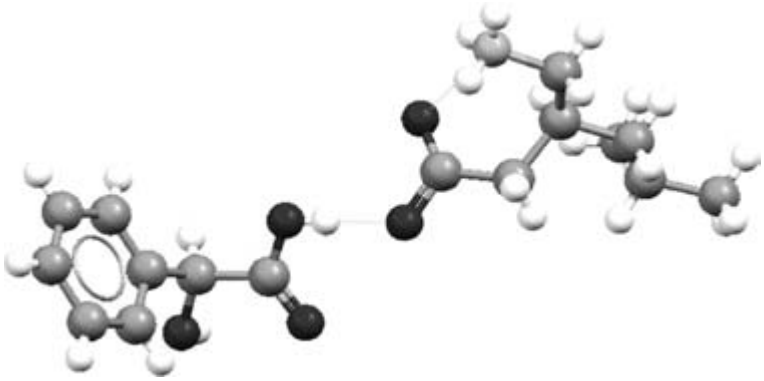

FIGURE 7 1:1 co-crystal of (*S*)-3-(ammonionmethyl)-5-methylhexanoate and (*S*)-mandelic acid.

known crystallization experiments (84), it is not the typical outcome to such an experiment. Rather, racemates are generally considered to be the outcome in around 90% of crystallizations of racemic mixtures (85). Chiral co-crystal formers offer an enhanced possibility of separating enantiomers by fractional crystallization because the resulting co-crystals are diastereomeric in nature. For example, (*S*)-mandelic acid has been used to resolve racemic pregabalin on an industrial scale (86), and it is able to resolve racemic 2-aminobutyric acid (87a) and phenylalanine (87b) through fractional crystallization. On the other hand, racemic mandelic acid can be resolved by (*S*)-alanine and *R*-cysteine (88). A diastereomeric co-crystal of (*S*)-mandelic acid is illustrated in Figure 7.

- Many of the crystal engineering principles and protocols that have been exploited for the generation of pharmaceutical co-crystals might also be invoked for the design and isolation of other types of co-crystal. In this context, molecular targets that would be particularly attractive and amenable for study because of technological opportunities and their hydrogen-bonding capabilities include the following: nucleobases (drug design and detection of oligonucleotides), molecules with high polarizability (new classes of NLO material), explosives/propellants (reformulation, enhanced thermal stability, enhanced properties), agrichemicals (reformulation, enhanced properties), renewable substrates (solid-state, polymer, and green chemistry), and volatile organics (air pollution).

CASE STUDIES OF PHARMACEUTICAL CO-CRYSTALS

An early example of studies that are related to pharmaceutical co-crystals was a series of studies conducted in the 1950s by Higuchi and his coworkers, who studied complex formation between macromolecules and certain pharmaceuticals (89). For example, complexes of polyvinylpyrrolidone (PVP) with sulfathiazole, procaine hydrochloride, sodium salicylate, benzylpenicillin, chloramphenicol, mandelic acid, caffeine, theophylline, and cortisone were isolated (89–90). However, these compounds would not be classified as pharmaceutical co-crystals according to the criteria applied herein. Whitesides et al. addressed the use of substituted barbituric acid, including barbital and melamine derivatives, to generate supramolecular "linear tape," "crinkled tape," and "rosette" motifs sustained by robust supramolecular synthons with three-point hydrogen bonding (34). Despite their success in co-crystal formation, the focus of these studies was not so much the physical properties of the resulting co-crystals but rather the supramolecular functionality of barbitals and their complementarity with melamine. Nevertheless, these studies illustrated the potential diversity of crystal forms that can exist for a particular API, as more than 60 co-crystals were structurally characterized in this series of studies. Herein we shall focus upon case studies that exemplify the formation of pharmaceutical co-crystals with altered physical properties of clinical relevance.

Pharmaceutical Co-crystals of Carbamazepine (Tegretol®)

Carbamazepine (CBZ) has been in use for over three decades for the treatment of epilepsy and trigeminal neuralgia even though it has multiple challenges associated with its oral drug delivery, including a small therapeutic window, autoinduction of metabolism, and dissolution limited bioavailability. A CSD analysis on CBZ reveals that it has 45 entries that include four fully characterized polymorphs (91), a dihydrate (92), 14 solvates (acetone, furfural, DMSO, trifluoroethanol, DMF, NMP, nitromethane, acetic acid, formic acid, butyric acid, formamide, trifluroacetic acid, tetrahydrofuran, *N*,*N*′-dimethyl acetamide) (93,96a), two ammonium salts (94), a solid solution with dihydrocarbamazepine (95), and 16 co-crystals including co-crystal hydrate/solvates and co-crystal polymorphs (67g,96). Most recently, Hilfiker et al. (97), at Solvias AG, identified three new forms and a dioxane solvate using high-throughput screening and Childs et al. (45) demonstrated the preparation of 27 unique solid phases of carbamazepine utilizing 18 carboxylic acids as co-crystal formers and four different screening methods. CBZ probably has more reported co-crystals than any other API, and some of these co-crystals have also been studied in terms of their dissolution and bioavailability. CBZ is therefore an

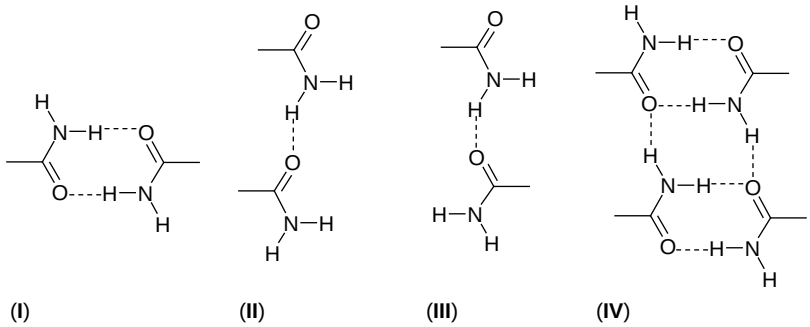

FIGURE 8 The four supramolecular homosynthons typically exhibited by primary amides.

appropriate starting point for case studies. CBZ exhibits a simple molecular structure in terms of its hydrogen-bonding capabilities because it possesses a single hydrogen-bonding moiety, a primary amide. The supramolecular homosynthons typically exhibited by primary amides are presented in Figure 8.

The primary amide dimer, I, like the carboxylic acid dimer, is a well-documented supramolecular homosynthon. A survey of the CSD reveals that there are 1,464 crystal structures that consist of at least one primary amide functional group, and I is exhibited in 589 of these structures even in the presence of competing hydrogen bond donors/acceptors. However, this represents a raw set of data, and a more refined search of the occurrence of this moiety in the absence of competing hydrogen bond donors and/or acceptors revealed 61 crystal structures that contain an amide moiety in the absence of other hydrogen bond donor or acceptor groups. Fifty-two (85 %) of these structures exhibit I and 9 (15 %) exhibit catemer motif II, suggesting that I is favored over II when no competing groups are present. Once the dimer is formed between the amide moiety, the anti-hydrogen atom either forms a hydrogen bond to an adjacent amide so as to form molecular tapes or sheets or it hydrogen bonds to a different functional group via a supramolecular heterosynthon. However, this is not the case with CBZ, in which the anti-hydrogen atom is not involved in hydrogen bonding, presumably due to steric constraints imposed by the azepine ring of CBZ (Fig. 9). That the CBZ dimer does not engage its peripheral hydrogen-bonding capabilities represents one avenue for crystal engineering and makes CBZ an excellent candidate for formation of pharmaceutical co-crystals. A second strategy involves breakage of the dimer motif and formation of supramolecular heterosynthons. Both strategies have been successful, and have afforded a number of CBZ co-crystals that exhibit improved physicochemical properties. Several of these co-crystals are described herein.

Carbamazepine:Nicotinamide 1:1 Co-crystal (1a) (96a)

In the pharmaceutical co-crystal of CBZ and nicotinamide, **1a**, CBZ molecules form supramolecular homosynthon **I** around a crystallographic inversion center. These CBZ dimers H-bond to the *syn* positions of nicotinamide amide groups, and the aromatic nitrogen atoms of the nicotinamide molecules are not involved in hydrogen bonding (Fig. 10).

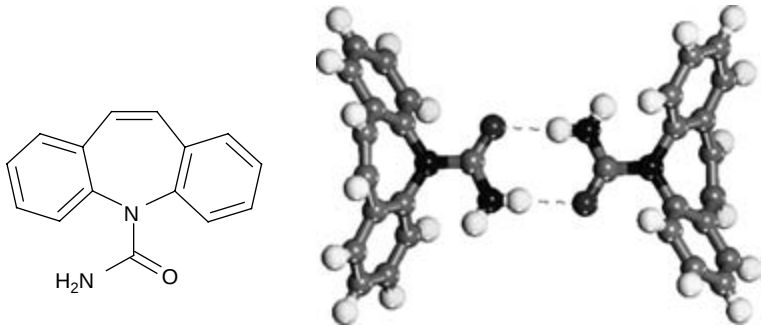

FIGURE 9 Molecular structure of carbamazepine (CBZ; *left side*) and the amide dimer (**I**; *right side*) that occurs in pure CBZ polymorphs.

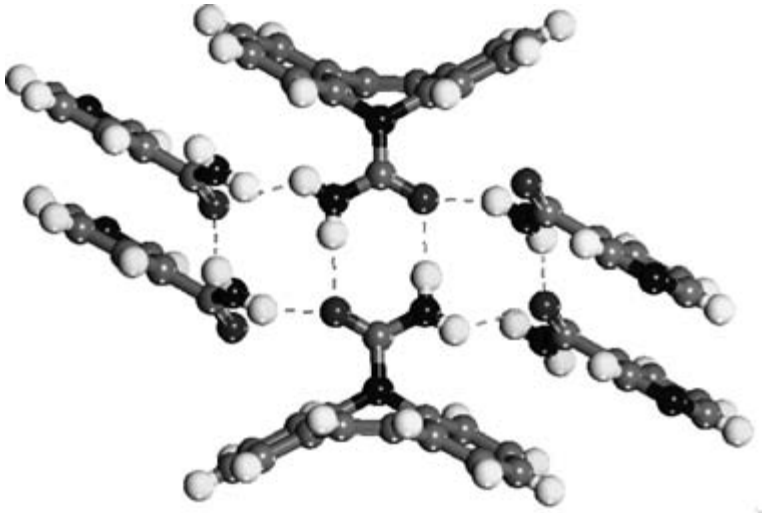

FIGURE 10 Illustration of the interaction between CBZ dimers and nicotinamide. Nicotinamide links the CBZ dimers by forming hydrogen-bonded tapes.

Rodriguez-Hornedo and coworkers have studied CBZ to develop an approach called reaction crystallization for the rapid formation of co-crystals in microscopic and macroscopic scales under ambient conditions (40). Reaction crystallization exploits solubility differences between the API, co-crystal former and co-crystal, and involves analysis of the ternary phase diagram. **1a** was selected as a model system to study the reaction pathways and kinetics in both aqueous and organic media. The phase solubility diagram for **1a** as a function of the concentration of co-crystal former in EtOH was reported, and the co-crystallization process of **1a** using anhydrous CBZ form III and nicotinamide in EtOH was monitored by Raman spectroscopy (Fig. 11). This formation of **1a** was the result of dissolution of

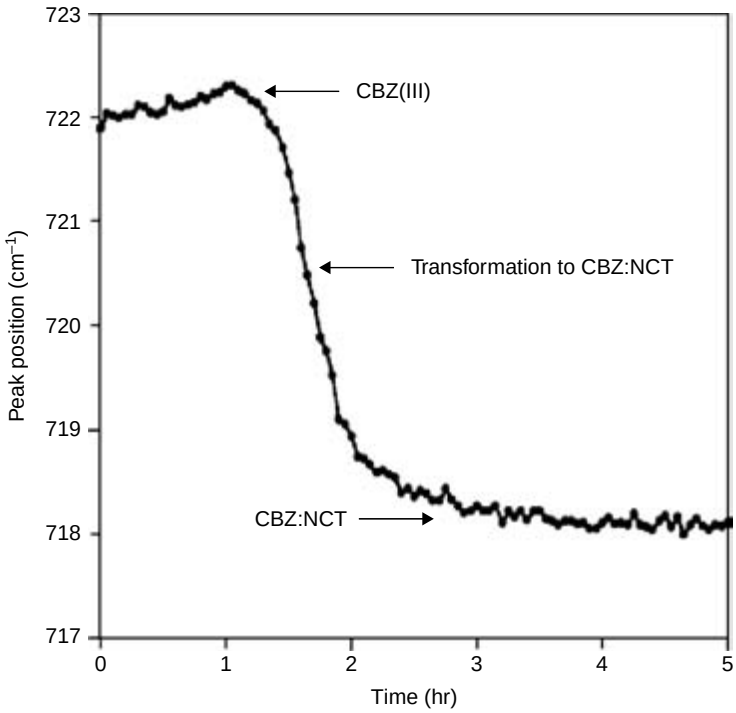

FIGURE 11 Raman peak position with respect to time showing the slurry conversion or transformation of solid phase CBZ(III) to co-crystal **1a** at 25°C after adding 0.16 M solution of nicotinamide in ethanol to CBZ(III).

anhydrous CBZ form III, leading to supersaturation of co-crystal **1a**. In situ preparation of **1a** using covered depression slides on a polarizing optical light and Raman microscope by addition of a few drops of solvent such as ethanol, ethyl acetate, or 2-propanol to the solid API and co-crystal former was also described. This study suggests broadly applicable screening methods for the preparation of co-crystals.

The factors that can control amorphous phase-mediated co-crystallization using **1a** as a model system were also addressed in order to evaluate whether amorphous phases lead to co-crystal formation and if there is a relation between temperature and crystallization pathways (98). The results suggested that amorphous phases can indeed generate co-crystals, and that temperature affects the crystallization pathways in significant ways. A new phase of **1a** (Form II) was identified during the thermal analysis.

Rodriguez-Hornedo et al. also developed a mathematical model to describe the solubility of co-crystals by taking into consideration the equilibria between co-crystal, co-crystal components, and solution complexes with **1a** as a model [Fig. 12(A)] (99). Nicotinamide solutions with varying concentrations were prepared using solvents such as ethanol, 2-propanol, or ethyl acetate [Fig. 12(B)]. The co-crystal solubility was measured by suspending co-crystals in these solutions, and it was observed that the solubility of co-crystal decreases with the increase in nicotinamide concentration.

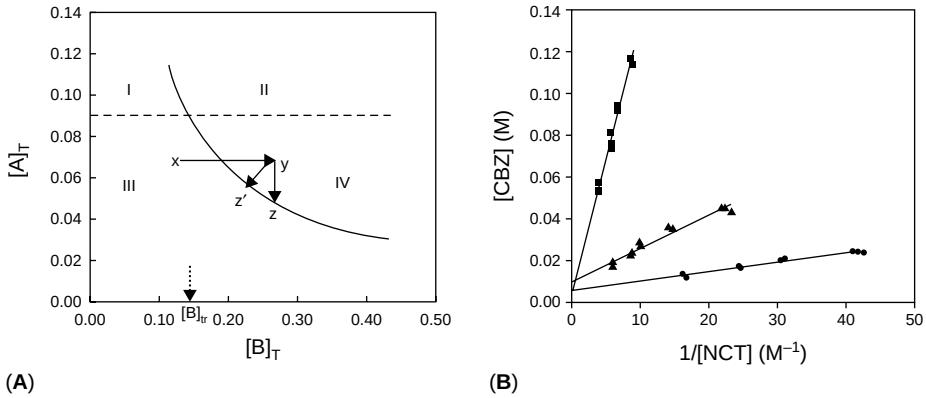

FIGURE 12 (**A**) Effect of co-crystal former B concentration on the solubility of co-crystal AB (*solid line*) and the solubility of single-component crystal (for instance API) A (*dashed line*). The transition of the co-crystal former concentration $[Br]_{tr}$ occurs when the solubility of A equals the solubility of AB. (**B**) Total CBZ concentration in equilibrium with co-crystal, **1a**, at 25°C as a function of the inverse total nicotinamide concentration in ethanol (*top*), 2-propanol (*middle*), and ethyl acetate (*bottom*), showing the linear dependence as per the prediction.

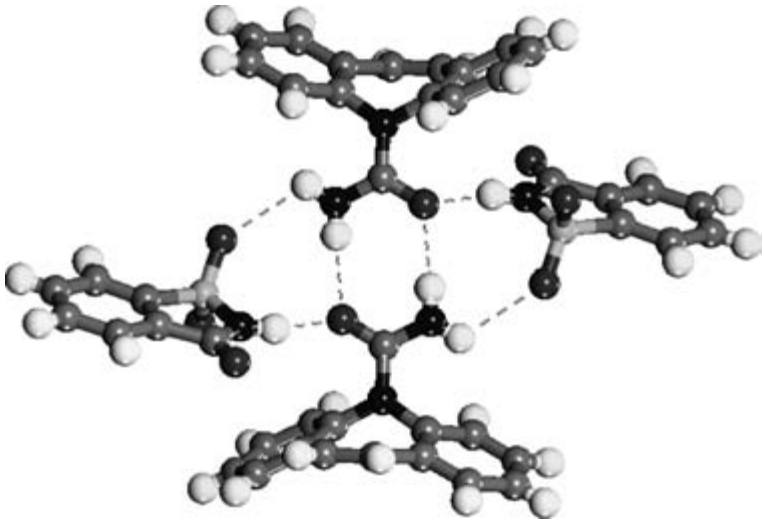

FIGURE 13 Illustration of the interactions between CBZ dimers and saccharin (**1b**).

Carbamazepine:Saccharin 1:1 Co-crystal (1b) (96a)

1b exhibits a structure similar to that of **1a** in that CBZ molecules form supramolecular homosynthon I related by inversion symmetry. The saccharin molecules serve as both hydrogen-bond donors (N–H moiety) and acceptors (S=O group) by forming hydrogen bonds with both the carbonyl and N–H moieties of CBZ. The carbonyl and the second S=O of saccharin molecules are not involved in hydrogen bonding (Fig. 13).

Almarsson and coworkers (50) studied **1b** with regard to multi-gram scale-up, propensity for crystal polymorphism, physical stability, in vitro dissolution, and oral bioavailability in comparison with the marketed form III of CBZ (Tegretol®). **1b** was scaled up to 30 g with a conventional cooling crystallization process from alcohol solution without seeding. The physical stability of the co-crystal **1b** was found to be superior compared to that of solvates of CBZ and similar to that of the marketed form of CBZ. It was also found that co-crystal **1b** is resistant to hydrate formation over a period of 15 days under direct exposure to ICH storage conditions. The oral pharmacokinetics (PK) of co-crystal **1b** were studied in dogs and compared with the marketed form of Tegretol®. The study was conducted at a dose equivalent to 200 mg of anhydrous CBZ, and was administered orally in a two-way cross-over design to four fasted beagle dogs. The study suggested that co-crystal could serve as a practical alternative to anhydrous CBZ in oral formulation because the bioavailability appears to be improved. Other benefits of the co-crystal **1b** include the following: (i) it has better solubility compared to the CBZ dihydrate or pure CBZ forms; (ii) it is stable in water for >24 hours; (iii) it has similar chemical stability compared to other forms of CBZ; (iv) although pure CBZ has four polymorphs co-crystal is not overtly polymorphic (1200 screen CRYSTALMAX experiments that include high-throughput screening, neat grinding, solvent-drop grinding with various solvents, and slurry conversion in different solvents). In general, if CBZ represents a microcosm of issues related to crystal form selection of APIs then pharmaceutical co-crystals could indeed represent a viable approach for improving the diversity and performance of API crystal forms.

Polymorphs of 1a and 1b (96d)

Utilization of functionalized cross-linked polymers as heteronuclei has been used as effective strategy for polymorph discovery of active pharmaceutical ingredients, and CBZ co-crystal polymorphs have been discovered using such an approach. Matzger and coworkers demonstrated that **1a** and **1b** are polymorphic when grown from solution in the presence of polymer heteronuclei. The single-crystal X-ray structure of form II of **1b** revealed the formation of supramolecular heterosynthons between CBZ and saccharin molecules as shown in Figure 14, in contrast to the amide–amide dimers observed in Form I.

Polymorphs of the Carbamazepine:Isonicotinamide 1:1 Co-crystal (1c) (100)

Horst and coworkers investigated two polymorphs of **1c** through a solvent-mediated transformation process in which a dry mixture of the pure components was suspended in ethanol. Co-crystals with two different morphologies and stabilities were obtained. Metastable, needle-like crystals (Form II) were obtained first followed by stable plate-like single crystals (Form I). Single-crystal X-ray structure determination revealed that Form I is constituted of chains of alternating dimers of CBZ and dimers of isonicotinamide, whereas the powder X-ray diffraction pattern of Form II suggests that it is isostructural to the known 1:1 stoichiometric co-crystal of CBZ and nicotinamide (i.e., centrosymmetric CBZ dimers hydrogen bonded to chains of nicotinamide molecules). Figure 15 compares the crystal structures of the two polymorphs of **1c**.

The ternary phase diagram reveals that excess isonicotinamide favors formation of co-crystals, whereas 1:1 stoichiometry affords either CBZ crystals or mixtures of CBZ and co-crystals. Generally APIs are slightly or moderately soluble

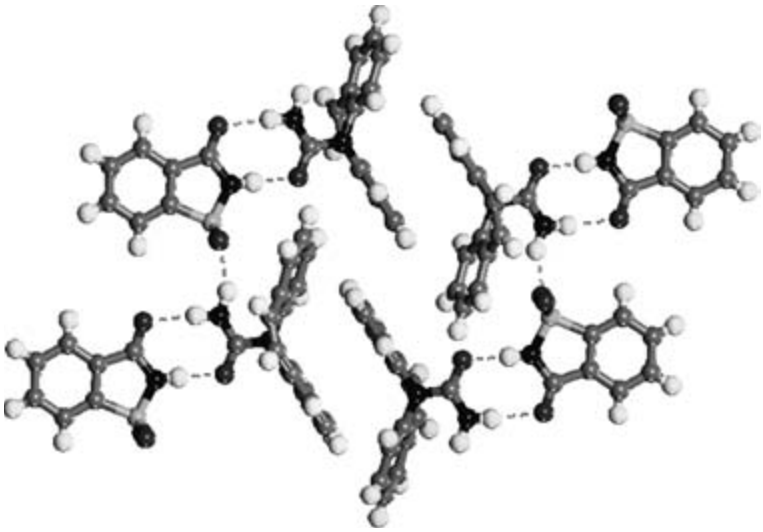

FIGURE 14 Molecular packing in CBZ:saccharin form II co-crystal.

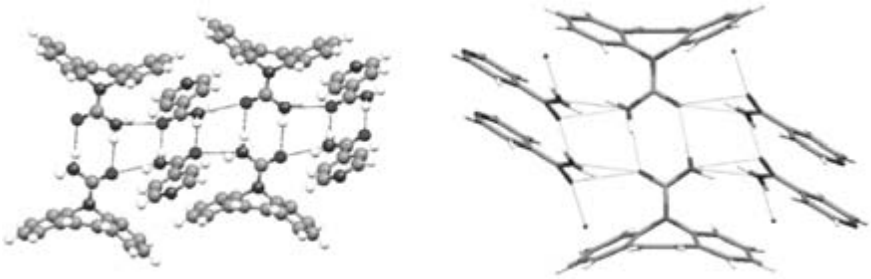

(**A**) (**B**)

FIGURE 15 Single-crystal X-ray structure of CBZ:isonicotinamide co-crystals: (**A**) Form I; (**B**) proposed structure of Form II, showing the principal hydrogen bonding synthons.

in solvents acceptable in pharmaceutical industries. Taking this into consideration a typical schematic phase diagram for an API (A), a co-crystal former (B), and solvent is as shown in Figure 16. This phase diagram highlights how solvent-mediated transformations such as reaction crystallization can offer a simple, flexible, and adaptable method for identifying the presence of co-crystal polymorphs.

Pharmaceutical Co-crystals of Fluoxetine Hydrochloride (Prozac®) (48)

Fluoxetine hydrochloride (fluoxetine HCl) is the API found in the common antidepressant drug Prozac®. It is a solid under ambient conditions, and only one crystalline phase is known. Childs et al. (48) demonstrated the preparation of co-crystals of

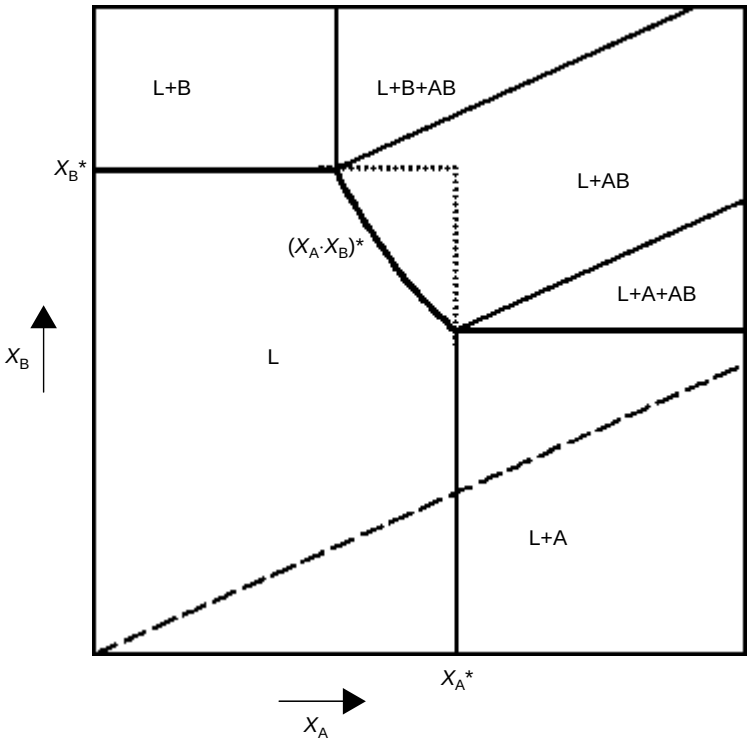

FIGURE 16 A schematic phase diagram for slightly soluble components and co-crystal. In the region L+AB co-crystallization occurs and ultimately equilibrium is reached between the AB co-crystal and the solution. In the regions L+A+AB and L+B+AB both the co-crystal and a pure component crystal phase are formed and the system moves to the three-phase equilibrium point where the two solubility lines meet. The dashed line indicates a 1:1 stoichiometric solution.

fluoxetine HCl using pharmaceutically acceptable carboxylic acids that form hydrogen bonds with the chloride ions. That chloride is perhaps the most preferred anion for generating salts of APIs makes co-crystals of fluoxetine HCl prototypal for many APIs. Fluoxetine HCl was co-crystallized with benzoic acid (1:1), succinic acid (2:1), and fumaric acid (2:1) via traditional evaporation techniques. For all three co-crystals, the carboxylic acid was found to hydrogen bond to the chloride ion, which in turn, interacted with the protonated amine. Powder dissolution experiments were carried out in water for the three novel co-crystals, resulting in a spread of dissolution profiles (Fig. 17). The fluoxetine HCl:benzoic acid co-crystal was found to have a decrease in aqueous solubility of ca. 50%, and the fluoxetine HCl:fumaric acid co-crystal had only a slight increase in aqueous solubility. However, the fluoxetine HCl:succinic acid co-crystal exhibited an approximately two-fold increase in aqueous solubility after only five minutes. The dissolution profile is consistent with the complex between succinic acid and fluoxetine HCl falling apart in solution to generate its pure components after about one hour. An intriguing aspect of this study is that by simply hydrogen bonding a hydrochloride salt of an API with similar

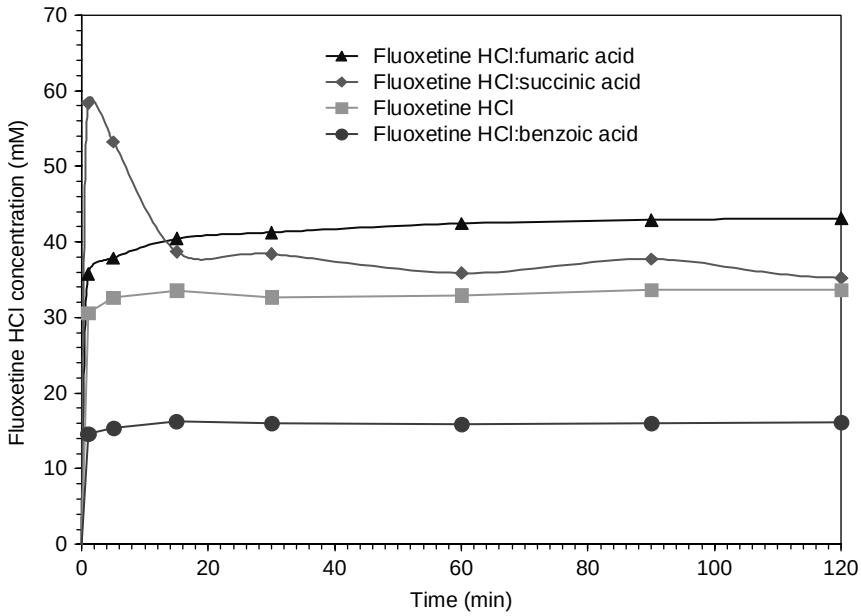

FIGURE 17 Powder dissolution profile for various forms of fluoxetine HCl illustrate how intrinsic dissolution can be modified through co-crystallization.

co-crystal formers one can generate distinctively different dissolution profiles in a manner that could not be achieved through, for example, particle size control.

Pharmaceutical Co-crystals of Itraconazole (Sporanox®) (47)

Itraconazole (Fig. 18) is an extremely water-insoluble (aqueous solubility is estimated at ~1 ng/mL at neutral pH and ~4 μg/mL at pH 1) (101) triazole antifungal agent. It is administered both orally and intravenously. The oral administration is formulated with the amorphous form of itraconazole coated on the surfaces of sucrose beads of 0.4–0.5-mm diameter and marketed as Sporanox® capsules. In addition, co-administration of acidified HP-β-cyclodextrin beverages with Sporanox® capsules is required to achieve the maximal absorption of the API, even though such a co-administration can cause diarrhea.

Intriguingly, a survey of the patent literature revealed that there is no data available on crystalline salts of itraconazole, even though salt formation using itraconazole and an acidic salt former would seem to be a logical approach to improve the absorption properties of the API. Crystalline phases of itraconazole can be crystal engineered by introduction of additional molecules to match hydrogen-bond donors and acceptors. The 2:1 co-crystal of itraconazole and succinic acid is shown in Figure 19, and it reveals hydrogen bonding via carboxylic acid-triazole supramolecular heterosynthons. The aqueous dissolution of itraconazole co-crystals was studied; two of the co-crystals exhibit a dissolution profile more akin to the Sporanox® form than to the crystalline form of pure API. In a further pharmacokinetic study of itraconazole co-crystals, it was revealed that the co-crystal formulation of the API

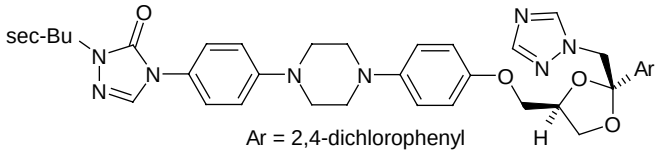

FIGURE 18 Molecular structure of itraconazole.

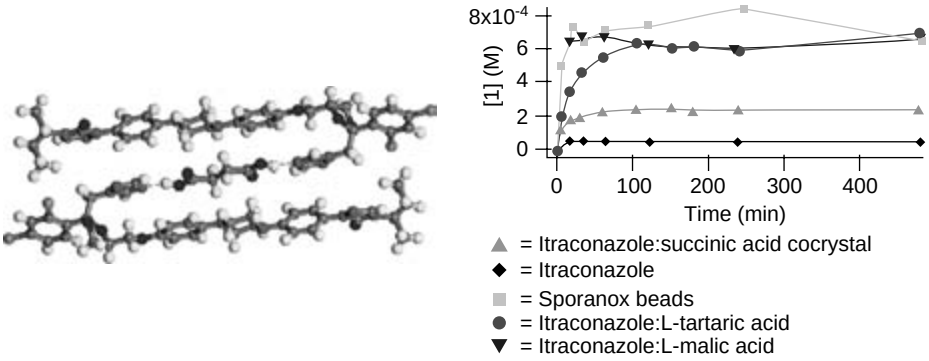

FIGURE 19 (**A**) The 2:1 co-crystal of itraconazole and succinic acid forms a trimeric unit. (**B**) Dissolution profiles in 0.1 N HCl at 25°C.

gives similar oral bioavailability to the Sporanox® form in the animal trial using a dog model.

Pharmaceutical Co-crystals of Sildenafil (Viagra®) (64)

Sildenafil, 1-[[3-(6,7-dihydro-1-methyl-7-oxo-3-propyl-1*H*-pyrazolo[4-3-*d*]pyrimidin-5-yl)-4-ethoxyphenyl]sulphonyl]-4-methylpiperazine [Fig. 20(A)] is a drug utilized in the treatment of a number of disorders including pulmonary arterial hypertension, stable, unstable, and variant angina, congestive heart failure, atherosclerosis, conditions of reduced blood vessel patency, peripheral vascular disease, bronchitis, chronic and allergic asthama, as well as male erectile dysfunction and female sexual disorders. Sildenafil is available as a citrate salt form, and has been commercially developed and marketed by Pfizer under the trademark Viagra®. Although it is available as a salt form it is moderately soluble in water and thus exhibits erratic or incomplete absorption, low bioavailability, and slow onset of action. It has been observed that sildenafil in a pharmaceutical co-crystal form could provide an improved solubility of the API under acidic conditions. In addition, such an improvement of solubility of sildenafil could be particularly advantageous for its orally administrable formulation. Sildenafil has been successfully co-crystallized with acetylsalicylic acid (1:1 molar ratio) by slurry or under reflux conditions. The crystal structure of the co-crystal of sildenafil and acetylsalicylic acid has been determined

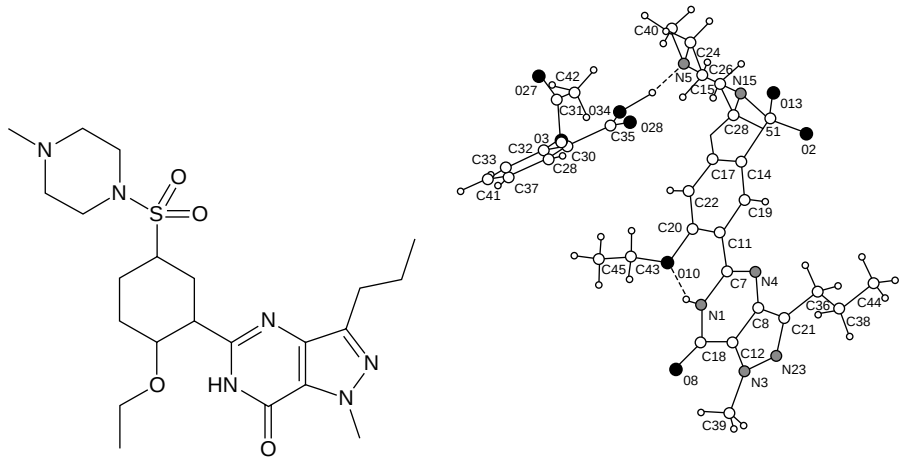

(**A**) (**B**)

FIGURE 20 (**A**) Molecular structure of sildenafil. (**B**) Crystal structure of 1:1 sildenafil:acetyl salicylic acid co-crystal.

by single-crystal X-ray diffraction [Fig. 20(B)], and in addition, the composition of matter was confirmed by powder X-ray diffraction and infrared spectrometry. The melting point of the co-crystal is approximately 143°C, and it remains thermodynamically stable up to ca. 165°C. An intrinsic dissolution study in simulated gastric body fluid (pH = 1.2) shows that the co-crystal exhibits an intrinsic dissolution rate (IDR) of ca. 11.75 mg·min^{-1} cm^{-2} versus 6.64 mg·min^{-1} cm^{-2} for sildenafil citrate under the same conditions.

Pharmaceutical Co-crystals of 2-[4-(4-Chloro-2-Fluorophenoxy)Phenyl] Pyrimidine-4-Carboxamide (SCB), a Sodium Channel Blocker (49)

2-[4-(4-Chloro-2-fluorophenoxy)phenyl]pyrimidine-4-carboxamide (SCB) is a BCS class II drug that belongs to a class of sodium channel blockers and was developed as a potential drug candidate for the treatment or prevention of surgical, chronic, and neuropathic pain. SCB was observed to exhibit low in vitro dissolution, and upon oral administration to dogs it showed low in vivo plasma concentration. Efforts to increase the bioavailability of SCB by forming salts, solvates, hydrates, polymorphs, or amorphous material failed to produce a viable solid form for drug formulations. Hence, co-crystallization was used to improve the pharmaceutical properties of SCB. Co-crystal screening was carried out employing two methods: melt crystallization or highly saturated solution. A total of 26 carboxylic acids were screened out of which a co-crystal containing SCB and glutaric acid in 1:1 molecular ratio was identified and characterized by single-crystal X-ray analysis (Fig. 21), **5**. **5** can be scaled up in gram quantities, is non-hygroscopic, and chemically and physically stable to thermal stress.

The intrinsic dissolution rate profile suggests that the co-crystal increases the in vitro rate of dissolution by 18 times when compared to the pure API. Single-dose

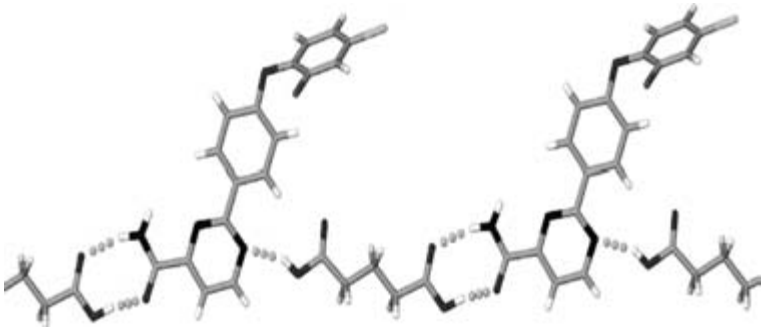

FIGURE 21 Hydrogen bonding in co-crystal **5** showing the interactions between the carboxylic acid groups of glutaric acid molecules and the amide and pyridine groups of the drug molecules, SCB.

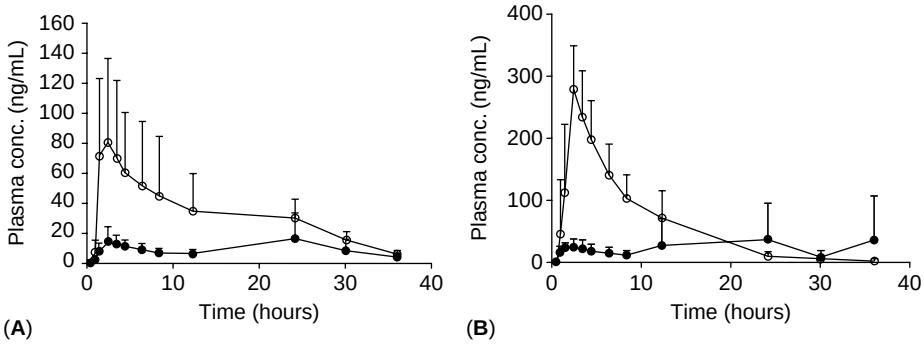

FIGURE 22 Dog plasma concentration with time for (**A**) 5 mg/kg dosing and (**B**) 50 mg/kg of API, SCB (solid circles) and co-crystal (open circles). Error bars show +1 standard deviation.

bioavailability studies on dogs confirmed that the co-crystal improved the plasma area under the curve (AUC) values by three times at both low (5 mg/kg) and high dose (50 mg/kg) as shown in Figure 22.

Pharmaceutical Co-crystals of "AMG 517" (102)

Transient receptor potential vanilloid 1 or TRPV1 is a nonselective ligand-gated cation channel that can be activated by a wide variety of external and internal stimuli such as a temperature greater than 43°C, an acidic medium or a neurotransmitter such as anandamide, or the capsaicin-active components in chilli pepper. TRPV1 receptors are found in central and peripheral nervous systems, and they are responsible for transmission and modulation of pain along with the integration of diverse painful stimuli. AMG 517 is a transient receptor potential vanilloid 1 antagonist that was developed by Amgen for the treatment of acute and chronic pain. The free base of AMG 517 is associated with problems such as insolubility in water and buffers at physiological pH. AMG 517 has three isolated forms: a monohydrate (stable for at

least three years at ambient temperature and humidity), a metastable nonsolvated form, and a stable free base. In addition numerous salts and solvates have been prepared, isolated, and characterized. However, the salts disproportionate in aqueous medium and convert into the hydrated form of AMG 517. Bak and coworkers (102) investigated 10 co-crystals of AMG 517 with the following carboxylic acids: sorbic acid, benzoic acid, *trans*-cinnamic acid, 2,5-dihydroxybenzoic acid, glutaric acid, glycolic acid, *trans*-2-hexanoic acid, 2-hydroxycaproic acid, L(+)-lactic acid, and L(+)-tartaric acid. The hydrogen bonding in two co-crystals is as shown in Figure 23. The physicochemical properties such as particle size, solubility, stability, hygroscopicity, thermal behavior, and structural characteristics of these co-crystals were studied in detail.

Solubility experiments on the AMG 517:sorbic acid co-crystal showed that the co-crystal has better initial solubility compared to AMG 517; however, it converts back to a form of the free base hydrate after prolonged slurrying in FaSIF (fasted simulated intestinal fluid, pH 6.8). Pharmacokinetic studies of the co-crystal in rats using 10% (w/v) Pluronic F1081 in OraPlus1 suspensions revealed that a 30 mg/kg dose in suspension had comparable exposure to a 500 mg/kg dose of the free base. Further solubility measurements on AMG 517 co-crystals with glutaric acid, glycolic acid, *trans*-2-hexanoic acid, lactic acid, and benzoic acid showed that the co-crystals reach a maximum solubility within 1–2 hours and, similar to the sorbic acid co-crystal, the dissolution profile indicates conversion of the co-crystals to AMG 517 hydrate.

Correlations between the melting point of the co-crystal formers and the co-crystals and between the melting point and solubility of the co-crystals were also addressed. The melting point of all co-crystals was between the co-crystal formers and AMG 517, and linear regression indicated that the melting points of co-crystal formers and co-crystals are directly proportional with 78% correlation. However, the melting point and solubility of the co-crystals are related with only 55% correlation.

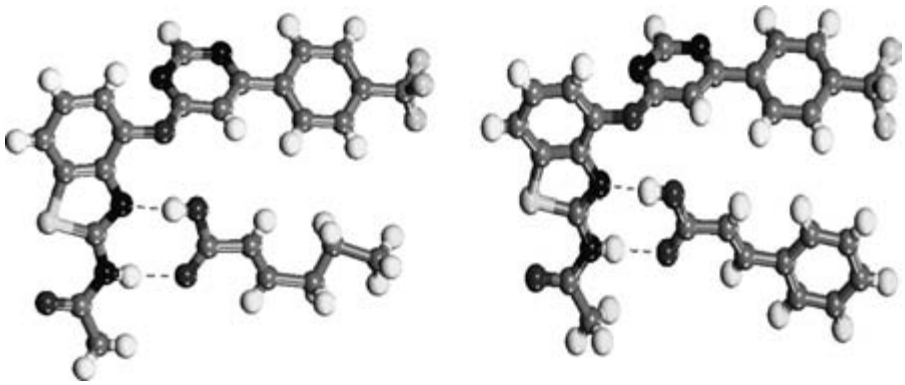

(**A**) (**B**)

FIGURE 23 Molecular recognition between AMG 517 and (**A**) *trans*-cinnamic acid (**B**) *trans*-2-hexanoic acid.

Co-crystals of Melamine and Cyanuric acid (103)

In early 2007 there was a major pet food recall by the FDA based on the receipt of numerous complaints regarding the deaths of animals after ingestion of a variety of pet food products. It was reported that the majority of these deaths were associated with acute renal failure in these animals. Melamine, 2,4,6-triamino-1,3,5 triazine, was the primary suspect for contamination in the tainted pet food products because melamine had been intentionally added to raise the apparent protein content in the pet food. However, melamine is considered relatively nontoxic [LD_{50} values of 3100 mg/kg (rat male) and 3900 mg/kg (rat female)] and oral administration of 125 mg/kg body weight of melamine to dogs leads to diuretic effects but is not fatal. Indeed, the quantity of melamine observed in the pet food was not at the lethal dosage. In the course of the pet food recall investigation, cyanuric acid, another relatively nontoxic compound, was also identified in the pet food as a co-contaminant. Although melamine and cyanuric acid are relatively safe individually, no data could be found in the literature that determines the potential toxicity of melamine and cyanuric acid in combination. From the crystal engineering viewpoint, melamine and cyanuric acid (1:1 molar ratio) form an extensive two-dimensional networks in the solid state based on robust three-point molecular recognition (Fig. 24) and

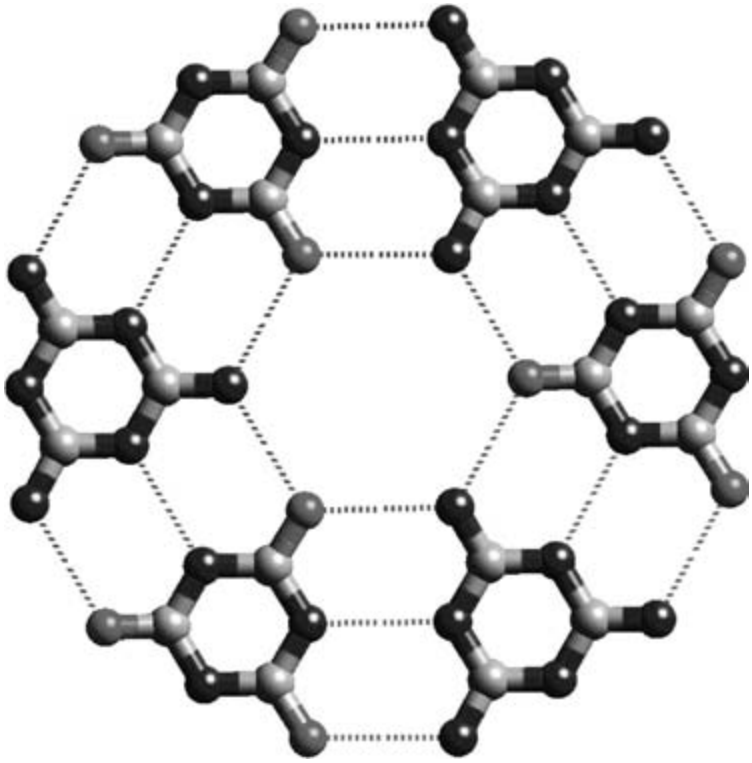

FIGURE 24 The rosette network formed between melamine and cyanuric acid.

the resulting melamine:cyanuric acid co-crystal is, perhaps unsurprisingly, highly insoluble in water.

Puschner et al. investigated the toxicity of melamine and cyanuric acid individually and also in combination when administered to cats, and demonstrated clinical pathologic changes, gross or histologic lesions, associated with the contaminants in the recalled pet food. The oral administration of 181 mg/kg body weight of melamine alone at 0.5% and 1% of their diet to three cats for 11 days did not show any evidence of renal failure. Similar results were obtained on administration of cyanuric acid alone in the diet at 0.2%, 0.5%, and 1% dosage respectively. However, it was observed that a single oral exposure of cats to the combination of melamine and cyanuric acid at a dosage as low as 32 mg/kg body weight leads to acute renal failure. A study conducted at the Bergh Memorial Animal Hospital in New York revealed that co-crystals blocked the tubes leading from the kidneys to the bladder in one cat. Thus, it seems clear that the formation of a low solubility co-crystal of melamine and cyanuric acid is responsible for these incidents. This case study of melamine:cyanuric acid co-crystals might be the first example of co-crystals altering clinically relevant physical properties in a negative manner.

POLYMORPHISM IN CO-CRYSTALS AND PHARMACEUTICAL CO-CRYSTALS

Polymorphism (19,104–105), the existence of different crystal forms of the same compound, is long recognized from a scientific perspective. Mitscherlich introduced the concept of isomorphism, an important development in structural chemistry, in 1819 (106), and in 1932 Wöhler and Liebig (107) described dimorphism of benzamide, perhaps the first example of a polymorphic organic substance. That polymorphism can impact physical properties is perhaps best exemplified in elements, where it is known as "allotropy," as exemplified by carbon, which exhibits three crystal forms with dramatically different physical properties: graphite, diamond, and fullerenes. The phenomenon of polymorphism is now well appreciated both academically and industrially because it impacts preparation and formulation of specialty chemicals, pharmaceuticals, dyes, explosives, and foods (108). McCrone's definition (109) of polymorphism, that is, "a solid crystalline phase of a given compound resulting from the possibility of at least two different arrangements of the molecules of that compound in the solid state," is apt in the context of this chapter's focus upon structural chemistry.

Crystallization of polymorphs is governed by a combination of thermodynamic and kinetic factors (110). The occurrence of polymorphs often follows Ostwald's rule of stages (111), which states that the meta-stable form is often obtained first and the stable form crystallizes subsequently. Depending upon the arrangement of molecules and/or conformation adopted by the functional groups present in the molecule, polymorphs may be classified into several categories: that is, conformational polymorphs (112), concomitant polymorphs (107,113) structural polymorphs (114), and configurational polymorphs (115). Nevertheless, a CSD analysis tabulated in Table 1 reveals that polymorphism is not prevalent in either single-component crystals (1,882/134,086) or in co-crystals (40/2,083).

This chapter focuses upon pharmaceutical co-crystals, and we present herein a structural analysis of selected co-crystals that exhibit polymorphism in addition to the polymorphic co-crystals of CBZ discussed earlier in the section "Pharmaceutical Co-crystals of Carbamzepine (Tegretol®)."

TABLE 1 Cambridge Structural Database Statistics of Polymorphic Single and Multicomponent Crystal Structures

	Number of entries	Percentage of organic structures
Organic crystal structures	186,053[a]	100[d]
Single-component molecular organic structures	134,086	72.1[d]
Single-component polymorphic structures	1,882[b]	1.4[e]
Hydrates	13,843	7.4[d]
Co-crystals	2,083[c]	1.1[d]
Polymorphic co-crystals	40	1.9[f]

CSD August 2008 update, 456,628 entries.
[a]Structures containing Na, Li, K, As were excluded.
[b]Only one refcode was counted for each polymorphic compound.
[c]Co-crystals sustained by strong hydrogen bonds.
[d]Percentages with respect to organic crystal structures only.
[e,f]Percentages with respect to 134,086 and 2083 sub-totals, respectively.

1:1 Co-crystals of Caffeine and Glutaric Acid (EXUQUJ–EXUQUJ01)

The crystal structures of the polymorphic forms of 1:1 co-crystals of caffeine and glutaric acid were described by Jones et al. (42) in 2004. Both crystal forms, rods and blocks, were obtained concomitantly from a solution containing a 1.3:1 ratio of caffeine and glutaric acid, respectively. The "rods" are monoclinic (Form I), whereas the "blocks" are triclinic (Form II). Both Forms I and II exhibit identical secondary architecture because they form sheets resulting from hydrogen bonds (O–H···N) between one of the –COOH moieties of glutaric acid and the free aromatic nitrogen atom (N_{arom}) of caffeine. The two polymorphs exhibit differences in the torsion angle of the methylene carbon atoms of glutaric acid (Fig. 25). The authors noted how solvent-drop grinding could be used to afford a co-crystal polymorph exclusively: dry grinding and solvent-drop grinding using nonpolar solvents such as *n*-hexane, cyclohexane, or heptane yielded only Form I; solvent-drop grinding using polar solvents such as chloroform, dichloromethane, acetonitrile, and water produced only Form II.

2:1 Co-crystals of 4-Cyanopyridine and 4,4′-Biphenol (TEHNAW–TEHNAW01)

Zaworotko et al. (116) reported that crystallization of a 2:1 ratio of 4-cyanopyridine and 4,4′-biphenol in methanol:ethyl acetate afforded concomitant polymorphs of the 2:1 co-crystal of 4-cyanopyridine and 4,4′-biphenol. The single-crystal X-ray structures revealed that Form I (irregular hexagonal plates) and Form II (parallelepiped plates) exhibit conformational differences in the 4,4′-biphenol molecules (Fig. 26), but O–H···N supramolecular heterosynthon sustain both forms, suggesting that O–H···N(pyridine) supramolecular heterosynthons are favored over competing O–H···N(cyano) supramolecular heterosynthons. Form I crystallized in $C2/c$ with half a 4,4′-biphenol molecule and one 4-cyanopyridine molecule in the asymmetric unit, whereas Form II crystallized in $P2_1/n$ with four 4-cyanopyridine and two 4,4′-biphenol molecules in the asymmetric unit. Form I can be obtained by dissolving Form II in MeOH, EtOAc, or acetone where Form II can be obtained by solvent drop grinding of the starting materials or Form I.

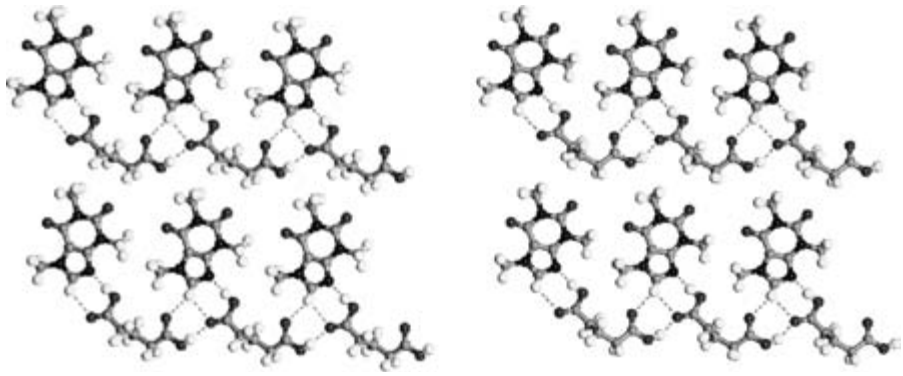

FIGURE 25 Crystal structures of monoclinic (Form I) and triclinic (Form II) forms of caffeine:glutaric acid co-crystals. Although the crystal packing is similar there is a difference in the torsion angle of the methylene carbon atoms of glutaric acid.

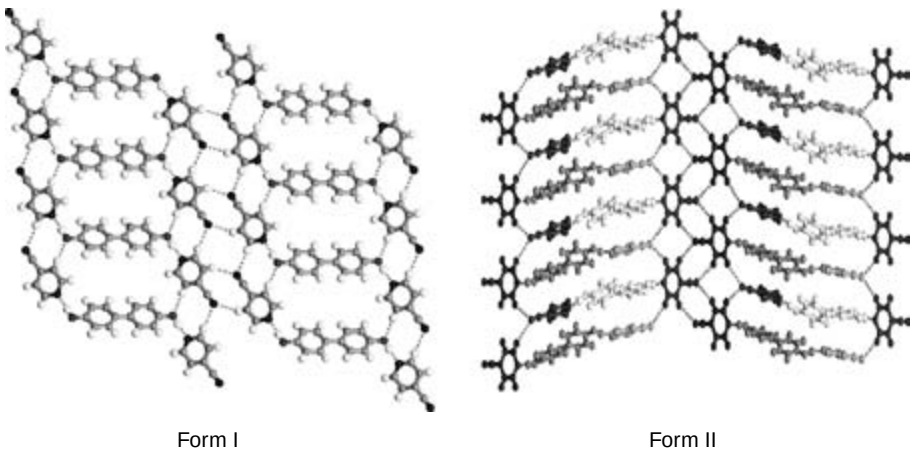

FIGURE 26 Crystal packing of Form I and Form II of the 2:1 co-crystal of 4-cyanopyridine: 4,4′-biphenol.

1:1 Co-crystals of Hydroquinone/*p*-Benzoquinone (QUIDON–QUIDON02) (117–119)

Quinhydrone is a 1:1 co-crystal of hydroquinone and *p*-benzoquinone. It is the prototypal co-crystal that was first reported in 1844, and it is also the earliest entry of a co-crystal in the CSD for which atomic coordinates are available. Quinhydrone exists in two polymorphic crystal forms: monoclinic and triclinic. The monoclinic form ($P2_1/c$ space group, QUIDON02) was reported by Matsuda et al. in 1958.

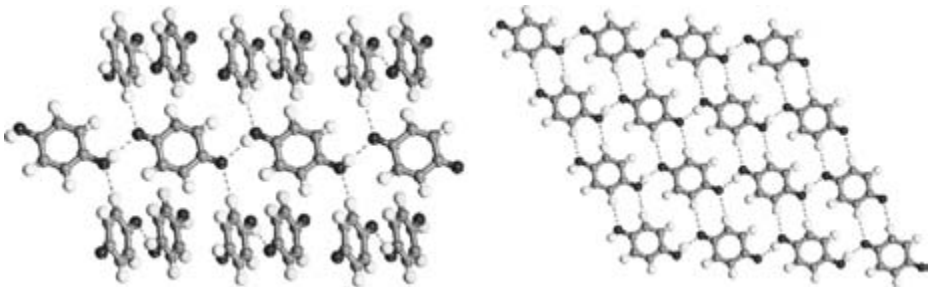

(**A**) (**B**)

FIGURE 27 Crystal structures of the (**A**) monoclinic and (**B**) triclinic forms of quinhydrone.

The crystal structure reveals that both hydroquinone and *p*-benzoquinone molecules reside on an inversion center generating linear tapes through O–H···O and C–H···O hydrogen bonds. Such tapes are further connected to generate a 3D network as illustrated in Figure 27(A). In the triclinic polymorph (*P*-1 space group, QUIDON), H-bonded tapes are also formed; however, the tapes are packed parallel to generate molecular sheets [Fig. 27(B)]. The crystal packing of Forms I and II is therefore different although the supramolecular synthons remain the same.

Polymorphism in the 1:1 Co-crystal of *N*,*N*-Bis(4-bromophenyl)melamine/5,5-Diethylbarbituric acid (JICTUK01–JICTUK10)

In 1994, Whitesides and coworkers (34) reported polymorphism in 1:1 co-crystals of *N*,*N-bis*(4-bromophenyl) melamine and 5,5-diethylbarbituric acid. Form I crystallized in a monoclinic crystal system ($P2_1/n$, JICTUK01), whereas Form II crystallized in a triclinic system (*P*-1, JICTUK10). Both polymorphs form linear tapes through three-point molecular recognition involving N–H···O and N–H···N hydrogen bonds. Once again, the same supramolecular synthons are observed in both crystal forms; however, the rotation of the phenyl ring along the C–N bond in Form II generates a different arrangement of linear tapes. (Fig. 28).

1:1 Co-crystals of Oxalic Acid and Iso-nicotinamide (ULAWAF01–ULAWAF02)

The crystal structures of the polymorphs of the 1:2 co-crystal of oxalic acid and iso-nicotinamide were reported by Wilson and coworkers in 2007 (120). The co-crystal exist in two forms: Form I crystallizes in the monoclinic space group $C2/c$ as earlier reported by Nangia and coworkers (75b), whereas Form II crystallizes in the triclinic space group *P*-1. These polymorphs can be obtained concomitantly from 1:1 ethanol:water. The fundamental difference between the two polymorphs is a *cis*/*trans* isomerism observed in the hydroxyl groups of oxalic acid. Form I exhibits the *cis*-configuration, whereas Form II contains the *trans*-configuration. The oxalic acid and iso-nicotinamide molecules form trimeric units sustained through O–H···N hydrogen bonds. These trimeric units are, in turn, connected through centrosymmetric amide dimers between iso-nicotinamide molecules, and thereby forming tapes that H-bond to form sheets. The overall crystal packing in both Form I and Form II can be described as stacked sheets (Fig. 29).

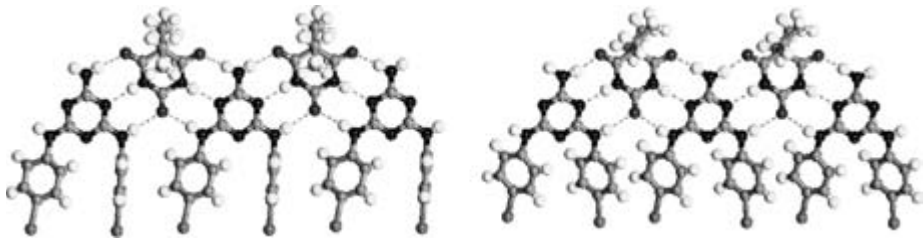

Form I Form II

(**A**) (**B**)

FIGURE 28 Linear tapes as observed by *N*,*N*-bis(4-bromophenyl)melamine and 5,5-diethylbarbituric acid co-crystals: (**A**) JICTUK01; (**B**) JICTUK10. The supramolecular synthons are identical in both forms and only salient difference between the structures lies with the orientation of the phenyl rings.

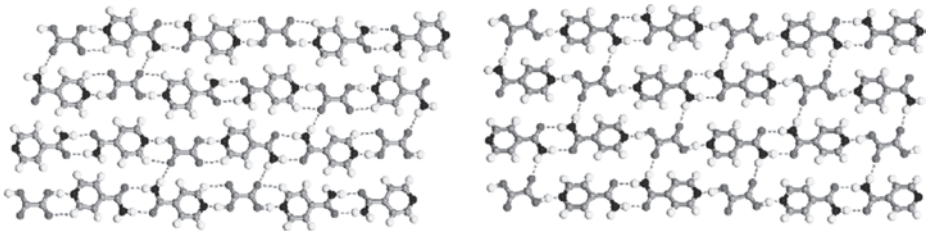

Form I Form II

(**A**) (**B**)

FIGURE 29 Crystal structures of Form (**A**) I and (**B**) Form II of the 1:1 oxalic acid:iso-nicotinamide co-crystal.

In summary, the series of polymorphic co-crystals presented herein is representative of the limited information within the CSD that addresses polymorphism in co-crystals and indicates that polymorphism in co-crystals in not typically the result of competing supramolecular synthons. However, the paucity of data precludes sweeping conclusions about polymorphism in co-crystals. That co-crystals are attracting wider interest means that there will likely be an increase in the number of systematic studies devoted to co-crystals and a corresponding increase in the number of polymorphic co-crystals. Intriguingly, this increase in the number of studies on co-crystals has afforded several recent reports of failed co-crystallizations that have instead resulted in new polymorphs of long known compounds such as benzidine and aspirin. Bernstein and coworkers (121) recently reported four new forms of benzidine obtained accidentally in the attempts to co-crystallize benzidine with different co-crystal formers. Zaworotko and coworkers (96b) first obtained Form II of aspirin during co-crystallization experiments involving aspirin and the antiseizure compound levetiracetam from hot acetonitrile. Such generation of new polymorphs could be a result of the creation of a new medium for crystallization via

the presence of co-crystal formers, and if so, it has implications for high-throughput screening as a methodology for discovering new polymorphs.

CONCLUSIONS

The pharmaceutical industry has only recently paid more than passing attention to pharmaceutical co-crystals, but there are several conclusions that can already be drawn:

- New pharmaceutical co-crystals should be patentable as novel crystal forms because their crystal structures are not obvious until prepared.
- New pharmaceutical co-crystals can be generated via rational design and multiple synthetic approaches for nearly all APIs by using crystal engineering strategies.
- Pharmaceutical co-crystals significantly diversify the number of crystal forms available for an API and always modify the physical properties of the API, thereby offering an opportunity to solve clinical problems through control of physicochemical properties of the API.

However, this does not mean that pharmaceutical co-crystals will become commonplace in marketed drug products because there remain practical handicaps that must be overcome such as the costs associated with the significant amounts of additional experimental research that are required and the risks associated with a patent and regulatory landscape that is presently in flux. As stated by Remenar (66), "If making a co-crystal of a specific molecule helps to enable an application or solve a problem, then it's the right thing to do, but you don't design a molecule in the real world simply because you are looking for a co-crystal strategy." This is probably a realistic assessment of where matters stand today in terms of pharmaceutical co-crystals and new drug development. However, there are certain niches where pharmaceutical co-crystals might be expected to find a role in drug development including high-throughput solid-state synthesis, new formulations of existing APIs, and processing of "difficult" APIs that are hard to crystallize and/or purify.

REFERENCES

1. Haleblian JK. Characterization of habits and crystalline modification of solids and their pharmaceutical applications. J Pharm Sci 1975; 64: 1269–88.
2. Byrn SR. Solid State Chemistry of Drugs, 2nd edn. SSCI Inc, 1999.
3. Salts: (a) Berge SM, Bighley LD, Monkhouse DC. Pharmaceutical salts. J Pharm Sci 1977; 66: 1–19. (b) Bastin RJ, Bowker MJ, Slater BJ. Salt selection and optimization procedures for pharmaceutical new chemical entities. Org Process Res Dev 2000; 4: 427–35 and references therein. (c) Gould PL. Salt selection for basic drugs. Int J Pharm 1986; 33: 201–17. (d) Banerjee R, Bhatt PM, Ravindra NV, et al. Saccharin salts of active pharmaceutical ingredients, their crystal structures, and increased water solubilities. Cryst Growth Des 2005; 5: 2299–309.
4. Hydrates/Solvates and polymorphs: (a) Remenar JF, MacPhee JM, Larson BK, et al. Salt selection and simultaneous polymorphism assessment via high-throughput crystallization: The case of Sertraline. Org Process Res Dev 2003; 7: 990–6. (b) Vishweshwar P, Beauchamp DA, Zaworotko MJ. An acetic acid solvate of trimesic acid that exhibits triple inclined interpenetration and mixed supramolecular homosynthons. Cryst Growth Des 2006; 6: 2429–31. (c) Banerjee R, Bhatt PM, Desiraju GR. Solvates of sildenafil saccharinate. A new host material. Cryst Growth Des 2006; 6: 1468–78. (d) Barnett SA,

Tocher DA, Vickers M. The solvates of o-acetamidobenzamide. CrystEngComm 2006; 8: 313–19. (e) Hosokawa T, Datta S, Sheth AR, et al. Isostructurality among five solvates of phenylbutazone. Cryst Growth Des 2004; 4: 1195–201.
5. Desiraju GR. Supramolecular synthons in crystal engineering – a new organic synthesis. Angew Chem Int Ed 1995; 34: 2311–27.
6. Lehn J-M. Supramolecular Chemistry: Concepts and Perspectives. Weinheim: VCH, 1995.
7. Atwood JL, Davies JED, MacNicol DD, et al., eds. Comprehensive Supramolecular Chemistry, Vol 6. Oxford: Pergamon, 1996.
8. MacDonald JC, Whitesides GM. Solid-state structures of hydrogen-bonded tapes based on cyclic secondary diamides. Chem Rev 1994; 94: 2383–420.
9. Schmidt GMJ. Photodimerization in the solid state. Pure Appl Chem 1971; 27: 647–78.
10. Etter MC. A new role for hydrogen-bond acceptors in influencing packing patterns of carboxylic acids and amides. J Am Chem Soc 1982; 104: 1095–6.
11. Desiraju GR. Crystal Engineering: The Design of Organic Solids. Amsterdam: Elsevier, 1989.
12. Dunitz JD. Phase transitions in molecular crystals from a chemical viewpoint. Pure Appl Chem 1991; 63: 177–85.
13. Mathias JP, Stoddart JF. Constructing a molecular LEGO set. Chem Soc Rev 1992; 21: 215–25.
14. Dunitz JD, Taylor R. Organic fluorine hardly ever accepts hydrogen bonds. Chem Eur J 1997; 3: 89–98.
15. Braga D. 15. Crystal engineering, Where from? Where to? Chem Commun 2003: 2751–4.
16. Moulton B, Zaworotko MJ. From molecules to crystal engineering: supramolecular isomerism and polymorphism in network solids. Chem Rev 2001; 101: 1629–58.
17. Tiekink ERT, Vittal JJ, eds. Frontiers in Crystal Engineering, Chichester, UK: Wiley, 2006.
18. Desiraju GR. Crystal engineering: a holistic view. Angew Chem Int Ed 2007; 46: 8342–56.
19. (a) Bernstein J. Polymorphism in Molecular Crystals. Oxford: Clarendon Press, 2002. (b) Hilfiker R. Polymorphism in the Pharmaceutical Industry. New York: Wiley VCH, 2006. (c) Special issue on polymorphism in crystals. Cryst Growth Des 2004; 4: 1085–444. (d) Special issue on pharmaceutical solid polymorphism in drug development and regulation. Adv Drug Delivery Rev 2004; 56: 235–418. (e) Brittain HG. Polymorphism in Pharmaceutical Solids. New York: Marcel Dekker Inc., 1999.
20. Amidon GL, Lennernas H, Shah VP, et al. A theoretical basis for a biopharmaceutic drug classification: the correlation of *in vitro* drug product dissolution and *in vivo* bioavailability. Pharm Res 1995; 12: 413–20.
21. Desiraju GR. Crystal and co-crystal. CrystEngComm 2003; 5: 466–7.
22. Dunitz JD. Crystal and co-crystal: a second opinion. CrystEngComm 2003; 4: 506.
23. Bond AD. What is a co-crystal? CrystEngComm 2007; 9: 833–4.
24. Aakeröy CB, Fasulo ME, Desper J. Cocrystal of salt: does it really matter? Mol Pharm 2007; 4: 317–22.
25. Stahly GP. Diversity in single- and multiple-component crystals. The search for the prevalence of polymorphs and cocrystals. Cryst Growth Des 2007; 7: 1007–26.
26. Zukerman-Schpector J, Tiekink ERT. What is a co-crystal? Zeit Fur Kristallogr 2008; 223: 233–4.
27. Parkin A, Gilmore CJ, Wilson CC. What is a co-crystal – and does it matter? Zeit Fur Kristallogr 2008: 223, 430.
28. Shan N, Zaworotko MJ. The role of cocrystals in pharmaceutical science. Drug Discov Today 2008; 13: 440–6.
29. (a) Aakeröy CB, Beatty AM, Helfrich BA. "Total synthesis" supramolecular style: design and hydrogen-bond-directed assembly of ternary supermolecules. Angew Chem Int Ed

2001; 40: 3240–2. (b) Aakeröy CB, Desper J, Helfrich BA. Heteromeric intermolecular interactions as synthetic tools for the formation of binary co-crystals. CrystEngComm 2004; 6: 19–24. (c) Aakeröy CB, Salmon DJ. Building co-crystals with molecular sense and supramolecular sensibility. CrystEngComm 2005; 7: 439–48. (d) Aakeröy CB, Hussain I, et al. Exploring the hydrogen-bond preference of N-H moieties in co-crystals assembled via O-H(Acid)…N(Py) intermolecular interactions. CrystEngComm 2007; 9: 46–54.
30. Ulrich J. Is melt crystallization a green technology? Cryst Growth Des 2004; 4: 879–90.
31. Almarsson Ö, Zaworotko MJ. Crystal Engineering of the composition of pharmaceutical phases. Do pharmaceutical co-crystals represent a new path to improved medicines? Chem Commun 2004: 1889–96.
32. Pepinsky R. Crystal engineering – a new concept in crystallography. Phys Rev 1955; 100: 971.
33. Etter MC. Hydrogen bonds as design elements in organic chemistry. J Phys Chem 1991; 95: 4601–10.
34. Zerkowski JA, MacDonald JC, Seto CT, et al. Design of organic structures in the solid state: molecular tapes based on the network of hydrogen bonds present in the cyanuric acid:melamine complex. J Am Chem Soc 1994; 116: 2382–91.
35. Desiraju GR, ed. Crystal Design: Structure and Function, New York: Wiley, 2003.
36. (a) Allen FH, Kennard O. Chem Des Automat News 1993; 8: 31–7. (b) Allen FH. The Cambridge Structural Database: a quarter of a million crystal structures and rising. Acta Crystallogr 2002; B58: 380–8.
37. Zerkowski JA, Seto CT, Whitesides GM, et al. Solid-state structures of 'Rosette' and 'Crinkled Tape' motifs derived from the cyanuric acid melamine lattice. J Am Chem Soc 1992; 114: 5473–5.
38. Vishweshwar P, McMahon JA, Bis JA, et al. Pharmaceutical co-crystals. J Pharma Sci 2006; 95: 499–516.
39. Special issue on pharmaceutical co-crystals. Mol Pharm 2007; 4: 299–486.
40. Wöhler F. Untersuchungen über das Chinon. Justus Liebigs Ann Chem 1844; 51: 153.
41. Shan N, Toda F, Jones W. Mechanochemistry and Co-crystal formation: effect of solvent on reaction kinetics. Chem Commun 2002: 2372–3.
42. Trask AV, Motherwell WDS, Jones W. Solvent-drop grinding: green polymorph control of cocrystallization. Chem Commun 2004; 10: 890–1.
43. Trask AV, Jones W. Crystal engineering of organic cocrystals by the solid-state grinding approach. Top Curr Chem 2005; 254: 41–70.
44. Karki S, Friscic T, Jones W, et al. Screening for pharmaceutical cocrystal hydrates via neat and liquid-assisted grinding. Mol Pharma 2007; 4: 347–54.
45. Childs SL, Rodríguez-Hornedo N, Reddy LS, et al. Screening strategies based on solubility and solution composition generate pharmaceutically acceptable cocrystals of carbamazepine. CrystEngComm 2008; 10: 856–64.
46. Rodriguez-Hornedo N, Nehm SJ, Seefeldt KF, et al. Reaction crystallization of pharmaceutical molecular complexes. Mol Pharma 2006; 3: 362–7.
47. Remenar JF, Morissette SL, Peterson ML, et al. Crystal engineering of novel cocrystals of a triazole drug with 1,4-dicarboxylic acids. J Am Chem Soc 2003; 125: 8456–7.
48. Childs SL, Chyall LJ, Dunlap JT, et al. Crystal Engineering Approach to Forming Cocrystals of Amine Hydrochlorides with Organic Acids. Molecular Complexes of Fluoxetine Hydrochloride with Benzoic, Succinic, and Fumaric Acids. J Am Chem Soc 2004; 126: 13335–42.
49. McNamara DP, Childs SL, Giordano J, et al. Use of a Glutaric Acid Cocrystal to Improve Oral Bioavailability of a Low Solubility API. Pharma Res 2006; 23: 1888–97.
50. Hickey MB, Peterson ML, Scoppettuolo LA, et al. Performance comparison of a co-crystal of Carbamazepine with marketed product. Eur J Pharma Biopharma 2007; 67: 112–9.
51. Trask AV, Motherwell WDS, Jones W. Pharmaceutical Cocrystallization: Engineering a Remedy for Caffeine Hydration. Cryst Growth Des 2005; 5: 1013–21.

52. Trask AV. An overview of pharmaceutical cocrystals as intellectual property. Mol Pharma 2007; 4: 301–9.
53. Lindenberg M, Kopp S, Dressman JB. Classification of orally administered drugs on the World Health Organization model list of essential medicines according to the biopharmaceutics classification system. Eur J Pharm Biopharm 2004; 58: 265–78.
54. Lobenberg R, Amidon GL. Modern bioavailability, bioequivalence and biopharmaceutics classification system. New scientific approaches to international regulatory standards. Eur J Pharm Biopharm 2000; 50: 3–12.
55. Kanfer I. Report on the international workshop on the biopharmaceutics classification system (BCS): scientific and regulatory aspects in practice. Pharm J Pharmaceut Sci 2002; 5: 1–4.
56. Ling AR, Baker JK. Halogen derivatives of quinine. Part III. Derivatives of quinhydrone. J Chem Soc Trans 1893; 63: 1314–27.
57. Anderson JS. Structure of organic molecular compounds. Nature 1937; 140: 583–4.
58. Pekker S, Kovats E, Oszlanyi G, et al. Rotor-stator molecular crystals of fullerenes with cubane. Nat Mater 2005; 4: 764–7.
59. (a) Hoogsteen K. The structure of crystals containing a hydrogen-bonded complex of 1-methylthymine and 9-methyladenine. Acta Crystallogr 1959; 12: 822–3. (b) Hoogsteen K. Crystal and molecular structure of a halogen-bonded complex between 1-methylthymine and 9-methyladenine. Acta Crystallogr 1963; 16: 907–16.
60. O'Brien EJ. Crystal structures of two complexes containing guanine and cytosine derivatives. Acta Crystallogr 1967; 23: 92–106.
61. Sivakova S, Rowan SJ. Nucleobases as supramolecular motifs. Chem Soc Rev 2005; 34: 9–21.
62. French patent: von Heyden F, et al. 1934; 769, 586.
63. Eli lilly patent: Amos JG, Indelicato JM, Pasini CE, et al. Bicyclic beta-lactam/paraben complexes. US5412094 (A1), JP7048383 (A), FI943081 (A), BR9402561 (A) and EP0637587 (B1), 1995.
64. Viagra-Aspirin patent: Zegarac M, Mestrovic E, Dumbovic A, et al. Pharmaceutically acceptable cocrystalline forms of sildenafil. WO 2007/080362 A1, 2007.
65. Caira MR. Sulfa drugs as model cocrystal formers. Mol Pharm 2007; 4: 310–6.
66. Thayer AM. Form and function: the choice of pharmaceutical crystalline form can be used to optimize drug properties, and cocrystals are emerging as new alternatives. C & E News 2007; 85: 17–30.
67. (a) Huang CM, Leiserowitz L, Schmidt GMJ. Molecular packing modes. Part XI. Crystal structures of the 2:1 complexes of benzamide with succinic acid and furamide with oxalic acid. J Chem Soc Perkins Trans 2 1973; 5: 503–8. (b) Aakeröy CB, Beatty AM, Helfrich BA. A high-yielding supramolecular reaction. J Am Chem Soc 2002; 124: 14425–32. (c) Pedireddi VR, Chatterjee S, Ranganathan A, et al. A study of supramolecular hydrogen bonded complexes formed by aliphatic dicarboxylic acids with azaaromatic donors. Tetrahedron 1998; 54: 9457–74. (d) Nguyen TL, Fowler FW, Lauher JW. Commensurate and incommensurate hydrogen bonds. An exercise in crystal engineering. J Am Chem Soc 2001; 123: 11057–64. (e) Walsh RDB, Bradner MW, Fleischman SG, et al. Crystal engineering of the composition of pharmaceutical phases. Chem Commun 2003: 186–7. (f) Bis JA, Vishweshwar P, Weyna D, et al. Hierarchy of supramolecular synthons: persistent hydroxyl...pyridine hydrogen bonds in cocrystals that contain a cyano acceptor. Mol Pharm 2007; 4: 401–16. (g) McMahon JA, Bis JA, Vishweshwar P, et al. Crystal engineering of the composition of pharmaceutical phases. 3 1. Primary amide supramolecular heterosynthons and their role in the design of pharmaceutical co-crystals. Fur Kristallogr 2005; 220: 340–50.
68. (a) Sudhakar P, Srivijaya R, Sreekanth BR, et al. Carboxylic acid-pyridine supramolecular heterocatemer in a co-crystal. J Mol Struc 2008; 885: 45–9. (b) Bhogala BR, Nangia A. Ternary and quaternary co-crystals of 1,3-*cis*,5-*cis*-cyclohexanetricarboxylic acid and

4,4′-bipyridines. New J Chem 2008; 32: 800–7. (c) Broker GA, Tiekink ERT. Co-crystal formation between 2,2′-dithiodibenzoic acid and each of 4,4′-bipyridine, *trans*-1,2-bis (4-pyridyl)ethene and 1,2-bis(4-pyridyl)ethane. CrystEngComm 2007; 9: 1096–109.

69. (a) Aakeröy CB, Desper J, Fasulo ME. Improving success rate of hydrogen-bond driven synthesis of co-crystals. CrystEngComm 2006; 8: 586–8. (b) Edwards MR, Jones W, Motherwell WDS. Cocrystal formation of 4-methyl and 4-chlorobenzamide with carboxylic acids: chloro/methyl interchange and crystal structure. CrystEngComm 2006; 8: 545–51.
70. Hosseini MW. Self assembly and generation of complexity. Chem Commun 2005: 5825–9.
71. Lindsey JS. Self-assembly in synthetic routes to molecular devices. Biological principles and chemical perspectives: a review. New J Chem 1991; 15: 153–80.
72. Mann S. Molecular tectonics in biomineralization and biomimetic materials chemistry. Nature 1993; 365, 499–505.
73. Calama MC, Timmerman P, Reinhoudt DN. Guest-templated selection and amplication of a receptor by noncovalent combinatorial synthesis. Angew Chem Int Ed 2000; 39: 755–8.
74. (a) Shattock TR, Arora KK, Peddy V, et al. Hierarchy of supramolecular synthons: persistent carboxylic acid...pyridine hydrogen bonds in cocrystals that also contain a hydroxyl moiety. Cryst Growth Des 2008; 8: 4533–45. (b) Aakeröy CB, Fasulo M, Schultheiss N, et al. Structural competition between hydrogen bonds and halogen bonds. J Am Chem Soc 2007; 129: 13772–3.
75. (a) Sharma CVK, Zaworotko MJ. X-Ray crystal structure of $C_6H_3(CO_2H)_3$-1,3,5·1.5 (4,4'-bipya): 'super trimesic acid' chicken-wire grid. Chem Commun 1996: 2655–6. (b) Vishweshear P, Nangia A, Lynch VM. Molecular complexes of homologous alkanedicarboxylic acids with isonicotinamide: X-ray crystal structures, hydrogen bond synthons, and melting point alternation. Cryst Growth Des 2003; 3: 783–90. (c) Shan N, Batchelor E, Jones W. Co-crystal structures of 4,7-phenanthroline and carboxylic acids: synthon competition and prediction. Tetrahedron Lett 2002; 43: 8721–5. (d) Arora KK, Pedireddi VR. A rational study of crystal engineering of supramolecular assemblies of 1,2,4,5-benzenetetracarboxylic acid. J Org Chem 2003; 68: 9177–85.
76. (a) Leiserowitz L, Nader F. The molecular packing modes and the hydrogen-bonding properties of amide:carboxylic acid complexes. Acta Crystallogr 1977; B33: 2719–33. (b) Reddy LS, Nangia A, Lynch VM. Phenyl-perfluorophenyl synthon mediated cocrystallization of carboxylic acids and amides. Cryst Growth Des 2004; 4: 89–94.
77. (a) Biradha K, Zaworotko MJ. A supramolecular analogue of cyclohexane sustained by aromatic C−H...π interactions: complexes of 1,3,5-trihydroxybenzene with substituted pyridines. J Am Chem Soc 1998; 120: 6431–2. (b) Papaefstathiou GS, MacGillivray LR. Discrete versus infinite molecular self-assembly: control in crystalline hydrogen-bonded assemblies based on resorcinol. Org Lett 2001; 3: 3835–8. (c) Vishweshwar P, Nangia A, Lynch VM. Supramolecular synthons in phenol-isonicotinamide adducts. CrystEngComm 2003; 5: 164–8.
78. Anastas PT, Warner JC. Green Chemistry: Theory and Practice, Oxford University Press, 1998.
79. Cannon AS, Warner JC. Noncovalent derivatization: green chemistry applications of crystal engineering. Cryst Growth Des 2002; 2: 255–7.
80. Foxman BM, Guarrera DJ, Taylor LD, et al. Environmentally benign synthesis using crystal engineering: steric accommodation in non-covalent derivatives of hydroquinones. Crystal Engineering 1998; 1: 109–18.
81. Taylor LD, Warner JC. US 5338644 A 19940816 Cont. of U.S., 5, 177262, 1994.
82. Etter MC, Frankenbach GM, Bernstein J. Solid-state nucleophilic aromatic substitution reaction of a carboxylic acid cocrystal. Tetrahedron Lett 1989; 30: 3617–20.

83. Cheney ML, McManus GJ, Perman JA, et al. The role of cocrystals in solid-state synthesis: cocrystal-controlled solid-state synthesis of imides. Cryst Growth Des 2007; 7: 616–17.
84. (a) Pasteur L. Ann Chim Phys 1848; 24: 442. (b) Pasteur L. Ann Chim Phys 1853; 38: 437. (c) Wheeler KA, Grove RC, Davis RE, Kassel WS. Rediscovering Pasteur's quisiracemates. Angew Chem Int Ed 2008; 47: 78–81.
85. Wallach O. Justus Liebigs Ann Chem 1895; 286: 90–143.
86. Samas B, Wang W, Godrej DB. 1:1 Cocrystal of (*S*)-3-(ammoniomethyl)-5-methylhexanoate and (*S*)-mandelic acid Acta Crystallogr 2007; E63: o3938.
87. (a) Teng MY, Sun J, Ma CA, et al. (*S*)-2-Hydroxy-2-phenylacetic acid-(*R*)-2-aminobutanoic acid-water (1/1/0.5). Acta Crystallogr 2006; E62: o2454–o2456. (b) Fischer E, Mouneyrat A. Ber Chem Ges 1900; 33: 2383. (c) Fischer E, Schoeller WA. Ann Chem 1907; 357: 1.
88. (a) Hu ZQ, Xu DJ, Xu YZ, et al. (*R*)-Mandelic acid (*S*)-alanine hemihydrate. (b) (*S*)-Alanine-(*S*)-mandelic acid (1/1). Acta Crystallogr 2002; C58: o612–o614. (b) Hu ZQ, Xu DJ, Xu YZ. Acta Crystallogr 2004; E60: o269–o271.
89. Higuchi T, Roy K. Study of possible complex formation between macromolecules and certain pharmaceuticals. I. Polyvinylpyrrolidone with sulfathiazole, procaine hydrochloride, sodium salicylate, benzyl penicillin, chloramphenicol, mandelic acid, caffeine, theophylline, and cortisone. J Am Pharm Assoc 1954; 43: 393–7.
90. Higuchi T, Roy K. Study of possible complex formation between macromolecules and certain pharmaceuticals. II. Polyvinylpyrrolidone with p-aminobenzoic acid, aminopyrine, benzoic acid, salicylic acid, p-hydroxybenzoic acid, m-hydroxybenzoic acid, citric acid, and Phenobarbital. J Am Pharm Assoc 1954; 43: 398–401.
91. CBZ four polymorphs: (a) Reboul JP, Cristau B, Soyfer JC, et al. 5H-dibenz[b,f]azépine-carboxamide-5 (carbamazépine). Acta Crystallogr 1981; B37: 1844. (b) Lowes MMJ, Cairo MR, Lotter AP, et al. Physicochemical properties and x-ray structural studies of the trigonal polymorph of carbamazepine. J Pharm Sci 1987; 76: 744. (c) Grzesiak AL, Lang M, Kim K, et al. Comparison of the four anhydrous polymorphs of carbamazepine and the crystal structure of form I. J Pharm Sci 2003; 92: 2260. (d) Lang M, Kampf JW, Matzger AJ. Form IV of carbamazepine. J Pharm Sci 2002; 91: 1186.
92. CBZ dihydrate: Gelbrich T, Hursthouse MB. Systematic investigation of the relationships between 25 crystal structures containing the carbamazepine molecule or a close analogue: a case study of the XPac method. CrystEngComm 2006; 8: 449.
93. CBZ solvates: (a) Chang CH, Yang DSC, Yoo CS, et al. The crystal structures of (*S*) and (*R*) baclofen and carbamazepine. Acta Crystallogr 1981; A37: c71. (b) Johnston A, Florence AJ, Kennedy AR. Carbamazepine furfural hemisolvate. Acta Crystallogr 2005; E61: o1777. (c) Johnston A, Florence AJ, Kennedy AR. Carbamazepine *N,N*-dimethylformamide solvate. Acta Crystallogr 2005; E61: o1509. (d) Lohani S, Zhang Y, Chyall LJ, et al. Carbamazepine-2,2,2-trifluoroethanol (1/1). Acta Crystallogr 2005; E61: o1310–o1312. (e) Fernandes P, Bardin J, Johnston A, et al. Carbamazepine trifluoroacetic acid solvate. (f) Solvent inclusion in the structural voids of form II carbamazepine: single-crystal X-ray diffraction, NMR spectroscopy and Hirshfeld surface analysis. Acta Crystallogr 2007; E63: o4269. (f) Fabbiani FPA, Byrne LT, McKinnon JJ, et al. CrystEngComm 2007; 9: 728. (g) Johnston A, Johnston BF, Kennedy AR, et al. Targeted crystallization of novel carbamazepine solvates based on a retrospective Random Forest classification. CrystEngComm 2008; 10: 23.
94. Ammonium salts: Reck G, Thiel W. Pharmazie 1991; 46: 509.
95. A solid solution with dihydrocarbamazepine: Florence AJ, Leech CK, Shankland N, et al. Control and prediction of packing motifs: a rare occurrence of carbamazepine in a catemeric configuration. CrystEngComm 2006; 8: 746.
96. Co-crystals (hydrates/solvates and polymorphs): (a) Fleischman SG, Kuduva SS, McMahon JA, et al. Crystal engineering of the composition of pharmaceutical phases:

multiple-component crystalline solids involving carbamazepine. Cryst Growth Des 2003; 9: 909. (b) Vishweshwar P, McMahon JA, Oliveira M, et al. The predictably elusive form II of aspirin. J Am Chem Soc 2005; 127: 16802. (c) Babu NJ, Reddy LS, Nangia A. Amide N-oxide heterosynthon and amide dimer homosynthon in cocrystals of carboxamide drugs and pyridine N-oxides. Mol Pharm 2007; 4: 417. (d) Porter III WW, Elie SC, Matzger AJ. Polymorphism in carbamazepine cocrystals. Cryst Growth Des 2008; 8: 14.

97. Hilfiker R, Berghausen J, Blatter F, et al. Polymorphism – integrated approach from high-throughput screening to crystallization optimization. J Ther Ana Calor 2003; 73: 429–40.
98. Seefeldt K, Miller J, Alvarez N, Rodriguez-Hornedo N. Crystallization pathways and kinetics of carbamazepine-nicotinamide cocrystals from the amorphous state by in situ thermomicroscopy, spectroscopy and calorimetry studies. J Pharma Sci 2007; 96: 1147–58.
99. Nehm SJ, Rodriguez-Spong B, Rodriguez-Hornedo N. Phase solubility diagrams of cocrystals are explained by solubility product and solution complexation. Cryst Growth Des 2006; 6: 592–600.
100. ter Horst JH, Cains PW. Co-crystal polymorphs from a solvent-mediated transformation. Cryst Growth Des 2008; 8: 2537–42.
101. (a) Peeteers J, Neeskens P, Tollenaere JP, et al. Characterization of the interaction of 2-hydroxypropyl-β-cyclodextrin with itraconazole at pH 2, 4, and 7. J Pharm Sci 2002; 91: 1414–22. (b) Francois M, Snoeckx E, Putteman P, et al. A mucoadhesive, cyclodextrin-based vaginal cream formulation of itraconazole. AAPS Pharma Sci 2003; 5: 1–5.
102. (a) Bak A, Gore A, Yanez E, et al. The co-crystal approach to improve the exposure of a water-insoluble compound: AMG 517 sorbic acid co-crystal characterization and pharmacokinetics. J Pharm Sci 2008; 97: 3942–56. (b) Stanton MK, Bak A. Physicochemical properties of pharmaceutical co-crystals: a case study of ten AMG 517 co-crystals. Cryst Growth Des 2008; 8: 3856–62.
103. (a) Puschner B, Poppenga RH, Lowenstine LJ, et al. Assessment of melamine and cyanuric acid toxicity in rats. J Vet Diagn Invest 2007; 19: 616–24. (b) Ranganathan A, Pedireddi VR, Rao CNR. Hydrothermal synthesis of organic channel structures: 1:1 hydrogen bonded adducts of melamine and cyanuric and trithiocyanuric acids. J Am Chem Soc 1999; 121: 1752–3.
104. Dunitz JD, Bernstein J. Disappearing polymorphs. Acc Chem Res 1995; 28: 193–200.
105. Davey RJ. Pizzas, polymorphs and pills. Chem Commun 2003: 1463–7.
106. Morrow SI. One hundred and fifty years of isomorphism. J Chem Edu 1969; 46: 580–4.
107. Wöhler F, Liebig J. Untersuchungen über das Radikal der Benzoesäure. Annal Pharm 1832; 3: 249–82.
108. Siegrist T, Kloc C, Schön JH, et al. Enhanced physical properties in a pentacene polymorph. Angew Chem Int Ed 2001; 40: 1732–6.
109. McCrone WC. Polymorphism in Physics and Chemistry of the Organic Solid State, Vol. II. In: Fox D, Labes MM, Weissberger A, eds. New York: Interscience, 1965: 725–67.
110. Caira MR. Crystalline polymorphism of organic compounds. Top Curr Chem 1998; 198: 163–208.
111. Ostwald W, Physikal Z. Studies on the formation and transformation of solid compounds: report I. Supersaturation and practicing cooling. Chem 1897; 22: 289.
112. (a) Boman CE, Herbertsson H, Oskarsson A. The crystal and molecular structure of a monoclinic phase of iminodiacetic acid. Acta Crystallogr 1974; B30: 378–82. (b) Bernstein J. Conformational polymorphism. III. The crystal and molecular structures of form II and form III of iminodiacetic acid. Acta Crystallogr 1979; B35: 360–6. (c) Graeber EJ, Morosin B. The crystal structures of 2,2', 4,4', 6,6'-hexanitroazobenzene (HNAB), forms I and II. Acta Crystallogr 1974; B30: 310–7.

113. David WIF, Shankland K, Pulham CR, et al. Polymorphism in benzamide. Angew Chem Int Ed 2005; 44: 7032–5.
114. Kalman A, Fabian L, Argay G, et al. Dipole-induced polymorphs of *trans*-2-hydroxycycloheptanecarboxylic acid with virtually the same unit cell. J Am Chem Soc 2003; 125: 34–5.
115. Matthews JH, Paul IC, Curtin DY. Configurational isomerism in crystalline forms of benzophenone anils. J Chem Soc Perkin Trans 1991; 2: 113–8.
116. Bis JA, Vishweshwar P, Middleton RA, et al. Concomitant and conformational polymorphism, conformational isomorphism, and phase relationships in 4-cyanopyridine + 4,4'-biphenol cocrystals. Cryst Growth Des 2006; 6: 1048–53.
117. Matsuda H, Osaki K, Nitta I. Crystal structure of quinhydrone, $C_{12}H_{10}O_4$. Bull Chem Soc Jpn 1958; 31: 611–20.
118. Sakurai T. On the refinement of the crystal structures of phenoquinone and monoclinic quinhydrone. Acta Crystallogr 1968; B24: 403–12.
119. Sakurai T. The crystal structure of the triclinic modification of quinhydrone. Acta Crystallogr 1965; B19: 320–30.
120. Schmidtmann M, Gutmann MJ, Middlemiss DS, et al. Towards proton transfer in hydrogen bonded molecular complexes: joint experimental and theoretical modeling and an energy scale for polymorphism. CrystEngComm 2007; 9: 743–5.
121. Rafilovich M, Bernstein J. Serendipity and four polymorphic structures of Benzidine, $C_{12}H_{12}N_2$. J Am Chem Soc 2006; 128: 12185–91.

9 Thermoanalytical and Crystallographic Methods

Sisir Bhattacharya*

Department of Pharmaceutics, University of Minnesota, Minneapolis, Minnesota, U.S.A.

Harry G. Brittain

Center for Pharmaceutical Physics, Milford, New Jersey, U.S.A.

Raj Suryanarayanan

Department of Pharmaceutics, University of Minnesota, Minneapolis, Minnesota, U.S.A.

INTRODUCTION

The different physical forms of a compound can exhibit pronounced differences in physicochemical properties. The term "physical form" encompasses polymorphs, solvates (also referred to as solvatomorphs), the non-crystalline (amorphous) form, and partially crystalline forms. Although numerous analytical techniques are available to characterize the physical forms of pharmaceutical compounds, this chapter will focus on thermal and crystallographic characterization techniques. While discussing the analytical techniques and their applications, we will use the term "polymorphism" in its broadest sense, with the understanding that with appropriate modifications, the techniques can often be extended for the characterization of the other physical forms of pharmaceuticals. Although crystallography (through crystal structure) provides the most definitive evidence of polymorphism, thermoanalytical, spectroscopic, and microscopic techniques are often used in a complementary fashion for the characterization of polymorphs.

Comprehensive and in-depth discussions of different thermoanalytical techniques can be found in the literature (1,2), and this chapter will specifically discuss the applications of thermoanalytical and crystallographic techniques in the characterization of pharmaceuticals. The specific thermoanalytical techniques to be discussed are differential scanning calorimetry (DSC), thermogravimetric analysis (TGA), and hot-stage microscopy (HSM). Several recent reviews and book chapters have covered this topic, and the examples presented are designed to complement the information in the literature (1–4). In the second part of the chapter, applications of X-ray powder diffractometry (XRD) (5,6) are provided. Finally, applications of variable-temperature XRD (VT-XRD) are discussed, specifically to monitor phase transitions as a function of temperature.

THERMOANALYTICAL TECHNIQUES

Thermal analysis methods can be conveniently defined as those techniques in which some property of the analyte is measured as a function of an externally applied temperature. In most applications, one effects a linear increase in the temperature of the sample while the property of interest is recorded on a continuous basis. Thermoanalytical methods are used to monitor endothermic processes (i.e., melting, boiling,

**Current affiliation*: Forest Laboratories, Inc., Commack, New York, U.S.A.

sublimation, vaporization, desolvation, solid–solid phase transitions, and chemical degradation) as well as exothermic processes (i.e., crystallization and oxidative decomposition). Thermal methods are routinely used for the characterization of polymorphs, and in light of the experimental simplicity, often constitute the first line of techniques used to understand the polymorphic space of a system.

Differential Scanning Calorimetry (DSC)

In DSC, which is the most widely used technique for thermal characterization of pharmaceuticals, the analyte is subjected to a controlled temperature program and the temperature and the heat flow associated with a thermally induced transition is measured.

DSC has been developed along two lines: power-compensation DSC and heat-flux DSC. In power-compensation DSC, separate heating elements are in contact with the sample and reference cells, with the rate of heating by these elements being controlled and measured. Thus the sample and reference are maintained at the same temperature and the heat flow required to accomplish this is measured. The other methodology is that of heat-flux DSC, where the sample and reference cells are heated by the same element, and one monitors the direction and magnitude of the heat being transferred between the two.

A detailed theory of DSC is outside the scope of this chapter and has been discussed elsewhere (1,2). Briefly, the basic principle behind a change in the baseline of a typical DSC plot (power vs. temperature), signifying a thermal event, is a change in the heat capacity of the system under investigation. The basic equation (4) describing the relationship between the heat flux (Q) associated with a thermal event and the heat capacity (C_p) of the system under investigation is given by:

$$(\mathrm{d}Q/\mathrm{d}t) = C_p(\mathrm{d}T/\mathrm{d}t) \tag{1}$$

where $\mathrm{d}Q/\mathrm{d}t$ represents power at the constant heating or cooling rate, $\mathrm{d}T/\mathrm{d}t$. DSC plots are obtained as the differential rate of heating [in units of watts (joules/second) or calories/second] against temperature, and thus represent direct measures of the heat capacity of the sample. The area under a DSC peak is directly proportional to the heat absorbed or evolved by the thermal event, and integration of these peak areas yields the heat of reaction (in units of calories/seconds · gram or joules/seconds · gram).

The effectiveness of DSC to detect various polymorphic forms is illustrated in Figure 1 (7). Profiles 1, 2, and 3 (*from top*) show the reversible transitions between the enantiotropically related forms I and III. The fourth DSC curve shows the melting of form II followed by crystallization and melting of form I. The bottom DSC profile is a heating curve of a mixture of forms II and III, which shows the respective melting endotherms but no transition to form I. This was tentatively attributed to the absence of form I seeds in the mixture of forms II and III, which were concomitantly crystallized as opposed to the pure forms (profiles 1–4), which were crystallized separately using different methods.

Standard Reference Materials (SRMs) are available from the National Institute of Standards and Technology for calibration of temperature and enthalpy of fusion for differential scanning calorimeters. Indium (SRM 2232; melting temperature = 156.6°C; enthalpy of fusion = 28.5 J/g), tin (SRM 2220; melting point = 232.0°C; enthalpy of fusion = 60.2 J/g), and gallium (SRM 2234; melting temperature = 29.8°C;

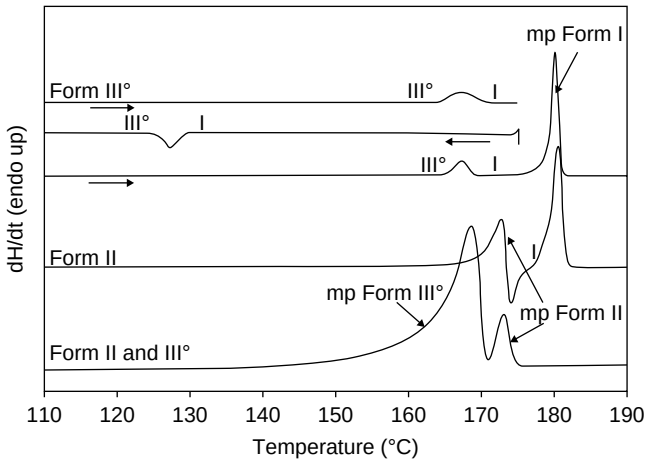

FIGURE 1 DSC profiles of cinacalcet hydrochloride polymorphs. The first (heating), second (cooling), and third (heating) profiles (*from top*) show the solid–solid transition (i.e., III° → I); the fourth profile shows melting of form II followed by crystallization and melting of form I; the fifth profile is a heating curve of a mixture of form II and form III° showing respective melting endotherms but no transition to form I signifying absence of form I seeds. *Note*: The direction of endotherm is *up*. *Source*: From Ref. (7).

enthalpy of fusion = 80.1 J/g) are suitable as calibration standards over the range of temperatures of interest in pharmaceutical analyses. Because DSC is also used at sub-ambient temperatures for the characterization of frozen solutions, mercury (SRM 2225; melting temperature = –38.9°C; enthalpy of fusion = 11.5 J/g) is a suitable calibration standard. Heat capacity calibration in a DSC is usually carried out with synthetic sapphire (SRM 720), copper (SRM RM5), polystyrene (SRM 705a), or molybdenum (SRM 781D2).

Depending on the protocol used for temperature programming, a DSC experiment could be classified as being conventional, modulated, or accelerated (also known as Hyper-DSC®). In the conventional mode, the heating rate is constant and typically ranges from 0.1°C/min to 20°C/min. The majority of DSC experiments are carried out in the conventional mode and may require optimization of the sample pan configuration (discussed later) and the experimental parameters to obtain the desired information (3). In Table 1, the effects of operational parameters are outlined.

In modulated DSC (MDSC), a changing (modulated) heating rate is superimposed on a constant average heating rate. The modulation is described by a frequency, determined by specific amplitude (±°C) and period (seconds), such as ±0.5°C every 60 seconds, with the choice of the amplitude and period being dictated by the nature of the transition (8–10). The advantage of MDSC over conventional DSC is that it can separate the reversible heat flow from the non-reversible heat flow (Fig. 2). Reversible heat flow corresponds to events that respond to the changing heating rate (e.g., heat capacity change, melting). On the other hand, non-reversible heat flow events (e.g., crystallization or decomposition) are not affected by changing heating rates.

TABLE 1 Influence of Operational Parameters on the Outcome of DSC Experimental Results

	Effects
Sample size	
Large	Advantages
	(i) Non-homogeneous samples
	(ii) Detects "weak" transitions
	Disadvantages
	(i) Broad peaks
	(ii) Temperature of the event may be inaccurate
	(iii) Poor resolution
	(iv) Requires slow heating rate
Small	Advantages
	(i) Sharp peaks
	(ii) Increased resolution
	(iii) Permits faster heating rate
	Disadvantages
	(i) Decreased sensitivity
Heating rate	
Fast	Advantages
	(i) Increased sensitivity
	Disadvantages
	(i) Decreased resolution
	(ii) Decreased temperature accuracy
Slow	Advantages
	(i) Increased resolution
	Disadvantages
	(i) Decreased sensitivity

Source: Adapted from Ref. (2).

MDSC has found limited utility in the characterization of polymorphs (11,12). However, the inherent capability of this technique to separate overlapping melting and crystallization events has been demonstrated for the polymorphs of tristearin (13,14). MDSC is especially suited for the characterization of amorphous materials (15,16), and has enabled the quantification of amorphous content in a partially crystalline material (17). Because crystallinity differences could affect material performance, it is important that analysts are aware of low levels of lattice disorder in highly crystalline materials that were brought about by processing and storage conditions. Saklatvala et al. investigated two batches of an investigational crystalline drug, which showed pronounced differences in their stability and water sorption profiles, and MDSC enabled detection and quantification of the amorphous content in the batch characterized by the lower chemical stability and the increased propensity to take up water (18).

Hyper-DSC® uses accelerated heating rates (up to 500°C/min) in order to selectively investigate phase transitions. The high heating rates result in selective inhibition of transitions that would normally take place over the longer timescales

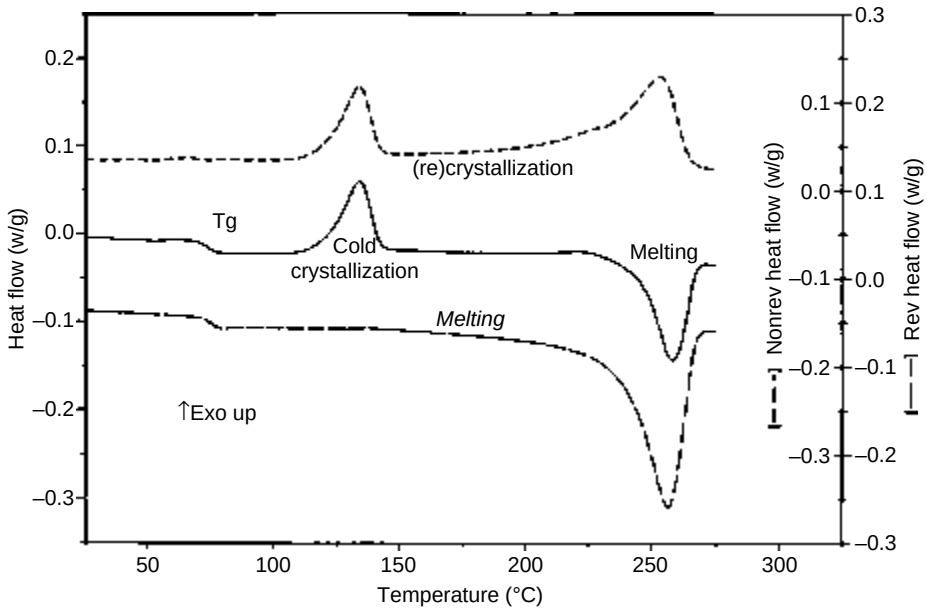

FIGURE 2 Modulated DSC profiles of quenched polyethylene terephthalate, showing the non-reversible (*uppermost trace*), total (*middle trace*), and reversible (*lowest trace*) heat flow curves. The exothermic recrystallization event is hardly discernible in the total heat flow but is prominent in the non-reversible heat flow. *Source*: From Ref. (66).

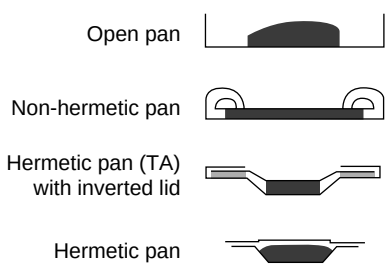

FIGURE 3 Diagrammatic representation of different DSC pan configurations. *Source*: From Ref. (9).

of conventional heating rates. A case in point are the polymorphs of carbamazepine, where a heating rate of 250°C/min was used to prevent simultaneous crystallization of form I during the melting of form III, thereby allowing determination of the enthalpy of fusion of form III (19).

In a typical DSC application, the sample is encapsulated in a pan and the lid is crimped, where the lid can be crimped either in a non-hermetic or in a hermetic manner (Fig. 3). In the hermetically crimped pan, a pinhole can be made in the lid to relieve pressure during the acquisition of the DSC curve. To minimize the head space, the lid can be inverted and then hermetically crimped.

The pan configuration can influence the outcome of a DSC experiment. This is especially true for solvates, because the desolvation kinetics, as well as the physical form of the product phase, can be profoundly influenced by the sample environment. In an open pan, there is no physical barrier to the escape of liberated solvent, and the purge gas (typically nitrogen) will facilitate removal of the liberated solvent. The reasonably unrestricted nature of a non-hermetically crimped pan will also permit ready escape of the liberated solvent. At the other extreme, the liberated solvent cannot escape in a hermetically crimped pan. In a sealed pan with a pinhole, the rate of vapor loss will become appreciable only when the vapor pressure exceeds atmospheric pressure. Different pan configurations, which result in varied desolvation conditions, have been used to generate different polymorphs of anhydrous carbamazepine and trehalose from their respective hydrates (20,21).

Pressure DSC (PDSC) enables DSC experiments to be carried out at elevated pressures as high as 1000 psi. PDSC is useful for the separation of overlapping dehydration and vaporization events that are observed following the dehydration of hydrates. Although the temperature of dehydration is likely to be unaffected by pressure, the boiling temperature of water is pressure dependent and can be ascertained from the Clausius–Clapeyron equation. In addition, the potential interaction of the liberated water with the anhydrous product phase can also be ascertained. Han and Suryanarayanan (22) used PDSC to successfully resolve overlapping dehydration and vaporization transitions observed when carbamazepine dihydrate was heated (Fig. 4, *upper left panel*). The conventional DSC of carbamazepine exhibited two overlapping endotherms over the temperature range of 85°C to 100°C, attributed to dehydration followed by vaporization, which were followed by the melting of non-solvated carbamazepine around 189°C. When the pressure was increased, only a single endotherm attributable to dehydration was observed at approximately 90°C. Interestingly, several thermal events were observed between the dehydration and the melting temperatures.

A limitation of DSC is that although it reveals the existence of thermally induced transitions, the nature of these transitions can be difficult to determine. In an effort to simulate the PDSC experiments, Han and Suryanarayanan (22) heated carbamazepine dihydrate in a "sealed" environment. Following dehydration, the released water caused an increase in pressure by being retained in the holder, although the pressure was uncontrolled. As shown in the *upper right panel* of Figure 4, the carbamazepine polymorphic transitions were further characterized by VT-XRD. The formation of β-carbamazepine at ~90°C was evident in the diffraction patterns on the basis of peaks observed at scattering angles of 13.1, 15.3, and 18.7° 2θ). Based on the disappearance of the characteristic peaks of carbamazepine dihydrate (at 8.9 and 12.3° 2θ), dehydration appeared to be complete by 100°C. Around 160°C, several characteristic peaks of γ-carbamazepine were observed, indicating a $\beta \rightarrow \gamma$ solid–solid phase transition. Based on the decrease in the intensities of the β-carbamazepine peaks, and the increase in the intensities of the γ-carbamazepine peaks, the $\beta \rightarrow \gamma$ phase transition was accelerated as the temperature was increased to 180°C. These VT-XRD results aided in the interpretation of the DSC results. When DSC was conducted under elevated pressure, usually four endotherms were observed. The first endotherm at ~90°C, as explained earlier, is attributed to dehydration. The two overlapping endotherms at ~120°C and 125°C are attributed to the $\beta \rightarrow \gamma$ carbamazepine phase transition and to the vaporization of water. The melting of γ-carbamazepine occurred at ~189°C. This scheme is

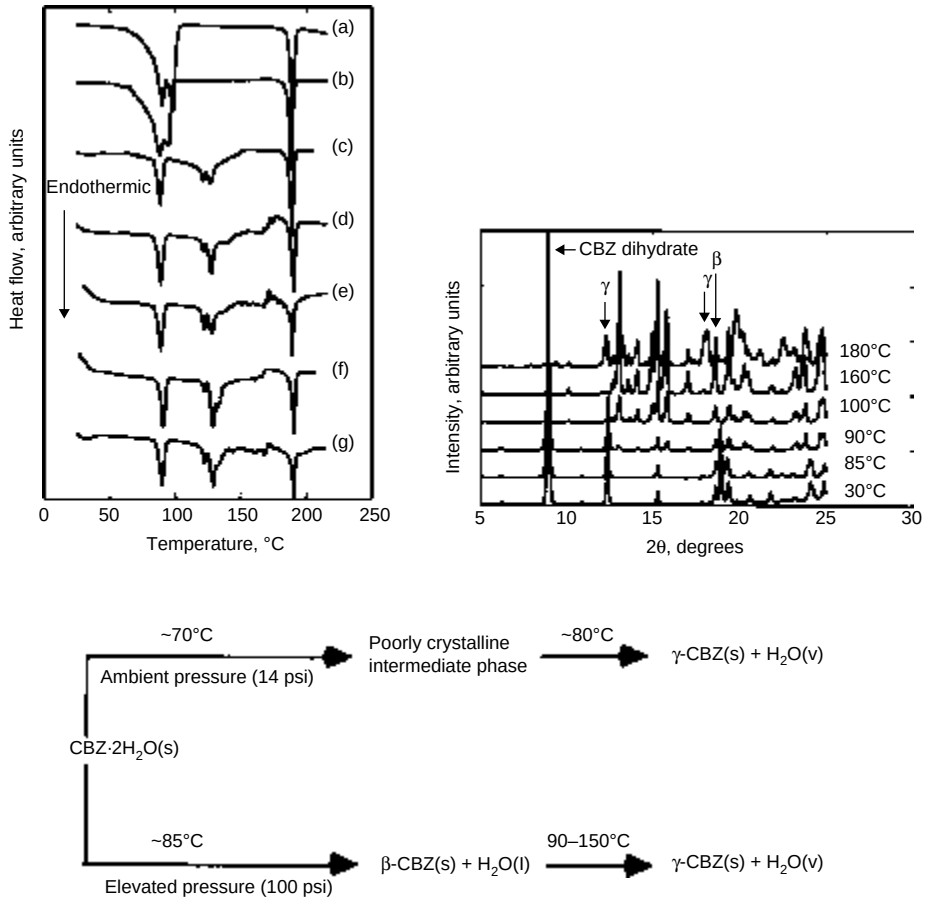

FIGURE 4 (*Upper left panel*) DSC of carbamazepine dihydrate at different pressures: (a) ambient pressure in conventional DSC cell, (b) ambient pressure in PDSC cell, (c) 100 psi, (d) 200 psi, (e) 300 psi, (f) 400 psi, (g) 600 psi. (*Upper right panel*) VT-XRD of carbamazepine dihydrate. Peaks characteristic of the dihydrate as well as anhydrous β and γ forms are shown. (*Lower panel*) Schematic showing carbamazepine dihydrate transitions under ambient and elevated pressures. *Source*: From Ref. (22).

illustrated in Figure 4 (*lower panel*) and shows the transitions of carbamazepine dihydrate at ambient and elevated pressures.

An emerging technique that could be considered as a variant of DSC is microthermal analysis, which combines the principles of DSC and scanning probe microscopy. Microthermal analysis was used to identify local regions of different polymorph content in a 50:50 mixture of two cimetidine polymorphs (23). This technique also has the potential to map a tablet surface for polymorph content uniformity.

Thermogravimetry

Thermogravimetry (TG, and also known as thermogravimetric analysis or TGA) is a technique where one uses a very sensitive balance to continuously determine the

weight of the analyte as a function of temperature or time. This simple technique provides valuable information that can aid in the identification and characterization of the thermal events associated with thermally induced reactions of solvates. For example, several hydrates of nedocromil sodium were identified and profiled using TG as one of the characterization tools (24). As the sample was heated, the weight loss occurred in a stepwise fashion, which facilitated calculation of the hydrate stoichiometries based on the percent weight loss at each step.

As discussed elsewhere in this book, there are different ways in which water can associate with solids. In authentic hydrates, water is incorporated in the crystal lattice, whereas in amorphous and partially crystalline materials, water can associate with disordered regions in the lattice. Water can also be adsorbed and also exist as "bulk water" in incompletely dried solids. TG analysis can also be used to distinguish between some of these states of water in solids. Compared with dehydration, desorption (adsorbed as well as bulk) typically occurs at lower temperatures, although these two processes can overlap. As shown in Figure 5, for carbamazepine dihydrate, when the TG experiment is carried out under isothermal conditions, there can be sequential loss of sorbed and lattice water (25).

TG analysis performed under isothermal conditions can be used to study the kinetics of phase transitions in solvatomorphs (26,27). Alkhamis et al. (26) carried out model-independent isoconversional analysis of the isothermal desolvation of the monohydrate and ethyl acetate solvate of fluconazole. One potential shortcoming of this technique is that a separate and direct technique might be required to confirm the cause of weight loss. In order to address this inadequacy, the TG instrument can be interfaced with additional instrumentation capable of identifying the vapor released upon heating. For example, TG has been used in combination with infrared absorption spectroscopy to understand the thermal behavior of a hydrate (28). In this study, two different thermal events resulting in weight loss were shown to be due to separate dehydration and decomposition processes.

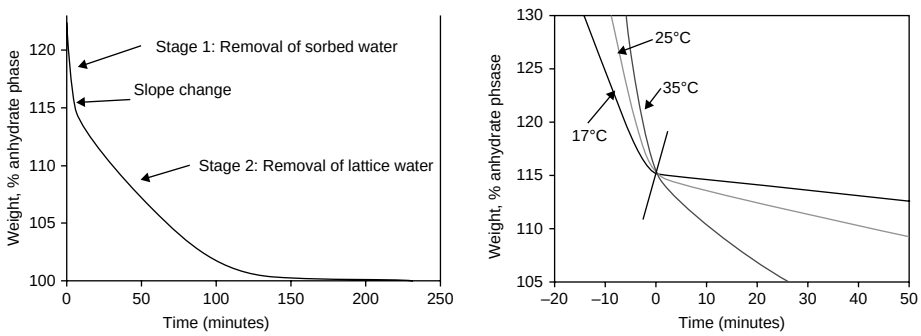

FIGURE 5 (*Left panel*) Dehydration of a wet sample of carbamazepine dihydrate at 0% RH (25°C). The plotted sample weight is based on the dry sample weight after complete dehydration. The first and second stages of dehydration are separated by the point of slope change. (*Right panel*) Effect of temperature on desorption and dehydration kinetics of carbamazepine dihydrate shown at three representative temperatures. For the purpose of comparison, the *x*-axis origin is the time point of transition from desorption to dehydration (point of slope change in left panel). *Source*: From Ref. (25).

Temperature calibration of TG instrumentation can be accomplished using melting point standards or the Curie point transition of a paramagnetic material (ASTM E1582) (29). Although not considered a "reference standard," calcium oxalate monohydrate is frequently used to validate the performance of a TG system (30).

Hot-Stage Microscopy

Visualization of solids using a microscope often provides unique insights not afforded by other techniques. The visual observation of the analyte, placed on a temperature controlled stage ("hot stage") of a microscope, forms the basis of HSM. For the characterization of polymorphs and solvates, HSM, with DSC and TG analyses, forms an optimal routine three-pronged approach. Vitez et al. (31) have briefly outlined the historical evolution of HSM from being merely a melting point determination tool to being an integral part of polymorph characterization. The practice and application of HSM has been reviewed and discussed in recent publications (3,32).

One of the primary advantages of HSM is the small amount of sample needed, which, given the limited availability of an active pharmaceutical ingredient (API) in the discovery phase, often represents a very important consideration. When characterizing solvates, the analyte is typically dispersed in silicone oil in order to aid in the visualization of the thermally induced release of any included solvent. As shown in Figure 6, a desolvation process is usually manifested by loss of transparency (perceived as a darkening of the crystals) (33), and in the formation of bubbles (specifically for hydrates) in the oil (34,35). Caution should be exercised in data interpretation because this observation could be potentially complicated by the release of entrapped air from the solids or by the simple presence of air bubbles in the dispersion medium. In addition, crystals may also darken as a result of decomposition.

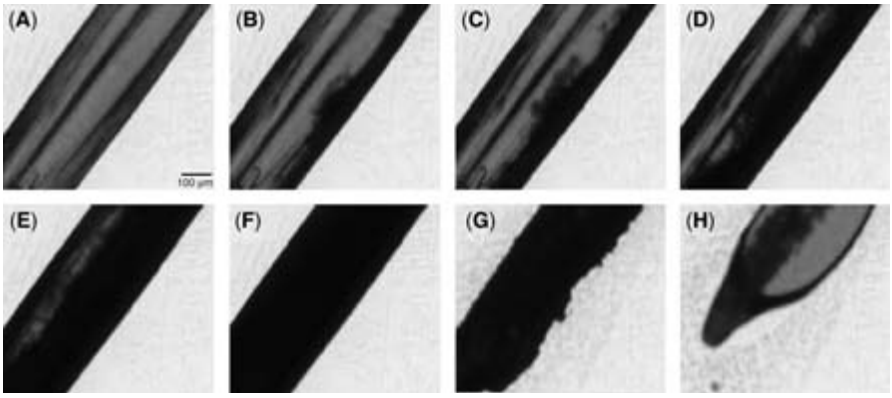

FIGURE 6 Hot-stage photomicrographs of toluene solvate of picryltoluidene, taken at various temperature values: (**A**) 25°C; (**B**) 35°C, onset of desolvation from crystal edges; (**C**) 45°C; (**D**) 55°C; (**E**) 65°C; (**F**) 80°C, completely desolvated anhydrous form; (**G**) 162.5°C, melting onset of the anhydrous form; (**H**) 163°C, remaining crystal of the anhydrous form in the melt. *Source*: From Ref. (33).

In some instances, desolvation may be accompanied by a change in crystal habit. For example, Tonder et al. used HSM to study the desolvation of different niclosamide solvates (36). Although the solvate crystals were characterized by different morphologies, desolvation resulted in the appearance of crystals having the same habit as that of the anhydrate form. In addition, the desolvated crystals were all observed to melt over the same temperature range as did the anhydrate, which was taken as confirming their transformation to the anhydrate phase.

Crystallization from the amorphous state can be demonstrated by the appearance of birefringence. In order to explain DSC observations, Bottom monitored the crystallization of a metastable spherulitic polymorph of sulfapyridine from the amorphous state through a solid-state phase transition to the stable needle-shaped form (12). Grooff et al. (37) used HSM as one of the tools to characterize crystallization of a metastable polymorph of nifedipine from the amorphous state. In this work, two other polymorphs were identified, and an enantiotropic relationship between two of the polymorphs was confirmed by direct observation of a reversible solid-state transition between the two crystal forms.

Microscope stage attachments are commercially available having a wide temperature range (less than –150°C to higher than 350°C) and excellent temperature stability (±0.1°C). In addition, most modern hot-stage systems are equipped with a high-resolution camera capable of rapid image collection, and which is controlled by a computer interface. All these accessories have drastically reduced the subjectivity associated with microscopy and have increased the efficiency of data collection. Consequently, HSM has evolved into one of the primary techniques that is used for the routine identification and characterization of pharmaceutical solids.

CRYSTALLOGRAPHIC CHARACTERIZATION TECHNIQUES

The technique of XRD is exceedingly important in the study of polymorphs and solvatomorphs because it represents the primary method whereby one can obtain fundamental information about the structure of a crystalline substance. The methodology is highly suited for the differentiation of crystal forms, as it would be only by pure coincidence that two compounds might form crystals having identical XRD patterns due to identical three-dimensional spacing of planes in all directions. One example of accidental isostructure is the trihydrate phases of ampicillin and amoxicillin (38), but such instances are uncommon. Typical applications of XRD methodology include the determination of crystal structures, evaluation of polymorphism and solvate structures, evaluation of degrees of crystallinity, and the study of phase transitions.

Every crystal consists of exceedingly small fundamental structural units, which are repeated indefinitely in all directions. In 1830, Hessel conducted a purely mathematical investigation of the possible types of symmetry for a solid figure bounded by planar faces, and deduced that only 32 symmetry groups were possible for such objects. The same conclusion was reached by Bravais in 1949, and Gadolin in 1867. These 32 crystallographic point groups are grouped into six crystal systems, denoted as triclinic, monoclinic, orthorhombic, tetragonal, trigonal, hexagonal, and cubic. Each crystal system is characterized by unique relationships existing among the crystal axes and the angles between these, and this information is summarized in Table 2.

TABLE 2 Characteristics of the Six Crystal Systems

System	Description
Cubic	Three axes of identical length (identified as a_1, a_2, and a_3) intersect at right angles.
Hexagonal	Four axes (three of which are identical in length, and denoted as a_1, a_2, and a_3) lie in a horizontal plane, and are inclined to one another at 120°. The fourth axis, *c*, is different in length from the others, and is perpendicular to the plane formed by the other three.
Tetragonal	Three axes (two of which are denoted as a_1 and a_2, and are identical in length) intersect at right angles. The third axis, *c*, is different in length with respect to a_1 and a_2.
Orthorhombic	Three axes of different lengths (denoted as *a*, *b*, and *c*) intersect at right angles. The choice of the vertical *c* axis is arbitrary.
Monoclinic	Three axes (denoted as *a*, *b*, and *c*) of unequal length intersect such that *a* and *c* lie at an oblique angle, and the *b* axis is perpendicular to the plane formed by the other two.
Triclinic	Three axes (denoted as *a*, *b*, and *c*) of unequal length intersect at three oblique angles.

Bragg (39) explained the diffraction of X rays by crystals using a model where the atoms of a crystal are regularly arranged in space, and that they can be regarded as lying in parallel sheets separated by a definite and defined distance. Then he showed that scattering centers arranged in a plane act like a mirror to X rays incident on them, so that constructive interference would occur in the direction of specular reflection. Within a given family of planes, defined by a Miller index of (*hkl*) and with an inter-planar distance *d*, each plane produces a specular reflectance of the incident beam. If the incident X rays are monochromatic (having wavelength equal to λ), then for an arbitrary glancing angle of θ, the reflections from successive planes are out of phase with one another. This yields destructive interference in the scattered beams. However, through the systematic variation of analysis angles, a set of values for θ can be found so that the path difference between X rays reflected by successive planes will be an integral number (*n*) of wavelengths, and then constructive interference would occur. One ultimately obtains the expression known as Bragg's law that explains the phenomenon:

$$2d\sin\theta = n\lambda \tag{2}$$

Unlike the diffraction of light by a ruled grating, the diffraction of X rays by a crystalline solid leads to constructive interference (i.e., reflection) only at critical Bragg angles. When reflection does occur, it is stated that the plane in question is reflecting in the *n*th order, or that one observes *n*th order diffraction for that particular crystal plane. Therefore, one will observe an X-ray scattering response for every plane defined by a unique Miller index of (*hkl*).

Single-Crystal X-Ray Diffractometry

Single-crystal XRD involves an assignment of the arrangement of atoms based on an electron density map generated by diffraction of a pure, regular, and adequately large crystal (40). Structural information derived from an XRD study of a single

crystal is the most fundamental description of a polymorph or solvatomorph, and helps to explain its physical properties.

Generally, polymorphic structures can be classified into one of two main categories. The first is associated with molecules that can only exist as a rigid grouping of atoms that can be stacked in different motifs to occupy the points of different lattices (i.e., packing polymorphism). One of the best-known instances of packing polymorphism is the allotropic system of carbon, namely graphite and diamond. As shown in Figure 7, in diamonds each carbon atom is tetrahedrally surrounded by four equidistant neighbors, and the tetrahedra are arranged to give a cubic unit cell. Graphite is composed of planar hexagonal nets of carbon atoms, which can be arranged to yield either a hexagonal unit cell (the α-form) or a rhombohedral unit cell (the β-form).

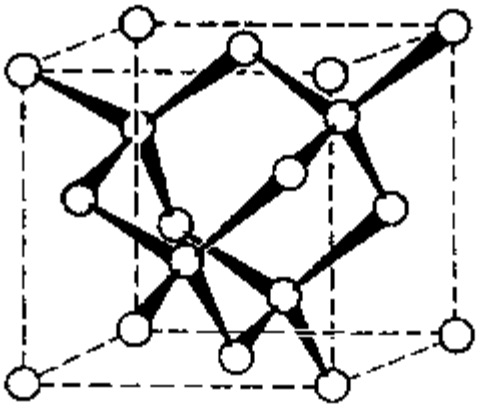

(**1**)

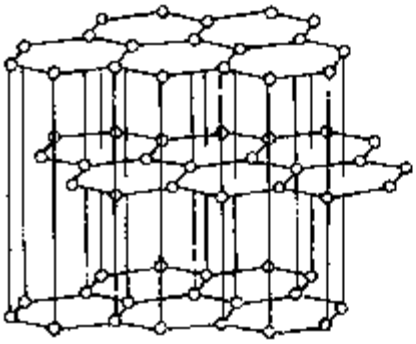

(**2a**)

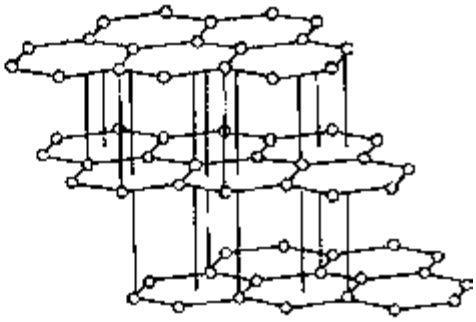

(**2b**)

FIGURE 7 Crystal structure of (**1**) diamond, showing the tetrahedral coordination of each carbon atom. Also shown are the crystal structures of the two polymorphs of graphite, specifically (**2a**) the hexagonal α-form, and (**2b**) the rhombohedral β-form.

The other category is associated with molecules that are capable of existing in conformationally different arrangements, each of which can crystallize in its own characteristic structure. This latter behavior has been termed conformational polymorphism (41), and the probucol system represents an extreme example of a compound where the polymorphism arises from the packing of different conformers (42). Although both polymorphs were found to be monoclinic, the unit cells belonged to different space groups and the molecular conformations of the title compound were quite different (Fig. 8). In form II, the C–S–C–S–C chain is extended,

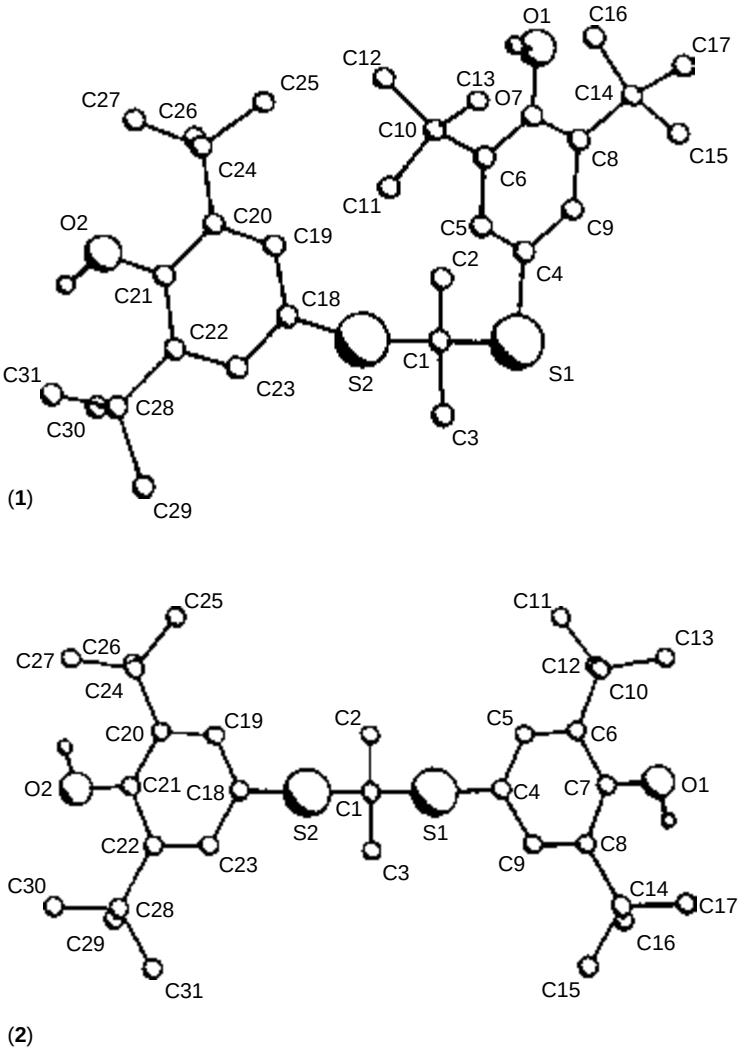

FIGURE 8 Conformation of the probucol molecule existing in **(1)** form I and in **(2)** form II. The figure was adapted from data contained in Ref. (42).

and the molecular symmetry approximates C_{2v}. This symmetry is lost in the structure of form I, where the torsion angles about the two C–S bonds deviate significantly from 180°. The extended conformer was shown to be less stable relative to the bent conformer, as simple grinding was sufficient to convert form II into form I.

Not all instances of conformational polymorphism are as dramatic as the probucol system, and often different conformers of a single sidechain are able to pack into different crystalline arrangements. For instance, the two polymorphs of *p*-(1*R*,3*S*)-3-thioanisoyl-1,2,2-trimethylcyclopentane carboxylic acid were found to be associated with different conformations of the carboxylate group (43). Torsion about a single C–N bond was shown to be the origin of the polymorphism detected for lomeridine dihydrochloride (44). Finally, relatively small differences in molecular conformation were detected for the two polymorphic and four solvated crystalline forms of spironlactone (45).

The analysis of single-crystal XRD data is divided into three parts (46–49). The first of these is the geometrical analysis, where one measures the exact spatial distribution of X-ray reflections and uses these to compute the size and shape of a unit cell. The second part entails a study of the intensities of the various reflections and uses this information to determine the atomic distribution within the unit cell. Finally, one looks at the X-ray diffraction pattern to deduce qualitative information about the quality of the crystal or the degree of order within the solid. This latter analysis may permit the adoption of certain assumptions that may aid in the solving of the crystalline structure.

A determination of the internal structure of a crystal requires the specification of the unit cell dimensions (axis lengths, and angles between these), and measurement of the intensities of the diffraction pattern of the crystal. For a given lattice, regardless of the content of the unit cell, the directions of reflection are the same. The experimental determination of these directions is used to deduce the reciprocal lattice of the crystal, which unambiguously yields the crystal lattice. In addition, the relative intensities diffracted by different planes depend on the contents of the unit cell. Their measurement leads to the determination of the crystal structure factor, and these data permit the determination of the atomic structure of crystals.

Crystallographic characterization of the physical form of an API may be used to understand its performance during pharmaceutical processing. One well-known case is that of polymorphic forms I and II of acetaminophen (also known as paracetamol). The crystal structures of both forms have been determined and the associated implications on their physical properties have been discussed (50). Monoclinic acetaminophen form I cannot be formulated into tablets by direct compression, but the presence of slip planes (illustrated in Fig. 9) in the orthorhombic form II allows its direct compression due to a plastic deformation process. This property is an immense advantage considering that direct compression is a cost-effective and time-efficient method of tablet production.

Crystallographic information is critical to understand dehydration of solvates that have channels in their crystal structures. As mentioned earlier, such solvatomorphs undergo desolvation under certain conditions, leading to the formation of isomorphic desolvates that tend to retain the three-dimensional structures of the parent compound (51,52).

Variable temperature and atmospheric-induced dehydration was characterized in form I of a small molecule developmental drug that was presented as a sodium salt and a trihydrate (53). It was shown that at 25°C, the compound lost 0.5% w/w

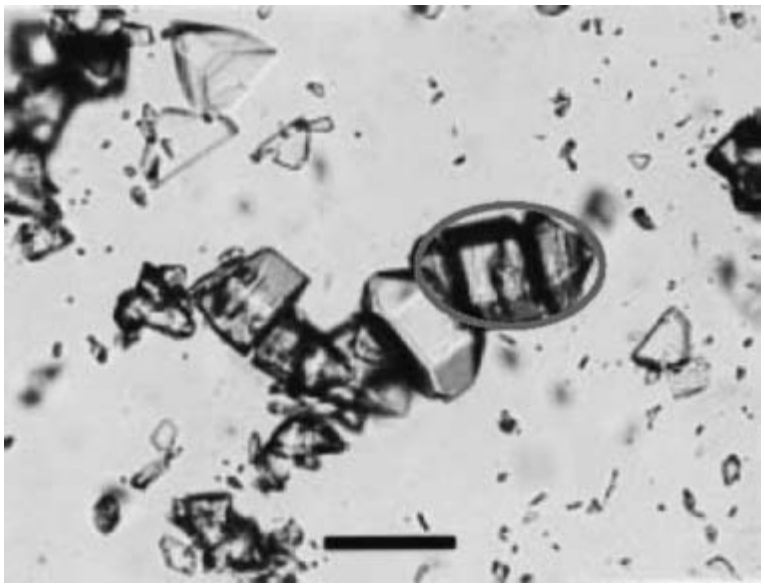

FIGURE 9 Pressure-induced formation of cleavages (*indicated by the ellipse*) in an acetaminophen form II crystal perpendicular to its length, showing the evidence of the existence of slip planes. *Source*: From Ref. (41).

water when the relative humidity was decreased from 90% to 15%, and that this water loss did not cause any change in the XRD pattern. A single-crystal XRD study revealed the existence of channels in the form I crystal structure (illustrated in Fig. 10), where one of the water molecules was weakly bound by hydrogen bonds and where the other two water molecules were bound to the sodium cation. Formation of the isomorphic dehydrate was attributed to the escape of some weakly bound water molecules through the channel, which did not compromise the integrity of the structure. Further decrease in relative humidity into the range of 5% to 15% resulted in a reversible phase transformation into form II, and at relativity humidities below 5%, XRD showed that the compound transformed into the semi-crystalline form III. A combination of techniques was used to show that form II was formed as a result of the escape of both weakly and strongly bound water molecules, which caused a partial collapse of the channels. Further dehydration of the solid resulted in disordered anhydrate form III.

The interplay between intramolecular conformational flexibility and intermolecular hydrogen bonding may influence the properties of a polymorph (54), such as in the classic example of ritonavir (55). In 1998, the commercial form of this drug substance (tradename of Norvir®, and marketed as a semi-solid formulation contained in capsules) had to be reformulated because the newer lots failed to meet established dissolution specifications. This was attributed to the sudden appearance of a polymorph (form II), which was much less soluble than the parent polymorph (form I) in the hydro-alcoholic medium of the formulation. Single-crystal XRD studies showed that both the hydrogen bonding capability and the packing density of

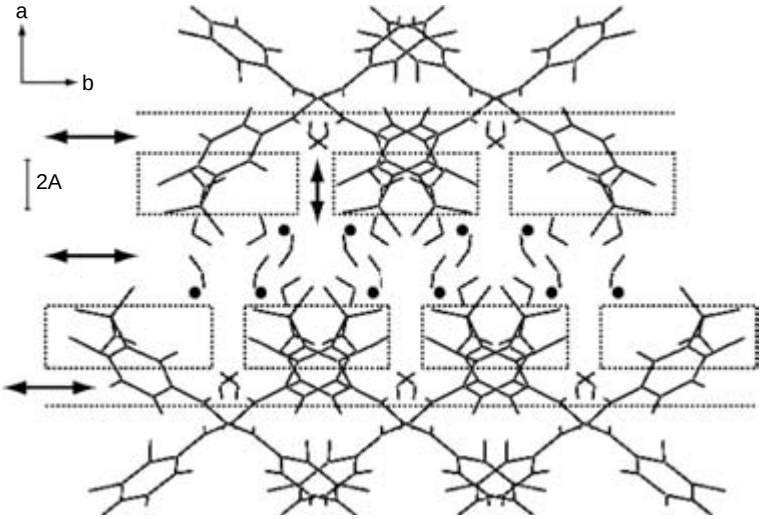

FIGURE 10 Top view along *c*-axis showing the crystal packing of form I of a developmental drug, the sodium salt of *N*-(3-(aminosulfonyl)-4-chloro-2-hydroxyphenyl)-*N′*-(2,3-dichlorophenyl) urea. Arrows indicate potential motion of water along the channels (*dashed lines*). Sodium atoms are represented by dark circles. *Source*: From Ref. (44).

form II was less than that of form I, which could be taken to suggest a greater stability of form I. However, the molecular conformation of ritonavir in form II was more favorable for crystal packing, and made this form the more stable polymorph.

It has been shown elsewhere that a thermodynamically stable polymorph may be characterized by the presence of unstable molecular conformations, such as the thermodynamically stable polymorph of oxybuprocaine hydrochloride, which was shown to have both stable and unstable molecular conformations in its crystalline forms (56).

X-Ray Powder Diffractometry

Although the solving of a crystal structure from an analysis of single-crystal diffraction provides the most fundamental structural understanding of polymorphic solids, the need for suitable single crystals and the degree of complexity associated with data analysis precludes this technique from being used on a routine basis for batch characterization. During routine synthesis, most drug substances are obtained as micro-crystalline powders, for which it is usually sufficient to establish only the physical form (usually polymorphic identity) of the solid, and to verify that the isolated compound is indeed of the desired structure. For these reasons, and in light of the experimental simplicity, the technique of XRD is the predominant tool for the study of polycrystalline materials (57–60), and is eminently suited for the routine characterization of polymorphs and solvates.

A properly prepared sample of a powdered solid will present a substantially random selection of all possible crystal faces and the diffraction patterns will therefore provide information regarding all possible spacings (atomic or molecular) in

the crystal lattice. To measure a powder pattern, a randomly oriented powdered sample is prepared in an effort to expose all the planes in the lattice. The scattering angle is determined by slowly rotating the sample and measuring the angle of diffracted X rays (typically using a scintillation detector) with respect to the angle of the incident beam. Alternatively, the angle between sample and source can be kept fixed, while moving the detector to determine the angles of the scattered radiation. Knowing the wavelength of the incident beam, the spacing between the planes (identified as the *d*-spacings) is calculated using Bragg's Law.

The XRD pattern will therefore consist of a series of peaks detected at characteristic scattering angles. These angles, and their relative intensities, can be correlated with the computed *d*-spacings to provide a full crystallographic characterization of the powdered sample. After indexing all the scattered lines, it is possible to derive unit cell dimensions from the powder pattern of the substance under analysis. For routine work, however, this latter analysis is not normally performed, and one typically compares the powder pattern of the analyte to that of reference materials to establish the polymorphic identity. Because every compound produces its own characteristic powder pattern owing to the unique crystal structure, powder XRD is clearly the most powerful and fundamental tool for polymorphic identity of an analyte.

The United States Pharmacopeia contains a general chapter on XRD (61), which sets the criterion that identity is established if the scattering angles in the powder patterns of the sample and reference standard agree to within the calibrated precision of the diffractometer. It is noted that it is generally sufficient that the scattering angles of the ten strongest reflections obtained for an analyte agree to within either ± 0.10 or $\pm 0.20°\ 2\theta$, whichever is more appropriate for the diffractometer used. Older versions of the general test contained an additional criterion for relative intensities of the scattering peaks, but it has been noted that relative intensities may vary considerably from that of the reference standard, making it impossible to enforce a criterion based on the relative intensities of corresponding scattering peaks.

For identification purposes, it is usually convenient to identify the angles of the 10 most intense scattering peaks in a powder pattern, and to then list the accepted tolerance ranges of these based on the diffractometer used for the determinations. Useful tabulations of the XRD patterns of a number of compounds have been published by Koundourellis and coworkers, including 12 diuretics (62), 12 vasodilators (63), and 12 other commonly used drug substances (64).

The literature abounds with countless examples that illustrate how powder diffraction has been used to distinguish between polymorphs. It is safe to state that one could not publish the results of a phase characterization study without the inclusion of XRD data. Nowhere is this more crucial than in intellectual property controversies, where the different XRD patterns of polymorphs are used for patentability purposes. For example, two polymorphic forms of ibandronate sodium have been the subject of two United States patent applications (65), and although the XRD patterns of these are somewhat similar (Fig. 11), a sufficient number of differences in scattering peak angles exist so as to permit their identification. In the patent applications, some of the claims define the two polymorphs on the basis of five characteristic XRD scattering peaks, which enables one to tabulate the data and determine whether or not a given sample of ibandronate sodium is within the scope of these XRD claims.

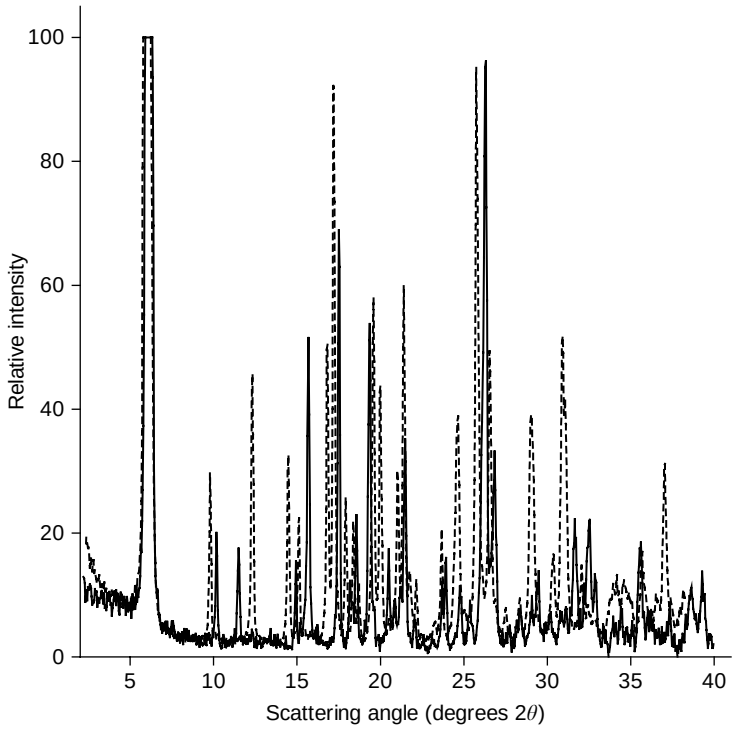

FIGURE 11 X-ray powder diffraction patterns of ibandronate sodium, Form A (*solid trace*) and Form B (*dashed trace*). The patterns have been adapted from data in United States patent applications 2006/0172975 and 2006/0172976 (65).

Once the characteristic XRD patterns of one or more analytes have been established, it is usually possible to develop methods for phase quantification. The methodology is based on the premise that each component will contribute to the overall scattering by an amount that is proportional to its weight fraction in a mixture, and that the powder pattern of each analyte contains one or more peaks whose scattering angle is unique to that analyte. Quantitative analysis typically requires the use of reference standards that contribute known scattering peaks at appropriate scattering intensities. This can be achieved through the use of internal standards, where one would mix reference materials such as elemental silicon or lithium fluoride into the sample matrix.

Although simple intensity correction techniques can be used to develop suitable quantitative XRD methods, the introduction of more sophisticated data acquisition and handling techniques can greatly improve the quality of the developed method. For instance, improvement of the powder pattern quality through use of the Rietveld method has been used to evaluate mixtures of two anhydrous polymorphs of carbamazepine and the dihydrate solvatomorph (66). The method of whole pattern analysis developed by Rietveld (67) has found widespread use in crystal structure refinement and in the quantitative analysis of complex mixtures.

Using this approach, the detection of analyte species was possible even when their concentration was less than 1% in the sample matrix. It was reported that good quantitation of analytes could be obtained in complex mixtures even without the requirement of calibration curves.

Well-characterized and stable (both physically and chemically) Standard Reference Materials are available from the National Institute of Standards and Technology (NIST) (68). These materials are used both to calibrate powder XRD equipment and to measure the instrument sensitivity. Silicon powder (SRM 640c) is typically used for the calibration of *d*-spacing or line position, and also can be used as an internal reference for quantitative applications. NIST SRM 674b is a set of four metal oxides (CeO_2, Cr_2O_3, TiO_2, and ZnO) that are also used as internal standards in quantitative work.

The use of parallel beam optics as a means for determining the polymorphic composition in powder compacts has been evaluated (69). In this study, compressed mixtures of known polymorphic composition were analyzed in transmission mode, and the data processed using profile fitting software. The advantage of using transmission, rather than reflectance, was that the results were not sensitive to the geometrical details of the compact surfaces, and that spurious effects associated with preferential orientation were minimized.

The effects of preferred orientation in XRD analysis can be highly significant, and are most often encountered when working with systems characterized by plate-like or tabular crystal morphologies. A viable XRD sample is one that is free from the deleterious effects of preferential orientation, and any sample packing effect that serves to introduce a non-random pattern of crystal faces can strongly affect the observed intensities and any quantitative results. The problem has been investigated for the three needle-like polymorphs of mannitol, and it was found that through the use of small particles, the preferential orientation effects were held to a minimum, enabling quantification of the polymorphs around the 1% level (70).

The use of powder XRD has been investigated to determine whether one may use pattern indexing as another tool for polymorph screening studies (71). In this work, data were collected on six compounds using two diffractometers that employed transmission geometry, primary monochromatic radiation, and a position-sensitive detector. The data were found to exhibit good angular resolution, and therefore lattice parameters were easily obtained using the indexing program DICYOL-91. The extent of preferred orientation in each pattern was estimated using the DASH implementation of the March–Dollase function. It was concluded that the combination of experimental techniques used would be highly effective compared to just one technique that would require a large number of samples per day with the aim of obtaining the type of high-quality data necessary for pattern recognition and indexing.

Practical complications associated with preferential orientation effects have been discussed in detail (72). A number of sample-packing methods were considered (vacuum free-fall, front-faced packing vs. rear-faced packing, etc.), but the best reduction in preferential orientation was achieved by using materials having small particles that were produced by milling. Through the use of sieving and milling, excellent linearity in diffraction peak area as a function of analyte concentration was attained. The authors deduced a protocol for development of a quantitative XRD method consisting of (a) calculation of the mass attenuation coefficient of the drug substance, (b) selection of appropriate diffraction peaks for quantification,

(c) evaluation of the loading technique for adequate sample size, (d) determination of whether preferred orientation effects can be eliminated through control of the sample particle size, (e) determination of appropriate milling conditions to obtain reproducibility in peak areas, and (f) generation of calibration curves from physical mixtures.

Profile-fitting analysis has been combined with powder XRD to develop a quantitative method to determine the relative amounts of two prazosin hydrochloride polymorphs in their powder mixtures (73). Powder patterns of the pure α- and δ-polymorphs were initially obtained, and then patterns of calibration samples containing the α-form at concentrations ranging from 0.5% to 10% w/w in bulk δ-form. As is evident from Figure 12, the α-form exhibits a strong scattering peak at 27.5° 2θ where the δ-form exhibits little scattering, thus making this peak suitable for use in developing a quantitative method for phase composition. Using mathematical profile fitting, the background intensity level of the δ-form and the integrated intensity of peaks due to the α-form were determined, enabling a detection limit of 0.5%.

Powder XRD and diffuse reflectance infrared absorption spectroscopy analyses were used to develop two independent quantitative phase composition methods

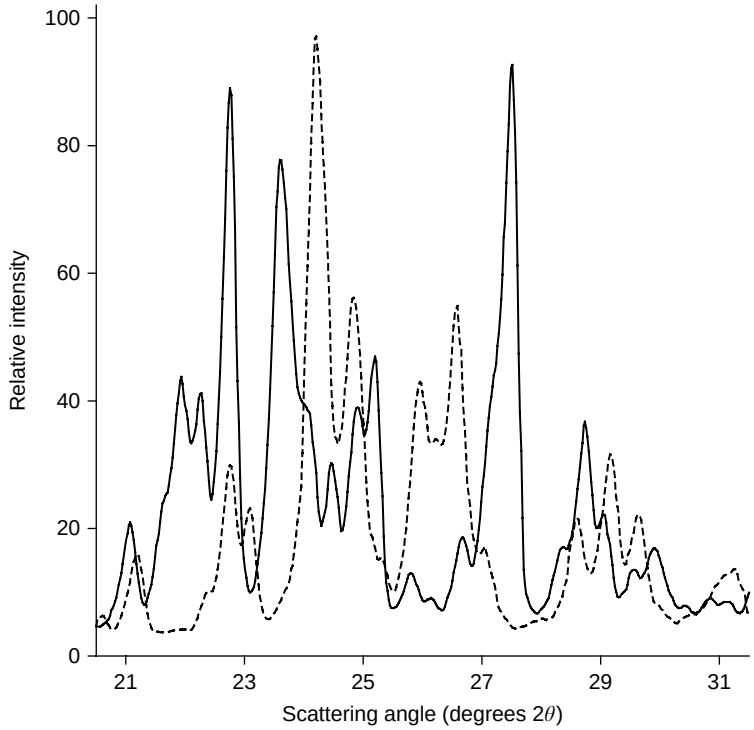

FIGURE 12 Expanded X-ray powder diffraction patterns of prazosin hydrochloride, α-form (*solid trace*) and δ-form (dashed trace), illustrating the peak at 27.5° 2θ that was used for quantitation purposes. The patterns have been adapted from data in Ref. (73).

for the determination of quantities of cefepime dihydrochloride dihydrate in samples of cefepime dihydrochloride monohydrate (74). For the XRD method, over a working concentration range 2.5% to 15% w/w, the limit of detection and quantification of the dihydrate in monohydrate were respectively 0.75% and 2.5% w/w. For the infrared method, a working range of 1.0% to 8.0% w/w was established with a minimum quantifiable level of 1.0% w/w and a limit of detection of 0.3% w/w dihydrate in monohydrate.

When reference samples of the pure amorphous and pure crystalline phases of a substance are available, calibration samples of known degrees of crystallinity can be prepared by mixing these reference samples. Establishment of a calibration curve (XRD response vs. degree of crystallinity) permits quantification of crystallinity in unknown samples. In one such study, a quantitative method was developed by beginning with commercially available crystalline digoxin and ball-milling of this substance to obtain various samples having various degrees of amorphous phase (75). Calibration mixtures were prepared as a variety of blends prepared from the 100% crystalline and 0% crystalline materials, and acceptable linearity and precision was obtained in the calibration curve of XRD intensity versus actual crystallinity.

In the absence of standard materials having known degree of crystallinity, one may determine the degree of crystallinity from the simple relation:

$$\mathrm{DOC} = (A_C/A_T)(100) \tag{3}$$

where A_C is the integrated intensity attributable to the crystalline regions, and A_T is the total diffracted intensity. The evaluation of A_C and A_T is illustrated in Figure 13, where the reported XRD pattern of lenalidomide Form H (76) is shown along with its associated amorphous background. One would obtain A_C as the sum of the areas of the peaks above the dashed line, whereas A_T would be measured as the total area under the curve.

Determination of Crystal Structures from Powder Diffraction Data

As discussed above, a powder pattern will consist of a series of peaks having varying intensities, detected at various scattering angles. Through the indexing process, the *d*-spacings computed from the values of the scattering angles are assigned to diffraction from the crystal planes defined by their Miller (*hkl*) indices to provide a full crystallographic characterization of the powdered sample. After the indexing procedure is complete, it is possible to derive unit cell dimensions and other crystallographic information from a high-resolution powder pattern of a substance, eventually developing an approximate structural model that can be refined against experimental powder XRD data (structure refinement) (77–81). This procedure is best conducted on diffraction data collected using a high-flux synchrotron source (82).

Of the three crystal forms of telmisartan, the structure of solvated Form C was determined using single-crystal XRD and the structures of non-solvated forms A and B were determined from high-resolution powder XRD data using the method of simulated annealing for structure solution followed by Rietveld refinement (83). With 13 degrees of freedom (three translational, three orientational, and seven torsion angles), the structure solution was accomplished in approximately two hours of computer time, demonstrating that the crystal packing and the molecular conformation

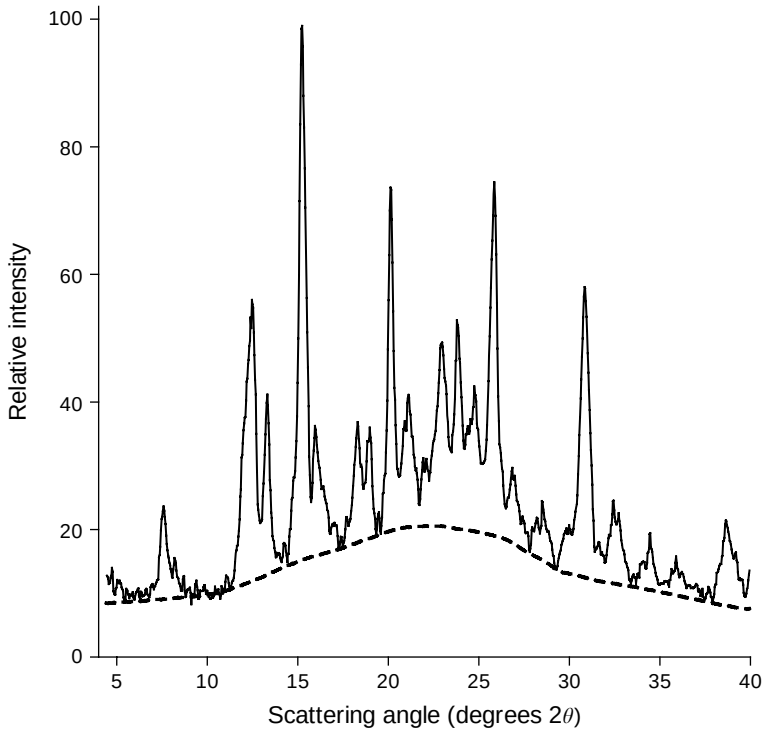

FIGURE 13 XRD pattern of lenalidomide form H (*solid trace*), and an estimation of the amorphous background (*dashed line*). The powder pattern of form H was adapted from data in Ref. (74).

of medium-sized pharmaceutical compounds could be solved quickly and routinely from high-resolution powder XRD data.

Other examples where structural properties have been derived from powder XRD data include enalapril maleate form II (84) and bupivacaine base (85).

Variable-Temperature X-Ray Diffractometry

XRD, performed on a hot stage, enables one to obtain powder patterns at elevated temperatures, and permits the deduction of structural assignments for thermally induced phase transformation reactions. By conducting VT-XRD studies, one can bring the system to conditions that had been indicated to be of interest during the conduct of thermal analysis studies. XRD systems equipped with hot-stage sample holders have been described, with this instrumentation being capable of obtaining powder patterns at temperatures of pharmaceutical interest (86,87). VT-XRD studies conducted under isothermal conditions can also be used for the calculation of activation energies of solid-state reactions.

VT-XRD is ideally suited to explain potentially complex solid-state transformations involving pharmaceutical hydrates. For example, Terakita et al. examined the dehydration behavior of calcium benzoate trihydrate, a system where the solid state transformations involved, in addition to crystalline and amorphous phases,

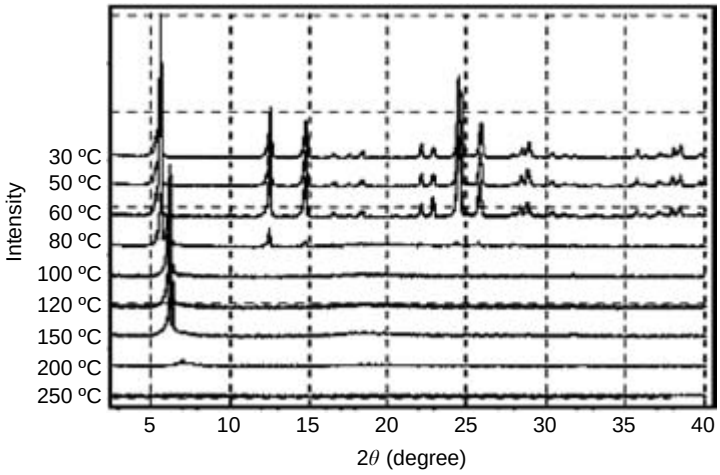

FIGURE 14 VT-XRD patterns obtained during the drying of calcium benzoate trihydrate, showing the gradual dehydration to a mesophase (100°C), which eventually culminated in the formation of an amorphous phase (250°C). *Source*: From Ref. (88).

a mesophase (88). As the temperature was increased, the trihydrate crystal form gradually formed a mesophase, as indicated by a sharp low-angle peak. As illustrated in Figure 14, further heating resulted in complete amorphization and the disappearance of all XRD peaks. A ground sample of the trihydrate was found to contain traces of calcium benzoate monohydrate, which was confirmed by VT-XRD to have formed by a recrystallization process. In this work, VT-XRD was shown to function both as an aid in the identification of crystalline phases, as well as in decoding the mechanism of their formation. Understanding such transformations and the knowledge of the conditions under which phase transitions occur, could aid in optimizing process parameters, such as the drying temperature of granules.

By virtue of their higher free energy compared to their more stable counterparts, metastable polymorphs of drug substances can significantly affect drug release from a dosage form. For example, theophylline monohydrate was observed by VT-XRD to dehydrate to the anhydrous form via an intermediate metastable anhydrate (89). The dissolution performance of tablets containing stable and metastable anhydrous theophylline was compared, where surprisingly the dissolution rate of the metastable form was found to be slower than that of the stable form. This phenomenon was shown to be due to the relatively rapid conversion of the metastable anhydrate form to the monohydrate form in the dissolution medium.

Isomorphic desolvates, formed by desolvation of solvates, represent the type of lattice structures that can be inherently unstable owing to their molecular packing. Consequently, such materials tend to be quite reactive and prone to instability, especially during their secondary processing into drug products (90). Miroshynk et al. used VT-XRD to investigate processing-induced phase transformations in erythromycin dihydrate (91). Dehydration resulted in shifts in the XRD peak positions, where some peaks shifted to higher angles owing to lattice expansion, whereas other peaks shifted to lower angular values as a result of lattice contraction.

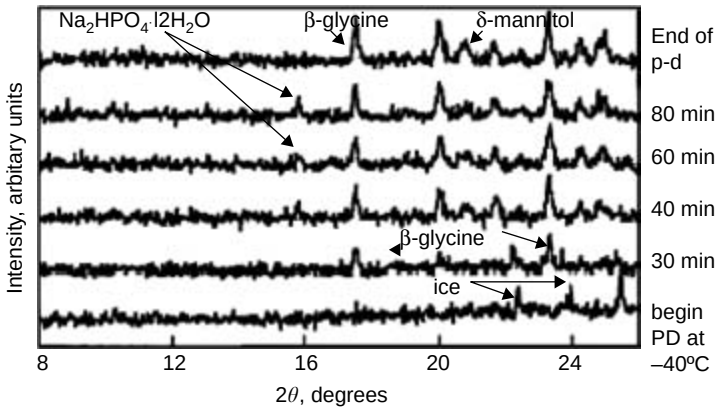

FIGURE 15 In situ VT-XRD patterns obtained during the primary drying (PD) of a frozen aqueous solution consisting of buffer salts, mannitol, and glycine. The solution was first cooled to –70°C at 2°C/min, which was then followed by heating to the primary drying temperature (–40°C) at 5°C/min. Primary drying was carried out for 4 hours. *Source*: From Ref. (92).

At higher temperatures, the XRD patterns indicated that the solids rearranged to form anhydrous erythromycin.

Although the typical use of VT-XRD is at elevated temperatures, the technique can also be used for work under sub-ambient conditions. For example, Pyne et al. characterized freeze-dried buffered aqueous systems of mannitol and glycine, and found that δ-mannitol and β-glycine crystallized during primary drying (92). By monitoring the intensities of the characteristic peaks of δ-mannitol and β-glycine both during primary and secondary drying, it was possible to determine the rate of crystallization of these solutes. Interestingly, one of the buffer salts, disodium hydrogen phosphate, crystallized as its dodecahydrate phase at the start of primary drying, but became dehydrated to an amorphous anhydrate at the end of the drying cycle (Fig. 15). It is important to note that conventional XRD of the final lyophile would not have revealed the crystallization of the buffer salt. The selective crystallization of disodium hydrogen phosphate only became evident by monitoring the phase transitions that took place *during* the freeze–drying process.

While attempting to simulate pharmaceutical processing steps, it is important to consider the effect of sample geometry on the phase transition kinetics. The relative quantities of stable and metastable anhydrous theophylline were found to be significantly different when theophylline monohydrate granules were dried in a microscale fluid bed dryer and in the sample stage of a powder X-ray diffractometer, with these differences being attributed primarily to differences in sample geometry (93). Although the VT-XRD sample bed was stationary, resulting in a slow drying rate, the sample in the fluid bed drier was dried rapidly due to fluidization.

XRD studies conducted at elevated temperatures can also be run under controlled water vapor pressures, using humidified nitrogen to control the vapor pressure. Han et al. proposed this technique to rapidly evaluate the physical stability of pharmaceutical hydrates, and studied the isothermal dehydration kinetics

of amoxicillin trihydrate at 68°C and at different water vapor pressures (94). The product they obtained was a poorly crystalline anhydrate. From these kinetic studies, the transition water vapor pressure of amoxicillin trihydrate was determined to be approximately 10.5 Torr at 68°C.

In addition to being extremely useful in the study of phase transformations, VT-XRD can also be used to obtain information on substance decomposition during a variable-temperature study. The commercially available form of aspartame is hemihydrate form II, which is known to transform into hemihydrate form I when milled, but a 2.5-hydrate species is also known (95,96). Through the use of VT-XRD, it was found that when either hydrate form was heated to 150°C, they dehydrated into the same anhydrous phase. Further heating of the anhydrate to 200°C resulted in a thermally induced cyclization, forming 3-(carboxymethyl)-6-benzyl-2, 5-dioxopiperazine. The 2.5-hydrate was shown to dehydrate to hemihydrate form II when heated to 70°C, and this dehydration product was shown to undergo the same decomposition sequence as directly crystallized hemihydrate form II.

REFERENCES

1. Wendlandt W. Thermal Analysis. New York: John Wiley & Sons, 1986.
2. Ford J, Timmins P. Pharmaceutical Thermal Analysis: Techniques and Applications. New York: E. Horwood, 1989.
3. Craig D. Pharmaceutical applications of DSC. In Thermal Analysis of Pharmaceuticals. In: Craig D, Reading M, eds. New York: CRC Press, 2006: 53–100.
4. Craig D. Characterization of polymorphic systems using thermal analysis. In: Polymorphism in the Pharmaceutical Industry. In: Hilfiker R, ed. Weinheim: Wiley-VCH, 2006: 43–79.
5. Jenkins R, Snyder RL. Introduction to X-Ray Powder Diffractometry. New York: John Wiley & Sons, 1996.
6. Suryanarayanan R. X-Ray powder diffractometry. In: Brittain HG, ed. Physical Characterization of Pharmaceutical Solids. New York: Marcel Dekker, 1995.
7. Braun DE, Tobbens DM, Kahlenberg V. Structural and thermodynamic features of crystal polymorphs of R-cinacalcet hydrochloride. Cryst Growth Des 2008; 8: 4109–19.
8. Coleman N, Craig D. Modulated temperature differential scanning calorimetry: a novel approach to pharmaceutical thermal analysis. Int J Pharm 1996; 135: 13–29.
9. Hill V, Craig D, Feely L. The effects of experimental parameters and calibration on MTDSC data. Int J Pharm 1999; 192: 21–32.
10. Simon S. Temperature-modulated differential scanning calorimetry: theory and application. Thermochim Acta 2001; 374: 55–71.
11. Kawakami K, Ida Y. Application of modulated-temperature DSC to the analysis of enantiotropically related polymorphic transitions. Thermochim Acta 2005; 427: 93–9.
12. Bottom R. The role of modulated temperature differential scanning calorimetry in the characterization of a drug molecule exhibiting polymorphic and glass forming tendencies. Int J Pharm 1999; 192: 47–53.
13. Singh S, Jalali A, Alden M. Modulated temperature differential scanning calorimetry for examination of tristearin polymorphism: I. Effect of operational parameters. J Am Oil Chem Soc 1999; 76: 499–505.
14. Singh S, Jalali A, Alden M. Modulated temperature differential scanning calorimetry for examination of tristearin polymorphism: 2. Isothermal crystallization of metastable forms. J Am Oil Chem Soc 1999; 76: 507–10.
15. Kaushal A, Bansal A. Thermodynamic behavior of glassy state of structurally related compounds. Eur J Pharm Biopharm 2008; 69: 1067–76.

16. Graeser K, Strachan C, Patterson J. Physicochemical properties and stability of two differently prepared amorphous forms of simvastatin. Cryst Growth Des 2008; 8: 128–35.
17. Guinot S, Leveiller F. The use of MTDSC to assess the amorphous phase content of a micronized drug substance. Int J Pharm 1999; 192: 63–75.
18. Saklatvala R, Royall P, Craig D. The detection of amorphous material in a nominally crystalline drug using modulated temperature DSC: a case study. Int J Pharm 1999; 192: 55–62.
19. McGregor C, Bines E. The use of high-speed differential scanning calorimetry (Hyper-DSCTM) in the study of pharmaceutical polymorphs. Int J Pharm 2008; 350: 48–52.
20. McMahon L, Timmins P, Williams A. Characterization of dihydrates prepared from carbamazepine polymorphs. J Pharm Sci 1996; 85: 1064–9.
21. Sussich F, Urbani R, Princivalle F. Polymorphic amorphous and crystalline forms of trehalose. J Am Chem Soc 1998; 120: 7893–9.
22. Han J, Suryanarayanan R. Applications of pressure differential scanning calorimetry in the study of pharmaceutical hydrates: I. Carbamazepine dihydrate. Int J Pharm 1997; 157: 209–18.
23. Sanders G, Roberts C, Danesh A. Discrimination of polymorphic forms of a drug product by localized thermal analysis. J Microsc 2000; 198: 77–81.
24. Khankari R, Chen L, Grant DJW. Physical characterization of nedocromil sodium hydrates. J Pharm Sci 1998; 87: 1052–61.
25. Surana R, Pyne A, Suryanarayanan R. Solid-vapor interactions: influence of environmental conditions on the dehydration of carbamazepine dihydrate. AAPS PharmSci 2003; 4: 1–10.
26. Alkhamis K, Salem M, Obaidat R. Comparison between dehydration and desolvation kinetics of fluconazole monohydrate and fluconazole ethyl acetate solvate using three different methods. J Pharm Sci 2006; 95: 859–70.
27. Miyazaki T, Sivaprakasam K, Tantry J, et al. Physical characterization of dibasic calcium phosphate dihydrate and anhydrate. J Pharm Sci 2009; 98: 905–16.
28. Rastogi S, Zamansky I, Roy S. Solid-state phase transitions of AG337, an antitumor agent. Pharm Dev Tech 1999; 4: 623–32.
29. Blaine RL, Fair PG. Estimate of the true magnetic transition temperatures for the ICTA reference materials GM761. Thermochim Acta 1983; 67: 233–40.
30. Hill JO. Thermogravimetric analysis. In Encyclopedia of Chemical Processing, Volume 5. In: Lee S, Lee L, eds. New York: CRC Press, 2006: 3009–22.
31. Vitez I, Newman A, Davidovich M. The evolution of hot-stage microscopy to aid solid-state characterizations of pharmaceutical solids. Thermochim Acta 1998; 324: 187–96.
32. Bernstein J. Polymorphism in Molecular Crystals. Clarendon: Oxford University Press, 2002.
33. Braun D, Gelbrich T, Jetti R. Colored polymorphs: thermochemical and structural features of N-picryl-p-toluidine polymorphs and solvates. Cryst Growth Des 2008; 8: 1977–89.
34. Zhu H, Grant DJW. Dehydration behavior of nedocromil magnesium pentahydrate. Int J Pharm 2001; 215: 251–62.
35. Zhu H. Dehydration behavior and structural characterization of the GW275919X monohydrate. Int J Pharm 2006; 315: 18–23.
36. Tonder E, Mahlatji M, Malan S. Preparation and physicochemical characterization of five niclosamide solvates and one hemisolvate. AAPS PharmSciTech 2004; 5: 1–10.
37. Grooff D, De Villiers M, Liebenberg W. Thermal methods for evaluating polymorphic transitions in nifedipine. Thermochim Acta 2007; 454: 33–42.
38. Boles MO, Girven RJ, Gane PAC. The structure of amoxicillin trihydrate and a comparison with the structures of ampicillin. Acta Cryst 1978; B34: 461–6.
39. Bragg WH, Bragg WL. X-Rays and Crystal Structure. London: G. Bell & Sons, 1918.

40. Cullity BD, Stock SR. Elements of X-Ray Diffraction. Upper Saddle River, NJ: Prentice Hall, 2001.
41. Bernstein J. Conformational polymorphism, chapter 13 in Organic Solid State Chemistry. In: Desiraju GR, ed. Amsterdam: Elsevier, 1987: 471–518.
42. Gerber JJ, Caira MR, Lötter AP. Structures of two conformational polymorphs of the cholesterol-lowering drug probucol. J Cryst Spect Res 1993; 23: 863–9.
43. Rambaud J, Bouassab A, Pauvert B, et al. Comparative study of the two polymorphic forms of p-(1R, 3S) 3-thioanisoyl-1, 2,2-trimethylcyclopentane carboxylic acid. J Pharm Sci 1993; 82: 1262–5.
44. Hiramatsu Y, Suzuki H, Kuchiki A, et al. X-ray structural studies of lomeridine dihydrochloride polymorphs. J Pharm Sci 1996; 85: 761–6.
45. Agafonov V, Legendre B, Rodier N, et al. Polymorphism of spironolactone. J Pharm Sci 1991; 80: 181–5.
46. Woolfson MM. X-Ray Crystallography. Cambridge: Cambridge University Press, 1970.
47. Stout GH, Jensen LH. X-Ray Structure Determination: A Practical Guide. New York: Macmillan Co, 1968.
48. Clegg W, Blake AJ, Gould RO, et al. Crystal Structure Analysis: Principles and Practice. New York: Oxford University Press, 2001.
49. Giacovazzo C. Fundamentals of Crystallography. New York: Oxford University Press, 2002.
50. Nichols G, Frampton C. Physicochemical characterization of the orthorhombic polymorph of paracetamol crystallized from solution. J Pharm Sci 1998; 87: 684–93.
51. Reutzel-Edens S, Kleemann R, Lewellen P. Crystal forms of LY334370 HCl: isolation, solid-state characterization, and physicochemical properties. J Pharm Sci 2003; 92: 1196–205.
52. Stephenson G, Groleau E, Kleemann R. Formation of isomorphic desolvates: creating a molecular vacuum. J Pharm Sci 1998; 87: 536–42.
53. Vogt F, Brum J, Katrincic L. Physical, crystallographic, and spectroscopic characterization of a crystalline pharmaceutical hydrate: understanding the role of water. Cryst Growth Des 2006; 6: 2333–54.
54. Nangia A. Conformational polymorphism in organic crystals. Acc Chem Res 2008; 41: 595–604.
55. Bauer J, Spanton S, Henry R. Ritonavir: an extraordinary example of conformational polymorphism. Pharm Res 2001; 18: 859–66.
56. Griesser U, Jetti R, Haddow M. Conformational polymorphism in oxybuprocaine hydrochloride. Cryst Growth Des 2008; 8: 44–56.
57. Klug HP, Alexander LE. X-ray Diffraction Procedures for Polycrystalline and Amorphous Materials, 2nd edn. New York: Wiley-Interscience, 1974.
58. Suryanarayanan R. X-ray Powder diffractometry, chapter 7 in Physical Characterization of Pharmaceutical Solids. In: Brittain HG, ed. New York: Marcel Dekker, 1995: 187–221.
59. Brittain HG. X-ray Diffraction of pharmaceutical materials, chapter 7, in Profiles of Drug Substances, Excipients, and Related Methodology, volume 30. In: Brittain HG, ed. Amsterdam: Elsevier Academic Press, 2003: 273–319.
60. Blachére JR, Brittain HG. X-ray diffraction methods for the characterization of solid pharmaceutical materials, Chapter 3.4, in Preformulation in Solid Dosage Form Development. In: Adeyeye MC, Brittain HG, eds. New York: Informa Healthcare Press, 2008: 229–52.
61. X-Ray Diffraction, General test <941>. United States Pharmacopoeia 32, Volume 1. Rockville, MD: The United States Pharmacopoeial Convention, 2009: 390–2.
62. Koundourellis JE, Markopolou CK, Underwood FA, et al. The x-ray characterization of 12 diuretics. J Chem Eng Data 1992; 37: 187–91.
63. Koundourellis JE, Malliou ET, Sullivan RAL, et al. X-ray characterization of 12 vasodilators in current use. J Chem Eng Data 1999; 44: 656–60.

64. Koundourellis JE, Malliou ET, Sullivan RAL, et al. X-ray powder diffraction data for 12 drugs in current use. J Chem Eng Data 2000; 45: 1001–6.
65. Eiermann U, Junghans B, Knipp B, et al. Ibandronate polymorph, United States Patent Applications 2006/0172975 and 2006/0172976, published August 3, 2006.
66. Iyengar SS, Phadnis NV, Suryanarayanan R. Quantitative analyses of complex pharmaceutical mixtures by the Rietveld metnod. Powder Diffraction 2001; 16: 20–4.
67. Rietveld HM. A profile refinement method for nuclear and magnetic structures. J Appl Crystallogr 1969; 2: 65–71.
68. https://srmors.nist.gov/tables/view_table.cfm?table=209-1.htm: Accessed: November 9, 2008.
69. Cao W, Bates S, Peck GE, et al. Quantitative determination of polymorphic composition in intact compacts by parallel-beam X-ray powder diffractometry. J Pharm Biomed Anal 2002; 30: 1111–19.
70. Campell Roberts SN, Williams AC, Grimsey IM, et al. Quantitative analysis of mannitol polymorphs. X-ray powder diffractometry: exploring preferred orientation effects. J Pharm Biomed Anal 2002; 28: 1149–59.
71. Florence AJ, Baumgartner B, Weston C, et al. Indexing powder patterns in physical form screening: instrumentation and data quality. J Pharm Sci 2003; 92: 1930–8.
72. Kidd WC, Varlashkin P, Li CY. The applicability of powder X-ray diffraction to the quantification of drug substance polymorphs using a model organic system. Powder Diffraction 1993; 8: 180–7.
73. Tanninen VP, Yliruusi J. X-ray powder diffraction profile fitting in quantitative determination of two polymorphs from their powder mixture. Int J Pharm 1992; 81: 169–77.
74. Bugay DE, Newman AW, Findlay WP. Quantitation of cefepime·2HCl dihydrate in cefepime·2HCl monohydrate by diffuse reflectance IR and powder X-ray diffraction techniques. J Pharm Biomed Anal 1996; 15: 49–61.
75. Black DB, Lovering EG. Estimation of the degree of crystallinity in digoxin by X-ray and infrared methods. J Pharm Pharmacol 1977; 29: 684–7.
76. Jaworsky MS, Chen RS-C, Muller GW, et al. Polymorphic forms of 3-(4-amino-1-oxo-1,3 dihydro-isoindol-2-yl)-piperidin-e-2,6-dione. United States Patent Application 2005/0096351, published May 5, 2005.
77. Poojary DM, Clearfield A. Application of X-ray powder diffraction techniques to the solution of unknown crystal structures. Acc Chem Res 1997; 30: 414–22.
78. Stephenson GA. Structure determination from conventional powder diffraction data: application to hydrates, hydrochloride salts, and metastable polymorphs. J Pharm Sci 2000; 89: 958–66.
79. Harris K, Tremayne M, Kariuki B. Contemporary advances in the use of powder X-ray diffraction for structure determination. Angew Chem Int Ed 2001; 40: 1626–51.
80. Harris KDM. New opportunities for structure determination of molecular materials directly from powder diffraction data. Cryst Growth Des 2003; 3: 887–95.
81. Habershon S, Cheung EY, Harris KDM, Johnston RL. Powder diffraction indexing as a pattern recognition problem: a new approach for unit cell determination based on an artificial neural network. J Phys Chem A 2004; 108: 711–16.
82. Cernik R, Louer D. Indexing unit cells from synchrotron X-ray powder diffraction data. J Appl Cryst 1993; 26: 277–80.
83. Dinnebier RE, Sieger P, Nar H, Shankland K, David WIF. Structural characterization of three crystalline modifications of telmisartan by single crystal and high-resolution X-ray powder diffraction. J Pharm Sci 2000; 89: 1465–79.
84. Kiang Y-H, Huq A, Stephens PW, et al. Structure determination of enalapril maleate form II from high-resolution X-ray powder diffraction data. J Pharm Sci 2003; 92: 1844–53.
85. Cheung EY, Harris KDM, Johnston RL, et al. Rationalizing the structural properties of bupivacaine base – a local anesthetic – directly from powder X-ray diffraction data. J Pharm Sci 2004; 93: 667–74.

86. Epple M, Cammenga HK. Investigation of solid state reactions and solid-solid phase transformations with time- and temperature-resolved X-ray diffractometry. Ber Bunsenges Phys Chem 1992; 96: 1774–8.
87. Conflant P, Guyot-Hermann A-M. Contribution of X-ray powder diffraction versus temperature to the solid state study of pharmaceutical raw materials. Eur J Pharm Biopharm 1994; 40: 388–92.
88. Terakita A, Byrn SR. Structure and physical stability of hydrates and thermotropic mesophase of calcium benzoate. J Pharm Sci 2006; 95: 1162–72.
89. Phadnis N, Suryanarayanan R. Polymorphism in anhydrous theophylline: implications on the dissolution rate of theophylline tablets. J Pharm Sci 1997; 86: 1256–63.
90. Govindarajan R, Suryanarayanan R. Processing induced phase transformations and their implications on pharmaceutical product quality, chapter 13 in Polymorphism in the Pharmaceutical Industry. In: Hilfiker R, ed. Weinheim: Wiley-VCH, 2006: 333–61.
91. Miroshnyk I, Khriachtchev L, Mirza S. Insight into thermally induced phase transformations of erythromycin A dihydrate. Cryst Growth Des 2006; 6: 369–74.
92. Pyne A, Chatterjee K, Suryanarayanan R. Solute crystallization in mannitol-glycine systems: implications on protein stabilization in freeze-dried formulations. J Pharm Sci 2003; 92: 2272–83.
93. Airaksinen S, Karjalainen M, Räsänen E. Comparison of the effects of two drying methods on polymorphism of theophylline. Int J Pharm 2004; 276: 129–41.
94. Han J, Suryanarayanan R. A method for the rapid evaluation of the physical stability of pharmaceutical hydrates. Thermochim Acta 1999; 329: 163–70.
95. Leung SS, Grant DJW. Solid state stability studies of model dipeptides: aspartame and aspartylphenylalanine. J Pharm Sci 1997; 86: 64–71.
96. Rastogi S, Zakrzewski M, Suryanarayanan R. Investigation of solid-state reactions using variable temperature X-ray powder diffractrometry. I. Aspartame hemihydrate. Pharm Res 2001; 18: 267–73.

10 Vibrational Spectroscopy

Harry G. Brittain
Center for Pharmaceutical Physics, Milford, New Jersey, U.S.A.

INTRODUCTION

In addition to the crystallographic techniques of X-ray diffraction and optical crystallography, methodologies based on molecular spectroscopy have become extremely important for the characterization of polymorphs and solvatomorphs (1). These methods become particularly useful when information must be obtained from a small amount of sample in a short period of time, and because most of the methods are non-destructive in nature, the analyzed material can be recycled for additional study once the measurements are complete. A number of techniques have been developed for the characterization of compounds in the solid state, and those based on probing the periodic motion of atoms and groups of atoms in molecules in solids will form the scope of this chapter.

The vibrational patterns existing in molecules are characterized by repetitious departures and returns about the center of gravity, and these correlated motions are termed the vibrational modes of the molecule. Energies associated with the lowest energy vibrational modes of a chemical compound will lie within the range of 400 to 4000 cm^{-1}, a spectral region of the electromagnetic spectrum denoted as the mid-infrared. Transitions among states associated with these vibrational modes can be observed directly through their absorbance in the mid-infrared region of the spectrum, or alternatively through an inelastic scattering of incident energy via the Raman effect. Transitions involving the excitation of multiple vibrational states are known as overtone bands or combination bands, and these are observed in the near-infrared (NIR) region of the spectrum (4000–13,350 cm^{-1}).

Infrared absorption spectroscopy is an enormously useful technique for the physical characterization of solids having pharmaceutical interest. When the crystallography of a given molecule sufficiently perturb the frequencies of vibrational modes relative to the energies of the modes for a free molecule, one can use changes in the spectra as a means to study the solid-state chemistry of the system. For example, being especially sensitive to changes in molecular conformation between different solid-state forms, infrared absorption spectra are frequently used to evaluate the polymorphic space of a drug substance system. In addition, the technology can be very useful in studies of solvent molecules contained within a solvatomorph.

The vibrational energy levels of a molecule in its solid form can also be evaluated using Raman spectroscopy. Because most compounds of pharmaceutical interest are characterized by low or no molecular symmetry, the same bands observed in the infrared absorption spectrum will also be observed in the Raman spectrum. However, the fundamentally different nature of the selection rules associated with the Raman effect leads to the existence of significant differences in intensity among peaks as measured by the two methods. In general, symmetric

vibrations and non-polar groups yield the most intense Raman scattering bands, whereas antisymmetric vibrations and polar groups yield the most intense infrared absorption bands.

The spectral features observed in the NIR region of the electromagnetic spectrum are associated with overtones and combinations of the same fundamental bands detected in infrared absorption or Raman spectroscopies. Some of the spectral features that have found the greatest utility are those functional groups that contain unique hydrogen atoms. For example, studies of water in solids can be easily performed through systematic characterization of the characteristic –OH band, usually observed around 5170 cm^{-1}. The determination of hydrate species in an anhydrous matrix can also be easily performed using near-IR analysis.

In this chapter, a brief overview of the necessary theoretical bases for all three types of vibrational spectroscopy will be presented, and it should be noted that more extensive details regarding molecular spectroscopy (2–6) and vibrational spectroscopy (7–17) are available. The utility of vibrational spectroscopy in the physical characterization of pharmaceutical compounds has been reviewed many times (18–32).

Motion of Atoms in Molecules

Because all forms of vibrational spectroscopy have their origin in the patterns of motion executed by the atoms and groups in the molecule, it is clear that the energies associated with these motions provide the basis to an understanding of the observed spectra. Consequently, it is appropriate to briefly consider the nature of these motions, and the manner in which energy can become distributed among the various modes. For this part of the discussion, the perturbing effects of other molecules in a condensed state will not be considered, but instead, only the state of a molecule will be considered, which is essentially free to move through space. The perturbing effects of the solid state on the vibrational properties of the component molecule in a crystal will be the focus of illustrative examples.

The number of degrees of freedom that any body may possess is related to the number of independent coordinates that are needed to specify its position in space. For instance, a sphere that is able to move randomly in space would require the specification of all three of the Cartesian coordinates (X, Y, and Z) to define its position. One therefore states that this free object has three degrees of freedom. However, if the object were constrained to move only in the XY-plane, then the value of the Z-coordinate would be fixed and only the X and Y coordinates would have to be specified during the motion. In that case, the object would have only two degrees of freedom. If it is further required that the object move along a line in this plane, then one would only have to specify the coordinate along which the object moved (i.e., one degree of freedom).

If one now considers a molecule consisting of N atoms, it is clear that one must specify the three X, Y, and Z coordinates for each atom, and therefore, the total number of degrees of freedom possible for this molecule would be equal to $3N$. At the same time, the atoms in the molecule are bound, and this bonding will affect how the $3N$ degrees of freedom would be distributed among the different types of motion available to the molecule. In a molecule, each atom is not free to move independently of the others, but instead, the molecule must translate and rotate as a whole. For non-linear molecules, three degrees of freedom are associated with translational motion, and three more degrees of freedom are associated with

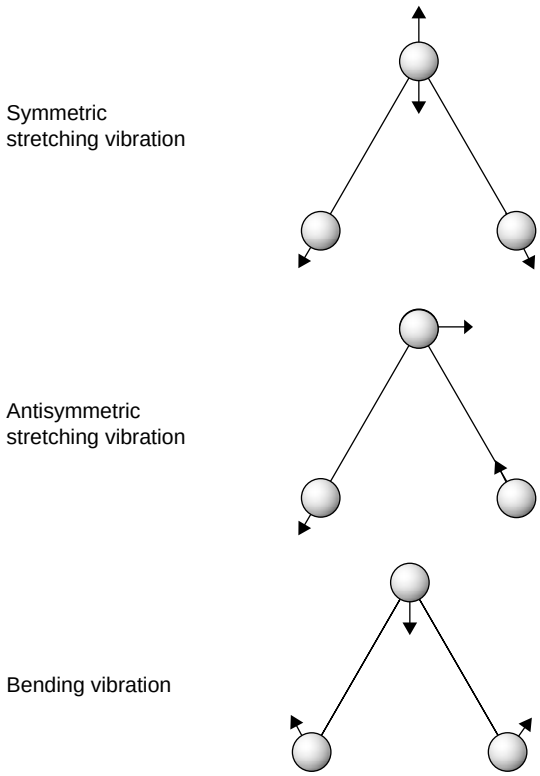

FIGURE 1 Motions of the atoms in each of the genuine vibrational modes of a nonlinear triatomic molecule.

rotational motion, so for polyatomic molecules consisting of N atoms, there will be $(3N - 6)$ degrees of freedom due to the various types of internal motion known as the vibrational modes.

Consider the case of a non-linear triatomic molecule, for which the number of authentic vibrations will therefore equal [3(3) – 6]. The three normal vibrational modes of motion are illustrated in Figure 1. To preserve the pure vibrational nature of the symmetric stretching motion, the central atom must move an equal amount in the direction opposite to the motion of the end atoms, so that the net result of the simultaneous motions of the end and central atoms is a symmetric stretching of the bonds. The atomic motions for the asymmetric stretching vibration gives rise to a compression of one bond and a stretching of the other bond, whereas the atomic motions for the bending vibration yield an opening and closing of the bond angle.

The Harmonic Oscillator Model and Spectroscopy Associated with Fundamental Vibrational Modes

A full understanding of vibrational spectroscopy requires a solution of the wave functions associated with vibrational motion, which are usually developed as quantum

mechanical expressions independent of the expressions for electronic motion. For a simple diatomic molecule, the Hamiltonian operator for nuclear motion is given by the sum of the kinetic and the potential energy operators, and so the Schrödinger equation for nuclear motion can be written as:

$$\{T_N + V(r)\}\boldsymbol{\psi} = E\boldsymbol{\psi} \tag{1}$$

where T_N is the kinetic energy operator, $V(r)$ is the potential energy function, and it is understood that $\boldsymbol{\psi}$ is the wave function for nuclear motion. For the diatomic molecule A-B, equation (1) becomes:

$$\frac{1}{m_A}\nabla_A{}^2\boldsymbol{\psi} + \frac{1}{m_B}\nabla_B{}^2\boldsymbol{\psi} + \frac{2}{\hbar^2}\{E - V(r)\}\boldsymbol{\psi} = 0 \tag{2}$$

where m_A and m_B are the masses of the two atoms comprising the molecule.

After elimination of terms associated with translation of the nuclei, the motion of the atoms is determined by the effect of the potential field directed along the internuclear axis. Mathematically, this situation is equivalent to that of a single particle moving in the field defined by $V(r)$, where the mass of this equivalent particle is given by the reduced mass (μ) of the two atoms:

$$\mu = \frac{m_A m_B}{m_A + m_B} \tag{3}$$

The wave equation now becomes:

$$\nabla^2\boldsymbol{\psi} + \frac{2\mu}{\hbar^2}\{E - V(r)\}\boldsymbol{\psi} = 0 \tag{4}$$

After the wave function is transformed into spherical polar coordinates, it can be factored into radial and angular functions that each consist of a single variable. The usual procedure is to define the radial distribution function, $\mathbf{S}(r)$, and after much work the radial portion of the wave equation becomes:

$$\frac{\mathrm{d}\mathbf{S}}{\mathrm{d}r^2} + \frac{2\mu}{\hbar^2}\{E - V(r)\}\mathbf{S} = 0 \tag{5}$$

Equation (5) cannot be considered further until one chooses a form for the potential function, but highly useful solutions are obtained if $V(r)$ is assumed to have the form associated with simple harmonic motion:

$$V(r) = \tfrac{1}{2}\, k\, r^2 \tag{6}$$

In equation (6), k is the force constant associated with the magnitude of the restoring force on the particle.

The mathematical solution to the harmonic oscillator wave function is beyond the scope of this chapter, but has been amply described in numerous texts on quantum mechanics (33–37). At the end of the process, one obtains expressions for the energies (E_V) of the vibrational wave functions that are functions of the reduced mass, the bond force constant, and a quantum number v for each wave function:

$$E_V = \eta\,\{k/\mu\}^{1/2}\,(v + \tfrac{1}{2}) \tag{7}$$

Because the classical vibrational frequency (υ_{OSC}) of a harmonic oscillator is:

$$\upsilon_{OSC} = (1/2\pi)\ \{\ k\ /\mu\ \}^{½} \tag{8}$$

it follows that the energies (in units of ergs) of the vibrational states are also equal to:

$$E_V = h\ \upsilon_{OSC}\ (v\ + ½) \tag{9}$$

It is more typical to express the energy of a given vibrational state in units of reciprocal centimeters (cm^{-1}), which is obtained by dividing equation (9) by the speed of light:

$$G_V = \frac{h\ \upsilon_{OSC}}{c}(v + ½) \tag{10}$$

Defining the oscillator energy as ω (in units of cm^{-1}), one obtains the expression:

$$G_V = \omega\ (v\ + ½) \tag{11}$$

For most molecules, ω will have values in the range of 200 to 4000 cm^{-1}.

In order for a molecule to absorb infrared energy to promote the system from the ground $E(v = 0)$ ground state to an excited $E(v \neq 0)$ excited states, the molecule must possess a permanent dipole moment. The intensity of this electric dipole transition is determined by the magnitude of the transition probability, $\mathbf{P}_{ij}$, which is calculated from the lower vibrational state ($\mathbf{S}_i$) to the upper vibrational state ($\mathbf{S}_j$):

$$\mathbf{P}_{ij} = \int S_i \boldsymbol{\mu} \mathbf{S}_j d\tau \tag{12}$$

For a molecule having a permanent dipole moment, it can be shown that equation (12) will equal zero unless the following harmonic oscillator selection rule is met:

$$\Delta v = \pm 1 \tag{13}$$

The energetics of vibrational energy levels is such that the ground vibrational state of a given molecule will be characterized by $v = 0$. The implication of the harmonic oscillator selection rule is that the only allowed vibrational transition would be $\mathbf{S}_0 \rightarrow \mathbf{S}_1$, which is known as the *fundamental* vibrational transition. In the harmonic oscillator model, transitions from $\mathbf{S}_0$ to higher excited states $\mathbf{S}_V$ are forbidden.

In the harmonic oscillator model, therefore, the energy of the $E(v = 0)$ state is given by:

$$E_0 = \frac{\hbar}{2}\{k/\mu\}^{½} \tag{14}$$

and the energy of the $E(v = 1)$ state is given by:

$$E_1 = \frac{3\hbar}{2}\{k/\mu\}^{½} \tag{15}$$

Therefore, energy of the ($v = 0$) → ($v = 1$) transition is given by:

$$E_1 - E_0 = \hbar \{k/\mu\}^{1/2} \tag{16}$$

or:

$$G_1 - G_0 = \omega \tag{17}$$

According to equation (17), the energy of a vibrational transition may be seen to be partially defined by the magnitude of the force constant (which is interpreted as a measure of the bond strength). In particular, it can be shown that one can calculate a value for the force constant of a harmonic oscillator using the relation:

$$k = \mu(4\pi^2\omega^2c^2) \tag{18}$$

where the reduced mass μ is give in units of grams/molecule, ω is in units of cm^{-1}, and the speed of light c equals 2.9979246×10^{10} cm/sec.

The energy of a vibrational transition is also dependent on the reduced mass of the atoms involved in the vibrational motion. Using the average bond stretching force constants of Wilson, Decius, and Cross [p. 175 of Ref. (17)], and the relation:

$$\omega = \frac{\{k/\mu\}^{1/2}}{2\pi c} \tag{19}$$

it is possible to calculate the transition energies for the fundamental vibrational transitions of some chemically relevant bond types. For instance, the energy of the C–H stretching mode is calculated to be 3444 cm^{-1}, and the energy of the C–C stretching mode is calculated to be 1189 cm^{-1}. In addition, the energy of the N–H stretching mode is calculated to be 3425 cm^{-1}, and the energy of the N–N stretching mode is calculated to be 1044 cm^{-1}. Finally, the energy of the O–H stretching mode is calculated to be 3737 cm^{-1}, and the energy of the C–C stretching mode is calculated to be 950 cm^{-1}.

From this analysis, the general trend emerges that the stretching frequencies of molecules containing a hydrogen atom will be much higher than the stretching frequencies of molecules that do not contain a hydrogen atom. The spectroscopic consequence of this trend (which will be developed further in forthcoming sections) is that vibrational transitions associated with atom–hydrogen stretching modes will be observed at much higher energies than will be the transitions of other functional groups.

Even for polyatomic molecules, the harmonic oscillator model can be adequately used to describe their fundamental vibrational transitions, because the vibrational spectra of complicated molecules can often be assumed to be summations of a number of harmonic oscillators. The concept of group frequencies is based on the fact that many vibrational wave functions are be essentially localized on the atoms of a functional group and its nearest neighbors. Because the bond force constants are fairly constant from molecule to molecule, and because the reduced masses often are comparable as well, it follows that the vibrational frequency of a given functional group is determined primarily by the identity of the atoms

involved. This concept has led to the concept of *group frequencies*, which have been summarized in several monographs (38–40).

Returning to the example of the non-linear triatomic molecule exhibiting three modes of vibration, the symmetric stretching mode will be identified as (ν_1, the "scissors" bending mode as ν_2, and the anti-symmetric stretching mode as ν_3. Because the individual vibrational modes are independent of each other, the vibrational wave function describing the states of this non-linear triatomic molecule will be:

$$\psi\ (\nu_1, \nu_2, \nu_3) = \psi(\nu_1)\psi(\nu_2)\psi(\nu_3) \tag{20}$$

The ground state of this non-linear triatomic molecule will be characterized by $\psi(\nu_1)$, $\psi(\nu_2)$, and $\psi(\nu_3)$ each being in their respective $v = 0$ states, and its wave function will be abbreviated as ψ_{000}. The lowest energy excited states will be characterized by two of the $\psi(\nu_1)$, $\psi(\nu_2)$, or $\psi(\nu_3)$ functions each being in the $v = 0$ state and the third function being in the $v = 1$ state. These three possible excited states would be identified by the functions ψ_{100}, ψ_{010}, and ψ_{001}.

Because the harmonic oscillator selection rule is $\Delta v = \pm 1$, it follows that the only possible fundamental vibrational spectroscopic transitions for the non-linear triatomic molecule water are:

$$\psi_{000} \rightarrow \psi_{100} \text{ (the } \nu_1 \text{ mode)} \tag{21}$$

$$\psi_{000} \rightarrow \psi_{010} \text{ (the } \nu_2 \text{ mode)} \tag{22}$$

$$\psi_{000} \rightarrow \psi_{001} \text{ (the } \nu_3 \text{ mode)} \tag{23}$$

For water in the gas phase, it has been found that the energy of the ν_1 vibrational mode equals 3652 cm^{-1}, the energy of the ν_2 mode equals 3756 cm^{-1}, and the energy of the ν_3 mode equals 1545 cm^{-1}. However, as shown in Figure 2, in bulk water these frequencies are substantially shifted to 1634, 3262, and 3341 cm^{-1}, respectively, owing to the extensive degree of hydrogen bonding.

The Anharmonic Oscillator Model and Spectroscopy Associated with Overtones and Combinations of Fundamental Vibrational Modes

Because the harmonic oscillator selection rule states that only transitions for which $\Delta v = \pm 1$ are allowed, and because, the majority of molecules will be in the $v = 0$ state at room temperature, only fundamental transitions can be observed in either the infrared absorption or Raman spectra. A more realistic description of the energy level sequence can be achieved by using potential energy functions that allow for molecular distortion in excited vibrational states. The inclusion of anharmonic effects serves to weaken the $\Delta v = \pm 1$ selection rule, and permits transitions to higher quantum states. The development of appropriate technology has permitted the development of a wide variety of applications in the pharmaceutical and other industries.

The most widely used anharmonic potential energy function is the Morse potential:

$$V(r) = D_e[1 - e^{-a(r - re)}]^2 \tag{24}$$

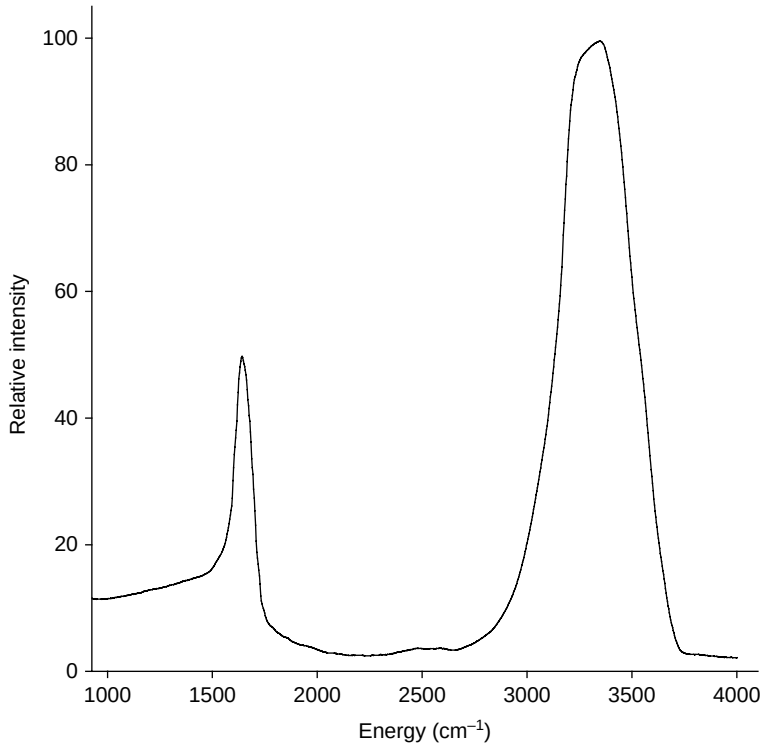

FIGURE 2 Infrared absorption spectrum of bulk water, obtained using the attenuated total reflectance sampling mode.

where D_e is the energy required to dissociate the bond. The rigorous approach would then be to substitute this form for the potential energy function back into the Hamiltonian equation, and to then solve the resulting Schrödinger equation in the usual manner. However, this approach is not trivial, and hence, more empirical approaches are usually taken.

A more practical approach toward vibrational spectroscopy is to expand the harmonic oscillator equation in an infinite power series based on $(v + ½)$ to include anharmonic effects:

$$G'_{\mathrm{V}} = \omega_e(v + ½) - \omega_e X_e(v + ½)^2 + \omega_e Y_e(v + ½)^3 + ... \tag{25}$$

where ω_e is the harmonic oscillator constant, and where X_e and Y_e are anharmonic constants. The dissociation energy is given by the sum:

$$D_e = \sum \Delta\, G'(v + ½) \tag{26}$$

where the summation is performed over the range of $v = 0$ to the highest vibrational level for which the bond in the molecule is still intact. Usually the $\omega_e X_e$ term is

considerably larger than the $\omega_e Y_e$ term, and thus most experimentally determined vibrational spectra can be fitted to the simplified equation:

$$G'_V = \omega_e(v + ½) - \omega_e X_e(v + ½)^2 \tag{27}$$

For most molecules, the $\omega_e X_e$ term will be positive in character, so the separation between successively higher excited states will decrease as v increases. In this simplified model, the separation between the G'_V state and the G'_{V+1} state will be given by:

$$\Delta G'_V = \omega_e - \omega_e X_e(2v + 2) \tag{28}$$

In this simplified model of the anharmonic oscillator, the dissociation energy is given by:

$$D_e = \omega_e / 4X_e \tag{29}$$

Equation (28) indicates that progressions of experimentally observed vibrational transitions can be considered as being composed of a harmonic and an anharmonic part. But at ambient conditions the majority of molecules will be in the $v = 0$ state because the thermal energy available at 25°C is not sufficient to raise more than a few percent of molecules into the $v = 1$ state. This gives rise to the reality that for a transition from $v = 0$ to $v = 1$, the contribution from the anharmonic terms is relatively minor; therefore, fundamental transitions can be adequately treated using the harmonic oscillator model.

With the inclusion of anharmonic effects in vibrational energy states, the strict harmonic oscillator selection rule of $\Delta v = \pm 1$ becomes relaxed and transitions from the ground vibrational state to higher vibrationally excited states to gain some degree of allowedness. Because the overtone transitions can only take place through relaxation of the primary selection rule transitions, where $\Delta v = 2, 3, 4$, etc., will be less intense than the corresponding fundamental transition. Nevertheless, overtone transitions are easily detected, and are observed in the NIR region of the electromagnetic spectrum (41–45).

Returning to the non-linear triatomic molecule, once the effects of anharmonicity are factored into the transition moment calculations, almost any type of vibrational excitation becomes possible. One could observe sequences of simple *overtone* transitions, such as:

$$\Psi_{000} \rightarrow \Psi_{200}, \Psi_{300}, \Psi_{400}, \text{etc.} \tag{30}$$

$$\Psi_{000} \rightarrow \Psi_{020}, \Psi_{030}, \Psi_{040}, \text{etc.} \tag{31}$$

$$\Psi_{000} \rightarrow \Psi_{002}, \Psi_{003}, \Psi_{004}, \text{etc.} \tag{32}$$

or any one of a number of *combination* transitions, some of which can be written as:

$$\Psi_{000} \rightarrow \Psi_{110}, \Psi_{101}, \Psi_{011}, \text{etc.} \tag{33}$$

$$\Psi_{000} \rightarrow \Psi_{120}, \Psi_{201}, \Psi_{021}, \text{etc.} \tag{34}$$

TABLE 1 Overtone and Combination Vibrational Transitions of Water in the Vapor Phase

Upper State			Energy (cm^{-1})	Wavelength (nm)	Intensity
ν_1	ν_2	ν_3			
0	1	1	5,332.0	1875.5	Medium
0	2	1	6,874.0	1454.8	Weak
1	0	1	7,251.6	1379.0	Medium
1	1	1	8,807.1	1135.4	Strong
2	0	1	10,613.1	942.2	Strong
0	0	3	11,032.4	906.4	Medium
2	1	1	12,151.2	823.0	Medium
3	0	1	13,830.9	723.0	Weak
1	0	3	14,318.8	698.4	Weak

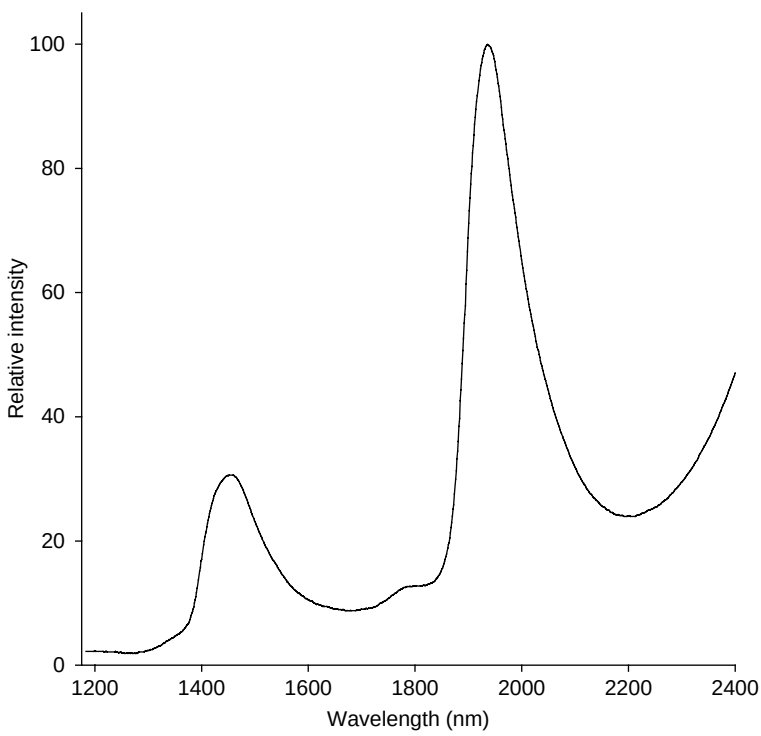

FIGURE 3 NIR absorption spectrum of bulk water, obtained using the reflectance sampling mode.

A summary of the overtone and combination bands of water in the vapor phase is given in Table 1, and a portion of its liquid phase absorption spectrum is shown in Figure 3. For bulk water, the moderate band observed at 1455 nm can be assigned to the $\psi_{000} \rightarrow \psi_{101}$ transition, the weak band at 1806 nm can be assigned to the $\psi_{000} \rightarrow \psi_{021}$ transition, and the strong band at 1936 nm can be assigned to the $\psi_{000} \rightarrow \psi_{011}$ transition.

INFRARED ABSORPTION SPECTROSCOPY FOR THE CHARACTERIZATION OF POLYMORPHS AND SOLVATOMORPHS

The acquisition of high-quality infrared spectra on solid materials has been made possible using Fourier transform technology, because the use of this methodology minimizes transmission and beam attenuation problems. Essentially all FTIR spectrometers use a Michelson interferometer, where infrared radiation entering the interferometer is split into two beams: one of which follows a path of fixed distance before being reflected back into the beam splitter, and the other traveling a variable distance before being recombined with the first beam. The recombination of these two beams yields an interference pattern, where the time-dependent constructive and destructive interferences have the effect of forming a cosine signal. Each component wavelength of the source yields a unique cosine wave, having a maximum at the zero pathlength difference (ZPD) and which decays with increasing distance from the ZPD. The radiation in the central image of the interference pattern impinges on the detector, and intensity variations in the recombined beam become measurable manifest as phase differences. If the component cosine waves can be resolved, then the contribution from individual wavelengths can be observed. The frequency domain spectrum is obtained from the interferogram by performing the Fourier transformation mathematical operation. More detailed descriptions of the components of a FTIR spectrophotometer are available (46–48).

Numerous modes of sampling may be used with FTIR spectrophotometers, although only a few of these are appropriate for the study of polymorphs and solvatomorphs. The classic alkali halide pellet method is probably the least useful for this type of work, as the sample may under so a solid-state transformation due to the pressure used to form the pellet, or one may encounter halide exchange between the KBr or KCl matrix and the sample (49). The use of mineral oil mulls avoids the problems noted for the pellet technique, but the mineral oil itself exhibits a number of intense absorption bands (2952, 2923, 2853, 1458, and 1376 cm^{-1}) that may overlap important absorption bands associated with the sample and obscure important spectral regions. Use of diffuse reflectance sampling avoids all of the problems just mentioned (50,51), but usually requires dilution of the analyte with either KBr or KCl at a level of 1% to 5% w/w. The diffuse reflectance technique lends itself to studies of polymorphic composition because it is non-invasive, its use causes no changes in polymorph character due to its inherent limited sample handling, and the technique can be used for quantitative purposes.

Probably the most useful sampling method for the study of polymorphs and solvatomorphs uses attenuated total reflectance accessories (52,53). In the ATR technique, infrared radiation is passed through a crystal at an angle less than the critical angle, which causes the light to undergo total internal reflection. At each such reflection, the radiation penetrates a small distance beyond the crystal surface, and if an analyte is in physical contact with the crystal, then the internally reflected

energy will be attenuated at those frequencies corresponding to changes in molecular vibrational states. The advantage of the ATR approach is that it requires effectively no sample preparation, because one simply clamps the analyte onto the surface of the crystal with moderate pressure to ensure a sufficient degree of optical contact. Because the internal reflectance process does not permit the infrared beam to pass very deeply into the sample, it is typical to determine the composition of an analyte up to a sampling depth in the range of 5 to 10 μm.

Not surprisingly, the sensitivity of infrared absorption spectroscopy to subtle changes in crystal structure have led to its application in a wide variety of investigations of polymorphic solids, often in conjunction with Raman spectroscopic studies. For example, FTIR spectra of different polymorphs of mepivacaine hydrochloride were obtained in Nujol mulls and via ATR sampling, with the ATR method providing better distinction between the polymorphs (54). This has been illustrated in Figure 4, where the infrared absorption spectra of mepivacaine hydrochloride (Form-II) is seen to be superior when obtained using the attenuated total reflectance

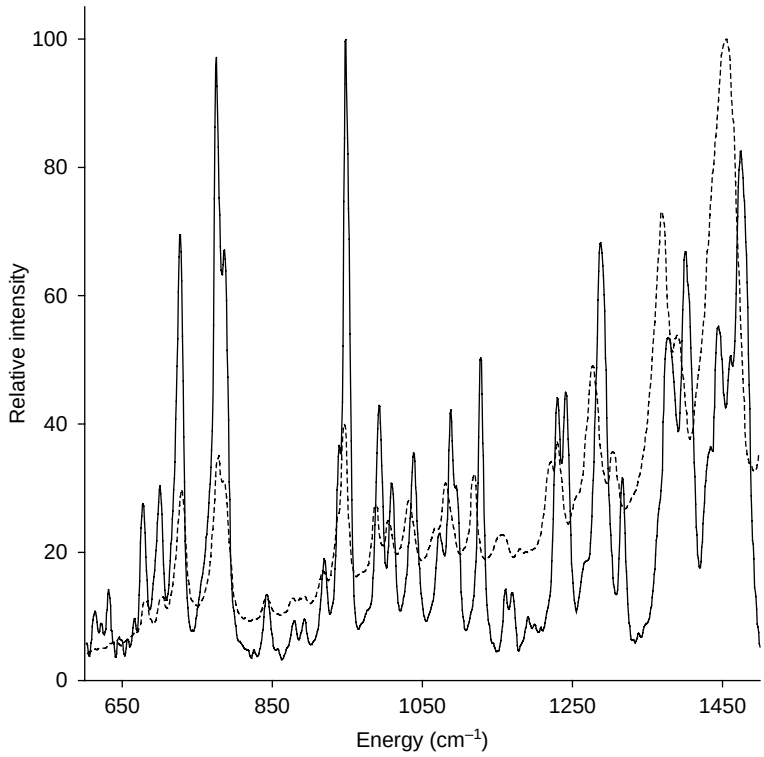

FIGURE 4 Infrared absorption spectra of mepivacaine hydrochloride, Form-II, obtained using the attenuated total reflectance (*solid trace*) and Nujol mull (*dashed trace*) sampling modes. Each spectrum has been normalized so that the relative intensity of the most intense band equals 100%, and the normalized spectra were generated from data given in Ref. (54).

sampling mode as opposed to a Nujol mull. When coupled with artificial neural network methods, a diffuse reflectance FTIR spectroscopic method was developed that permitted the simultaneous quantification of three polymorphs of carbamazepine in ternary mixtures (55).

FTIR–ATR spectroscopy was used to characterize the salt-induced crystallization of a metastable polymorph of flufenamic acid, and to characterize the product obtained after a subsequent interface-mediated polymorphic transition (56). The FTIR–ATR method was also used to characterize the fluconazole products obtained using the supercritical antisolvent process, with the technique being able to identify the polymorphic forms produced as a result of variation of operating conditions such as temperature, pressure, and solvent type (57). Three concomitant polymorphs of 1,3-bis(*m*-nitrophenyl)urea had been reported in 1899 as yellow prisms (the α-form), white needles (the β-form), and yellow tablets (the γ-form), and FTIR-microscopy was used during a more detailed investigation of the system (58). In this work, complete assignments for the absorption bands associated with hydroxyl, amide, nitro, and benzene-ring functional groups were developed in order to obtain a deeper understanding of the conformational differences in the molecules constituting the various crystal forms.

Five differently colored solid-state forms of 5-methyl-2-[(2-nitrophenyl) amino]-3-thiophenecarbonitrile, where the color of the polymorphic crystal forms is related to changes in the energies of molecular orbitals of the systems have been studied using infrared absorption spectroscopy (59). The spectra for three of the solid-state forms were characterized by frequency shifts originating from the structural differences, with the nitrile stretching frequency varying by approximately $10\,cm^{-1}$ each for the yellow, orange, and red solid-state forms of the compound. In a study of the amorphous salt formed by the co-precipitation of cimetidine and diflunisal, solid-state infrared absorption spectroscopy was used to prove the existence of the salt species (60). The prominent carbonyl absorption band observed at $1650\,cm^{-1}$ in crystalline diflunisal could not be observed in the spectrum of the amorphous salt, but a new peak was noted at $1580\,cm^{-1}$ that was assigned to an asymmetric stretching mode of a carboxylate group.

Diffuse reflectance sampling was used to study the anhydrates and hydrates of ampicillin and nitrofurantoin, with the presence of water in the hydrate crystal forms causing new bands to appear in the infrared absorption spectrum (61). On the other hand, FTIR spectroscopy was not useful in distinguishing between the hydrate forms of diclofenac sodium as the frequencies in the spectra of the polymorphic tetrahydrates were nearly identical, and only differed in band relative intensities (62). The utility of combined FTIR and solid-state ^{13}C nuclear magnetic resonance studies enabled the deduction that although the water molecules of topotecan hydrochloride trihydrate were intrinsic parts of the crystal lattice, the pentahydrate possessed additional structural channels where water could hydrogen bond to specific portions of the topotecan molecules (63).

Fluconazole has been isolated in a number of solvated and non-solvated forms, and infrared spectroscopy has proven to be an important tool in the characterization of these. In one study involving two non-solvated polymorphs (Forms I and II) and several solvatomorphs (the ¼-acetone solvate, a 1/7-benzene solvate, and a monohydrate), the infrared spectra of the different forms showed differentiation in bands associated with the triazole and 2,4-difluorobenzyl groups, and in the propane backbone (64). In another study, the diagnostic infrared spectral

characteristics of non-solvated Form-III and two solvatomorphs (the ¼-ethyl acetate solvate, and a monohydrate) were used to demonstrate the novelty of the new forms relative to those in the literature (65). In yet another work, the kinetics associated with the dehydration and desolvation of fluconazole solvatomorphs were studied by three physical methods, and then used to understand the mechanisms of the processes involved (66).

It has been found that the carbonyl frequency of niclosamide anhydrate and two of its monohydrates was particularly sensitive to the crystal form of the drug substance, and hence, infrared spectroscopy could be used to demonstrate the conformational state of the compound in the solvatomorphs (67). Similarly, infrared spectra obtained in the fingerprint and high-frequency regions for four non-solvated polymorphs of tenoxicam, and of its acetonitrile, dioxane, dimethyl formamide, ethyl acetate, acetone, and isopropanol solvates, facilitated a differentiation between the various crystal forms (68). A combination of thermogravimetric analysis and infrared absorption spectroscopy was used to develop a quantitative method for the determination of pantoprazole sodium monohydrate in bulk quantities of the sesquihydrate solvatomorph (69).

Because the pattern of vibrational modes is usually sufficiently perturbed by crystallographic differences, infrared absorption spectroscopy can be profitably used to study the phase transformation process between polymorphic forms of a substance. For example, infrared absorption spectroscopy has been used to study the solution-mediated phase transformation of metastable β-glycine to the stable α-phase, making use of disappearance of the weak band at 1660 cm^{-1} and shifts in energy for the anti-symmetric stretch of the carboxyl group (1580–1590 cm^{-1}), the deformation of the NH_3^+ group (1515–1500 cm^{-1}), and the O–C=O group bend (around 700 cm^{-1}) (70). In another work, characteristic absorption bands around 1145 to 1165 cm^{-1} were found to be useful in understanding the effect of experimental variables on the solution-mediated Form-II to Form-I phase transformation of buspirone hydrochloride (71).

Infrared spectroscopy has been used to follow the isothermal transformation of mefenamic acid Form-I into Form-II at a sufficient number of temperatures so as to calculate the activation energy for the process (72). The value of 71.6 kcal/mol, obtained using the infrared spectroscopic method, was significantly smaller than the previously reported value of 86.4 kcal/mol that had been determined using of differential scanning calorimetry. Conventional FTIR spectroscopy in conjunction with FTIR micro-spectroscopy has been used to study the polymorphic interconversion of famotidine metastable Form-B into stable Form-A during grinding in a ceramic mortar (73). The particle size reduction that resulted from the grinding process was also found to lead a decrease in the transition temperature for the Form-B to Form-A phase transformation.

Changes in infrared absorption spectra have also been used to study the phase transformation process between solvatomorphs. For example, granulation of anhydrous lactose with water results in conversion of the anhydrate phase to the monohydrate phase, as well as a change from the β-anomer to the α-anomer. Figure 5 shows the FTIR–ATR spectra obtained in the high-frequency region for different stages in the solution-mediated conversion of lactose anhydrate to lactose monohydrate phase of lactose monohydrate, where it is clear that the absorbance band at 3522 cm^{-1} could be used to follow the kinetics of formation of the monohydrate (74).

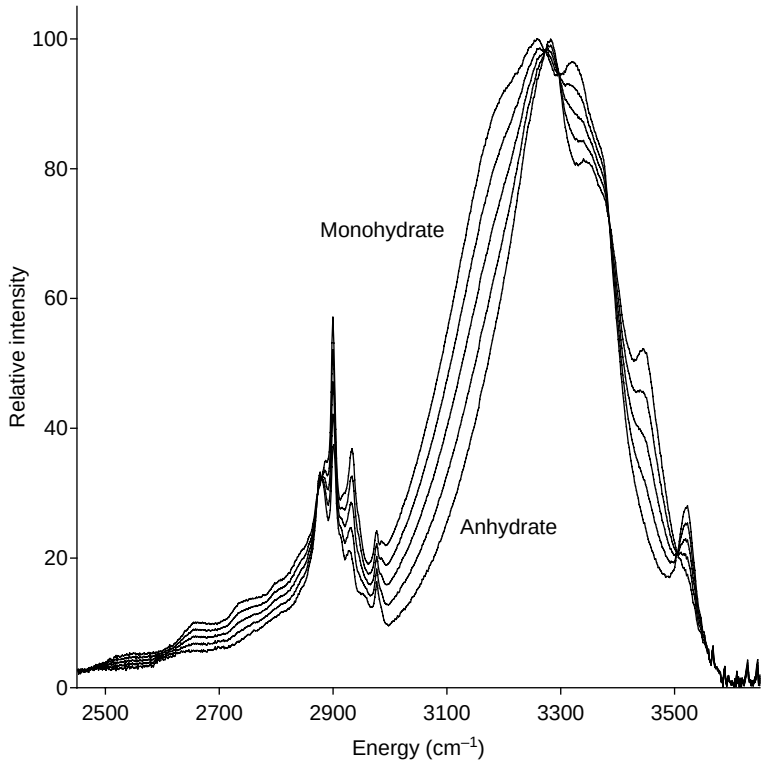

FIGURE 5 FTIR–ATR spectra obtained in the high-frequency region of lactose anhydrate (*lowest trace*), and during various stages of its solution-mediated phase transformation into the monohydrate phase (*uppermost trace*). H.G. Brittain, unpublished results (70).

Trehalose dihydrate undergoes a dehydration transition around 100°C, and the infrared spectra obtained during this process were found to change significantly over the 1500 to 1800 cm^{-1} region (75). For example, the band intensities at 1640 and 1687 cm^{-1} decreased sharply around 65°C, but remained relatively constant at higher temperatures. During the rehydration process where trehalose anhydrate became trehalose dihydrate, the liquid-like water became solid-like water over the same temperature range. It was postulated that this phase transition could be related to the protective effect of trehalose in preserving protein stability.

NIR SPECTROSCOPY FOR THE CHARACTERIZATION OF POLYMORPHS AND SOLVATOMORPHS

Because the energy separation of the ground vibrational state and the lowest vibrational excited states is large relative to kT at room temperature, molecules at ambient temperature will reside almost entirely in their ground vibrational states. According to the harmonic oscillator selection rule of $\Delta v = \pm 1$, only the fundamental vibrational transitions that are studied by ordinary infrared absorption spectroscopy

or Raman spectroscopy will be allowed. As long as the harmonic oscillator selection rules can be considered as being valid, vibrational transitions corresponding to $\Delta v = \pm 2$, $\Delta v = \pm 3$, $\Delta v = \pm 4$, etc., or combinations of these, are not allowed.

However, the harmonic oscillator model should be considered as being the first term in a solution of the vibrational Hamiltonian equation where the potential term can also include anharmonic effects. As discussed above, the strict $\Delta v = \pm 1$ selection rule can be relaxed by the inclusion of anharmonicity, and the relaxation of this fundamental selection rule enables the observation of transitions from the ground vibrational state to higher vibrationally excited states. However, because the fundamental selection rule is merely relaxed and not broken, these overtone transitions will generally be less intense than their fundamental transition.

The NIR region of the spectrum is generally considered to span 750 nm (13,350 cm^{-1}) to 2500 nm (4000 cm^{-1}). Through the design of appropriate instrumentation, the overtone and combination transitions can be detected and quantitated, with these being observed in the NIR region of the spectrum (76–83). In general, the spectral features of greatest utility entail overtone transitions associated with functional groups that contain unique hydrogen atoms. For example, NIR spectroscopy has been successfully used to develop methods for moisture determination, whole tablet assay, and powder blending (84–87). Owing to the usually broad nature of the absorption bands, the raw spectra themselves tend not to be most useful in the study of polymorphs and solvatomorphs, but when the spectra are differentiated and the resulting derivative spectra combined with multi-component analysis, real analytical utility emerges.

NIR spectroscopy has been shown to be capable of differentiating between polymorphs of sulfathiazole and sulfamethoxazole, as well as hydrates of ampicillin and lactose (88). For example, the raw absorption spectra of sulfathiazole Form-I and Form-III are shown in Figure 6 along with their corresponding second derivative spectra. It is evident that use of the derivative spectra eliminates the sloping baseline of the raw absorption spectra, readily identifying bands at 1376 and 1528 nm that were useful in differentiating between the polymorphic forms. These spectra differences were exploited to develop a quantitative analytical method for determination of the amount of Form-III in Form-I that was characterized by recovery errors less than 3%.

Although NIR spectroscopy can definitely be used as a means of polymorph identification, its real power lies in the ability of workers to readily develop quantitative assays for phase composition. The quantification of sulfathiazole Form-I and Form-III in binary mixtures was addressed in another work, here using univariate, multiple linear regression, and partial least-squares regression methods to generate the validation set (89). Quantitative methods for the two polymorphs of bicifadine hydrochloride have been developed using differential scanning calorimetry coupled with thermogravimetric analysis, X-ray powder diffraction, infrared absorption spectroscopy, and NIR spectroscopy, with the NIR methods being found to yield the best accuracy and ease of operation (90). The utility of Raman and NIR spectroscopies combined with multivariate analysis for the quantitation of ternary mixtures of α-, γ-, and amorphous indomethacin was investigated, with comparable root-mean-square errors of prediction being obtained for the two methods (91).

Distinctions between the solvated and non-solvated forms of a drug substance are often easy to detect using NIR spectroscopy, making the technique a valuable part of a multi-disciplinary study such as that carried out on the baclofen anhydrate

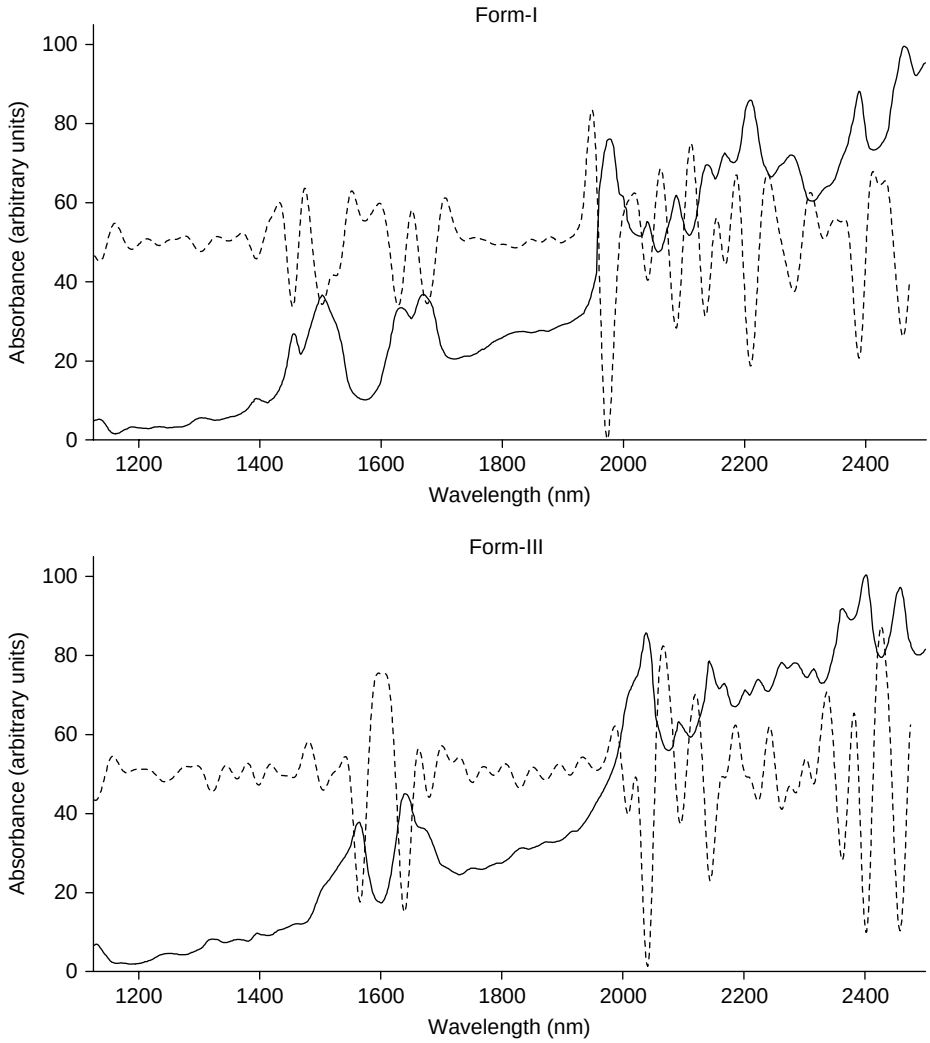

FIGURE 6 NIR spectra obtained for sulfathiazole Form-I (*upper spectra*) and Form-III), showing both the raw absorption spectrum (*solid traces*) and the corresponding second derivative spectrum (*dashed traces*) for each. The spectra are shown in arbitrary units, and have been adapted from Ref. (88).

and monohydrate (92). The factors associated with the quantitative analysis of anhydrate/hydrate powder mixtures have been discussed (93), and these issues illustrated in work establishing the phase boundaries in the anhydrate/hydrate system of caffeine (94). The interconversion between the anhydrate, monohydrate, and dihydrate forms of azithromycin have been studied, with the spectral region associated with the first overtone of water (1800–2200 nm) being most useful (95). In another work, the monohydrate/dihydrate composition of magnesium

stearate samples was established using NIR spectroscopy and multivariate calibration (96).

NIR spectroscopy was used to monitor the degree of conversion between the stable Form-A of a new chemical entity and the metastable Form-B produced at the elevated temperature and humidity conditions of its wet granulation (97). Because a reference method was not available for quantitation of Form-B in bulk quantities of Form-A, a calibration set was developed from the NIR spectra of the drug substance, the premix blend, and wet granulated samples, because narrow spectral regions unique to Form-B were found that were insensitive to differences in physical properties between the premix blend and wet granulation. The final univariate method was used for either for off-line, or for on-line, monitoring of phase conversion during the wet granulation process.

In-line NIR spectroscopy was used to demonstrate that the process-induced transformation of erythromycin A dihydrate to its dehydrated form did not take place easily during pellet manufacture via extrusion/spheronization and drying, although partial phase transformation was noted for pellets dried at 60°C (98). NIR spectroscopy was one of several techniques used to obtain quantitative determinations of phase compositions of a developmental compound in its bulk drug substance and in compressed tablets, with a partial least-squares regression algorithm being used to obtain good multivariate calibration (99).

TERAHERTZ SPECTROSCOPY FOR THE CHARACTERIZATION OF POLYMORPHS AND SOLVATOMORPHS

The ability to acquire absorption spectra in the far-infrared region of the spectrum (10–450 cm^{-1}) became much easier to obtain when dispersive technology was replaced by Fourier transform methodology. Initial applications of far-infrared spectroscopy included studies of pure rotational spectra, skeletal bending modes, molecular motion in four-, five-, six, and seven-membered rings, torsional vibrations, vibrational modes involving heavy atoms, and weak intermolecular interactions (100). Other investigational work involved studies of organic crystalline solids, where the translational and librational modes of molecular crystals below 250 cm^{-1} could be evaluated. In one such study, the four lattice modes of crystalline films of elemental nitrogen and carbon monoxide at 10 K were studied over the range of 20 to 250 cm^{-1}, and it was determined that although the translational modes were moderately strong, the librational modes were weak in intensity (101).

Fairly recently, it has been recognized that the developing field of terahertz (THz) spectroscopy can also be used to study low-frequency modes that hitherto had been the domain of far-infrared spectroscopy. Because 1 THz is equivalent to 33.33 cm^{-1}, it turns out that the spectral region of interest (i.e., 3–400 cm^{-1}) corresponds to frequencies of 0.09 to 12 THz. With the development of appropriate instrumentation, the technique has been applied to the study of a wide variety of materials (102,103), and has been used to study the crystallinity of materials having pharmaceutical interest (104–106). With the introduction of the attenuated total reflectance sampling mode (107), it is anticipated that application of THz spectroscopy to the characterization of polymorphs and solvatomorphs will become even more widespread.

The incident THz radiation is obtained as femtosecond pulses that are generated by the excitation of charge carriers in a semiconductor material through the

use of ultra-short pulses of light that is higher in energy than the bandgap of the semiconductor. These pulses can be detected with an ultra-fast antenna receiver, providing simultaneous amplitude and phase information over a wide frequency range in a single measurement. It is to be noted that this type of measurement is based on frequency (in the form of the instantaneous value of the electric field itself) and not on an intensity measurement of the type that would be used during the conduct of conventional far-infrared spectroscopy. The frequency-dependent absorption coefficient and index of refraction of the analyte are obtained from the attenuation, delay, and distortion of the femtosecond THz pulse transmitted through the sample. Additional details of the different modes of measurement technology are available in the book by Dexheimer (103).

The utility of pulsed THz spectroscopy as a tool for the differentiation of the two polymorphs or ranitidine hydrochloride has been demonstrated (108). As shown in Figure 7, the THz spectra of the two crystal forms are quite different, and the authors concluded that the region around 1.10 THz (36.7 cm^{-1}) was the most useful for identification of the polymorphic form contained in tablet formulations. It was also noted that the plastic bags commonly used for drug substance storage

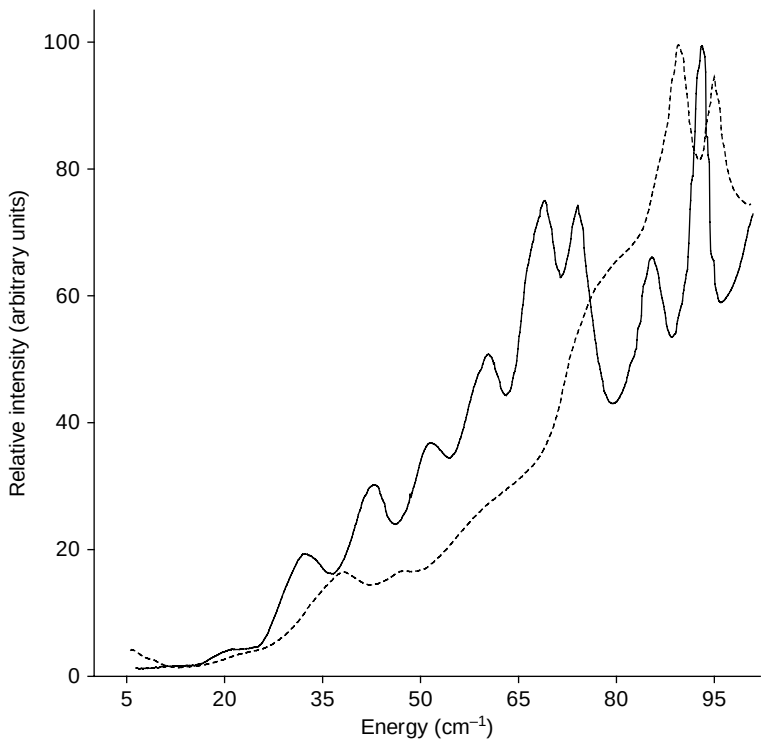

FIGURE 7 THz pulsed spectra of ranitidine hydrochloride, Form-I (*solid trace*), and Form-I (*dashed trace*). Each spectrum has been normalized so that the relative intensity of the most intense band equals 100%, and the normalized spectra were generated from data given in Ref. (104).

were transparent to THz radiation, thus making it possible to use the technology for substance identification without having to remove a sample for analysis.

The utility of pulsed THz spectroscopy for quantitative analysis of phase composition was demonstrated for various forms of carbamazepine, enalapril maleate, indomethacin, and fenoprofen calcium (109). Distinct THz spectra were measured for the various crystal forms owing to the unique patterns of lattice vibrations associated with each compound type and crystal form, and these differences were exploited to develop quantitative methods of analysis. Harmonic lattice dynamics calculations were performed on the four polymorphs of carbamazepine in order to derive assignments for the bands observed in the THz spectra, and to understand the observed trends in frequencies of similar hydrogen bond vibrations in the polymorphs (110). In fact, the sensitivity of THz spectroscopy toward differences between crystal structures has led to its inclusion as one of the identification tools in a polymorph screening study (111).

With the inclusion of a hot-stage in a THz spectrometer, acquisition of temperature-dependent spectra in real time could be used to study a variety of thermally induced phenomena. The methodology was first applied to a study of the phase transition of carbamazepine Form-III to Form-II, as well as the solid-state transformation under isothermal conditions below the melting point (112). When heated between 20°C and 160°C, the spectral features of Form-III broadened, decreased in intensity, and underwent a shift to lower energies. Further heating to 180°C led to melting of Form-III and recrystallization to Form-I, with the THz spectra reflecting the formation of the phase form. Sequences in the disappearance of Form-III spectral features, and in the appearance of Form-I features, indicated that the conversion mechanism entailed more than one step.

The far-infrared spectroscopic characteristics of five polymorphs of sulfathiazole have been studied by THz pulsed spectroscopy and thermal analysis, and then variable-temperature spectroscopic studies were conducted to monitor thermally induced phase transitions among the different forms (113). Time–domain THz spectroscopy was used to obtain the defining characteristics of two anhydrous polymorphs of theophylline and its monohydrate, and then variable-temperature studies were used to monitor phase transformations (114). Details of the phase transformation processes associated with the hydration and dehydration of theophylline have also been studied using THz pulsed spectroscopy (115).

THz time–domain spectroscopy has been used to study the anhydrous and hydrate forms of caffeine, theophylline, glucose, and ampicillin, with the aim of demonstrating the utility of this method as a process analytical tool in production and quality control (116). Crystallization and relaxation phenomena in amorphous carbamazepine have been studied using THz pulsed spectroscopy, and the technique was shown to be capable of determining glass transition temperatures (117).

Raman Spectroscopy for the Characterization of Polymorphs and Solvatomorphs

With the introduction of Fourier-transform methodology into measurement instrumentation, the use of Raman spectroscopy as a tool to solve problems having pharmaceutical interest has become widespread, and the technique is now as essential to the study of polymorphs and solvatomorphs as infrared absorption spectroscopy. Comparable to the use of attenuated total reflectance in FTIR spectroscopy, the sampling modes used in the acquisition of Raman spectra are non-destructive

in nature, and spectra can even be obtained in a non-invasive manner using fiber optics. Unlike diffuse reflectance sampling in FTIR spectroscopy, analytes are not required to be diluted with a spectroscopically inert filler before study. A number of detailed reviews are available regarding the use of Raman spectroscopy in areas of pharmaceutical interest (20–29,31,32).

When substances are irradiated with intense beams of monochromatic radiation, the majority of the photons are scattered at the same frequency as that of the incident beam (i.e., elastic or Rayleigh scattering). However, it has been found that a small amount of the incident light will also be scattered at non-resonant frequencies, some at frequencies more than and some at frequencies less than the frequency of the Rayleigh line. The differences in frequency between the incident radiation and the shifted frequencies correspond to the frequency of molecular vibrations of the molecules in the sample. The scattering peaks observed at lower frequencies relative to the Rayleigh line are known as the *Stokes* bands, and the scattering peaks observed at higher frequencies are known as the *anti-Stokes* bands. Owing to their stronger intensity, most Raman spectroscopic studies use only the Stokes peaks.

For those molecular systems having non-degenerate ground electronic states that are irradiated with intense beams of electromagnetic radiation whose energy does not permit a transition among electronic states, the theory states that the intensities of vibrational Raman transitions are determined by the matrix elements of the electronic polarizability. Therefore, only molecular transitions characterized by a change in polarizability will exhibit an allowed Raman transition. Because the magnitude of the frequency shifts of Raman bands relative to the frequency of the incident beam is determined by the energy differences of the associated vibrational states, the intensity of a given Raman band is related to the transition probability the transition, and as long as the harmonic oscillator model can be used to describe the system, the usual selection rule of $\Delta v = \pm 1$ will hold.

The intensity of scattered light will depend on the magnitude of the induced dipole moment, **P**, which can be defined in analogy with equation (12) for a transition between states *i* and *j* that are defined by the wavefunctions $\boldsymbol{\psi}_i$ and $\boldsymbol{\psi}_j$, and which is given by the matrix formed from the integrals:

$$\mathbf{P}_{ij} = \int \boldsymbol{\psi}_i \mathbf{P} \boldsymbol{\psi}_j \mathrm{d}\tau \tag{35}$$

The polarizability operator, **P**, being a matrix quantity, requires that the elements of transition moment along each of the Cartesian axes will be:

$$\mathbf{P}_X^{ij} = \mathbf{E}_X \int \boldsymbol{\psi}_i \alpha_{XX} \boldsymbol{\psi}_i \mathrm{d}\tau + \mathbf{E}_Y \int \boldsymbol{\psi}_i \alpha_{XY} \boldsymbol{\psi}_j \mathrm{d}\tau + \mathrm{E}_Z \int \boldsymbol{\psi}_i \alpha_{XZ} \boldsymbol{\psi}_j \mathrm{d}\tau \tag{36}$$

$$\mathbf{P}_Y^{ij} = \mathbf{E}_X \int \boldsymbol{\psi}_i \alpha_{YX} \boldsymbol{\psi}_j \mathrm{d}\tau + \mathbf{E}_Y \int \boldsymbol{\psi}_i \alpha_{YY} \boldsymbol{\psi}_j \mathrm{d}\tau + \mathbf{E}_Z \int \boldsymbol{\psi}_i \alpha_{YZ} \boldsymbol{\psi}_j \mathrm{d}\tau \tag{37}$$

$$\mathbf{P}_Z^{ij} = \mathbf{E}_X \int \boldsymbol{\psi}_i \alpha_{ZX} \boldsymbol{\psi}_i \mathrm{d}\tau + \mathbf{E}_Y \int \boldsymbol{\psi}_i \alpha_{ZY} \boldsymbol{\psi}_j \mathrm{d}\tau + \mathbf{E}_Z \int \boldsymbol{\psi}_i \alpha_{ZZ} \boldsymbol{\psi}_j \mathrm{d}\tau \tag{38}$$

$\mathbf{E}_X$, $\mathbf{E}_Y$, and $\mathbf{E}_Z$ are the amplitudes of the incident electromagnetic radiation along each Cartesian direction.

The three diagonal matrix elements of the transition moment ($\int \boldsymbol{\psi}_i \alpha_{XX} \boldsymbol{\psi}_i \mathrm{d}\tau$, $\int \boldsymbol{\psi}_i \alpha_{YY} \boldsymbol{\psi}_j \mathrm{d}\tau$, and $\int \boldsymbol{\psi}_i \alpha_{ZZ} \boldsymbol{\psi}_i \mathrm{d}\tau$) correspond to the Rayleigh scattering, whereas the six off-diagonal elements ($\int \boldsymbol{\psi}_i \alpha_{XY} \boldsymbol{\psi}_j \mathrm{d}\tau$, $\int \boldsymbol{\psi}_i \alpha \alpha_{XZ} \boldsymbol{\psi}_j \mathrm{d}\tau$, $\int \boldsymbol{\psi}_i \alpha_{YX} \boldsymbol{\psi}_j \mathrm{d}\tau$, $\int \boldsymbol{\psi}_i \alpha_{YZ} \boldsymbol{\psi}_j \mathrm{d}\tau$, $\int \boldsymbol{\psi}_i \alpha_{ZX} \boldsymbol{\psi}_j \mathrm{d}\tau$, and $\int \boldsymbol{\psi}_i \alpha_{ZY} \boldsymbol{\psi}_j \mathrm{d}\tau$) correspond to the Raman scattering. The $\boldsymbol{\psi}_i \rightarrow \boldsymbol{\psi}_j$ transition will be

Raman allowed if at least one of the six off-diagonal elements does not equal zero. Such determinations can be qualitatively made using symmetry-based group theory, but for low symmetry organic molecules all fundamental (i.e., $\Delta v = \pm 1$) Raman transitions will be allowed.

Although Raman spectra can be obtained using dispersive technology, the best spectra are acquired through the use of Fourier transform technology because FT-Raman systems can provide superior wavelength accuracy and minimization of any background fluorescence. In a typical system, a gas or diode laser is used to irradiate the sample, the sample is positioned in the laser beam, and the scattered radiation collected either in the 180° backscattering or the 90° right-angle configuration. The scattered photons are passed into an interferometer equipped with laser line filtering, and ultimately quantitated by a suitable detector. More detailed discussions of the spectrometer hardware can be found in the literature (13–16,118).

With appropriate collection optics, Raman spectroscopy can be performed on very small samples, with solid samples of approximately 25 to 50 mg often being merely filled into metal or glass sample holders. Samples that are darkly colored can present practical difficulties because such materials tend to absorb the exciting energy and degrade. In such cases, one must dissipate the heat, which can be accomplished by reducing the laser power or by spinning the sample to avoid the irradiation of a single point.

As in the case of infrared absorption spectroscopy, the bands in a Raman spectrum can be assigned through the use of group frequencies correlation tables. Significant insight can be obtained from the compilations of functional group vibrational frequencies associated with infrared absorption spectroscopy (38–40), but of greater utility is the compilation of group frequencies specific to Raman spectroscopy (119). Because the transition moment of a Raman transition depends on the magnitude of polarizability, it follows that the vibrational modes exhibiting the strongest intensities in a Raman spectrum will be those that are associated with functional groups that are characterized by high degrees of polarizability. Examples of such functionalities include the C–S, S–S, C–C, N=N, and C=C groups.

Although excitation of a given vibrational mode gives rise to infrared absorption bands and Raman scattering bands having identical frequencies, the fact that the infrared absorption process is an electric dipole transition and the Raman process is based on changes in polarizability leads to the observation of differences in relative spectral intensities for a given material. This is illustrated in Figure 8, where the infrared absorption and Raman spectra of racemic ibuprofen in the fingerprint region are compared (120). Most notable is the complete absence of a peak associated with the asymmetric C=O stretching mode in the Raman spectrum that is very prominent at 1707 cm^{-1} in the infrared absorption spectrum. Also noteworthy are the differing phenyl ring vibrational modes, one of which is observed at 779 cm^{-1} in the infrared absorption spectrum, and another which is observed at 827 cm^{-1} in the Raman spectrum.

As was the case for the other vibrational spectroscopic methods discussed above, Raman spectroscopy can be profitably used to study polymorphic and solvatomorphic solids when the differing crystal structures results in a perturbation of the pattern of molecular vibrations. This is often the case, but the question arises as to how different the energies of Raman peaks associated with the same group vibration in two different crystal forms should be in order to be useful. This question was addressed through the use of descriptive statistics and analysis of variance

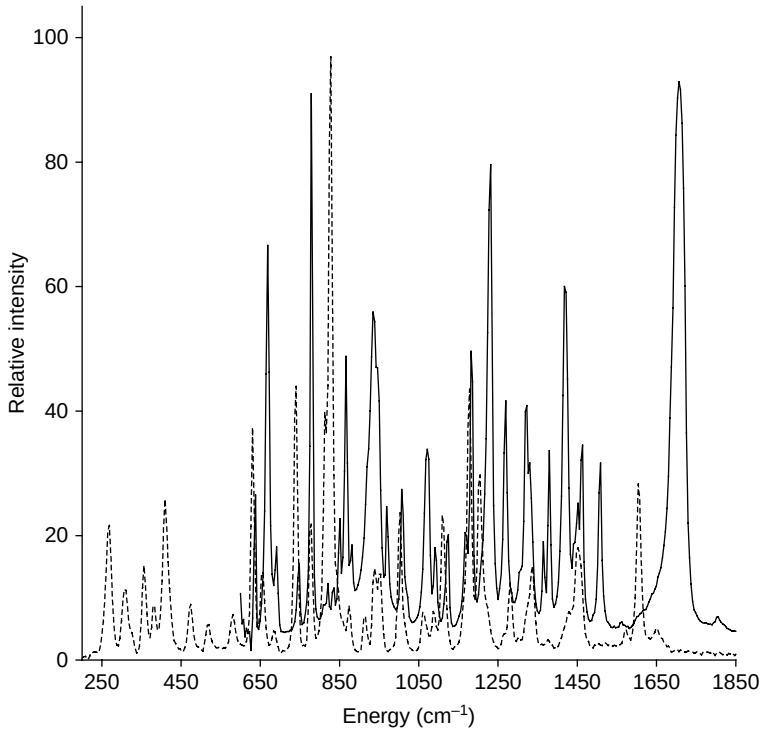

FIGURE 8 Fingerprint region infrared absorption spectrum of racemic ibuprofen (*solid trace*), and the fingerprint region Raman spectrum of the same compound (*dashed trace*). Each spectrum has been normalized so that the relative intensity of the most intense band equals 100%. H.G. Brittain, unpublished results (120).

methods for the development of a guideline that signify when Raman spectral differences could reliably signify the existence of different crystal structures for the same substance (121). From this analysis, it was proposed that the shift in the energy of a Raman peak would need to exceed 1.6 cm^{-1} to indicate the existence of polymorphism.

Nevertheless, the shifts commonly observed among polymorphic substances are frequently sufficiently large to permit the use of Raman spectroscopy as a triage method in screening protocols. In one such study, Raman spectroscopy was used to measure the amount of dissolved carbamazepine in a given solvent system, and subsequently to determine whether Form-I or Form-III crystallized upon cooling of the solutions (122). The advantage of the Raman method was that the analyses could be performed in sample volumes of 35 or 100 μL, and use of these small volumes allowed faster approaches to equilibrium through the use of smaller quantities of drug substance. The Raman method has been shown to be applicable to high-throughput studies conduced in multi-well plates (123) and in studies of epitaxial-induced crystallization (124).

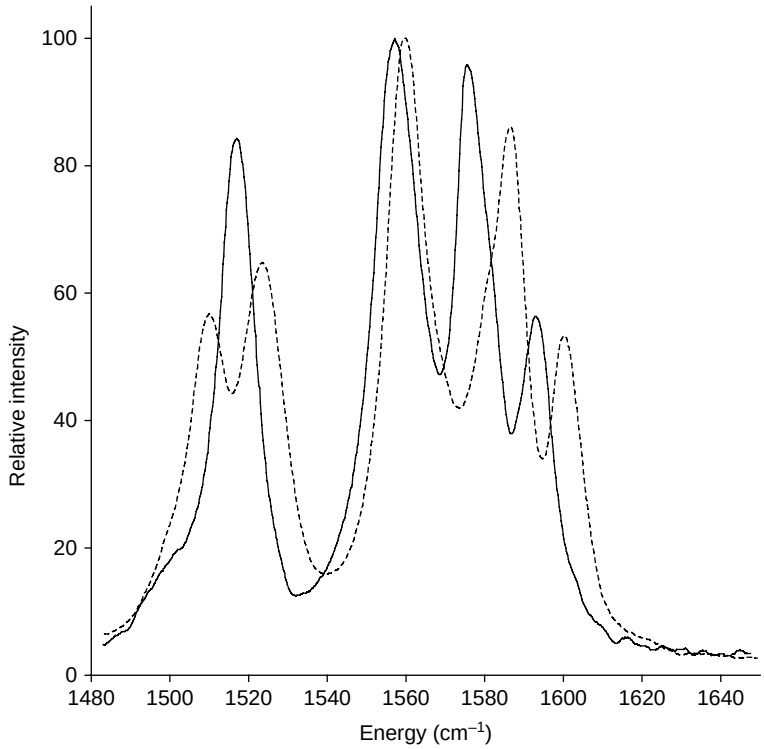

FIGURE 9 Raman spectra obtained in the high-frequency region for olanzapine Form-1 (*solid trace*) and Form-2 (*dashed trace*). Each spectrum has been normalized so that the relative intensity of the most intense band equals 100%, and the normalized spectra were generated from data given in Ref. (125).

A combination of infrared and Raman spectroscopic investigations was used to characterize two polymorphs of olanzapine, with spectral assignments being deduced for all observed bands in the two solid-state forms in order to obtain insight into the crystalline structures (125). As illustrated in Figure 9, the spectrum of Form-1 in the high-frequency region is characteristic of a hydrogen-bonded molecule, and the changes in the spectrum of Form-2 were determined to be consistent with atoms involved directly or indirectly to hydrogen bonds associated with the N–H group and not with any type of conformational difference between the molecules in the two crystal structures.

Schmidt has used Raman spectroscopy to study the polymorphic structures formed by benzocaine, butambene, and isobutambene as part of a program to characterize local anesthetic drugs having the general formula of lipo–CO–hyd, where the lipophilic end is mostly phenyl, CO is a negatively charged linkage (usually ester or amide), and the hydrophilic group (hyd) is usually a secondary or tertiary amine (126). Three polymorphs of sibenadet hydrochloride were found to exhibit varying degrees of dynamic disorder in a terminal phenyl group, with the

polymorphism being largely governed by skeletal symmetry changes rather than alterations in hydrogen-bonding patterns (127).

Raman spectroscopy has been found to be extremely useful for the quantitative analysis of phase composition. For example, two polymorphs of buspirone hydrochloride were characterized by a full range of techniques, with unique peaks in the Raman spectrum and chemometric analysis being used to develop quantitative methods for phase composition in mixtures of the two forms (128). A related approach was used to develop a quantitative method for the polymorphs of paracetamol in mixtures (129). An analytical method has been developed to determine the phase composition in mixtures of the two polymorphs of *N*-[5-chloro-4-[(4-chlorophenyl)cyanomethyl]-2-methylphenyl]-2-hydroxy-3,5-diiodobenzamide and its amorphous form, with these being quantitatively distinguished using Raman spectroscopy and a constrained linear regression model (130). The effect of particle size on quantitative phase determinations using Raman spectroscopy was studied for the case of flufenamic acid, noting that the intensity of Raman scattering tended to decrease with increasing particle size (131).

The use of X-ray powder diffraction in the study of amorphous solids is hampered by the lack of a useful response, but the vibrational transitions of such materials are still visible in both infrared absorption and Raman spectroscopies. Both techniques were used to evaluate the hydrogen-bonding patterns in a series of crystalline and amorphous dihydropyridine calcium channel blocker compounds, where it was learned that although significant variations existed in the various crystalline forms, similar patterns were detected for the amorphous states (132). The crystalline γ and amorphous modifications of indomethacin have been studied using vibrational spectroscopic and density functional theory computational methods, where it was deduced that the drug substance in the amorphate existed primarily in dimeric structures that were similar to those existing in the crystalline γ-form (133).

Raman spectroscopy has proven to be very useful as well in the study of the polymorphic content of drug substances in their formulations. For example, a detailed series of calibration samples was used to develop a method based on Raman spectroscopy for determination of the phase composition of the methyl ester of 5-*p*-fluoro-benzoyl-2-benzimidazolecarbamic acid in two formulations (134). The difficulty in this analysis lay in the fact that the drug substance was capable of existing in three polymorphic forms, and that a full statistical package based on the intensities of 78 selected bands was required to differentiate the forms.

The characterization of solvatomorphs by Raman spectroscopy is based on crystallographic effects on the energies of molecular vibrations. In addition to the known monohydrate and sesquihydrate crystal forms of pantoprazole sodium, two additional hydrate forms were studied using a full complement of spectroscopic characterization techniques, with both infrared absorption and Raman spectroscopies being capable of distinguishing between the various solvatomorphs (135). Four hydration states (an anhydrate, a monohydrate, a hemi-pentahydrate, and a variable hydrate containing fou to six waters) have been reported for risedronate sodium, with the Raman spectra of these forms being dominated by peaks associated with the substituted pyridine ring of the compound (136). Comparison of structures obtained by X-ray diffraction indicated the existence of strong intermolecular out-of-plane hydrogen bonding between the pyridine ring and an adjacent phosphate

group was capable of impacting the ring vibrational modes in the monohydrate and variable hydration forms.

Owing its ready adaptability as an in situ method of characterization, Raman spectroscopy has been shown to be useful in the study of solution-mediated phase transformation reactions. For example, a number of methods (including Raman spectroscopy) were used to follow the phase change of the metastable α-form of (*L*)-glutamic acid into its stable β-form, and as an aid develop the first-order kinetics for nucleation and growth kinetics of both polymorphs in a population balance model (137). The anhydrate/monohydrate equilibria of citric acid in aqueous solutions have been investigated with the aim of demonstrating the process analytical technology capabilities of in situ Raman spectroscopy (138). Flufenamic acid was used as the model system in a study of the use of in situ Raman spectroscopy as a method for the determination of transformation kinetics and transition temperatures, with good agreement being reported between results obtained by the spectroscopic method and those obtained using the more conventional van't Hoff approach (139).

The solution-mediated aqueous transformation of anhydrous carbamazepine to its dihydrate phase has proven to be a good model system for the use of Raman spectroscopy as a means to study the kinetics, because certain bands in the Raman spectra are diagnostic of the phase identity (Fig. 10). The thermodynamics associated with the system were studied in ethanol–water mixtures by measuring the solubility of both forms over the temperature range of 0°C to 60°C using a Raman immersion probe to establish the phase composition (140). In a related work, the Raman immersion probe was used to determine that crystallization of the stable form represented the rate-determining step (141). Raman spectroscopy was used to follow the kinetics associated with the conversion of the Form I, II, and II anhydrates to the dihydrate, where it was found that the morphology of the starting material seemed to determine the rates of reaction (142). The Raman technique, in combination with partial least squares regression analysis, was found to be the most robust method for the detection and quantification of mixtures of the carbamazepine solvatomorphs, with the possible biasing influences of particle size, morphology, mixing, and surface effects being evaluated (143).

Owing to its ease of acquisition, and non-invasive nature of sample handling, Raman spectroscopy has proven to be an ideal technique for the in situ study of thermally induced phase transformations. For example, variable-temperature Raman spectroscopy was used to study the low-temperature phase transitions in a biphenyl–fullerene single crystal, where three biphenyl vibrational modes and the C–H stretching mode were indicative of the phase transition, and changes in the planarity of the biphenyl molecule appeared to accompany the phase change (144). The behavior of most of the C_{60}–fullerene vibrational modes could be correlated with either of the transitions, indicating changes in its site symmetry. In contrast, Raman spectroscopy was used to demonstrate that single crystals of different polymorphs of pentacene did not undergo any phase transformation reactions over the temperature range of 79 K to 300 K (145).

Details of the phase transformation processes associated with the hydration and dehydration of theophylline have also been studied using Raman spectroscopy, because the bands in the high-frequency region were found to be especially sensitive toward the phase identity (146). The thermally induced dehydration of

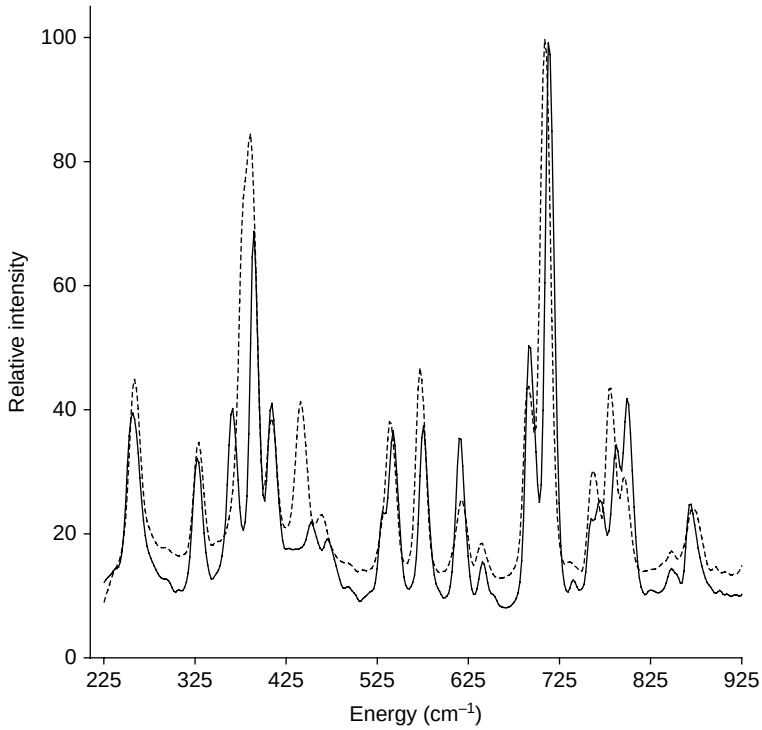

FIGURE 10 Raman spectra of carbamazepine anhydrate (*solid trace*) and carbamazepine dihydrate (*dashed trace*) over the lowest frequency region. Each spectrum has been normalized so that the relative intensity of the most intense band equals 100%. H.G. Brittain, unpublished results (120).

erythromycin A dihydrate has been studied using variable-temperature Raman spectroscopy, because the spectroscopic method was able to distinguish between the isomorphic dihydrate and its dehydrated product and being sufficiently responsive so as to be useful as an in-process technique for control over a drying process (147).

The use of principal component analysis and Raman spectroscopy in studies of the dehydration phenomena associated with various hydrated compounds, where it was found that the approach was effective in the fast screening of accumulated information, and its use facilitated the identification of critical temperatures or critical time points in the dehydration reactions (148). A Raman spectrometer interfaced with a moisture sorption gravimetric analyzer has been used to study modes of water–solid interactions in sulfaguanidine, cromolyn sodium, ranitidine hydrochloride, amorphous sucrose, and silica gel (149). Once again, principal components analysis was used to determine the genuine trends in the Raman data and facilitate the generation of information related the various types of interactions.

REFERENCES

1. Brittain HG. Spectroscopy of Pharmaceutical Solids. New York: Taylor & Francis, 2006.
2. Barrow GM. Molecular Spectroscopy. New York: McGraw-Hill, 1962.
3. King GW. Spectroscopy and Molecular Structure. New York: Holt, Rinehart and Winston, 1964.
4. Brittain EFH, George WO, Wells CHJ. Introduction to Molecular Spectroscopy. London: Academic Press, 1970.
5. Guillory WA. Introduction to Molecular Structure and Spectroscopy. Boston: Allyn and Bacon, 1977.
6. McHale JL. Molecular Spectroscopy. Upper Saddle River, NJ: Prentice Hall, 1999.
7. Rao CNR. Chemical Applications of Infrared Spectroscopy. New York: Academic Press, 1963.
8. Kendall DN. Applied Infrared Spectroscopy. New York: Reinhold Pub, 1966.
9. Conley RT. Infrared Spectroscopy. Boston, MA: Allyn and Bacon, 1966.
10. Colthup NB, Daly LH, Wiberley SE. Introduction to Infrared and Raman Spectroscopy, 2nd edition. London: Academic Press, 1975.
11. Nakanishi K, Solomon PH. Infrared Absorption Spectroscopy. San Francisco, CA: Holden-Day, 1977.
12. Bhagavantam S. Scattering of Light and the Raman Effect. New York: Chemical Publishing Co, 1942.
13. Grasselli JG, Snavely MK, Bulkin BJ. Chemical Applications of Raman Spectroscopy. New York: Wiley-Interscience, 1981.
14. Grasselli JG, Bulkin BJ. Analytical Raman Spectroscopy. New York: John Wiley & Sons, 1991.
15. Ferraro JR, Nakamoto K. Introductory Raman Spectroscopy. New York: Academic Press, 1994.
16. Lewis IR, Edwards HGM. Handbook of Raman Spectroscopy. New York: Marcel Dekker, 2001.
17. Wilson EB, Decius JC, Cross PC. Molecular Vibrations: The Theory of Infrared and Raman Vibrational Spectra. New York: McGraw-Hill Book Co, 1955.
18. Markovich RJ, Pidgeon C. Introduction to fourier transform infrared spectroscopy and applications in the pharmaceutical sciences. Pharm Res 1991; 8: 663–75.
19. Brittain HG, Bogdanowich SJ, Bugay DE, et al. Physical characterization of pharmaceutical solids. Pharm Res 1991; 8: 963–73.
20. Threlfall TL. Analysis of organic polymorphs. Analyst 1995; 120: 2435–60.
21. Bugay DE, Williams AC. Vibrational spectroscopy, chapter 3 in Physical Characterization of Pharmaceutical Solids. In: Brittain HG, ed. New York: Marcel Dekker, 1995: 59–91.
22. Brittain HG. Spectral methods for the characterization of polymorphs and solvates. J Pharm Sci 1997; 86: 405–12.
23. Findlay WP, Bugay DE. Utilization of fourier transform raman spectroscopy for the study of pharmaceutical crystal forms. J Pharm Biomed Anal 1998; 16: 921–30.
24. Brittain HG. Methods for the characterization of polymorphs and solvates, chapter 6 in Polymorphism in Pharmaceutical Solids. In: Brittain HG, ed. New York: Marcel Dekker, 1999: 227–78.
25. Bugay DE, Findlay WP. Pharmaceutical Excipients: Characterization by Raman IR and NMR Spectroscopy. New York: Marcel Dekker, 1999.
26. Frank CJ. Pharmaceutical applications of raman spectroscopy, chapter 6 in Analytical Applications of Raman Spectroscopy. In: Pelletier MJ, ed. Oxford: Blackwell Science, 1999: 224–75.
27. Brittain HG. Solid-state analysis, Chapter 3, in the Handbook of Pharmaceutical Analysis. In: Ahuja S, Scypinski S, eds. New York: Marcel Dekker, 2001: 57–84.

28. Bugay DE. Characterization of the solid-state: spectroscopic techniques. Adv Drug Del Rev 2001; 48: 43–65.
29. Brittain HG, Medek A. Polymorphic and solvatomorphic impurities, chapter 3 in Handbook of Isolation and Characterization of Impurities in Pharmaceuticals. In: Ahuja S, Alsante KM, eds. Academic Press, 2003: 39–73.
30. Bugay DE, Brittain HG. Infrared absorption spectroscopy, chapter 8, in Spectroscopy of Pharmaceutical Solids. In: Brittain HG, ed. New York: Taylor and Francis, 2006: 235–69.
31. Bugay DE, Brittain HG. Raman spectroscopy, chapter 9, in Spectroscopy of Pharmaceutical Solids. In: Brittain HG, ed. New York: Taylor and Francis, 2006: 271–312.
32. Brittain HG. Spectroscopic methods for the characterization of drug substances, chapter 3.5, in Preformulation in Solid Dosage Form Development. In: Adeyeye MC, Brittain HG, eds. New York: Informa Healthcare Press, 2008: 253–77.
33. Pauling L, Wilson EB. Introduction to Quantum Mechanics. New York: McGraw-Hill, 1935.
34. Eyring H, Walter J, Kimball GE. Quantum Chemistry. New York: John Wiley & Sons, 1944.
35. Kauzmann W. Quantum Chemistry. New York: Academic Press, 1957.
36. Davis JC. Advanced Physical Chemistry. New York: Ronald Press, 1965.
37. Levine IN. Quantum Chemistry. Boston: Allyn and Bacon, 1970.
38. Flett MC. Characteristic Frequencies of Groups in the Infra-Red. Amsterdam: Elsevier Pub, 1963.
39. Bellamy LJ. Advances in Infrared Group Frequencies. London: Methuen & Co, 1968.
40. Socrates G. Infrared and Raman Characteristic Group Frequencies – Tables and Charts, 3rd edn. Chichester: John Wiley & Sons, 2001.
41. Fearn T, Osborne BG. Near Infrared Spectroscopy in Food Analysis. Dublin, Ireland: Longman Scientific & Technical Pub, 1986.
42. Williams P, Norris K. Near-Infrared Technology in the Agricultural and Food Industries. Saint Paul, MN: American Association of Cereal Chemists, 2001.
43. Siesler HW, Ozaki Y, Kawata S, et al. Near-Infrared Spectroscopy: Principles, Instruments, Applications. Weinheim: Wiley-VCH Pub., 2002.
44. Burns DA, Ciurczak EW. Handbook of Near-Infrared Analysis, 2nd edn. New York: Marcel Dekker, 2001.
45. Ciurczak EW, Drennen JK. Pharmaceutical and Medical Applications of Near-Infrared Spectroscopy. New York: Marcel Dekker, 2002.
46. Anderson DH, Woodall NB. Infrared spectroscopy, chapter 1 in Physical Methods of Chemistry, volume I, part IIIB. In: Weissberger A, Rossiter BW, eds. New York: Wiley-Interscience, 1972: 1–84.
47. Griffiths PR, de Haseth JA. Fourier Transform Infrared Spectrometry. New York: John Wiley & Sons, 1986.
48. Fredericks P, Rintoul L, Coates J. Vibrational spectroscopy: instrumentation for infrared and Raman spectroscopy, chapter 7 in Ewing's Analytical Instrumentation Handbook, 3rd edn, Cazes J, ed. New York: Marcel Dekker, 2005: 163–238.
49. Mutha SC, Ludemann WB. Solid-state anomalies in IR spectra of compounds of pharmaceutical interest. J Pharm Sci 1976; 65: 1400–3.
50. Bugay DE, Newman AW, Findlay WP. Quantitation of cefepime dihydrochloride in cefepime dihydrochloride monohydrate by diffuse reflectance IR and powder X-ray diffraction techniques. J Pharm Biomed Anal 1996; 15: 49–61.
51. Culler SR. Diffuse Reflectance Spectroscopy: Sampling Techniques for Qualitative/Quantitative Analysis of Solids, in Practical Sampling Techniques for Infrared Analysis. In: Coleman PB, ed. Boca Raton, FL: CRC Press, 1993: 93–105.
52. Compton SV, Compton DAC. Optimization of data by internal reflectance spectroscopy, in Practical Sampling Techniques for Infrared Analysis. In: Coleman PB, ed. Boca Raton, FL: CRC Press, 1993: 55–92.

53. Urban MW. Attenuated Total Reflectance Spectroscopy of Polymers. Washington, DC: American Chemical society, 1996.
54. Giannellini V, Bambagiotti-Alberti M, Bartolucci G, et al. Solid-state study of mepivacaine hydrochloride. J Pharm Biomed Anal 2005; 39: 444–54.
55. Kipouros K, Kachrimanis K, Nikolakakis I, et al. Simultaneous quantification of carbamazepine crystal forms in ternary mixtures (I, III, and IV) by diffuse reflectance FTIR spectroscopy (DRIFTS) and multivariate calibration. J Pharm Sci 2006; 95: 2419–31.
56. Lee EH, Boerrigter SXM, Rumondor ACF, et al. Formation and solid-state characterization of a salt-induced metastable polymorph of flufenamic acid. Cryst Growth Des 2008; 8: 91–7.
57. Park HJ, Kim M-S, Lee S, et al. Recrystallization of fluconazole using the supercritical antisolvent (SAS) process. Int J Pharm 2007; 328: 152–60.
58. Rafilovich M, Bernstein J, Harris RK, et al. Groth's Original Concomitant Polymorphs Revisited. Cryst Growth Des 2005; 5: 2197–209.
59. Yu L, Stephenson GA, Mitchell CA, et al. Thermochemistry and conformational polymorphism of a hexamorphic crystal system. J Am Chem Soc 2000; 122: 585–91.
60. Yamamura S, Gotoh H, Sakamoto Y, et al. Physicochemical properties of amorphous salt of cimetidine and diflunisal system. Int J Pharm 2002; 241: 213–21.
61. Kojima T, Yamauchi Y, Onoue S, et al. Evaluation of hydrate formation of a pharmaceutical solid by using diffuse reflectance infrared fourier-transform spectroscopy. J Pharm Biomed Anal 2008; 46: 788–91.
62. Bartolomei M, Bertocchi P, Antoniella E, et al. Physicochemical characterization and intrinsic dissolution studies of a new hydrate form of diclofenac sodium: comparison with anhydrous form. J Pharm Biomed Anal 2006; 40: 1105–13.
63. Vogt FG, Dell'Orco PC, Diederich AM, et al. A study of variable hydration states in topotecan hydrochloride. J Pharm Biomed Anal 2006; 40: 1080–8.
64. Alkhamis KA, Obaidat AA, Nuseirat AF. Solid-state characterization of fluconazole. Pharm Dev Tech 2002; 7: 491–503.
65. Caira MR, Alkhamis KA, Obaidat RM. Preparation and crystal characterization of a polymorph, a monohydrate, and an ethyl acetate solvate of the antifungal fluconazole. J Pharm Sci 2004; 93: 601–11.
66. Alkhamis KA, Salem MS, Obaidat RM. Comparison between dehydration and desolvation kinetics of fluconazole monohydrate and fluconazole ethyl acetate solvate using three different methods. J Pharm Sci 2006; 95: 859–70.
67. van Tonder EC, Maleka TSP, Liebenberg W, et al. Preparation and physicochemical properties of niclosamide anhydrate and two monohydrates. Int J Pharm 2004; 269: 417–32.
68. Cantera RG, Leza MG, Bachiller CM. Solid phases of tenoxicam. J Pharm Sci 2002; 91: 2240–51.
69. Reddy VR, Rajmohan MA, Shilpa RL, et al. A novel quantification method of pantoprazole sodium monohydrate in sesquihydrate by thermogravimetric analyzer. J Pharm Biomed Anal 2007; 43: 1836–41.
70. Ferrari ES, Davey RJ, Cross WI, et al. Crystallization in polymorphic systems: the solution-mediated transformation of β to α glycine. Cryst Growth Des 2003; 3: 53–60.
71. Sheikhzadeh M, Murad S, Rohani S. Response surface analysis of solution-mediated polymorphic transformation of buspirone hydrochloride. J Pharm Biomed Anal 2007; 45: 227–36.
72. Gilpin RK, Zhou W. Infrared studies of the thermal conversion of mefenamic acid between polymorphic states. Vibrat Spectroscopy 2005; 37: 53–9.
73. Lin SY, Cheng WT, Wang SL. Thermodynamic and kinetic characterization of polymorphic transformation of famotidine during grinding. Int J Pharm 2006; 318: 86–91.

74. Brittain HG. unpublished results obtained at a resolution of 4 cm^{-1} using a Shimadzu model 8400S Fourier-transform infrared spectrometer, with each spectrum being obtained as the average of 40 individual spectra. The data were acquired using the attenuated total reflectance sampling mode, where the samples were clamped against the ZnSe crystal of a Pike MIRacleTM single reflection horizontal ATR sampling accessory.
75. Lin S-Y, Chien J-L. In vitro simulation of solid-solid dehydration, rehydration, and solidification of trehalose dihydrate using thermal and vibrational spectroscopic techniques. Pharm Res 2003; 20: 1926–31.
76. Fearn T, Osborne BG. Near Infrared Spectroscopy in Food Analysis. Dublin, Ireland: Longman Scientific & Technical Pub, 1986.
77. Williams P, Norris K. Near-Infrared Technology in the Agricultural and Food Industries. Saint Paul, MN: American Association of Cereal Chemists, 2001.
78. Siesler HW, Ozaki Y, Kawata S, Heise HM. Near-Infrared Spectroscopy: Principles, Instruments, Applications. Weinheim: Wiley-VCH Pub., 2002.
79. Burns DA, Ciurczak EW. Handbook of Near-Infrared Analysis, 2nd edn. New York: Marcel Dekker, 2001.
80. Ciurczak EW, Drennen JK. Pharmaceutical and Medical Applications of Near-Infrared Spectroscopy. New York: Marcel Dekker, 2002.
81. Cogdill RP, Drennen JK III. Near-Infrared spectroscopy, Chapter 10, in Spectroscopy of Pharmaceutical Solids. In: Brittain HG, ed. New York: Taylor & Francis, 2006: 313–412.
82. Ciurczak EW. Uses of Near-Infrared Spectroscopy in Pharmaceutical Analysis. Appl Spectrosc Rev 1987; 23: 147–63.
83. MacDonald BF, Prebble KA. Some applications of near-infrared reflectance analysis in the pharmaceutical industry. J Pharm Biomed Anal 1993; 11: 1077–85.
84. Roggo Y, Chalus P, Maurer L, Lema-Martinez C, et al. A review of near infrared spectroscopy and chemometrics in pharmaceutical technologies. J Pharm Biomed Anal 2007; 44: 683–700.
85. El-Hagrasy A, D'Amico F, Drennen JK III. A process analytical technology approach to near-infrared process control of pharmaceutical powder blending. Part I: D-optimal design for characterization of powder mixing and preliminary spectral data evaluation. J Pharm Sci 2006; 95: 392–406.
86. El-Hagrasy A, Delgado-Lopez M, Drennen JK III. A process analytical technology approach to near-infrared process control of pharmaceutical powder blending. Part II: qualitative near-infrared models for prediction of blend homogeneity. J Pharm Sci 2006; 95: 407–21.
87. El-Hagrasy A, Drennen JK III. A process analytical technology approach to near-infrared process control of pharmaceutical powder blending. Part III: quantitative near-infrared calibration for prediction of blend homogeneity and characterization of powder mixing kinetics. J Pharm Sci 2006; 95: 422–34.
88. Luner PE, Majuru S, Seyer JJ, et al. Quantifying crystalline form composition in binary powder mixtures using near-infrared reflectance spectroscopy. Pharm Dev Tech 2000; 5: 231–46.
89. Patel AD, Luner PE, Kemper MS. Low level determination of polymorph composition in physical mixtures by near-infrared reflectance spectroscopy. J Pharm Sci 2001; 90: 360–70.
90. McArdle P, Gilligan K, Cunningham D, et al. Determination of the polymorphic forms of bicifadine hydrochloride by differential scanning calorimetry–thermogravimetric analysis, X-ray powder diffraction, attenuated total reflectance–infrared spectroscopy, and attenuated total reflectance–near-infrared spectroscopy. Appl Spectrosc 2005; 59: 1365–71.
91. Heinz A, Savolainen M, Rades T, et al. Quantifying ternary mixtures of different solid-state forms of indomethacin by raman and near-infrared spectroscopy. Eur J Pharm Sci 2007; 32: 182–92.

92. Mirza S, Miroshnyk I, Rantanen J, et al. Solid-state properties and relationship between anhydrate and monohydrate of baclofen. J Pharm Sci 2007; 96: 2399–408.
93. Rantanen J, Wikström H, Rhea FE, et al. Improved understanding of factors contributing to quantification of anhydrate/hydrate powder mixtures. Appl Spectrosc 2005; 59: 942–51.
94. Krzyaniak JF, Williams GR, Ni N. Identification of phase boundaries in anhydrate/hydrate systems. J Pharm Sci 2007; 96: 1270–81.
95. Blanco M, Valdés D, Llorente I, et al. Application of NIR spectroscopy in polymorphic analysis: study of pseudo-polymorphs stability. J Pharm Sci 2005; 94: 1336–42.
96. Kauffman JF, Tumuluri V, Guo C, et al. Near-infrared spectroscopy of magnesium stearate hydrates and multivariate calibration of pseudo-polymorph composition. J Pharm Sci 2008; 97: 2757–67.
97. Li W, Worosila GD, Wang W, et al. Determination of polymorph conversion of an active pharmaceutical ingredient in wet granulation using NIR calibration models generated from the premix blends. J Pharm Sci 2005; 94: 2800–6.
98. Römer M, Heinämäki J, Miroshnyk I, et al. Phase transformations of erythromycin A dihydrate during pelletization and drying. Eur J Pharm Biopharm 2007; 67: 246–52.
99. Xie Y, Tao W, Morrison H, et al. Quantitative determination of solid-state forms of a pharmaceutical development compound in drug substance and tablets. Int J Pharm 2008; 362: 29–36.
100. Durig JR, Cox AW Jr. Current and past research in far-infrared interferometry, chapter 6 in Fourier Transform Infrared Spectroscopy, volume 1. In: Ferraro JE, Basile LJ, eds. New York: Academic Press, 1978: 215–74.
101. Friedmann H, Kimel S. Rotation-translation coupling spectrum of matrix-isolated diatomic molecules in the near and far infrared. J Chem Phys 1966; 44: 4359–60.
102. Beard MC, Turner GM, Schmuttenmaer CA. Terahertz spectroscopy. J Phys Chem B 2002; 106: 7146–59.
103. Dexheimer SL. Terahertz Spectroscopy: Principles and Applications. New York: Taylor and Francis, 2008.
104. Strachan CJ, Rades T, Newnham DA, et al. Using terahertz pulsed spectroscopy to study crystallinity of pharmaceutical materials. Chem Phys Lett 2004; 390: 20–4.
105. Zeitler JA, Rades T, Taday PF. Pharmaceutical and security applications of terahertz spectroscopy, chapter 8 in Terahertz Spectroscopy: Principles and Applications. In: Dexheimer SL, ed. New York: Taylor and Francis, 2008: 299–323.
106. Zeitler JA, Taday PF, Newnham DA, et al. Terahertz pulsed spectroscopy and imaging in the pharmaceutical setting. J Pharm Pharmacol 2007; 59: 209–23.
107. Newnham DA, Taday PF. Pulsed terahertz attenuated total reflection spectroscopy. Appl Spectrosc 2008; 62: 394–8.
108. Taday PF, Bradley IV, Arnone DD, et al. Using terahertz pulsed spectroscopy to study the crystalline structure of a drug: a case study of the polymorphs of ranitidine hydrochloride. J Pharm Sci 2003; 92: 831–8.
109. Strachan CJ, Taday PF, Newnham DA, et al. Using terahertz pulsed spectroscopy to quantify pharmaceutical polymorphism and crystallinity. J Pharm Sci 2005; 94: 837–46.
110. Day GM, Zeitler JA, Jones W, et al. Understanding the influence of polymorphism on phonon spectra: lattice dynamics calculations and terahertz spectroscopy of carbamazepine. J Phys Chem B 2006; 110: 447–56.
111. Aaltonen J, Strachan CJ, Pöllänen K, et al. Hyphenated spectroscopy as a polymorph screening tool. J Pharm Biomed Anal 2007; 44: 477–83.
112. Zeitler JA, Newnham DA, Taday PF, et al. Temperature dependent terahertz pulsed spectroscopy of carbamazepine. Thermochim Acta 2005; 436: 71–7.
113. Zeitler JA, Newnham DA, Taday PF, et al. Characterization of temperature-induced phase transformations in five polymorphic forms of sulfathiazole by terahertz pulsed spectroscopy and differential scanning calorimetry. J Pharm Sci 2006; 95: 2468–98.

114. Upadhya PC, Nguyen K, Shen YC, et al. Characterization of crystalline phase transformations in theophylline by time-domain terahertz spectroscopy. Spectrosc Lett 2006; 39: 215–24.
115. Zeitler JA, Kogermann K, Rantanen J, et al. Drug hydrate systems and dehydration processes studied by terahertz pulsed spectroscopy. Int J Pharm 2007; 344: 78–84.
116. Liu H-B, Chen Y, Zhang X-C. Characterization of anhydrous and hydrated pharmaceutical materials with THz time-domain spectroscopy. J Pharm Sci 2007; 96: 927–34.
117. Zeitler JA, Taday PF, Pepper M, et al. Relaxation and crystallization of amorphous carbamazepine studied by terahertz pulsed spectroscopy. J Pharm Sci 2007; 96: 2703–9.
118. Tobin MC. Laser Raman Spectroscopy. New York: Wiley-Interscience, 1971.
119. Dollish FR, Fateley WG, Bentley FF. Characteristic Raman Frequencies of Organic Compounds. New York: John Wiley & Sons, 1974.
120. Brittain HG. Unpublished results obtained for the infrared absorption spectrum of racemic ibuprofen obtained according to reference [74], and Raman spectrum obtained on this substance at a resolution of 5 cm^{-1} and using a Raman Systems model R-3000HR spectrometer (785 nm laser source). The data were acquired using front-face scattering from a thick powder bed contained in an aluminum sample holder.
121. Mehrens SM, Kale UJ, Qu X. Statistical analysis of differences in the raman spectra of polymorphs. J Pharm Sci 2005; 94: 1354–67.
122. Anquetil PA, Brenan CJH, Marcolli C, et al. Laser raman spectroscopic analysis of polymorphic forms in microliter fluid volumes. J Pharm Sci 2003; 92: 149–60.
123. Kojima T, Onoue S, Murase N, et al. Crystalline form information from multiwell plate salt screening by use of raman spectroscopy. Pharm Res 2006; 23: 806–12.
124. Grezesiak AL, Matzger AJ. New form discovery for the analgesics flurbiprofen and sulindac facilitated by polymer-induced heteronucleation. J Pharm Sci 2007; 96: 2978–86.
125. Ayala AP, Siesler HW, Boese R, et al. Solid-state characterization of olanzapine polymorphs using vibrational spectroscopy. Int J Pharm 2006; 326: 69–79.
126. Schmidt AC. Structural characteristics and crystal polymorphism of three local anesthetic bases. Int J Pharm 2005; 298: 186–97.
127. Cosgrove SD, Steele G, Austin TK, et al. Understanding the polymorphic behavior of sibenadet hydrochloride through detailed studies integrating structural and dynamical assessment. J Pharm Sci 2005; 94: 2403–15.
128. Sheikhzadeh M, Rohani S, Jutan A, et al. Solid-state characterization of buspirone hydrochloride polymorphs. Pharm Res 2006; 23: 1043–50.
129. Kachrimanis K, Braun DE, Greisser UJ. Quantitative analysis of paracetamol polymorphs in powder mixtures by FT-raman spectroscopy and PLS regression. J Pharm Biomed Anal 2007; 43: 407–12.
130. De Spiegeleer B, Baert B, Diericx N, et al. Assessment of the solid-state composition of an active salicylanilide compound by FT-raman spectroscopy. J Pharm Biomed Anal 2007; 44: 254–7.
131. Hu Y, Wikstrom H, Byrn SR, et al. Analysis of the effect of particle size on polymorphic quantitation by raman spectroscopy. Appl Spectrosc 2006; 60: 977–84.
132. Tang XC, Pikal MJ, Taylor LS. A spectroscopic investigation of hydrogen bond patterns in crystalline and amorphous phases in dihydropyridine calcium channel blockers. Pharm Res 2002; 19: 477–83.
133. Strachan CJ, Rades T, Gordon KC. A theoretical and spectroscopic study of γ-crystalline and amorphous indomethacin. J Pharm Pharmacol 2007; 59: 261–9.
134. De Spiegeleer B, Seghers D, Wieme R, et al. Determination of the relative amounts of three crystal forms of a benzimidazole drug in complex finished formulations by FT-Raman spectroscopy. J Pharm Biomed Anal 2005; 39: 275–80.
135. Zupančič V, Ograjšek N, Kotar-Jordan B, et al. Physical characterization of pantoprazole sodium hydrates. Int J Pharm 2005; 291: 59–68.

136. Redman-Furey N, Dicks M, Bigalow-Kern A, et al. Structural and analytical characterization of three hydrates and an anhydrate form of risedronate. J Pharm Sci 2005; 94: 893–911.
137. Schöll J, Bonalumi D, Vicum L, et al. In-situ monitoring and modeling of the solvent-mediated polymorphic transformation of L-glutamic acid. Cryst Growth Des 2006; 6: 881–91.
138. Caillet A, Puel F, Fevotte G. In-line monitoring of partial and overall solid concentration during solvent-mediated phase transition using raman spectroscopy. Int J Pharm 2006; 307: 201–8.
139. Hu Y, Wikström H, Byrn SR, et al. Estimation of the transition temperature for an enantiotropic polymorphic system from the transformation kinetics monitored using raman spectroscopy. J Pharm Biomed Anal 2007; 45: 546–51.
140. Qu H, Louhi-Kultanen M, Kallas J. Solubility and stability of anhydrate/hydrate in solvent mixtures. Int J Pharm 2006; 321: 101–7.
141. Qu H, Louhi-Kultanen M, Kallas J. Solvent-mediated phase transformation kinetics of an anhydrate/hydrate system. Cryst Growth Des 2006; 6: 2053–60.
142. Tian F, Zeitler JA, Strachan CJ, et al. Characterizing the conversion kinetics of carbamazepine polymorphs to the dihydrate in aqueous suspension using raman spectroscopy. J Pharm Biomed Anal 2006; 40: 271–80.
143. Tian F, Zhang F, Sandler N, et al. Influence of sample characteristics on quantification of carbamazepine hydrate formation by X-ray powder diffraction and raman spectroscopy. Eur J Pharm Biopharm 2007; 66: 466–74.
144. Palles D, Marucci A, Penicaud A, et al. Low-temperature phase transitions in a biphenyl-fullerene single crystal: a raman study. J Phys Chem B 2003; 107: 4904–11.
145. della Valle RG, Venuti E, Farina L, et al. Intramolecular and low-frequency intermolecular vibrations of pentacene polymorphs as a function of temperature. J Phys Chem B 2004; 108: 1822–6.
146. Amado AM, Nolasco MM, Ribeiro-Claro PJA. Probing pseudopolymorphic transitions in pharmaceutical solids using raman spectroscopy: hydration and dehydration of theophylline. J Pharm Sci 2007; 96: 1366–79.
147. Miroshnyk I, Kriachthev L, Mirza S, et al. Insight into thermally induced phase transformations of erythromycin A dihydrate. Cryst Growth Des 2006; 6: 369–74.
148. Jørgensen AC, Miroshnyk I, Karjalainen M, et al. Multivariate data analysis as a fast tool in evaluation of solid state phenomena. J Pharm Sci 2006; 95: 906–16.
149. Gift AD, Taylor LS. Hyphenation of raman spectroscopy with gravimetric analysis to interrogate water-solid interactions in pharmaceutical systems. J Pharm Biomed Anal 2007; 43: 14–26.

11 Solid-State Nuclear Magnetic Resonance Spectroscopy

Patrick A. Tishmack
SSCI, an Aptuit Company, West Lafayette, Indiana, U.S.A.

INTRODUCTION

Solid-state NMR (SSNMR) spectroscopy has been used to study polymorphism beginning with the analysis of hydroquinone by Ripmeester almost 30 years ago (1). The characterization of pharmaceutical polymorphs by SSNMR spectroscopy has become more common in the last 10 to 15 years as the technology has improved and NMR spectrometers have become easier to use, particularly for non-specialists. SSNMR spectroscopy provides unique information due to its selectivity and specificity compared to other analytical techniques, which makes it very valuable for characterization of pure compounds and well as mixtures.

SSNMR spectroscopy has also found an important role in establishing intellectual property in the pharmaceutical industry because it is critical to know the specific solid forms in which most drug substances exist. SSNMR spectroscopy tends to be the primary technique to establish the solid form of a drug in a formulated product due to its high specificity and relatively limited interference from excipients compared to X-ray powder diffraction (XRPD), and vibrational spectroscopy (IR or Raman). Therefore, it is prudent to have all solid forms characterized by SSNMR spectroscopy in addition to the typical XRPD data as part of a patent package. In general, ^{13}C cross-polarization magic angle spinning (CP/MAS) is sufficient for characterizing the solid form, but SSNMR spectroscopy of other nuclei might also be important for a particular drug.

A number of recent reviews have appeared about the use of SSNMR spectroscopy to analyze polymorphs and other solid forms (2–7). Three of the more extensive recent reviews covering many aspects of SSNMR spectroscopy of pharmaceutical compounds are by Harris (2), Medek (3), and Tishmack et al. (4). The reader is referred to the book chapter by Medek for a thorough review of many aspects of pharmaceutical SSNMR spectroscopy in addition to a theoretical discussion of NMR spectroscopy (3). The review by Harris is particularly interesting for solid-state structural determination, analysis of hydrates, and amorphous solids (2). The review by Tishmack et al. is a general overview of SSNMR spectroscopic analyses of pharmaceuticals through approximately 2002 (4).

In this chapter, the theory and applications of SSNMR spectroscopy will be discussed primarily in the context of pharmaceutical compounds. SSNMR spectroscopy is considered a necessary analytical characterization technique for every pharmaceutical solid that is marketed. The International Committee of Harmonization (ICH) specifically refers to SSNMR spectroscopy along with IR and Raman spectroscopic techniques as necessary for characterizing polymorphs in drug substances and drug products (8). It has been well established that characterization of pharmaceuticals generally requires multiple analytical techniques (e.g., diffraction, spectroscopy,

thermal analysis, microscopy, dissolution, etc.) to adequately understand their behavior with respect to production, stability, and bioavailability. Therefore, many of the literature references cited in this chapter use SSNMR spectroscopy as only one of several analytical techniques to study the compound(s) of interest to the authors. One of the difficulties in using SSNMR spectroscopy is that acquisition and interpretation of spectra usually requires a reasonably good understanding of the underlying physics. This may be the main reason that a relatively high percentage of the pharmaceutical literature examples use SSNMR spectroscopy as a secondary technique with minimal or even incorrect interpretation of the results. Hopefully this situation will improve in the future as SSNMR spectroscopy becomes even more powerful in analyzing solid materials.

The section on NMR theory in this chapter is not highly mathematical or extensive given that there are many excellent texts, reviews, and monographs on NMR theory that include details specific to SSNMR spectroscopy (9–23). Recent reviews by Baldus (9) and Reichert (10) cover general applications of SSNMR spectroscopy to many solid systems. Laws et al. wrote a particularly thorough review of SSNMR spectroscopy that is highly recommended (11). The SSNMR spectroscopy book by Duer is a useful reference for beginners and more advanced spectroscopists (12), and two older books are also excellent references for most aspects of SSNMR spectroscopy (13,14). The books by Friebolin (15), Chandrakumar (16), Harris (17), and Becker (18) are texts on general NMR spectroscopy with chapters devoted to the solid state. These books also provide reasonable reviews of the basic theory of NMR spectroscopy. Traficante's chapter is a basic introduction to NMR spectroscopy that is generally easy to understand (19). The older books by Carrington and McLachlan (20), Slichter (21), and Abragam (22) are fundamental resources on NMR spectroscopy with a much more mathematically detailed treatment of essentially every aspect of the quantum mechanical basis of the technique. Grant and Harris edit a large encyclopedia covering all aspects of NMR spectroscopy that is periodically updated with new information (23).

GENERAL THEORY OF NMR SPECTROSCOPY

NMR spectroscopy derives from the nuclear spin angular momentum, which is based on the number of protons and neutrons of an atom. Nuclear spin (I) is quantized in multiples of the Planck constant (h), $I = 0, 1/2, 1, 3/2, 2$, etc. Nuclei with even numbers of protons and neutrons have zero spin and thus no NMR signal such as ^{12}C and ^{16}O. Half integer nuclear spins result when the nucleus of an element has either an even or odd number of protons and an odd number for its mass. Integer nuclear spins result if a nucleus has an odd number of protons and an even mass. Most elements have a isotope that can be studied by NMR spectroscopy, but it is not always the isotope with the highest natural abundance. Unfortunately, nuclei with spins other than one-half have a quadrupole moment and thus an electric field gradient that will interact with the nuclear dipole moment and lead to broad peaks in most cases. Spin one-half nuclei such as ^{1}H, ^{13}C, ^{15}N, ^{19}F, and ^{31}P are studied most often because they have better resolution and sensitivity compared to quadrupolar nuclei. However, ^{13}C and ^{15}N have relatively low natural abundances (1.1% and 0.37%, respectively) and correspondingly lower sensitivity than the other commonly studied spin one-half nuclei. Some of the positive and negative aspects of NMR spectroscopy are summarized in Table 1.

TABLE 1 Summary of Some Advantages and Disadvantages of Solid-State NMR Spectroscopy

NMR property	Advantages	Disadvantages
High field strength	Better sensitivity. Possibly better resolution. Decreased effect of quadrupolar nuclei.	Longer T_1 relaxation times. Instrument cost and upkeep. Increased CSA effects. Increased anisotropic bulk magnetic susceptibility.
Very weak transition energies	Highest resolution spectroscopy. High specificity.	Lowest sensitivity spectroscopy. Larger samples may be required.
Multiple nuclei	High selectivity for compounds containing chosen nucleus.	Compounds without the chosen nucleus are not observed.
Signal is directly proportional to the number of nuclei producing it	Intrinsically quantitative technique.	Quantification efficiency depends on nuclear relaxation properties.
T_1 and $T_1\rho$ relaxation times	Dynamic and spatial properties can be measured.	Long T_1 increases total data collection time. A different T_1 for each nuclei or molecule requires careful optimization for each case particularly for mixtures.
T_2 relaxation time	Dynamic properties can be measured.	Short T_2 causes broader peak. Potential loss of signal during longer pulse sequences.
Chemical shift	Structural analyses are possible.	Difficult to predict accurately. Extensive overlap in complex molecules.
Coupling	Structural analyses are possible.	Complicates spectrum with peak broadening or splitting.
Quadrupolar nuclei	Comprise most of periodic table.	Not easy to observe due to broad peaks and rapid relaxation times. Special techniques may be required to obtain spectra.
Multi-dimensional NMR	Increased resolution. Correlations between multiple different nuclei possible. Bonding and spatial information for structural analyses.	Time consuming to obtain data. Significant skill usually required.

NMR active nuclei also have a magnetic quantum number (m_I), which has $2I + 1$ possible energy states (i.e., $m_I = I, I - 1, \ldots, -I$) that determine the orientations of the magnetic moments in a static magnetic field ($\mathbf{B_0}$). For a spin one-half nucleus, there are two possible energy states, $m_I = -½, +½$ that are either approximately anti-parallel or parallel to the magnetic field. Thhe nuclear magnetic moment (μ_0) is directly proportional to the nuclear spin: $\mu_0 = \gamma\hbar[I(I + 1)]^{½}$, where the spin angular momentum is $P = \hbar[I(I + 1)]^{½}$ and $\hbar = h/2\pi$ (Fig. 1). The magnetogyric ratio (γ) is a constant relating the magnetic moment to the spin angular momentum of a particular nucleus, and it determines the direction of precession of a magnetic moment in a magnetic field. The magnetic moment and spin angular momentum are usually aligned parallel to each other, but there are exceptions such as for ^{29}Si and ^{15}N. An anti-parallel orientation will affect certain NMR experiments such as those that involve the nuclear Overhauser effect (NOE) or CP. The interaction energy between the magnetic moment and the magnetic field is given by the equation: $E = -\mu_z\mathbf{B_0}$, and the energy difference between adjacent energy levels is $\Delta E = -\gamma\hbar\mathbf{B_0}$ or $\Delta E = h\nu$, where ν is the radiation frequency. Transitions occur between energy levels by applying the appropriate radiofrequency electromagnetic radiation given by the equation, $h\nu = |-\gamma\hbar\mathbf{B_0}\Delta m_I|$. The selection rule for transitions is $\Delta m_I = \pm 1$. Substituting in the appropriate values gives the resonance frequency or Larmor frequency of the nucleus, $\nu_L = |-\gamma\mathbf{B_0}/2\pi|$. The vertical bars in the equation mean absolute value to show that the Larmor frequency of a particular nucleus is always positive.

Electrons in molecules shield and deshield nuclei and lead to different resonant frequencies (chemical shifts) for each nucleus in a unique environment. The chemical shielding effect for a nucleus is, $\nu_i = \gamma\hbar\mathbf{B_0}(1 - \sigma_i)$, where σ_i is the shielding constant for the nucleus, and $\mathbf{B_0}$ is the applied magnetic field corrected for the effect of bulk magnetization, which depends on the shape of the sample and its bulk

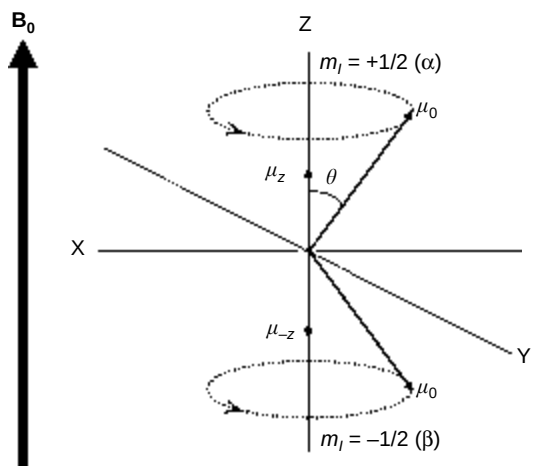

FIGURE 1 Spin one-half nuclear magnetic moments in a magnetic field ($\mathbf{B_0}$). The angle θ is 54.74° for spin one-half nuclei. μ_z is the z-component of the nuclear magnetic moments in $\mathbf{B_0}$. The α-state is lower energy and aligned parallel to $\mathbf{B_0}$, and the higher energy β-state is aligned anti-parallel to $\mathbf{B_0}$.

susceptibility. The electrons in molecular bonds also allow nuclear spins to interact or couple with each other, which results in fine splittings of the peaks produced by coupled spins. This is referred to as scalar coupling or J-coupling, and it is considered indirect because it is mediated by electrons. Dipolar coupling is referred to as direct coupling because it depends on the orientation and separation of nuclear dipoles that interact directly through space and not through bonding electrons. Dipolar coupling is a much stronger interaction than scalar coupling, and may cause significant peak broadening in solids. Dipolar coupling is not directly observed in NMR spectra of liquids or gases because it is averaged to zero by rapid motions. However, magnetic relaxation and the NOE rely on dipolar coupling, so it is a very important property for NMR structure determination in liquids. Other coupling mechanisms are also possible, but they are usually not important for spin one-half nuclei in common NMR samples.

The Boltzmann distribution of spins primarily determines the sensitivity for NMR spectroscopy. The NMR absorption and emission processes (i.e., transitions) between energy levels occur with equal probability, but the slight excess of spins in the lower energy state leads to absorption occurring more often. Each transition between energy states is a result of a spin flip from the α to β or β to α state. The equilibrium spin population ratio is: $n_\beta / n_\alpha = e^{-\Delta E/kT}$, where $n_{\alpha,\beta}$ are the spin populations in the α-state (lower energy) or β-state (higher energy) for the spin one-half case, k is the Boltzmann constant ($1.3806503 \times 10^{-23}$ J/K), ΔE is defined previously, γ for ^{1}H is 26.7515×10^7 rad·T^{-1}·s^{-1} and for ^{13}C is 6.7283×10^7 rad·T^{-1}·s^{-1}, the Planck constant ($\hbar = h/2\pi$) is $1.054571596 \times 10^{-34}$ J·s, and $\mathbf{B_0}$ is the magnetic field measured in tesla (kg·s^{-2}·A^{-1}) (24). In a magnetic field of 9.4 tesla at ambient temperature ($T \sim 298$ K), for every one million ^{1}H nuclei in the β-state, there will be one million and sixty-four in the α-state. The difference between the spin populations is graphed in Figure 2 for various magnetic field strengths represented by the corresponding ^{1}H frequency. The very small energy difference is the reason that NMR is inherently insensitive relative to other spectroscopic techniques. Low natural abundance also contributes to the decreased sensitivity of most nuclei relative to ^{1}H. A long T_1 relaxation time or short T_2 relaxation time for some nuclei may also adversely affect sensitivity. Relaxation properties will be discussed in more detail later. Dipolar coupling to the electric field gradient of quadrupolar nuclei or to unpaired electrons in paramagnetic systems can cause significant peak broadening and shifting that decreases the spectral resolution and also reduces the sensitivity. The weak transitions of NMR spectroscopy are also the reason that it has much higher resolution than any other spectroscopic techniques.

The magnetization vector in the positive z-axis (M_z) resulting from a summation of all the excess nuclear magnetic moments in the low energy state can be manipulated by modern NMR pulse sequences. Figure 3 shows what happens when a radiofrequency pulse (B_1) is applied perpendicular to M_z. M_z is equivalent to the equilibrium magnetization, M_0, when the time between pulses is sufficiently long to allow full relaxation of the particular nuclei being observed. The z component of the magnetization will rotate into the x–y plane if B_1 is applied for an appropriate length of time (i.e., a 90° pulse). The magnetization will then rotate in the x–y plane but not necessarily as a single vector, because each nucleus in a molecule may have a slightly different frequency (chemical shift) and may interact with other nuclei (coupling). This will break up the single magnetization vector into multiple vectors rotating at various rates orthogonally to the main field. The magnitude of each vector will also

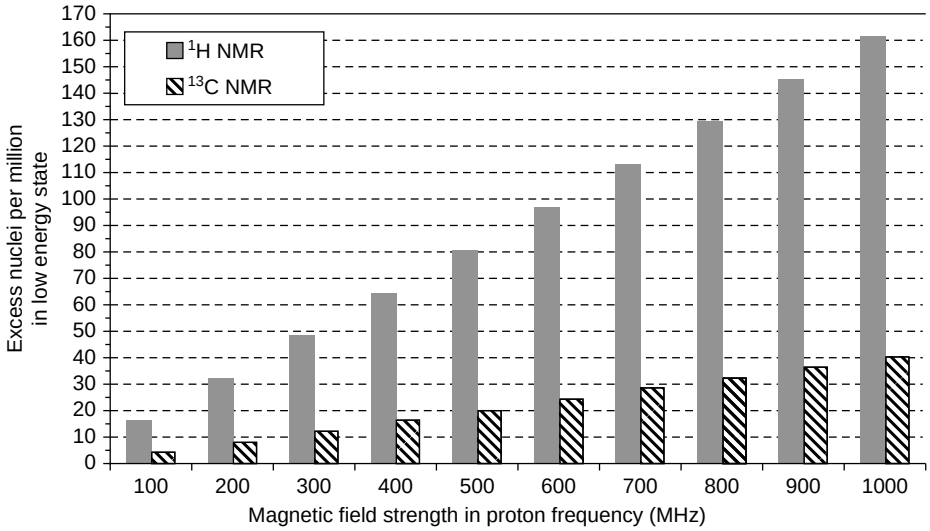

FIGURE 2 Bar graphs comparing the effect of the magnetic field strength on the number of excess nuclei in the lower energy state for two spin one-half nuclei. The effect of natural abundance is not taken into account for ^{13}C.

decrease over time due to interactions with electrons and nuclei in the sample that lead to relaxation. This is observed in the detector of the NMR spectrometer as a free induction decay (FID) where the signal intensity usually decays exponentially as the vectors dephase in the x–y plane due to random spin flips (T_2 relaxation) and as the equilibrium magnetization is re-established in the z-axis (T_1 relaxation) primarily through dipolar coupling. There is also another type of relaxation ($T_1\rho$) that occurs when the magnetization vector is continuously irradiated or spin-locked with a B_1 field that is typically in the kilohertz frequency region. The spin-lock is to achieve the Hartmann-Hahn matching condition, which is used in CP for solids or total correlation spectroscopy (TOCSY) and rotating frame Overhauser effect spectroscopy (ROESY) for liquids. In a solid, the time it takes for ^{13}C nuclei (or other low abundance nuclei) to be cross-polarized by ^{1}H nuclei (T_{CH}) is important because the ^{1}H $T_1\rho$ relaxation time determines how long the polarization will persist. Rapid ^{1}H $T_1\rho$ relaxation times may eliminate the sensitivity advantage that CP introduces. The ^{13}C T_1 and $T_1\rho$ relaxation times are usually not a significant factor for CP because they are almost always much longer than the ^{1}H relaxation times. The effects from relaxation due to the ^{1}H nuclei will occur long before those from ^{13}C nuclei can affect the magnetization. Accurate measurement of SSNMR relaxation times can be very important, and several of the most common techniques are compared by Frye (25). Figure 4 compares some of the effects of NMR parameters on the observed signal at various field strengths. Although it is generally beneficial to have a higher magnetic field strength, relaxation times may increase enough to adversely affect some samples and NMR experimental techniques. Higher field strength reduces the peak

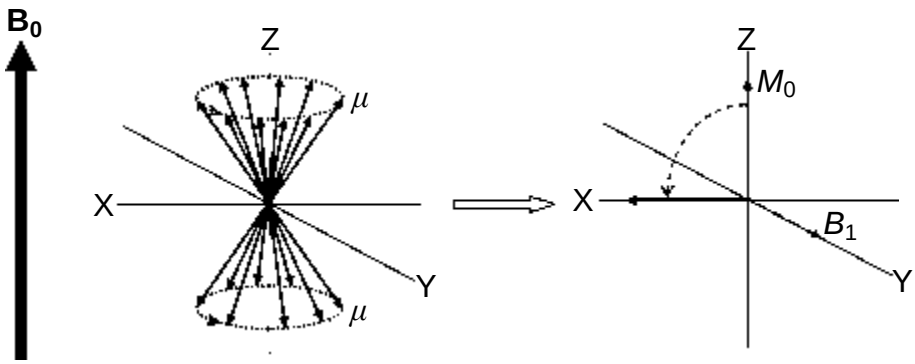

FIGURE 3 The magnetic moments for the excess nuclear spins in the lower energy state of a spin one-half nucleus in a magnetic field ($\mathbf{B_0}$) produce net magnetization (M_0) along the positive *z*-axis. A radiofrequency pulse (B_1) applied along the positive *y*-axis rotates the *z*-axis magnetization vector into the positive *x*-axis where it will begin to precess in the *x*,*y*-plane according to its Larmor frequency. If the nucleus exists in multiple unique environments as in a molecule, the magnetization vector will divide into vectors for each Larmor frequency corresponding to each chemical shift. Scalar coupling will also cause further separation of each vector in the *x*,*y*-plane, but usually this will be a much smaller effect because the frequency differences between peaks of multiplets are typically small relative to chemical shift differences.

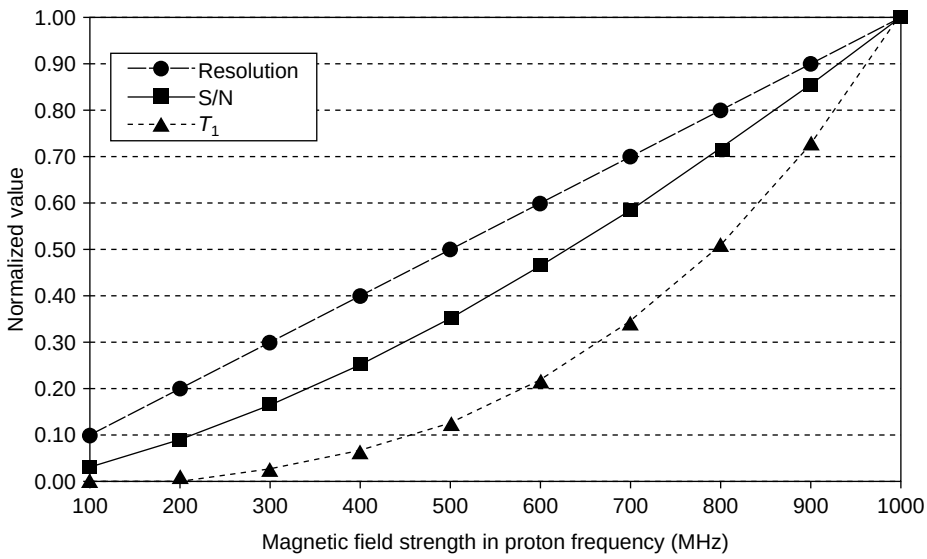

FIGURE 4 A graph of the effect of field strength on resolution, signal-to-noise ratio, and T_1 relaxation time. Although the resolution is expected to increase linearly with field strength, anisotropic bulk magnetic susceptibility, paramagnetic species, and quadrupolar coupling may significantly reduce this. In this comparison, the increase in the T_1 relaxation time has the largest deviation from linearity as the field strength increases.

broadening effect from quadrupolar nuclei, but it increases the longitudinal relaxation time (T_1) as well as the effects of chemical shielding anisotropy (CSA) and anisotropic bulk magnetic susceptibility (ABMS). These effects are particularly important for SSNMR spectroscopy.

SOLID-STATE NMR SPECTROSCOPY

NMR of solids presents significant problems compared to liquids. The rapid motions in liquids remove two effects that are largely responsible for the broad peaks typically observed in NMR spectra of solids: CSA and dipolar coupling. The T_2 relaxation time is also significantly shorter in solids, which increases the intrinsic peak widths. One of the main goals of SSNMR spectroscopy is to obtain spectra similar to what is observed for liquid-state NMR spectroscopy of the material in a solution. Figure 5 shows the structure of a simple organic molecule (DTPPAA) that has been used by the author to test pulse sequences for both liquid-state and SSNRMspectroscopy. The NMR spectra of DTPPAA are compared in Figure 6. Note that the chemical shifts are very close in the solid-state and liquid-state NMR spectra for DTPPAA with only one set of unresolved peaks (C14 and C17) in the SSNMR spectrum. This makes DTPPAA reasonably useful as a standard to test SSNMR pulse sequences and compare the results to the corresponding liquid-state NMR analyses. However, crystal packing forces and/or conformational changes will usually result in significant differences between liquid-state and SSNRMspectra.

For powdered solids, the nuclear magnetic moments are in fixed random orientations that result in broad peaks because both the CSA and dipolar coupling tensors have a $3\cos^2\theta - 1$ term, where θ is the angle of the tensor relative to the direction of $\mathbf{B_0}$. These phenomena will produce broad overlapped peaks in a SSNMR spectrum of a molecule with relatively few carbons. This would make SSNMR spectroscopy of limited use unless there was a means of reducing or eliminating the effects of CSA and dipolar coupling.

The isotropic component of chemical shielding averages to the isotropic frequency, ν_{iso}, in liquids due to rapid molecular motion, and the anisotropic component (CSA) vanishes. The CSA in solids depends on the orientation of nuclear magnetic moments with respect to the direction of $\mathbf{B_0}$. Nuclei of molecules in powdered solids have a distribution of parallel to perpendicular orientations relative to $\mathbf{B_0}$, and the peak shapes will depend on the crystallographic site symmetry at the nucleus (Fig. 7). Many different nuclei in a molecular solid will result in overlapping CSA patterns and a featureless spectrum with little useful information.

Dipolar coupling between spin one-half nuclei depends on the orientation of the dipolar vector between the nuclei relative to $\mathbf{B_0}$ as well as the distance between the nuclei. The distance dependence of dipolar coupling is very powerful for structural analysis of solids and partially ordered materials. The strength of the local field at each nucleus depends on the parallel to perpendicular orientations of dipolar vectors in the $\mathbf{B_0}$ field and gives rise to a distribution of resonance frequencies that produces peak shapes similar to axial CSA (Fig. 8). The two mirror image peaks are due to the two spin one-half transitions separated by the dipolar coupling constant (D_{CH}). The isotropic chemical shifts are identical for the two spin states and will be observed when the dipolar vector is at and angle of 54.74° relative to $\mathbf{B_0}$. There is no isotropic component of the dipolar coupling tensor, so it averages to zero in liquids due to rapid molecular motions, and has no direct effect on the spectrum. As for CSA,

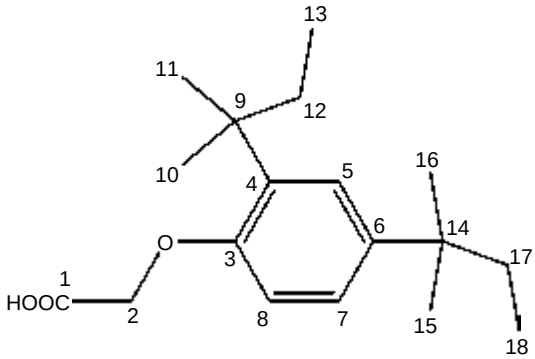

FIGURE 5 Chemical structure of (2,4-di-*tert*-pentylphenoxy)-acetic acid (DTPPAA) with numbering used for the assignments shown in Figure 6.

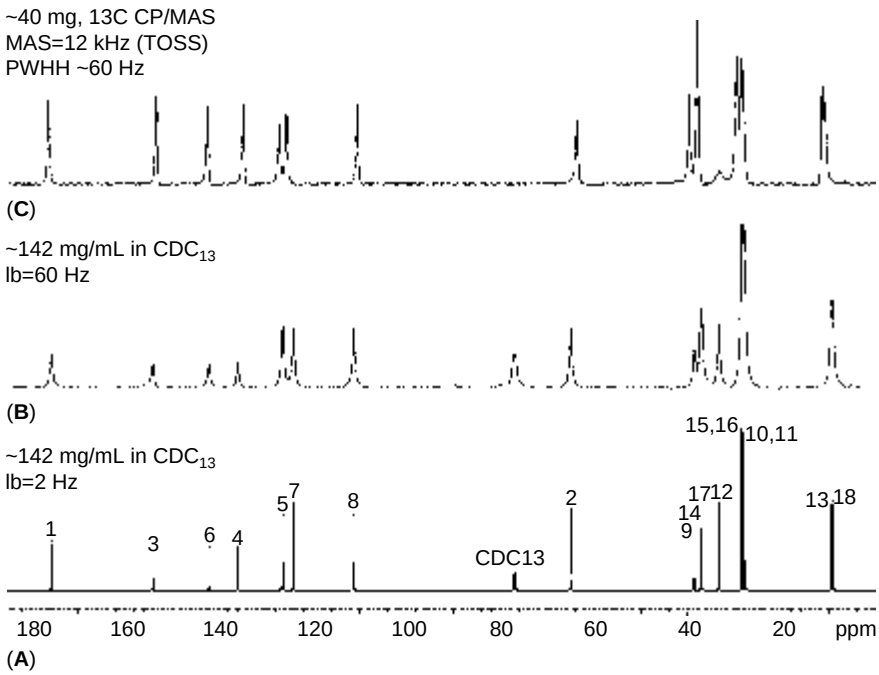

FIGURE 6 ^{13}C NMR spectra of DTPPAA at 9.4 T: (**A**) in $CDCl_3$ solution, (**B**) spectrum (**A**) with 60 Hz exponential multiplication, and (**C**) SSNMR spectroscopy of crystalline DTPPAA. The peak positions are similar for this molecule in the solid and liquid states. The peak labels in spectrum (**A**) are the resonance assignments for the structure in Figure 5. *Abbreviations*: CP/MAS, cross polarization magic angle spinning; TOSS, total side band suppression.

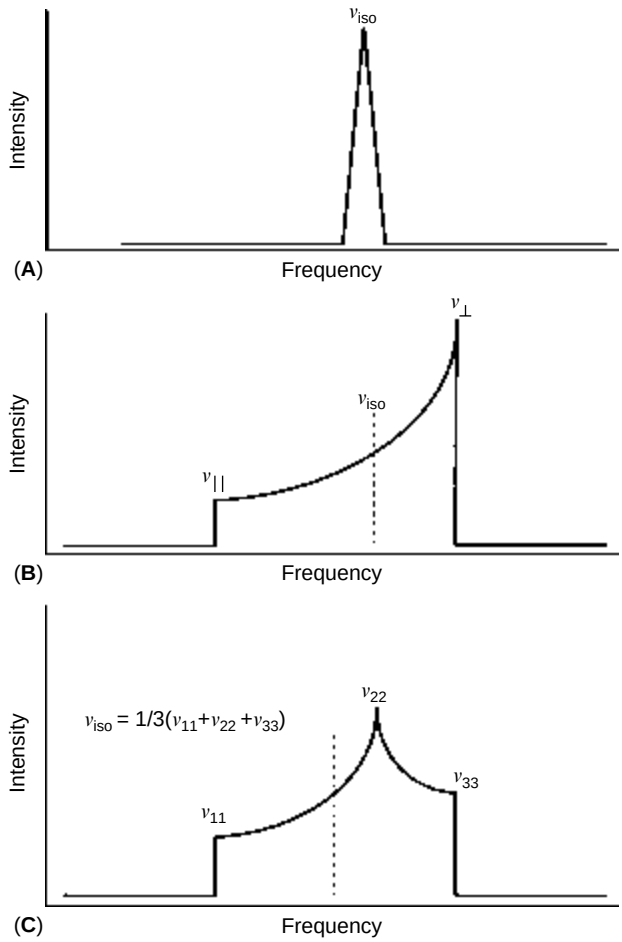

FIGURE 7 Representations of CSA powder patterns for (**A**) cubic, (**B**) axial, and (**C**) lower crystallographic site symmetry for a spin one-half nucleus relative to the magnetic field. Cubic symmetry results in only the isotropic frequency. For axial symmetry, the magnetic moment of the nucleus can vary between parallel and perpendicular orientations. The probability is much greater for a nuclear magnetic moment being in a perpendicular orientation, which results in the higher peak intensity for this case. The isotropic frequency for the axial case is a weighted average of the two extremes. The lower symmetry case results in a more complex peak shape, where υ_{22} will vary in position somewhere between the highest frequency (υ_{11}) and the lowest frequency (υ_{33}) with an isotropic frequency (υ_{iso}) as shown in the *bottom* diagram.

multiple dipolar coupled spins in a solid would result in many broad overlapped resonances and little useful information in the spectrum. Figure 9 shows the orientation dependence of dipolar coupling for two spin one-half nuclei in a solid. The results are similar for CSA except that only one peak will be present in each spectrum (i.e., the solid line spectrum of panel Fig. 9a and the corresponding peaks in Fig. 9b and c that align with frequencies for the parallel and perpendicular orientations.

The orientation dependence of CSA and dipolar coupling provides a means to reduce or eliminate their effects in SSNMR spectra. Andrew et al. discovered that rotating solid samples at 54.74° (the magic angle) relative to the magnetic field significantly reduced the peak widths in SSNMR spectra (26,27). Figure 10 shows the basic procedure for reducing CSA by rapid spinning at the magic angle, and it works essentially the same for dipolar coupling. In a powdered solid, all possible orientations of angles θ and β are present, but the angle of the rotor (θ_R) in the probe can be set by the operator.

Magic angle spinning (MAS) will cause modulations in the spectrum that extend out from the isotropic chemical shift position of each nucleus at integral multiples of the spinning speed. These spinning side bands move farther out and decrease in intensity as the spinning speed increases. The intensity of the isotropic peak increases with the spinning rate while the spinning side bands decrease until they are eliminated when the rate of rotation exceeds the CSA. An example of MAS for glycine (Fig. 11) is shown in Figure 12. Note the different CSA powder patterns for the carbonyl and methylene resonances in spectrum (a) of Figure 12. For ^{13}C SSNMR, the carbonyl resonance has a relatively large CSA (~150 ppm), whereas aliphatic carbons have significantly smaller CSA (~60 ppm). The CSA increases with field strength (e.g., for ^{13}C 100 ppm is ~10 kHz at 9.4 T and 15 kHz at 14.1 T), which means that faster spinning is required at higher field strengths to reduce the spinning side bands to the same extent. Smaller diameter rotors are required to achieve faster spinning speeds, but the reduced sample quantity results in lower sensitivity that may not be compensated by the higher field strength. If necessary, spinning side bands can be suppressed by using the total side band suppression (TOSS) technique first introduced by Dixon (28–33). In the typical four-pulse TOSS sequence, the 90° pulse width for the X-nucleus must be reasonably accurate for good suppression of the side bands. TOSS is particularly useful for removing overlapping side bands when the spinning speed is not fast enough to push them out past the peaks of

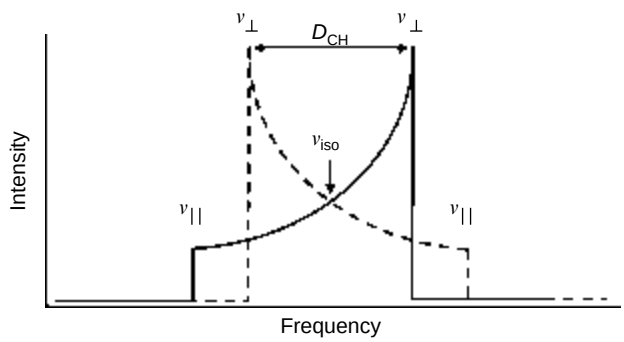

FIGURE 8 A diagram of a heteronuclear dipolar coupling powder pattern for the simple case of two coupled spins (e.g., ^1H and ^{13}C). The solid and dashed lines represent the two spin states for either of the spin one-half nuclei. Note the similarity of one peak of this pattern to the axial symmetry for CSA. The dipolar vectors also vary between the parallel and perpendicular orientations with respect to the magnetic field. The dipolar coupling constant is D_{CH}.

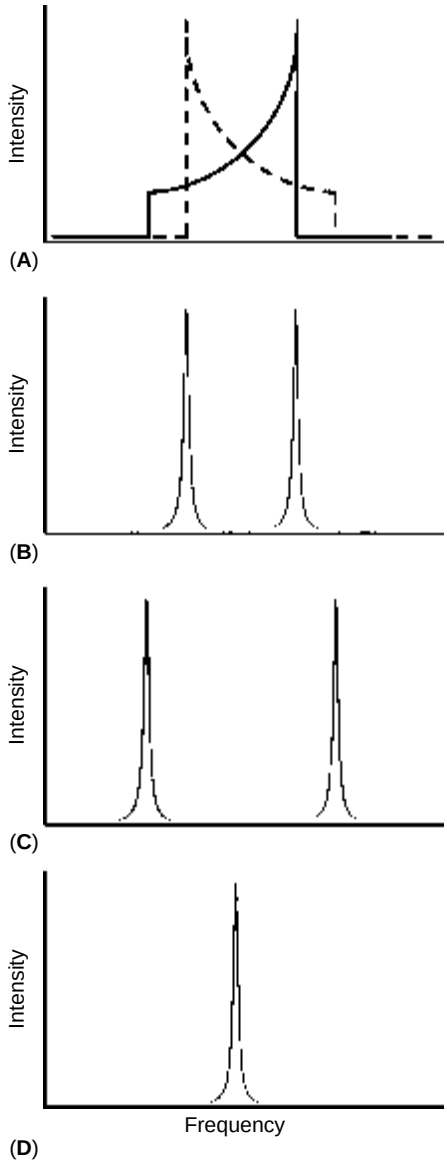

FIGURE 9 Representations of dipolar coupling for a two spin case: (**A**) powder pattern for randomly oriented dipolar vectors, (**B**) perpendicular orientation, (**C**) parallel orientation, (**D**) 54.74° orientation (the magic angle). Spectra (**B**)–(**D**) would be obtained for a single crystal positioned as specified.

interest such as with larger diameter rotors or at high magnetic field strengths. The ^{13}C CP/MAS spectrum (c) of Figure 6 was obtained with TOSS to eliminate potential overlap of the small isotropic peak at approximately 34 ppm with spinning side bands, which also helped confirm that it was a real peak.

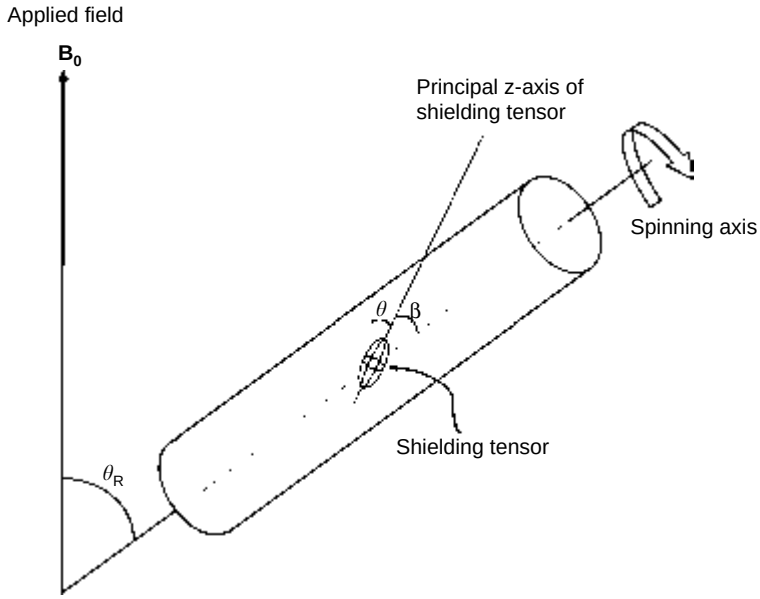

FIGURE 10 Spinning a sample rapidly at the magic angle (θ_R = 54.74°) will average the CSA (and the dipolar coupling) to zero because of $3\cos^2\theta - 1$ dependence of their orientation with respect to the magnetic field. Adapted from Ref. (12).

As with CSA, MAS will eliminate dipolar coupling only if it is significantly faster than the strength of the dipolar interaction (i.e., tens of kHz). Otherwise, it is scales the dipolar coupling in proportion to the spinning speed and gives broader peaks. MAS will usually remove the homonuclear dipolar coupling between ^{13}C nuclei because it is much weaker than $^{1}H/^{13}C$, $^{1}H/^{1}H$, $^{19}F/^{13}C$, or $^{19}F/^{1}H$ dipolar couplings (11). High-power ^{1}H decoupling is used to dramatically narrow the peaks in ^{13}C and ^{15}N detected SSNMR spectra. Simultaneous high-power ^{1}H and ^{19}F decoupling can also be used if both nuclei are present in the molecule of interest. Both scalar (through-bond) and dipolar (through-space) coupling are removed by decoupling. The decoupling power necessary to remove the dipolar interaction in solids is substantially greater than that used for broadband proton decoupling of the scalar coupling in liquid samples. Continuous wave decoupling was originally used, but dramatically improved results are possible with newer modulated techniques that will be discussed later.

Nuclei with low sensitivity (e.g., ^{13}C and ^{15}N) can be difficult to obtain spectra with good signal to noise in a reasonable time. Pines et al. first used the CP technique to increase the sensitivity of low natural abundance spins (34). This technique relies on dipolar coupling to transfer polarization from ^{1}H to ^{13}C nuclei, and its effectiveness is thus extremely dependent on the separation between the ^{1}H and ^{13}C nuclei in a solid. The enhancement of the ^{13}C signal is roughly proportional to the magnetogyric ratios of the nuclei. The high natural abundance and strong magnetic moment of protons results in an approximate four-fold enhancement of the ^{13}C signal or 10-fold enhancement of the ^{15}N signal. Because the ^{1}H T_1 relaxation time is

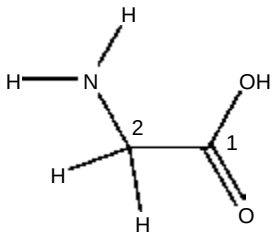

FIGURE 11 Chemical structure of the amino acid glycine.

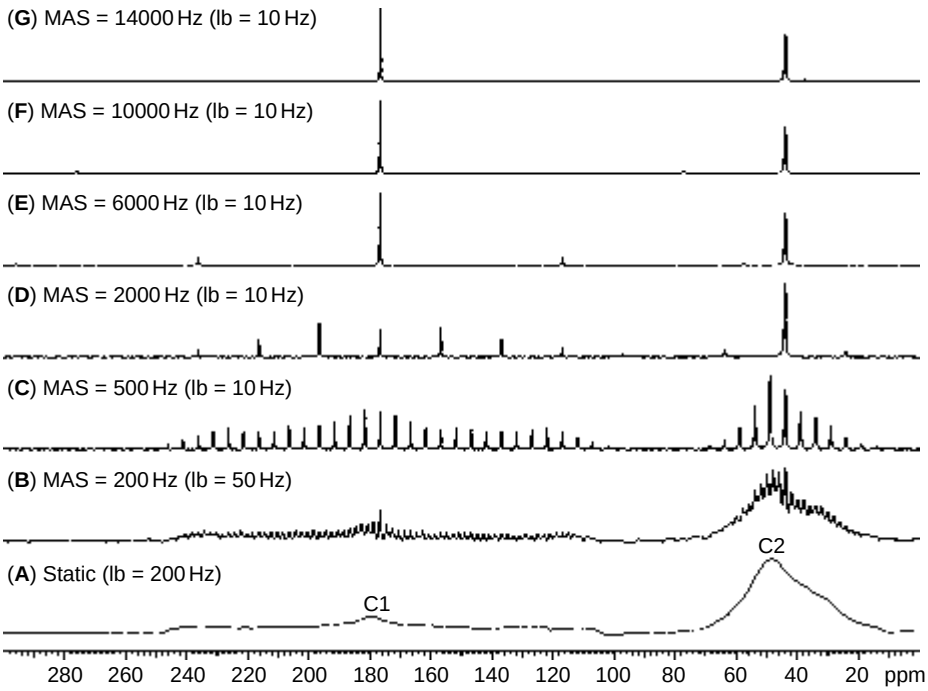

FIGURE 12 The effect of MAS on the ^{13}C SSNMR spectrum of glycine at 9.4 T. The peaks of the static pattern in (**A**) are broken up into spinning side bands that are separated by integral multiples of the spinning speed in spectra (**B**)–(**G**). The isotropic frequency is not readily apparent until the spinning speed is fast enough to reduce the spinning side bands significantly (2 kHz for methylene, 6 kHz for carbonyl). Note that the spinning side bands for the methylene resonance are essentially eliminated at 6 kHz because this is approximately equivalent to the CSA (60 ppm $\times$ 100 Hz/ppm = 6000 Hz). The spinning speed would need to be approximately 15 kHz to eliminate the spinning side bands for the carbonyl resonance, which has a CSA of ~150 ppm. *Abbreviation*: MAS, magic angle spinning.

usually much shorter than those of ^{13}C or ^{15}N, CP permits the acquisition of more scans in less time because the proton spin polarization determines how efficiently the X-nuclei are cross-polarized.

Stejskal and Shaefer first used a combination of magic angle spinning, high-power ^{1}H decoupling, and CP to obtain high-resolution ^{13}C SSNMR spectra (35,36). This CP/MAS technique is the standard procedure for obtaining high-resolution NMR spectra of solids. The effects of these three techniques on the ^{13}C SSNMR spectrum of glycine (Fig. 11) are shown in Figures 12 and 13. The CSA powder patterns are readily observed for the carbonyl and methylene carbon resonances of the static spectrum (a) of Figure 12. The enhancement due to CP is also apparent in spectra (b) and (d) of Figure 13. The high-power decoupling has the most dramatic effect on reducing the peak widths in the spectra (c) and (d) of Figure 13. An efficient modulated ^{1}H decoupling method [SPINAL-64 (57)] was used whenever decoupling was required because it is significantly better than the continuous wave decoupling procedure that was first used for ^{13}C CP/MAS spectra and is still used in many of the literature examples discussed in section "Solid-Form Characterization" on p. 398.

The basics of acquiring 1D SSNMR spectra has been demonstrated in an excellent article by Bryce et al., which is highly recommended to both novices and experienced NMR spectroscopists (37). Several things are important to clarify regarding this useful review. First, the authors state that glycine polymorphism may cause problems with using it as a standard for chemical shift referencing, CP, and sensitivity. However, the glycine polymorphs have such different relaxation properties, and it would not be difficult to determine if there was a polymorphic transformation in a glycine standard sample. The metastable α-glycine has significantly shorter relaxation times, which means that phase transformation is not likely to go unnoticed when obtaining SSNMR spectra (38). In this author's hands, the α-glycine polymorph appears to be stable for years under ambient storage conditions and in regular use as a ^{13}C CP/MAS SSNMR reference standard for signal-to-noise measurement, Hartmann-Hahn matching for CP, as a chemical shift reference, and to optimize ^{1}H decoupling (including at nonambient temperatures, –40°C to +80°C). The same sample of solid α-glycine has shown no detectable phase transformation or degradation affecting its ^{13}C CP/MAS spectrum for at least four years of regular use. Second, spectra C and D of Figure 7 in the review by Bryce et al. appear to be the same, which does not show the effect of two pulse phase modulated (TPPM) decoupling for spectrum D as the authors intended (37). Therefore, one should expect different results using the stated conditions. The peak for the methylene carbon of phenylacetic acid would actually be much like in spectrum B but with greater intensity due to the variable amplitude CP (VACP) in addition to the TPPM decoupling. The peak for the carbonyl resonance may not be narrowed as dramatically by TPPM, but it would likely be similar to what is shown in spectrum B of Figure 7 in the review by Bryce et al. (37).

Taylor has also written a more specific summary of the basic experimental set up procedures for ^{13}C CP/MAS SSNMR spectroscopy (39), and an interesting ^{13}C SSNMR spectroscopy study of the effect of low temperatures (–60°C) on the polymorphs of glycine (40). The changes in relaxation times (longer ^{1}H T_1 and shorter ^{1}H $T_1\rho$) for the glycine polymorphs at low temperature combine to make it significantly more difficult to acquire high sensitivity spectra in a reasonable amount of time. The carbonyl resonance is affected more dramatically because the magnitude of the changes in relaxation times is greater. This makes glycine somewhat problematic

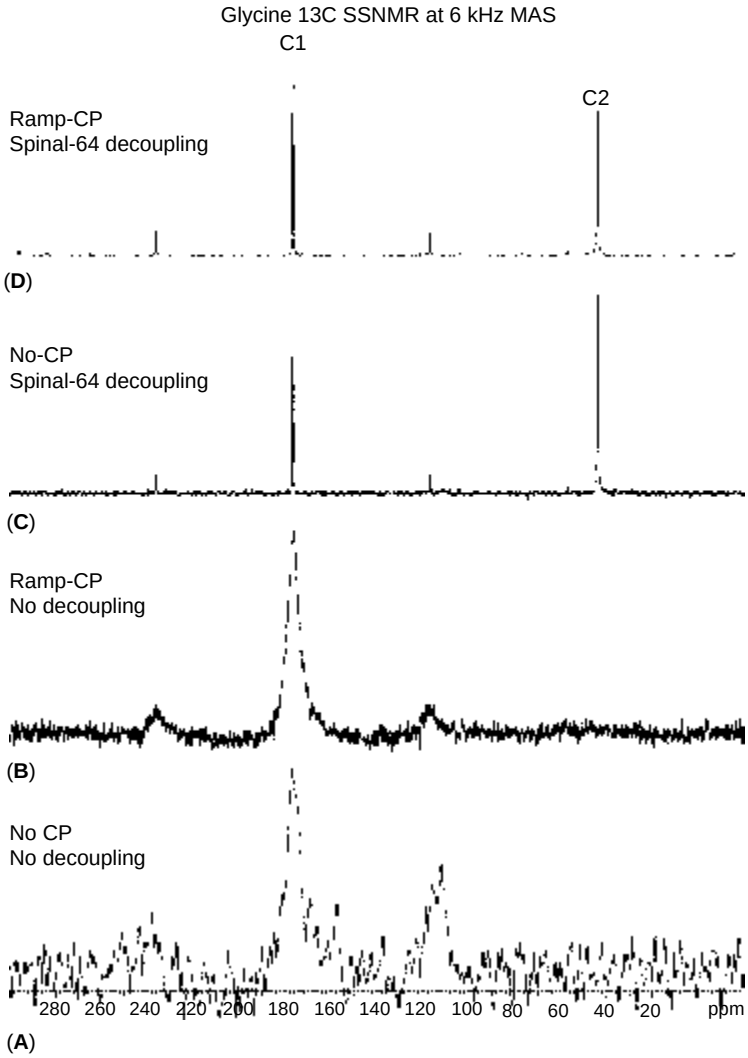

FIGURE 13 The effects of high-power ^{1}H decoupling and CP are shown for ^{13}C SSNMR spectra of glycine at 9.4 T and 6 kHz MAS. The MAS speed is too slow to reduce the dipolar coupling enough to observe the methylene resonance (C2) in spectra (**A**) and (**B**). CP dramatically increases the signal-to-noise ratio [compare spectra (**A**/**B**) or **C**/**D**)]. High-power ^{1}H decoupling is required to get the narrowest peaks in spectra (**C**) and (**D**). The apparent peak at approximately 115 ppm in spectrum (**A**) is due to the transmitter artifact partially overlapping a broad spinning side band combined with the very low signal-to-noise ratio of the spectrum. *Abbreviations*: CP, cross-polarization; MAS, magic angle spinning; RAMP-CP, ramped amplitude cross polarization; SSNMR, solid-state nuclear magnetic resonance.

as a reference standard to optimize the spectrometer at low-temperature conditions. However, this is not a significant problem in practice until the temperature is approximately –50°C, especially if amplitude- or frequency-modulated CP (41–48) and modulated decoupling are used (49–59).

Setting the magic angle accurately is obviously very important for obtaining the highest resolution SSNMR spectra. Frye and Maciel demonstrated the use of potassium bromide as a useful means of setting the magic angle for ^{13}C SSNMR spectroscopy (60). More recently, Antonijevic and Bodenhausen have used deuterated α-oxalic acid to set the magic angle to within 0.01° by minimizing the residual ^{2}H quadrupolar coupling (61). Barich et al. have shown that 3-methylglutaric acid (MGA) can be used to set the magic angle, optimize the Hartmann-Hahn match for CP, determine the signal-to-noise ratio, and as chemical shift reference for ^{13}C SSNMR spectroscopy (62). The two carboxylic acid carbonyl resonances for MGA are used to set the magic angle because carbonyl groups have a large CSA, which makes them very sensitive to the magic angle setting. However, adamantane is still the best molecule to use for optimizing the field homogeneity due to its very narrow ^{13}C SSNMR peak width (<0.05 ppm).

As noted earlier, SSNMR spectroscopy requires additional procedures compared to liquid-state NMR spectroscopy to obtain high-resolution spectra. The three procedures currently used are high-power ^{1}H decoupling, magic angle spinning, and CP. These have advanced in several ways since their inception. Magic angle spinning for spin one-half nuclei has been extended to double rotation (DOR) and dynamic angle spinning (DAS) for quadrupolar nuclei (63). Spinning speeds have also increased from several kHz when MAS was initially developed, to tens of kHz now. This is particularly helpful for ^{1}H and ^{19}F SSNMR, because these nuclei have strong dipolar coupling (40–50 kHz) compared to ^{13}C (10–20 kHz) and high natural abundance. Very fast spinning will reduce the dipolar coupling to give narrower peaks. High-power proton decoupling has progressed from continuous wave to various frequency and phase modulated decoupling methods (49–59). One of the best ^{1}H decoupling methods currently available for common use is the small phase incremental alternation (SPINAL-64) decoupling procedure (57), which is based on supercycles of the TPPM decoupling of Bennett et al. (59). TPPM decoupling itself was a dramatic improvement over existing decoupling techniques. CP has also advanced from the original continuous polarization to VACP and ramped amplitude (RAMP-CP) polarization techniques. RAMP-CP is more efficient than VACP and dramatically better than standard CP, particularly for rapidly spinning samples (>10 kHz). The result from using these techniques is higher sensitivity and resolution SSNMR spectra for all of the common nuclei. A minor drawback to using these modern techniques is that they require more complicated pulse sequences and additional effort to optimize them for obtaining spectra.

Temperature control for the sample is important for studying a variety of solid-state properties such as reactivity, relaxation properties, and molecular dynamics. Accurate temperatures in a SSNMR rotor have been significantly more difficult to obtain and determine than for liquids NMR (see Ref. (4) and references therein). Methanol or ethylene glycol is typically used for temperature calibration in liquid-state NMR spectroscopy, but they can work well for SSNMR spectroscopy in an appropriately sealed rotor. Antonijevic and Bodenhausen note that liquid methanol was used to calibrate the temperature in the rotor for their study (61). Methanol is used primarily for ambient and lower temperatures, whereas ethylene glycol is

used for ambient and higher temperatures. The overlap around room temperature is useful for connecting calibration curves for the entire temperature range of a probe. A significant advantage of using methanol and ethylene glycol is that only one or two samples are required to accurately determine an entire temperature calibration curve simply by measuring the frequency difference between the two peaks. The disadvantage is that a modified pulse sequence may be required to measure the temperature under similar CP/MAS conditions that will be used for solid samples. This is because the temperature calibration for either methanol or ethylene glycol must be determined with a ^{1}H pulse sequence, and liquids will not give NMR signals with CP as do solids.

SOLID-FORM CHARACTERIZATION

Molecular polymorphism can be divided into several types. Conformational polymorphism occurs when a molecule exists in two or more different conformations in a crystalline solid. Packing polymorphism occurs when a single conformation of a molecule is arranged in one of several unique orientations that have different long-range order. Polycrystalline powders are the typical samples for SSNMR spectroscopy and usually have a crystallite size in approximately the micrometer range (i.e., microcrystalline). Amorphous solids are essentially random arrangements of molecules, but they have some short-range order relative to each other because molecular motions are restricted in the solid state. Only the rapid tumbling of molecules in liquids or gases results in truly amorphous material. The molecules of amorphous solids can also have multiple conformations, which might suggest that these conformational differences would be observable by SSNMR spectroscopy or other techniques. However, the different conformations and the random spatial order of an amorphous solid tend to be indistinguishable by SSNMR spectroscopy because they have similar peak broadening effects on the spectrum. Nanocrystalline solids may also be distinguished from amorphous solids by SSNMR spectroscopy. Nanocrystallites will typically appear almost identical to microcrystallites or macrocrystallites (single crystals) by SSNMR spectroscopy using the typical CP/MAS technique. If nanocrystalline solids have significant disorder due to defects, they may be difficult to distinguish from amorphous solids.

The majority of the reports on polymorphism that are reviewed in this chapter were published within approximately the last eight years. Many published reports in the pharmaceutical literature use SSNMR spectroscopy as a secondary technique to analyze solid forms, and the interpretation tends to be rather minimal even when the results are quite interesting or potentially critical to a study. The complexity of NMR spectroscopy can be daunting at times, but the body of literature available on data acquisition and interpretation is extensive and reasonably easy to understand even for a novice (37,39). The value of SSNMR spectroscopy is significant for pharmaceutical solid-form analysis, and should be used to its greatest advantage as a complementary technique to XRPD, vibrational spectroscopy, microscopy, and thermal analyses. Hopefully, the examples provided in this chapter will demonstrate both the strengths and weaknesses of SSNMR spectroscopy in characterizing pharmaceutical solid forms.

Conformational polymorphism, where distinct conformations of a molecule result in different crystal forms, has been studied for decades (64,65). SSNMR spectroscopy is useful here because it is very sensitive to molecular conformations and

short-range order in solids. Griesser et al. studied conformational polymorphism in oxybuprocaine hydrochloride with spectroscopy, X-ray diffraction, and thermal analyses, and found it to have either a less stable bent conformation (U-type) or a more stable straight conformation (I-type) in the crystal forms (66). This local anesthetic drug has three polymorphs: modification I with one U-type conformer per asymmetric unit, modification III with two U-type conformers per asymmetric unit, and modification II° with one U-type and one I-type conformer in the asymmetric unit. Modification II° is the most stable polymorph below approximately 90°C, modification I is more stable above this temperature, whereas modification III is metastable over the temperature range studied. Both ^{13}C and ^{15}N SSNMR spectroscopy were useful in determining the number of molecules per asymmetric unit, and molecular mobility was studied using variable temperature analyses and the dipolar dephasing technique. The dipolar dephasing NMR experiment can be used to analyze molecular motion because dipolar coupling is reduced for more mobility for more mobile regions of a molecule.

Vogt et al. studied the two enantiotropic polymorphs of {4-(4-chloro-3-fluorophenyl)-2-[4-(methyloxy)phenyl]-1,3-thiazol-5-yl} acetic acid by ^{1}H, ^{13}C, ^{15}N, and ^{19}F SSNMR spectroscopy (67). A thorough SSNMR spectroscopy study was used to help understand the structures of each polymorph determined by X-ray diffraction. The solid-state transition temperature of the polymorphs was ~30°C. Form I was thermodynamically more stable below 35°C, but form II was more stable to milling and had lower hygroscopicity. The single-crystal structure of form I was determined, but form II did not produce suitable single crystals. The structure of form II was determined using XRPD, and various SSNMR spectroscopy analyses were used to provide additional restraints for the structure determination. Two 2D NMR pulse sequences that rely on dipolar coupling, ^{1}H DQ-BABA (double quantum back-to-back) and ^{1}H–^{13}C HETCOR (heteronuclear correlation), were used to determine conformational features of both polymorphs. The 2D PASS (phase-adjusted spinning sidebands) pulse sequence was used to determine chemical shielding tensors (CSTs) for ^{13}C resonances of form II to help refine the calculated structure. The orientation dependence of CSA is useful in providing unique structural details to support diffraction analyses. The authors suggest that, with additional work on other polymorphs, it may be possible to use SSNMR spectroscopy rather than the Burger–Ramberger IR rule for predicting the relative stability of polymorphs (68,69). The degree of peak overlap in the spectral region sensitive to hydrogen bonds is not nearly the problem for SSNMR spectroscopy as it is for IR spectroscopy. This study is an excellent example of using multinuclear, multidimensional SSNMR spectroscopy as a powerful technique to thoroughly characterize polymorphs. However, many of the analyses and the interpretation require a high level of expertise in NMR spectroscopy.

Maccaroni et al. studied the solid-state form interconversions for two linezolid (Fig. 14) polymorphs by ^{13}C SSNMR, XRPD, and thermal methods (70). Most of the SSNMR peaks were assigned for the two polymorphs by comparison to the ^{13}C NMR assignments of linezolid in a $CDCl_3$ solution. However, this procedure will not necessarily lead to correct assignments for the solid state unless the conformations are very similar or the electronic environment around each nucleus is coincidentally the same as shown for DTPPAA in Figure 6. It appears that the spectra of both polymorphs were acquired with the same parameters (e.g., contact time, pulse delay, number of scans), but form IV obviously has a longer ^{1}H T_1 relaxation time based on

the much lower signal-to-noise ratio in the spectrum (Fig. 15). The peak widths also are somewhat broader for form IV, which may result from unresolved peaks of two very similar molecules per asymmetric unit, as the authors state. The authors also note that the lowest frequency methyl carbon resonance of form IV is split into two peaks (nearly overlapping), which may be consistent with two molecules per asymmetric unit. However, this could also be explained by conformational exchange due to restricted rotation about the amide bond, which is quite well known for liquid-state NMR spectroscopy. The small symmetrical splitting of C2 (~170 ppm) in form II is likely due to conformational exchange rather than coupling to ^{14}N, because the quadrupolar broadening effect is not very large at this field strength (~9.4 T), and only some peak broadening is likely to be observed instead. The ^{13}C-^{14}N coupling usually produces asymmetrical splitting at lower field strengths where it is more readily observed (71–75). The ^{19}F atom directly bonded to the aromatic carbon (C9) produced significant broadening for this peak in the spectrum of form II due to the relatively strong scalar and dipolar coupling. The C8 resonance also shows broadening as do the C7 and C10 peaks to a lesser extent (Fig. 15). This is because ^{19}F decoupling is not commonly used simultaneously with ^{1}H decoupling for ^{13}C CP/MAS SSNMR spectroscopy unless the spectrometer and probe are specifically designed to do so. The MAS speed would need to be much faster than 7 kHz to reduce ^{19}F–^{13}C dipolar coupling significantly. The effect of ^{19}F coupling shows that for form II, C9 should be assigned to the broader peak at 154.9 ppm, and C6 should be assigned to the peak at 157.2 ppm. The C6 and C13–C16 resonances were apparently not observed for form IV supposedly because of broadening due to their proximity to oxygen and nitrogen in the molecule. However, the assignments for the C6 and C9 resonances are also swapped for form IV, which means that the C9 resonance is broadened (by ^{19}F coupling) into the baseline noise in this spectrum that already has a very low signal-to-noise ratio relative to the spectrum of form II (Fig. 15). This alternative interpretation of the spectrum of form IV is supported by the missing C13–C16 resonances (also broad in the spectrum of form II), which are likely broadened due to inefficient ^{1}H decoupling. Although the experimental details for the SSNMR spectroscopy data acquisition are very minimal in this report, it is quite likely that the older continuous wave ^{1}H decoupling scheme rather than one of the modern modulated decoupling methods was used to acquire the SSNMR spectra. The contact time (1 millisecond) is also relatively short, and may partly account for the low sensitivity of some quaternary carbons in the spectrum of form IV. The difficulties in correctly interpreting SSNMR spectra to compare solid forms can be reduced by using modern fast MAS and modulated decoupling or simultaneous ^{1}H and ^{19}F decoupling along with efficient CP. One or more of the various spectral editing methods would have been particularly useful in confirming the assignments in this case (76).

Two polymorphs of buspirone hydrochloride were compared using ^{1}H and ^{13}C SSNMR spectroscopy (observed and calculated values), XRPD, Fourier transform spectroscopy, infrared spectroscopy (FT-IR), and differential scanning calorimetry (DSC) (77). The single-crystal X-ray structure was determined for form I and found to be very similar to previous work. The authors used XRPD and DSC for quantitative analysis of mixtures of polymorphs and compared the results to previous quantitative FT-IR data. The XRPD patterns were difficult to use for quantification in this case. FT-IR spectroscopy gave superior quantitative data based on the summaries in Table 1 of their report (77), although the authors did not discuss

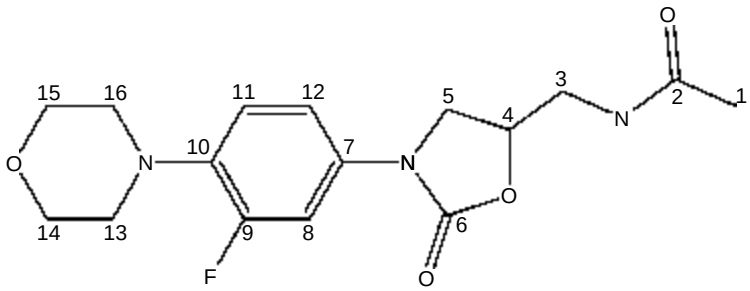

FIGURE 14 Chemical structure of linezolid. Adapted from Ref. (70).

this further. The ^{13}C SSNMR spectra clearly differentiated between the two forms, but form I appeared to have a longer ^{1}H relaxation time based on its relatively low signal-to-noise ratio. This may be why the authors were not able to obtain a ^{1}H SSNMR spectrum of form I, and also suggests that quantification by SSNMR spectroscopy may not be very practical in this case. The calculated ^{1}H and ^{13}C NMR chemical shifts were in generally good agreement with the observed values. The authors used the comparisons to determine which portions of buspirone hydrochloride had the greatest effect on the SSNMR spectroscopy differences observed for the two polymorphs. These comparisons with calculated chemical shifts are useful if the resonance assignments have not been previously obtained from a liquid-state NMR spectrum of the same molecule. Although calculated NMR chemical shifts have progressed greatly in recent years, it is still difficult to unambiguously determine them for cases when the molecular conformations are very close.

A recent study of donepezil hydrochloride used XRPD, SSNMR, vibrational spectroscopy, and thermal analyses to characterize five polymorphs, two hydrates, and an amorphous form (78). This work demonstrates the utility of multiple analytical techniques for characterizing pharmaceuticals. Unfortunately, each technique was not used to analyze every sample, which prevents a complete comparison of them. In general, the spectroscopic techniques could differentiate the solid forms. The authors apparently found three forms of a trihydate ("hydratemorphism") based on DSC, FT-IR, and water vapor sorption analyses. However, none of these hydrate forms were analyzed by any of the three most powerful solid-state techniques (XRPD, SSNMR spectroscopy, and Raman spectroscopy). These additional analyses would have greatly enhanced their case for "hydratemorphism." The authors also observed that hydrate I had slightly higher water content by Karl Fischer titration than a monohydrate, and one of three proposed reasons was that a small amount of amorphous material may cause this. The Karl Fischer results are explained by the observation of weak broad peaks in the SSNMR spectrum due to disordered material, and the XRPD pattern showed some diffuse scattering typical of disordered material. An interesting observation is that the carbonyl resonances in the ^{13}C SSNMR spectra are shifted to higher frequency for the hydrates, which is expected for hydrogen bonding with water.

Masuda et al. examined the α and γ forms of indomethacin by XRPD and ^{13}C CP/MAS SSNMR spectroscopy (79). They were able to determine that α-indomethacin

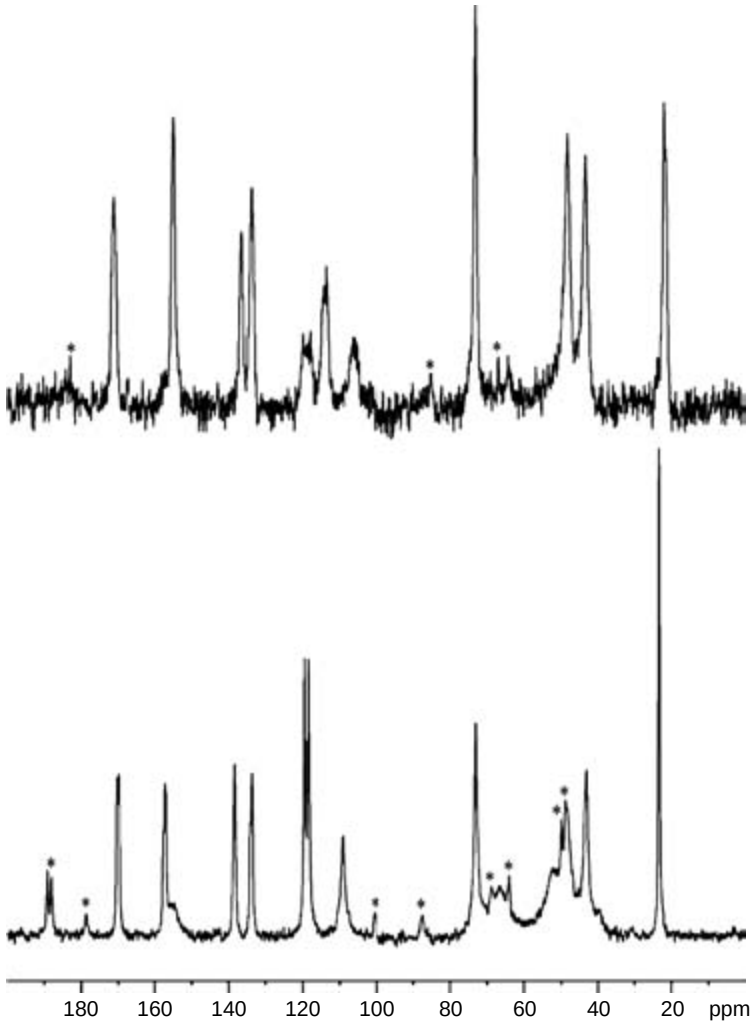

FIGURE 15 ^{13}C CP/MAS spectra of linezolid form II (*bottom*) and form IV (*top*) obtained at 9.4 T and 7 kHz MAS. Asterisks indicate spinning sidebands. Adapted from Ref. (70).

has three molecules per asymmetric unit while γ-indomethacin has only one based on the peak splitting (Fig. 16). However, the methoxy group (C12) and the aromatic carbon to which it was bonded (C5) of α-indomethacin also showed a slight splitting of the highest frequency peak at low temperature (203 K), which seemed inconsistent with three molecules per asymmetric unit. The variable temperature SSNMR analyses (at 203, 298, and 343 K) showed that this splitting was due to conformational exchange for one molecule in the asymmetric unit (Fig. 17). The flexible methoxy group (C12) of one molecule in the asymmetric unit is also in two slightly different conformations resulting in two nearly overlapping signals, and this apparently affects the aromatic carbon (C5) to which the methoxy group is bonded. The other

methyl group (C13) also shows some conformational flexibility, but it results in a broader peak rather than splitting. This is a good example of the sensitivity of SSNMR spectroscopy to molecular conformations of solid forms. Conformational flexibility is typically seen in an X-ray crystal structure as an enlarged thermal ellipsoid. The low temperature (<300 K) SSNMR spectrum shows that the methoxy carbon atom for one of the molecules in the asymmetric unit become "conformationally trapped" in one of two different environments. Above 300 K the methoxy group is apparently mobile enough to cause coalescence of the peaks. It was not clear from the report if temperature cycling or varying the cooling rate resulted in the same final spectrum at ambient temperature. This could demonstrate whether the two conformations became equally populated, or if they could be trapped unequally in the different conformations.

Apperley et al. also studied the solid forms of indomethacin as well as nifedipine by ^{1}H and ^{13}C SSNMR spectroscopy and ^{1}H T_1 and $T_1\rho$ relaxation analyses (80). The ^{13}C SSNMR spectroscopy peak widths of crystalline nifedipine were significantly narrower than for crystalline indomethacin, which suggests that molecular mobility is higher for nifedipine. The authors showed that amorphous nifedipine recrystallizes upon grinding while amorphous indomethacin does not. The onset points for the glass transition temperatures (T_g) of indomethacin and nifedipine are ~42°C and ~45°C, respectively. Nifedipine recrystallized at 55°C into a mixture of two different polymorphs (forms I and II), which converted almost completely to form I at 70°C.

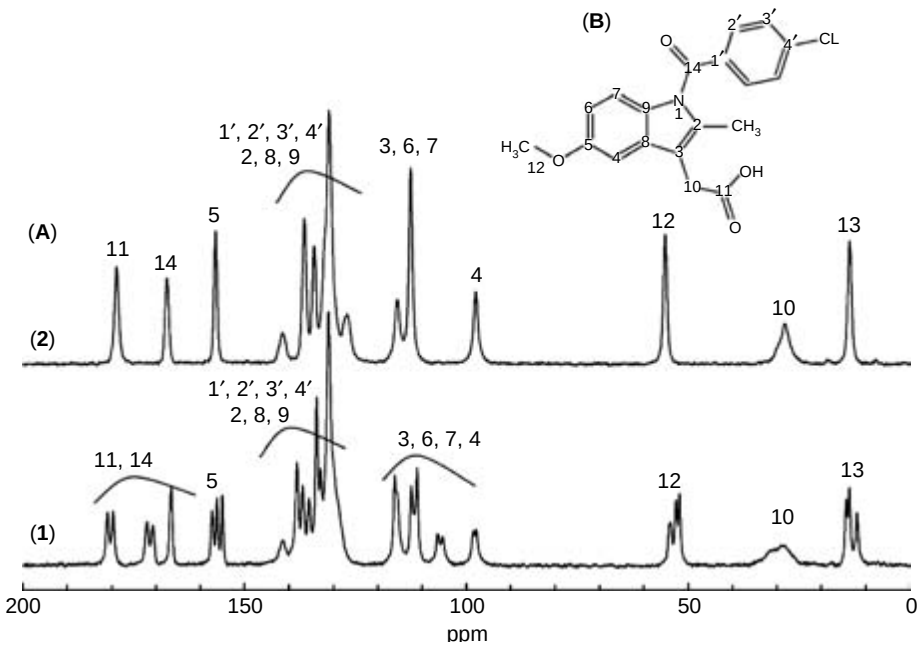

FIGURE 16 ^{13}C CP/MAS spectra of indomethacin at 9.4 T and 15 kHz MAS: (**A1**) α-form, (**A2**) γ-form, and (**B**) chemical structure of indomethacin. Adapted from Ref. (79).

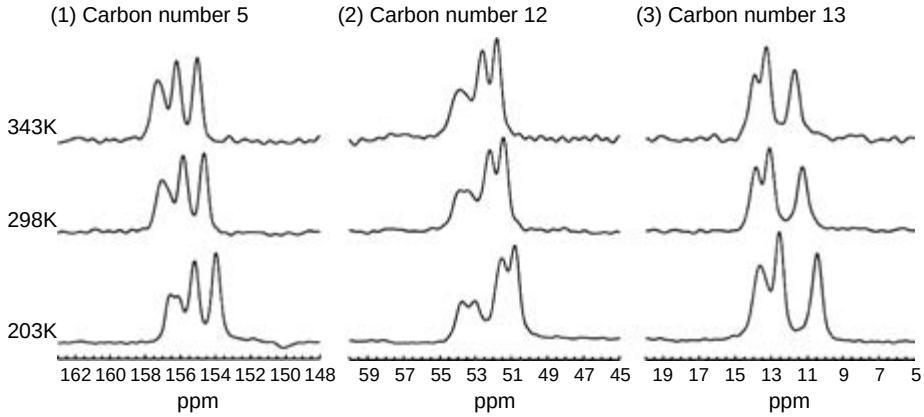

FIGURE 17 Expanded regions of the variable temperature ^{13}C CP/MAS spectra of α-indomethacin. The three groups of carbon resonances show conformational disorder for the highest frequency peak(s) in each region. The spectra also show that there are three molecules per asymmetric unit. Adapted from Ref. (79).

Nifedipine form II is a metastable polymorph. The ^{13}C SSNMR spectrum of amorphous indomethacin showed sharpening of peaks as the temperature was increased up to 80°C, but it did not recrystallize because the temperature was not increased high enough for this to occur in the ^{13}C SSNMR spectroscopy part of the study. The ^{1}H SSNMR spectra and relaxation measurements indicate that amorphous nifedipine has greater mobility below its glass transition temperature than indomethacin, and nifedipine tends to recrystallize first to a metastable form. The quadrupolar broadening effect of ^{35}Cl and ^{37}Cl was also examined in indomethacin at five different field strengths ranging from 4.7 to 18.8 T (50–200 MHz for ^{13}C). The quadrupole moment of both chlorine nuclides are much larger than for ^{14}N, which results in significantly more peak broadening as well as more complex splitting patterns. This can lead to much greater difficulty in SSNMR spectral interpretation for molecules having chlorine atoms unless high magnetic field strengths are used.

Schmidt et al. performed a series of studies on the polymorphism of local anesthetic drugs using spectroscopic, diffraction, microscopic, and thermal analyses (81–85). SSNMR spectroscopy was not a major part of any of these studies, but it provided unique complementary information for these compounds. In Part V (81), the authors showed ^{1}H SSNMR spectra in a study of hydrogen-bonding differences between modification II° and hydrated modification I, and ^{13}C SSNMR spectroscopy could easily differentiate modification II° from modification I and its hydrate. Modification I and its hydrate both appeared to have two molecules per asymmetric unit, which was confirmed by the single-crystal X-ray structures. Part IV (82) used ^{1}H, ^{13}C, and ^{15}N SSNMR spectroscopy to analyze polymorphism and molecular mobility in falicaine hydrochloride and isomorphic dyclonine hydrochloride. The SSNMR spectra showed that the polymorphs of both compounds have only one

molecule per asymmetric unit. Modification I of both falicaine hydrochloride and dyclonine hydrochloride had a significant amount of the corresponding modification II°. High-temperature ^{13}C SSNMR spectroscopy of the mixture of falicaine hydrochloride modifications I and II° showed that the aromatic ring is rotating at a rate that is intermediate on the NMR time scale at ambient temperature. This causes broadening of the protonated ring carbons for modification I such that they are not easily observed in the ^{13}C SSNMR spectrum. The authors state that a similar process is occurring for modification I in the dyclonine hydrochloride mixture, and this can be readily determined by the broad peaks near the baseline at the corresponding aromatic chemical shift positions in the ^{13}C CP/MAS spectrum. In Part VII (83), the author mentions that the ^{13}C SSNMR spectra of the three polymorphic systems did not have significant differences, although no spectra were shown for any of them. Only XRPD, thermal analyses, and microscopic data were shown for the polymorphs, but no IR, Raman, of SSNMR spectroscopic data was presented. A potentially interesting study would be to see if this were a series of polymorphs that can only be distinguished by specific analytical techniques. In Part VIII (84), the authors used ^{1}H and ^{13}C SSNMR spectroscopy to study several solid forms of hydroxyprocaine hydrochloride. The ^{1}H SSNMR spectroscopy was used to analyze the hydrogen bonding of the hydrate, and ^{13}C SSNMR spectroscopy was used to differentiate the two polymorphs and determine that the hydrate had two molecules per asymmetric unit. Part XI (85) also used ^{1}H SSNMR spectroscopy to study hydrogen-bonding differences for several hydrates. The relatively high chemical shifts of carboxylic acid protons made them useful for characterizing hydrogen bonds in several of these materials even though ^{1}H SSNMR peaks are typically very broad without very fast MAS or special pulse sequences like combined rotation and multiple pulse spectroscopy (CRAMPS).

Rubin-Preminger et al. studied polymorphs of ethambutol dihydrochloride diastereomers by single crystal X-ray diffraction, XRPD, SSNMR, and thermal analyses (86,87). The ^{13}C SSNMR spectroscopy was consistent with the crystal structure data showing that there was half a molecule per asymmetric unit for each form. Ethambutol dihydrochloride is a symmetrical molecule, and this property is maintained in the solid state resulting in the half molecule per asymmetric unit. The *S*,*S*-diastereomer has four polymorphs with two pairs that are enantiotropically related. The *R*,*S*-diastereomer has two enantiotropically related polymorphs. Variable temperature ^{13}C SSNMR spectroscopy of the *S*,*S*-diastereomer showed a solid-state phase transformation of a mixture of forms III and IV to form III at ~40°C and then back to form IV upon cooling again (87). A similar solid-state phase transformation occurs for form II to form I above ~70°C. The ^{13}C SSNMR spectra in these reports were very similar due to the similarity of the crystal structures for the polymorphs of each diastereomer. However, SSNMR spectroscopy was still sensitive and specific enough to easily distinguish the subtle differences among the solid forms.

Moynihan and O'Hare used IR, Raman, and SSNMR spectroscopic analyses to study two polymorphs of paracetamol (acetaminophen) (88). The authors note that IR and SSNMR spectra were useful for distinguishing the polymorphs, but the Raman spectra were not. The commercial form was monoclinic, and an orthorhombic form was produced as a mixture by melt quenching of the monoclinic material. A ^{13}C SSNMR spectrum of the orthorhombic form was obtained by subtracting the spectrum of the monoclinic form. The ^{13}C SSNMR spectra in this report use TOSS to suppress the spinning sidebands. The small out-of-phase peaks in each spectrum

are likely due to inefficient side band suppression from incorrectly setting the ^{13}C pulse width as noted in section "Solid-State NMR Spectroscopy" on p. 385.

Shaibat et al. used ^{13}C SSNMR spectroscopy to study polymorphs of the potential anti-leukemia compound Cu(II)(8-quinolinol)$_2$ (89). The paramagnetic copper atom increased the peak widths and shifted some of them to higher frequency for these molecules. The authors used relatively fast MAS of 20 kHz or more to decrease the peak broadening in the spectra. The interconversion of the polymorphs upon heating was also monitored by ^{13}C SSNMR. This study was a useful demonstration of SSNMR spectroscopy for characterizing molecular complexes having strong paramagnetic centers that cause peak broadening. Typically paramagnetic compounds have been very difficult to analyze by NMR spectroscopy because of the very broad peaks.

Enright et al. studied two anhydrous polymorphs of caffeine (Fig. 18) with single-crystal X-ray diffraction and SSNMR spectroscopy at low- and high-field strengths (90). The high-field ^{13}C CP/MAS SSNMR spectra had much better resolution compared to the low-field data because the interaction with the quadrupolar ^{14}N nucleus was dramatically reduced (Fig. 19). The anhydrous polymorphs appeared to be more disordered compared to the monohydrate, and the low-temperature anhydrous form had multiple molecules per asymmetric unit (Fig. 20). These results were confirmed by the single-crystal structures of each form.

Sheth et al. used ^{13}C SSNMR spectroscopy to study conversion of piroxicam polymorphs after cryogenically grinding them into "amorphous" solids (91). The "amorphous" material recrystallized to the original crystalline form during storage at 25°C and 0% relative humidity. This is not surprising given that forms I and II after cryogrinding for various times show different XRPD patterns for the most disordered forms, which are actually nanocrystalline piroxicam of the corresponding polymorph (92). The disordered nanocrystallites act as seeds for conversion back into larger crystallites of the same polymorph. SSNMR spectroscopy was not very useful in this case because the high degree of disorder in the cryoground samples resulted in broad peaks that masked the small amount of nanocrystalline material.

Harris et al. used ^{1}H and ^{13}C SSNMR spectroscopy to study the structures of four carbamazepine polymorphs, a dihydrate, and acetone and dioxane solvates (93).

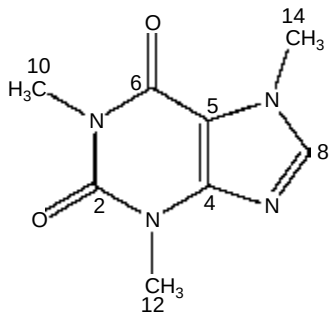

FIGURE 18 Chemical structure of caffeine with the numbering system as used for the assignments of Figure 19.

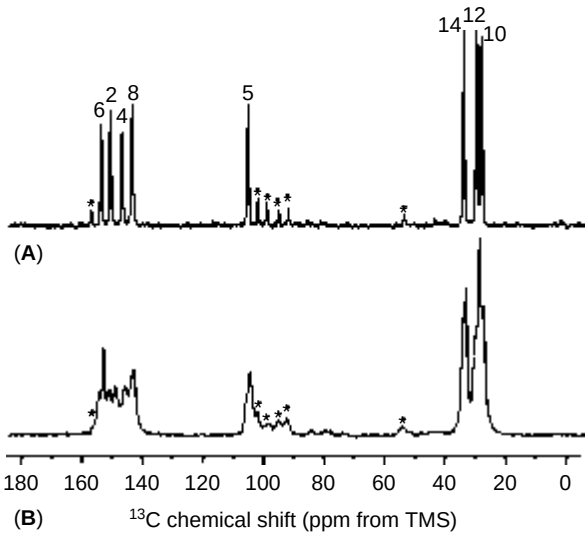

FIGURE 19 ^{13}C CP/MAS spectra of caffeine monohydrate: (**A**) 226.3 MHz (21.1 T) and 11.7 kHz MAS; (**B**) 50.3 MHz (4.7 T) and 2.6 kHz MAS. Asterisks indicate spinning sidebands. The assignments in spectrum (**A**) of the structure in Figure 18 are based on a spectrum obtained by liquid-state NMR spectroscopy. Adapted from Ref. (90).

The number of molecules per asymmetric unit was accurately determined for each case when compared to the crystal structures with only the triclinic form (with four molecules) having more than one. Computational analyses of the shielding constants of the P-monoclinic form were compared to the observed values and found to be reasonably close. The torsion angles for the P-monoclinic and trigonal forms of carbamazepine were also calculated and compared. The single-crystal X-ray structure of the dihydrate was also re-examined and determined to be monoclinic rather than orthorhombic as previous work had found, possibly due to micro-twinning.

Portieri et al. used ^{13}C and ^{15}N SSNMR, ^{1}H and ^{15}N T_1 and $T_1\rho$ relaxation data, and CSA to study polymorphs of sulfanilamide (94). The α, β, and γ forms were easily distinguished by ^{13}C SSNMR. The ^{1}H T_1 values for the α and γ forms were more than 10 times longer than for the β form, but the ^{1}H $T_1\rho$ values for the α and β forms were about twice as long as that of the γ form. This indicated that the solid-state molecular mobility was different for each polymorph. The authors note that the relaxation differences are large enough to result in potentially misleading information for mixtures of polymorphs. The peak intensities for the form with the shorter ^{1}H T_1 relaxation time may be relatively enhanced compared to the other if the SSNMR spectroscopy analyses are not set up to properly account for the differences. This is the reason that care should be used if one anticipates that mixtures of solid forms might be present in a sample to be analyzed by SSNMR spectroscopy. The ^{13}C SSNMR spectroscopy of each form obtained at this relatively low field strength (~50 MHz for ^{13}C) clearly showed the quadrupolar splitting of the carbon bonded to the quadrupolar ^{14}N nucleus. Selective ^{15}N-labeling at one of the two nitrogens was used to enable

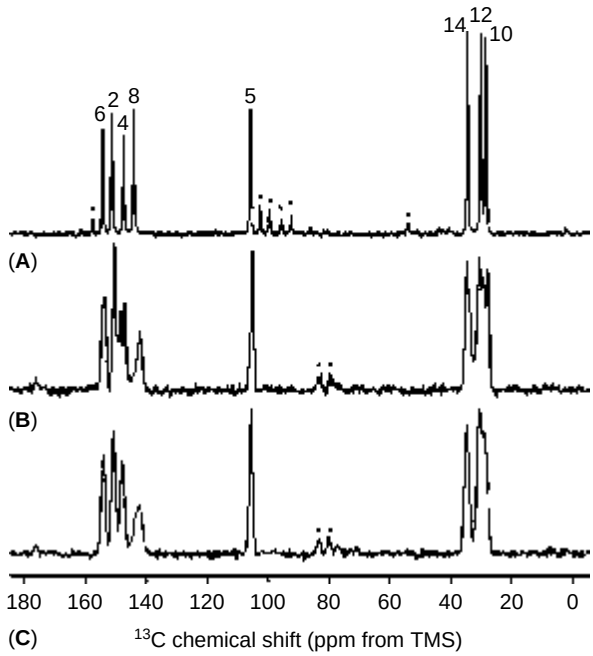

FIGURE 20 ^{13}C CP/MAS spectra of caffeine solid forms at 226.3 MHz (21.1 T): (**A**) caffeine monohydrate, (**B**) low-temperature anhydrous form, and (**C**) high-temperature anhydrous form. Asterisks indicate spinning sidebands. The spectra for the two anhydrous forms were acquired with 16 kHz MAS. Adapted from Ref. (90).

easier analysis of the nitrogen NMR parameters. The ^{15}N T_1 times for the secondary amine nitrogen in all three polymorphs were 100 seconds or longer as measured by the method of Torchia (95). The sulfonamide nitrogen T_1 relaxation times for all three polymorphs were less than three seconds. The $T_1\rho$ relaxation times for the secondary amine were 0.64 milliseconds for both the α and β forms, and 1.5 milliseconds for the γ form. The $T_1\rho$ relaxation times for the sulfonamide group were ~4 to 10 milliseconds. These results indicate that the mobility is substantially different in specific parts of this small molecule. The measured chemical shielding parameters were different for each nitrogen but almost the same among the three polymorphs. The calculated shielding parameters for ^{13}C and ^{15}N were reasonably useful for analyzing the differences in the polymorphs but also show that improvements in computational methods are still needed to accurately determine these values for detailed understanding of solid molecules.

Lee et al. used liquid-state ^{13}C NMR of several amphetamines to help assign the ^{13}C SSNMR spectra (96). The various amphetamines were easily distinguished by SSNMR spectroscopy. The authors also dry mixed 3,4-methylenedioxy-*N*-methylamphetamine-HCl [(*R*,*S*)-MDMA·HCl] with lactose monohydrate to mimic "Ecstasy" tablets. This simple mixing process involved rotating a vial of the two components without compression or shear forces, yet there was a very noticeable difference in the

^{13}C SSNMR spectrum compared to that of the pure drug. The authors noted shifts of about +5.5 ppm for C8 (methylene) and –6.2 ppm for C10 (methyl). Significant shifts of about 2.6 ppm for C1 and 1.3 ppm for C5 (both aromatic carbons) as well as a distinct increase in peak widths for the amphetamine in the mixture can also be seen in the spectra. A spectrum of pure lactose monohydrate was not shown for comparison, so the effect of mixing on it could not be determined. The authors also noted that the peaks shifted toward the positions of those observed in D_2O and attributed this to potential hydrogen bond formation in the solid mixture. The peak broadening may also be due to ABMS (138–140). However, the other amphetamines did not show similar spectral changes upon mixing with lactose monohydrate, so there appears to be a specific intermolecular interaction, such as hydrogen bonding, resulting in a conformational change that occurs with (*R*,*S*)-MDMA·HCl and causes both peak broadening and shifting.

Reutzel-Edens et al. used spectroscopic, diffraction, thermal, and water vapor sorption analyses to study three anhydrates, a dihydrate, and an acetic acid solvate of the developmental compound, LY33470 HCl (97). All of the forms had one molecule per asymmetric unit. An unusual observation was that form I had a much lower dissolution rate than the dihydrate. The liquid-state ^{13}C NMR spectrum was used to assign the peaks for the solid forms, but the peak shifting observed in the solid state was such that these assignments are tentative without supporting solid-state editing techniques or correlation spectroscopy. The peak of the fluorinated aromatic carbon was very near the amide carbonyl peak, and the large ^{19}F–^{13}C coupling constant (~150–375 Hz or ~1.5–3.7 ppm at 9.4 T field strength in this study) caused overlap with the amide resonance. The authors assigned three or four peaks in this region, although no more than two distinct peaks and a small shoulder were observable for any of the spectra they reported. The largest separation between the peaks above 160 ppm (excluding acetic acid) is about 3.3 ppm, which is within the range for ^{19}F–^{13}C coupling. The field strength used for the analyses was high enough that the proposed residual ^{13}C dipolar coupling to the quadrupolar ^{14}N nucleus of the amide group could not be responsible for this larger splitting, but may produce the shoulders observed for forms I, II, and the dihydrate. Restricted rotation about the amide bond is also a potential source of additional peaks that may be asymmetric depending on the conformational exchange rate. Therefore, the amide carbonyl and fluorinated aromatic carbon resonances appear to be overlapped with ambiguous chemical shift assignments without further information. A good example of the effects of ^{19}F–^{13}C coupling is shown for flurbiprofen by Antonioli and Hodgkinson (98).

Wang et al. studied four polymorphs of a fluorinated NK1 receptor agonist referred to as Compound A (Fig. 21) using variable temperature XRPD and ^{13}C SSNMR spectroscopy as well as differential scanning calorimetry, thermogravimetry, and microscopy (99). They found two sets of enantiotropically related polymorphs. Forms III and IV (Fig. 22) are the high-temperature polymorphs of forms I and II (Fig. 23), respectively. The highest frequency carbon resonance was due to the fluorinated aromatic carbon at ~160 to 165 ppm, which formed an asymmetrical doublet similar to that observed in the spectrum of LY334370 HCl (97) but without any possible overlap from amide carbonyl peaks or spinning side bands that could lead to misinterpretation (Figs. 22 and 23). The two trifluoromethyl carbon resonances (~120–130 ppm) were very broad in forms I and II (Fig. 23), but less so in forms III and IV (Fig. 22). The high-temperature forms of compound A appear to be conformational polymorphs of the low-temperature forms given the similarity of most

peak positions and the potential for flexibility for the methyl carbons and morpholine ring. The authors suggested that form I may have multiple molecules per asymmetric unit based on doublets at ~48 and ~100 ppm, but this could also be a conformational difference in the morpholine ring system (~48 ppm for N–CH_2 and ~100 ppm for O–CH–O) given that no other peak splittings were observed in the spectrum of form I to support this hypothesis. However, the spectrum of form II shows four peaks between 20 ppm and 30 ppm corresponding to the single methyl group, indicating that it is in four different environments in the unit cell (Fig. 23). This could result from conformational exchange for the mobile methyl group, but no variable temperature SSNMR spectra of form II were obtained to help clarify this.

Isotopic labeling is a very useful means of enhancing the sensitivity of NMR spectroscopy, particularly for biological molecules. It is used much less often for small molecules due to the difficulty in synthesizing molecules with isotopes at specific locations. Booy et al. specifically ^{13}C-labeled two ethynyl and one methyl carbon of a steroid (Org OD 14) as a means to enhance the sensitivity for detecting two polymorphs in formulations having 0.5% or 2.5% API loads (100). From the ^{13}C SSNMR spectra, form I had two molecules per asymmetric unit, and form II had one. Under the conditions used by the authors for ^{13}C SSNMR, the natural abundance steroid peaks were easily observed at 2.5% loading along with the much larger peaks from the isotopic labels. The polymorphic form was also readily determined from the natural abundance peaks at this loading level. For the 0.5% loading, the peaks of the natural abundance steroid were just visible above the noise in the baseline, and it was very difficult to determine the polymorphic form except by using the peaks of the labeled material. A spectrum of the pure labeled sample showed both sharp ethynyl carbon peaks overlapped on broader peaks, and this was also observed for

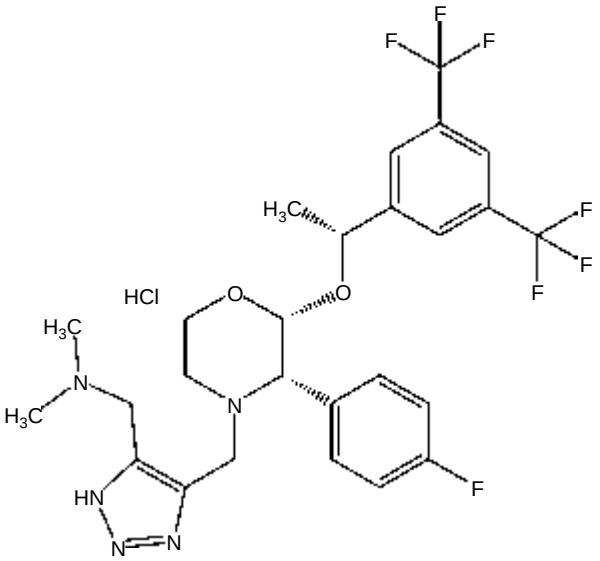

FIGURE 21 Chemical structure of Compound A. Adapted from Ref. (99).

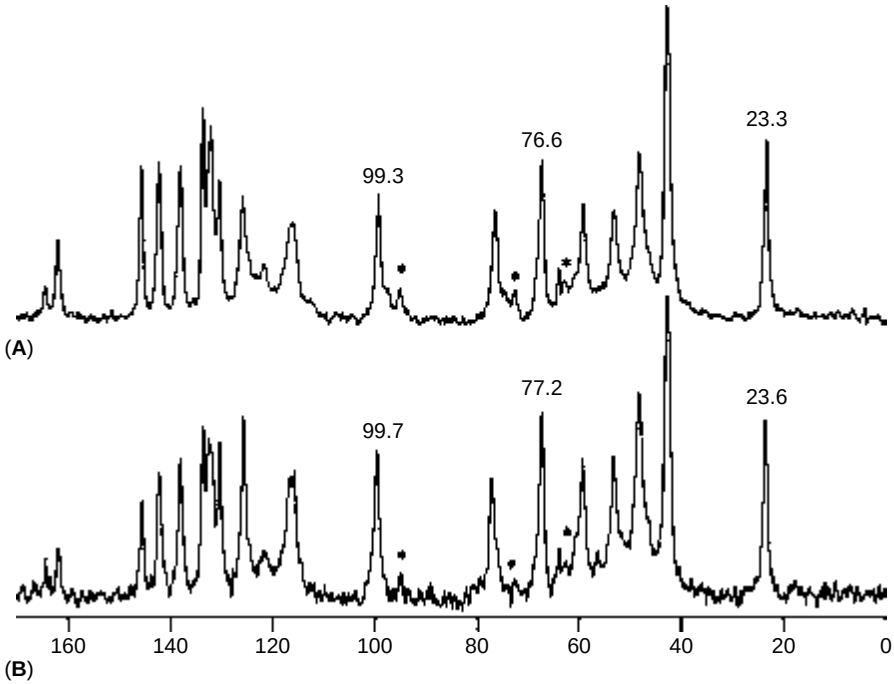

FIGURE 22 ^{13}C CP/MAS spectra of Compound A at 9.4 T and 7 kHz MAS: (**A**) form III and (**B**) form IV. Asterisks indicate spinning sidebands. Adapted from Ref. (99).

the spinning side bands. Although the authors attribute this to ^{13}C–^{13}C dipolar coupling, it is more likely due to some disordered ^{13}C-labeled material, because spinning at 8 kHz would dramatically reduce or eliminate the relatively small homonuclear ^{13}C coupling as noted in section "Solid-State NMR Spectroscopy" on p. 385. Synthetic isotopic labeling methods can be very useful for characterizing solid forms in low load formulations as long as the time and expense required for labeling the API is justified. It may eventually be a required technique if high potency pharmaceuticals become more prevalent as the current trend indicates.

Olejniczak et al. used 1D and 2D ^{13}C and ^{15}N SSNMR, CSA tensor analysis, and theoretical calculations to analyze polymorphs of *N*-benzoylphenylalanine (101). The carbonyl carbons were ^{13}C-labeled, and the amide nitrogen was ^{15}N-labeled. This permitted rapid 2D ^{1}H–^{13}C, ^{13}C–^{15}N, and ^{1}H–^{15}N HETCOR analyses of the molecule. CSA tensor analyses (^{13}C and ^{15}N) and $T_1\rho_H$ measurements were used to estimate the relative strengths of the hydrogen bonds. The authors noted that ^{15}N CSA tensor values were less reliable than the ^{13}C values for evaluating hydrogen bonding. The ^{15}N chemical shift tends to be very sensitive to the effects of chemical bonding and coupling, which makes them somewhat unpredictable even in relatively simple molecules. Polymorphs I and II each had two molecules per asymmetric unit. Polymorph III was only obtained as a mixture with one or more other polymorphs that were not isolated and studied. The isotopic labeling as done in this study can be further exploited for structural

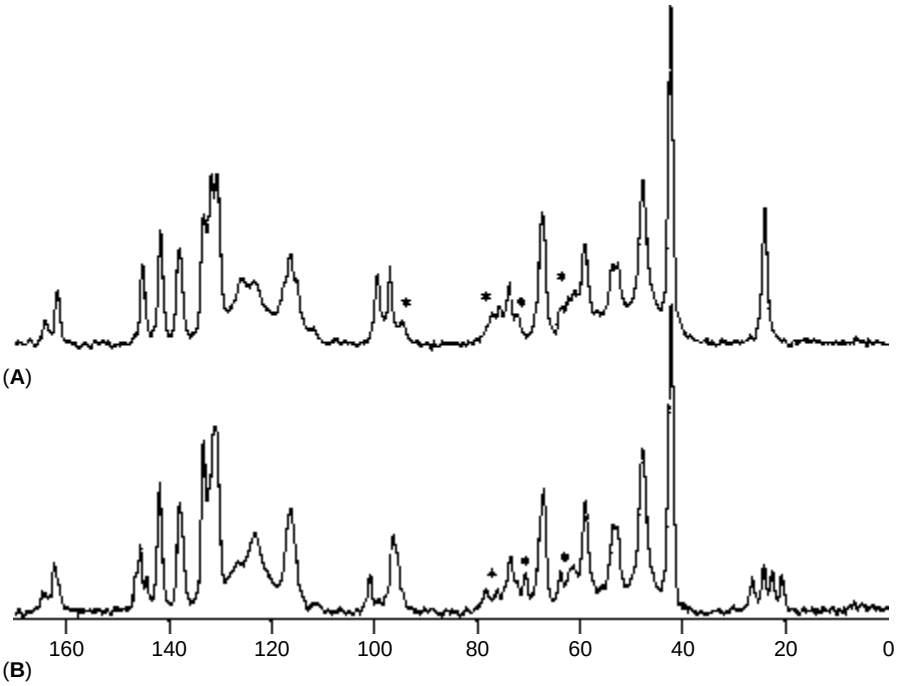

FIGURE 23 ^{13}C CP/MAS spectra of Compound A at 9.4 T and 7 kHz MAS: (**A**) form I and (**B**) form II. Asterisks indicate spinning sidebands. Adapted from Ref. (99).

analysis by using rotational echo double resonance (REDOR) to determine accurate internuclear distances within molecules (102,103).

Zhou et al. used both ^{1}H MAS and ^{2}H MAS SSNMR spectroscopy to study what they called "isotopomeric polymorphism" in a complex of pentachlorophenol with 4-methylpyridine (104). This complex could also be considered a co-crystal. They found that the fully protonated material only produces the triclinic polymorph with a strong hydrogen bond, whereas the 55% or 90% deuterated material forms the disordered monoclinic polymorph with a weaker hydrogen bond. The reason for deuterium causing weaker hydrogen bonding is not clear. It would be interesting to correlate the deuteron and proton covalent bond strengths with intermolecular hydrogen (or deuterium) bond strengths to determine what controls the resulting solid form. Neutron diffraction analyses and IR spectroscopy would be useful analytical techniques to study this further.

In some cases, SSNMR spectroscopy is more useful than XRPD in distinguishing solid forms. Othman et al. used ^{1}H and ^{13}C SSNMR spectroscopy (CP and direct polarization) and XRPD to study four polymorphs and four isomorphous solvate hydrates of finasteride (105). The solvate hydrates were readily distinguished by SSNMR spectroscopy but not by XRPD. The solvents in the crystal structures do not change the packing pattern significantly, but they influence the local electronic environments that affect the NMR chemical shifts. The solvent molecules (other than

water) also have unique chemical shifts that are observed in the SSNMR spectra. This study further emphasizes the need to use multiple analytical techniques when characterizing solid forms, because there is no reliable way to predict which analytical technique will be appropriate for properly characterizing solid materials. XRPD may be the gold standard for studying solid materials, but spectroscopic techniques provide unique data that complements or occasionally surpasses the value of XRPD.

Apperley et al. used ^{13}C and ^{15}N SSNMR spectroscopy to study hydrogen bonding in sildenafil citrate (active ingredient of Viagra™) upon exposure to water vapor (106). One of the citrate carbonyl peaks shifted to higher frequency upon exposure to water vapor over a seven-day period. The other two citrate carbonyl peaks did not change. The authors interpreted this as one citrate carboxyl group forming a hydrogen bond with water. The chemical shifts of the propyl and ethoxy groups of sildenafil also changed upon exposure to water vapor, which the authors suggest is due to water molecules occupying sites close to these groups and presumably changing the electronic environment surrounding these nuclei. However, the chemical shift changes may also result from modification of molecular mobility, and thus the conformations in the crystal, due to incorporation of water. The ^{15}N SSNMR spectroscopy chemical shifts of sildenafil varied by 0.2 to 1.5 ppm upon exposure to water vapor over seven days, which are relatively small changes that suggest weak interactions with the water molecules. The N2 and N3 nitrogens are bonded in sildenafil, which resulted in the typical 1:2 doublet peaks due to the interaction of the ^{15}N dipole with the electric field gradient of the ^{14}N nuclear quadrupole. The authors determined residual dipolar coupling constants of 33 Hz for $^{14}N3$–$^{15}N2$ and 37 Hz for $^{14}N2$–$^{15}N3$. The ^{15}N dipolar dephasing experiment showed that N26 was the only protonated nitrogen of sildenafil. The N5 peak was slightly suppressed by the dipolar dephasing experiment, which was interpreted to be a hydrogen bond at this position. The ^{13}C and ^{15}N SSNMR spectroscopy data are consistent with one citrate carbonyl donating a proton to N26 of sildenafil to form a salt, while a second citrate carbonyl is free to interact with water introduced into the sample. The third citrate carboxylate may have a pK_a that significantly reduces the exchange rate of its proton, which results in essentially no observed chemical shift changes for the corresponding carbonyl resonance upon exposure to water vapor.

Rafilovich et al. used a number of analytical techniques including ^{13}C SSNMR spectroscopy to study polymorphs of 1,3-bis(*m*-nitrophenyl)urea (107). This is the compound where concomitant polymorphs were first discovered. The authors found a new polymorph, designated δ, and a monohydrate that they believe was previously reported as the γ form. They were able to obtain only the β form as a pure phase. The α and δ forms have one molecule per asymmetric unit, and the monohydrate and β forms have half a molecule per asymmetric unit based on the X-ray diffraction data. This was generally supported by the ^{13}C SSNMR spectra. However, the spectrum of the α form did not show the expected 13 peaks, although the seven peaks observed were substantially broader than those in the spectra of the other forms. This may be indicative of some disorder in the crystal structure that may be sufficient to broaden the peaks and prevent observation of all of them. The authors were not able to obtain a ^{13}C SSNMR spectrum of the δ form, which was expected to show new peaks as a mixture with the β form. Only peaks from the β form were observed, so it was not certain whether any of the δ form was present or if it was indistinguishable from the β form. Small splittings for one peak due to ^{13}C dipolar coupling to the quadrupolar ^{14}N nucleus was observed for the monohydrate and β

forms that were analyzed at ~7.1 T but not for the α form that was analyzed at ~11.7 T, which is consistent with the field strength effect on dipolar coupling to quadrupolar nuclei. Some small chemical shift differences were observed in the ^{13}C SSNMR spectra that are consistent with the differences in hydrogen bonding among the polymorphs. An interesting result noted by the authors was the hydrogen bonding interactions observed for this molecule in acetone solution where a small amount of added water caused specific shifting of several peaks in the spectrum. This demonstrates that water specifically interacts with 1,3-bis(*m*-nitrophenyl)urea in the liquid-state, which is analogous to hydrates of solid forms.

Dong et al. prepared polymorphs of neotame anhydrate and studied them by XRPD, spectroscopy, microscopy, water vapor sorption, and thermal analyses (108). Forms A, D, F, and G were characterized more fully than the three forms that were more difficult to make in adequate quantities (B, C, and E). The polymorphs were readily distinguished by XRPD, FT-IR, and ^{13}C SSNMR spectroscopy. The ^{13}C SSNMR spectra of forms D and F had broader peaks, indicating some disordered material was present, which was also consistent with the XRPD data. Form D also appeared to have two polymorphs per asymmetric unit based on its ^{13}C SSNMR spectrum. The ^{13}C SSNMR spectra were obtained at a magnetic field strength of 7.1 T, so splitting due to dipolar coupling of ^{13}C with the ^{14}N nucleus was observed for the amide carbonyl resonance.

A recent brief communication by Griffin et al. demonstrated the use of ^{1}H double quantum combined rotation and multiple pulse (DQ CRAMPS (109)) NMR spectroscopy to distinguish the anhydrous and monohydrate pharmaceutical compounds in a tablet with $CaHPO_4 \cdot 2H_2O$ as the primary excipient (110). The identity of the compound and the loading level were not reported by the authors. However, the ^{1}H DQ CRAMPS analysis showed that the anhydrous form was present in the tablet, which would have been difficult to determine using 1D ^{1}H SSNMR due to overlap of some key resonances. The authors did not show a corresponding spectrum of the monohydrate in the same formulation, which would help validate this potentially useful technique.

Zhou and Rienstra used ^{1}H detected fast-MAS HETCOR to study acetaminophen and ibuprofen in tablet formulations (111). Fast MAS of 40 kHz was used with a 1.6 mm rotor that could hold about 6 mg of material. The fast MAS reduced the ^{1}H-^{1}H dipolar coupling without using homonuclear decoupling. A major advantage of this technique was that it did not require the tedious calibration procedures typical of CRAMPS experiments as used by Griffin et al. (110). The authors also used the technique to study hydrogen bonding and molecular motions. The ^{1}H detected HETCOR was much faster than the usual ^{13}C detected version particularly for acetaminophen (Fig. 24), which had a proton T_1 relaxation time about 30 times longer than that of ibuprofen (Fig. 25). The spectra in Figure 24 also show that it is important to acquire enough scans to obtain all of the correlations particularly for compounds with long relaxation times.

Harris et al. studied two anhydrates, a monohydrate, a higher hydrate, and an acetic acid solvate of terbutaline sulfate by ^{1}H, ^{13}C, and ^{15}N SSNMR spectroscopy as well as XRPD, single-crystal XRD (hydrates only), and thermal analyses (112). The ^{1}H and ^{13}C chemical shifts were also calculated and compared to the observed values. Modification A had broader ^{13}C SSNMR spectroscopy peaks that were attributed to disorder or crystal defects for this form, and it has only one molecule per asymmetric unit. Modification A also appeared to be contaminated with modification B. Based

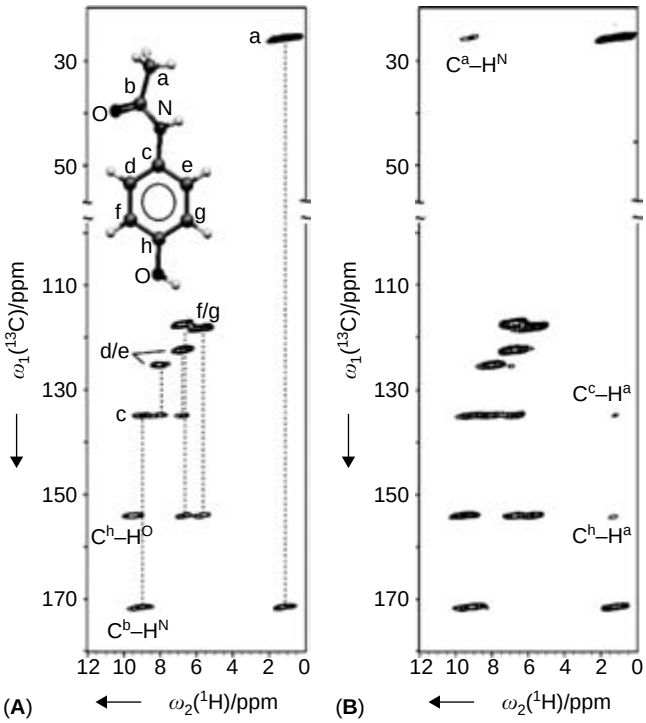

FIGURE 24 (**A**) ^{1}H detected ^{13}C–^{1}H HETCOR spectra at 17.6 T and 40 kHz MAS for 6 mg of a formulation containing 5.5 mg of acetaminophen (~93% load) with assignments for the labeled acetaminophen crystal structure shown in the inset of spectrum (**A**). Spectrum (**A**) was acquired in six hours with two scans per row, and spectrum (**B**) was acquired in 18 hours with six scans per row. The recycle delay for both spectra was 35 seconds. The ^{1}H T_1 relaxation time for acetaminophen was 63 seconds. Note the higher sensitivity in spectrum (**B**) that provided additional correlations. Adapted from Ref. (111).

on the peak splitting observed in their ^{13}C SSNMR spectra, modification B, the monohydrate, and the acetic acid solvate each have two molecules per asymmetric unit. The ^{13}C chemical shifts for each molecule in the asymmetric unit of modification B were computed, but the authors were not able to assign them to the independent molecules in this case. The ^{1}H SSNMR data and computational calculations indicated that strong hydrogen bonds may be present in all the forms, but further work is required to obtain better evidence for this.

Martin-Islán et al. used XRPD, FT-IR, ^{13}C SSNMR spectroscopy, and thermal analyses to study sodium pravastatin (113). The authors found a new polymorph (designated M) for this compound by very slow evaporation from a solution of 2-propanol. They also observed that sodium pravastatin tends to crystallize out as mixtures of multiple polymorphs (concomitant polymorphs). The polymorphs also tend to be disordered, which is typical of some statins due to the flexibility of the alkyl groups connected to the ring structures. Therefore, it is difficult to determine

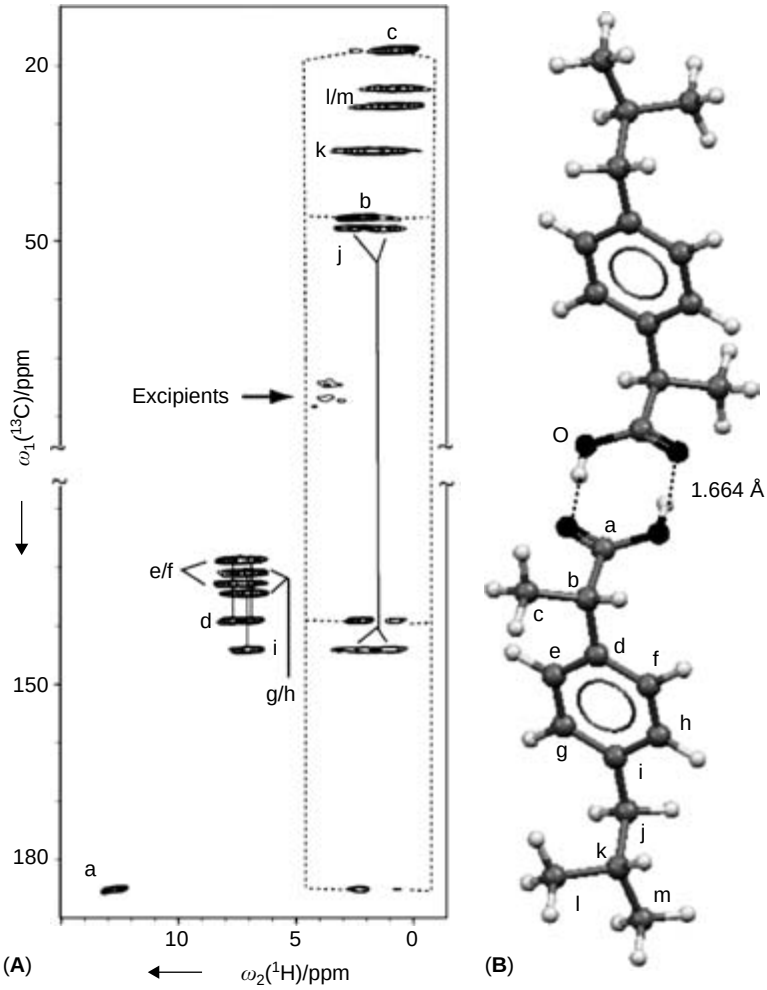

FIGURE 25 (**A**) ^{1}H detected ^{13}C–^{1}H HETCOR spectrum at 17.6 T and 40 kHz MAS for 6 mg of a formulation containing 3.8 mg of ibuprofen (~63% load) with assignments for the labeled ibuprofen crystal structure shown in (**B**). The spectrum was obtained in 33 minutes with two scans per row. The ^{1}H T_1 relaxation time for ibuprofen was 1.7 seconds. Adapted from Ref. (111).

the phase purity by most analytical methods unless truly pure phases can be obtained and compared. Without a crystal structure available for sodium pravastatin, no calculated XRPD patterns were possible. However, the authors used the crystal structure of *tert*-octylammonium pravastatin to build a model structure for sodium pravastatin, although they did not try to use this to calculate an XRPD pattern to compare with any of the forms they analyzed. The authors suggested that previously reported polymorphs of sodium pravastatin may actually be mixtures due to its propensity to crystallize out in multiple forms quite readily.

Maurin et al. studied two enantiotropically related polymorphs of roxifiban by XRPD, spectroscopy, and thermal analyses (114). The FT-IR spectra were essentially identical for both forms, and the FT-Raman spectra were almost indistinguishable. The standard DSC data for each form were the same, but the modulated DSC data showed some differences. The isothermal microcalorimetry data also showed differences between the two forms. The XRPD and ^{13}C SSNMR spectroscopy data easily differentiated both forms, although some peak regions were almost identical for the SSNMR spectra indicating that only part of the molecule experienced a change in electronic environment between the two polymorphs. Form I is the stable form above 132°C, and the *n*-butyl group of roxifiban showed splitting for three of the four aliphatic carbon resonances compared to form II. The splitting of the aliphatic resonances in the spectrum of form I is not necessarily indicative of two molecules per asymmetric unit because roxifiban has several amide groups that may have restricted rotation resulting in conformational exchange. Variable-temperature SSNMR spectroscopy would be useful in clarifying this issue, and single-crystal structures of both forms would show whether there was greater disorder for the aliphatic region of form I.

SSNMR Spectroscopy of Quadrupolar Nuclei in Pharmaceuticals

Several studies have shown that nuclear quadrupolar resonance (NQR) spectroscopy can be useful in analyzing polymorphs (115,116). Blinc et al. studied polymorphs of five sulfa drugs by using polarization enhancement of the ^{14}N NQR signal from protons (115). All of the drugs and their polymorphs were readily distinguished by this technique. Quantification was possible because the signal was directly proportional to the amount of sample that contains nitrogen, but it requires 10 mg or more of the compound in a sample. The authors also note that tablets can be analyzed without removing them from the bottle.

Pérez et al. used ^{35}Cl NQR spectroscopy without enhancement to analyze chlorpropamide and sodium diclofenac (116). Chlorpropamide had two polymorphs with one molecule per asymmetric unit in each, and variable temperature ^{35}Cl NQR spectroscopy revealed a third low-temperature form with a phase transition at –85°C. Quantification was also demonstrated in this study in which the limit of detection was near 10 mg and the limit of quantification limit was approximately 20 mg. NQR is not very useful with disordered or amorphous materials because the typically broad peaks even for crystalline materials become too broad to observe reliably.

NQR spectroscopy would not be a generally applicable technique for studying pharmaceuticals, but it can be useful in certain cases.

SSNMR Spectroscopy and Structure Determination

Structural determination in the solid state has been primarily done using diffraction techniques because of their atomic resolution. SSNMR spectroscopy is potentially very powerful for determining the conformation of a molecule in the solid state, but it is practically useless for determining long-range order in solids due to its strong dependence on the local electronic environment surrounding each nucleus. The conformations of molecules in the asymmetric unit and interactions with nearest neighbors provide useful information about different solid forms. There are numerous NMR pulse sequences used for structural determinations in liquid solutions, and some of them have been modified for use in the solid state. The orientationally

dependent properties of dipolar coupling and CSA have also been exploited to determine structure of solids at relatively high resolution. The various SSNMR spectroscopy techniques can also be applied to disordered solids to analyze their structures, although the broader peaks can make the data interpretation much more difficult. The rapid developments occurring in SSNMR spectroscopy will hopefully overcome some of the current limitations, particularly the broad peaks of ^{1}H SSNMR spectroscopy. Theoretical computations of chemical shifts in solid samples is also quite common as shown in several previous examples in section "Solid-Form Characterization" on p. 398, but improvements are required to obtain more accurate chemical shifts particularly for very similar conformations that may exist in the unit cell.

Harper et al. compared the ^{13}C detected HETCOR and 2D INADEQUATE experiments for analyzing the different molecules in the asymmetric units α-santonin, catechin, and calcium acetate (117). The resolution in the proton dimension of the HETCOR analysis tends to be low, which can make it difficult to assign the resonances appropriately. The ^{13}C–^{13}C INADEQUATE experiment has very low sensitivity (e.g., several days of data acquisition) but can show the carbon-to-carbon connections of a small molecule. Although the INADEQUATE experiment takes significantly longer than the HETCOR analysis, it usually has better resolution because there is no ^{1}H dimension.

Harris et al. used the refocused INADEQUATE (Figs. 26 and 27) and the HETCOR (Figs. 28 and 29) SSNMR spectroscopy experiments to determine most of the ^{1}H and ^{13}C resonance assignments for the two different molecules in the asymmetric unit for oxybuprocaine hydrochloride modification II° (118). This required a significant amount of data acquisition time as the INADEQUATE experiment took five days, whereas the HETCOR took 17 hours. The authors also observed unusually low chemical shifts for one of the ethyl amine groups ($CH_3CH_2NH^+$) that is likely due to the *γ-gauche* shielding effect.

Harper et al. used CST data to study a polymorph of paclitaxel with two molecules per asymmetric unit (119). Although they obtained useful data from the CST results for use with the XRPD structural refinement, they could not assign the specific peaks to one or the other molecule in the asymmetric unit. Paclitaxel is quite complex compared to most of the molecules so far discussed, which is why it is much more difficult to interpret it SSNMR spectra.

Harris et al. used the ^{13}C–^{13}C INADEQUATE experiment to assign the resonances of the two molecules in the asymmetric unit of the α form of testosterone (120). The SSNMR spectroscopy information was also used to test the accuracy of computed chemical shifts. Although the chemical shift calculations were reasonably close to the observed values, they were not accurate enough to differentiate between the molecules in the asymmetric unit.

Mifsud et al. used ^{1}H–^{1}H DQ-CRAMPS, ^{1}H–^{13}C INEPT-HSQC, and computation of ^{1}H and ^{13}C chemical shifts to study crystalline penicillin G (121). The resonance assignments were determined using through-space ^{1}H–^{1}H correlations from the DQ-CRAMPS technique and the through-bond ^{1}H–^{13}C correlations from the INEPT-HSQC technique. The computational results worked reasonably well for both ^{1}H and ^{13}C chemical shifts, although the aromatic resonances are probably the least reliable considering that five to six peaks are observed in a rather narrow chemical shift range. The variety of SSNMR techniques currently available allows one to analyze solids in many ways, which will lead to improved computational predictions of NMR properties and much better structural determinations of solids.

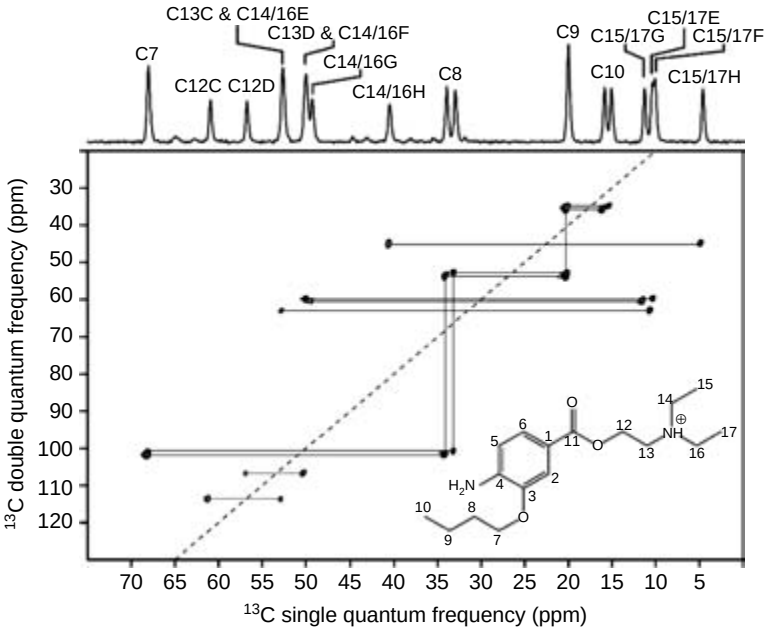

FIGURE 26 Solid-state ^{13}C INADEQUATE spectrum (low-frequency region) of oxybuprocaine hydrochloride (inset) modification II° at 11.7 T and 10 kHz MAS. The connections are shown for the two independent molecules in the asymmetric unit, and the ^{13}C resonance assignments are labeled in the 1D spectrum. Adapted from Ref. (118).

SSNMR Spectroscopy of Biopharmaceuticals

Biopharmaceuticals have been a rapid growth area in the pharmaceutical industry. Biopharmaceuticals are usually large molecules produced by living organisms, and most of those currently developed as pharmaceuticals tend to be proteins, particularly monoclonal antibodies. However, biopharmaceuticals can also be oligonucleotides, polysaccharides, and lipids with beneficial pharmacological properties. SSNMR spectroscopy is a very useful technique for studying crystalline and amorphous forms of proteins. Most pharmaceutical proteins are delivered in the lyophilized form primarily because protein crystals usually need a significant amount of liquid water to remain crystalline. The value of crystalline protein pharmaceutical formulations has been discussed in the literature (122). Production of crystalline formulation rather than the typical amorphous formulation may be beneficial for manipulating the stability or bioavailability of a biopharmaceutical.

Several studies have shown that SSNMR spectroscopy readily differentiates protein polymorphs (123,124). Five polymorphs of the protein GB1 (β1 immunoglobulin binding domain of protein G, 56 residues, ~6202 Da) were analyzed by ^{13}C SSNMR spectroscopy and XRPD (123). SSNMR spectroscopy showed the characteristic sharp peaks for the crystalline forms (Figs. 30 and 31). Although there was significant overlap due to the number of carbons in the molecule, the resolution was sufficient to easily identify the polymorphs.

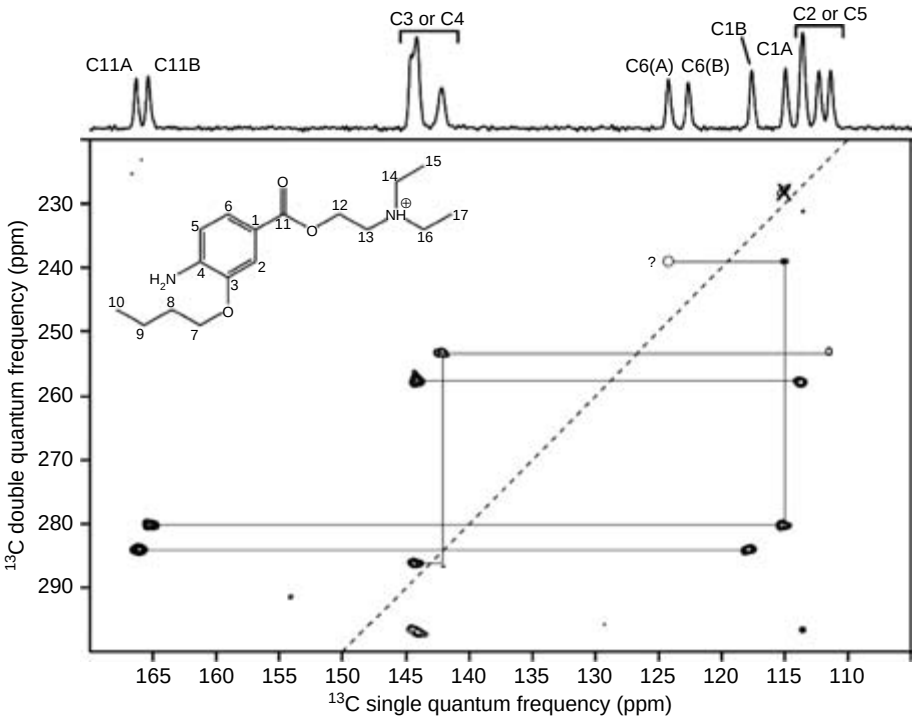

FIGURE 27 Solid-state ^{13}C INADEQUATE spectrum (high-frequency region) of oxybuprocaine hydrochloride (inset) modification II° at 11.7 T and 10 kHz MAS. The connections are shown for the two independent molecules in the asymmetric unit, and the ^{13}C resonance assignments are labeled in the 1D spectrum. Adapted from Ref. (118).

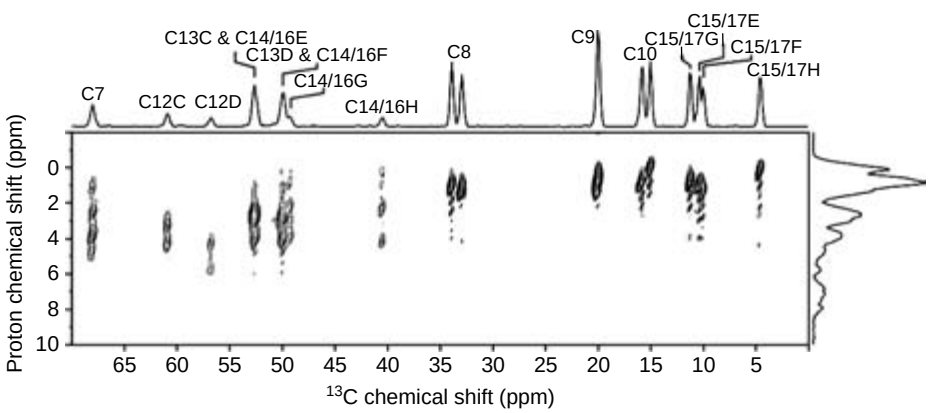

FIGURE 28 Solid-state ^{13}C–^{1}H HETCOR spectrum (low frequency region) of oxybuprocaine hydrochloride modification II° at 11.7 T and 10 kHz MAS. The ^{13}C resonance assignments are labeled in the 1D spectrum. Adapted from Ref. (118).

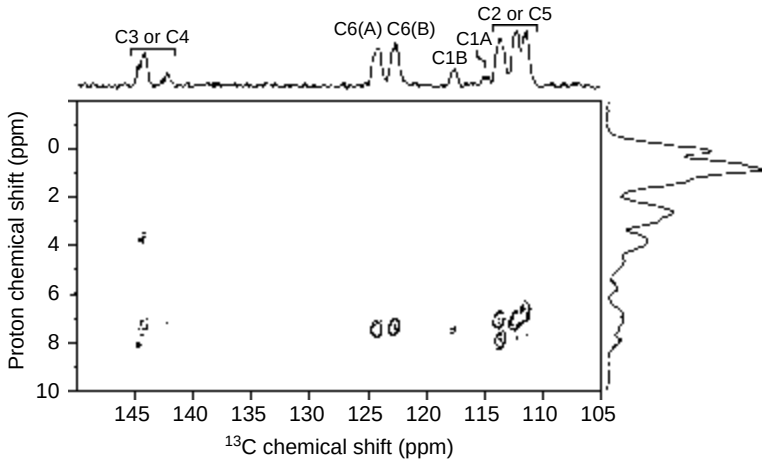

FIGURE 29 Solid-state ^{13}C–^{1}H HETCOR spectrum (high-frequency region) of oxybuprocaine hydrochloride modification II° at 11.7 T and 10 kHz MAS. The ^{13}C resonance assignments are labeled in the 1D spectrum. Adapted from Ref. (118).

Martin and Zilm analyzed five proteins with MW between ~8 and 56 kDa by ^{13}C SSNMR spectroscopy and XRPD (Figs. 32 and 33) (124). They showed that microcrystalline and nanocrystalline proteins produced essentially identical SSNMR spectra for cases where the nanocrystals were 100 nm or larger (Fig. 33). The authors also demonstrated some potentially useful procedures for making batch quantities of submicrometer size crystals and preparing small samples of wet crystals for SSNMR spectroscopy.

The need for molecular-level characterization of biopharmaceutical solids is likely to increase in the coming years as more of these molecules are developed to treat a wide variety of diseases. SSNMR spectroscopy of biopharmaceuticals may be a useful extension of liquid-state NMR spectroscopy of these large molecules. NMR spectroscopy of proteins, oligonucleotides, and polysaccharides in aqueous or organic solutions provides a detailed fingerprint of the molecule, which is a very powerful tool for comparing biopharmaceuticals. SSNMR spectroscopy is particularly useful for characterizing biopharmaceuticals because amorphous forms can be also analyzed and usually have unique spectra. Comparability of biologicals in the solid state has the potential to be a major application of SSNMR spectroscopy in pharmaceutical development.

Quantification with SSNMR Spectroscopy

The difficulties in performing quantitative SSNMR spectroscopy have been discussed by Harris (125). Stephenson et al. have reviewed quantitative X-ray diffraction, vibrational spectroscopy, and SSNMR spectroscopy (126). The main problem for quantitative SSNMR spectroscopy is ensuring that the relative peak areas are accurate for the components in the sample. For CP methods (e.g., ^{13}C CP/MAS) where the sensitivity enhancement is provided by ^{1}H to ^{13}C magnetization transfer, there are three main relaxation processes that need to be considered (127): (1) The CP time

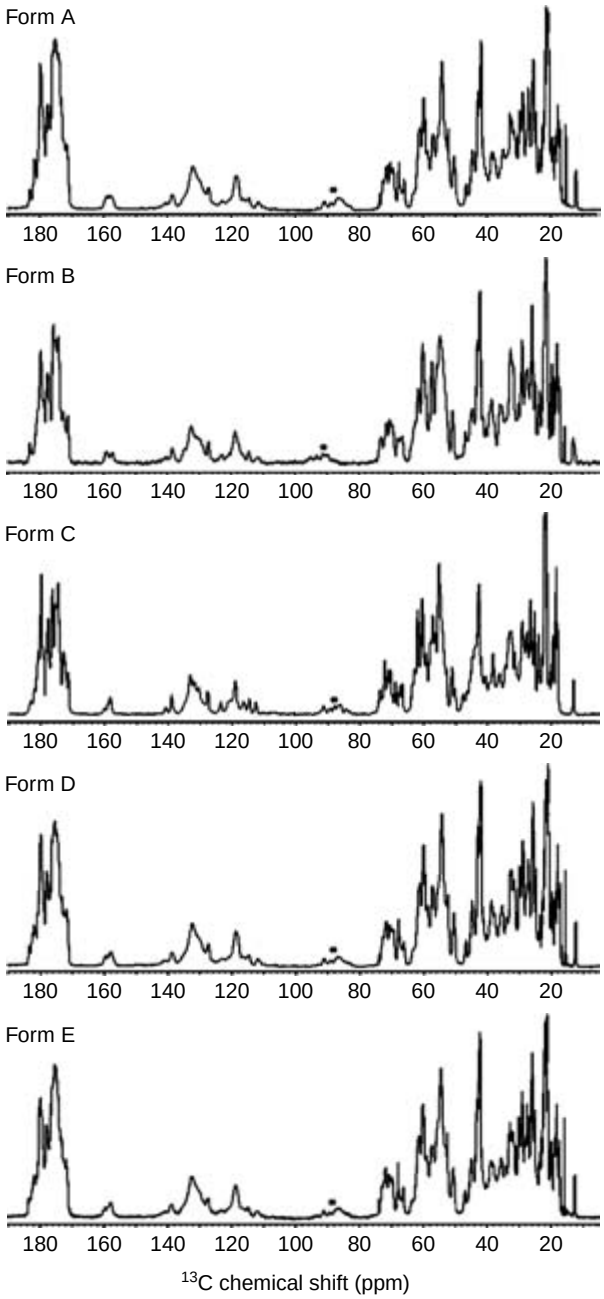

FIGURE 30 ^{13}C CP/MAS spectra of five forms of microcrystalline GB1. The spectra of forms A, D, and E were acquired at 11.7 T and 11.11 kHz MAS. The spectrum of form B was acquired at 14.1 T and 13.3 kHz MAS. The spectrum of form C was acquired at 17.6 T and 16.67 kHz MAS. Asterisks indicate spinning sidebands. Adapted from Ref. (123).

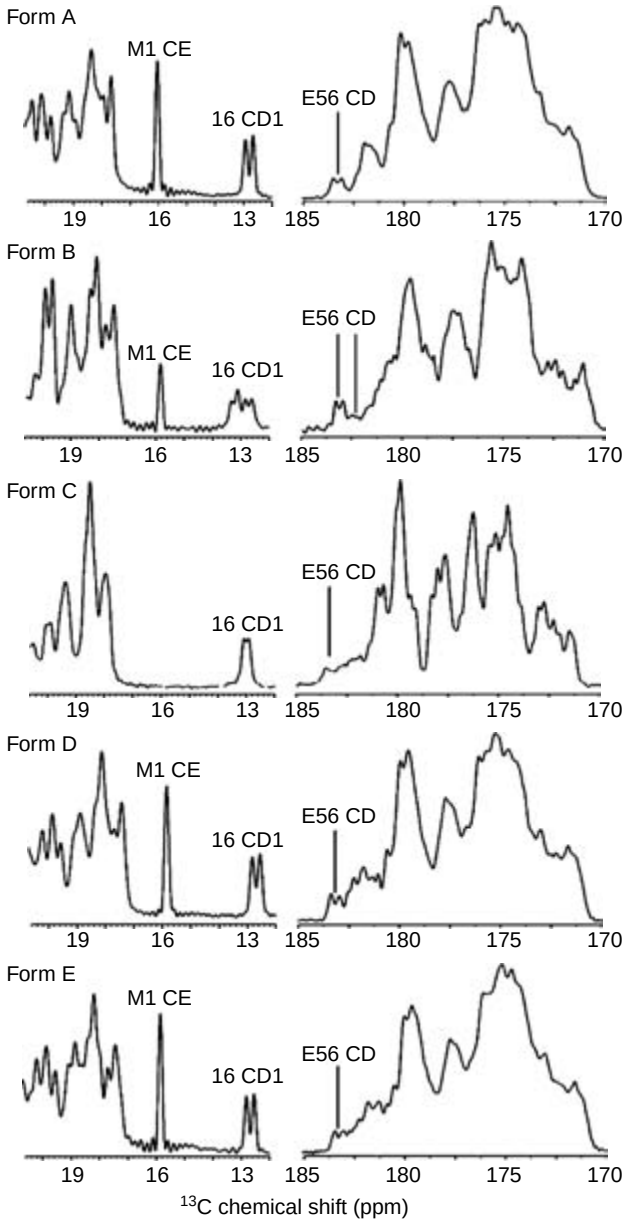

FIGURE 31 Expanded regions of the ^{13}C CP/MAS spectra of five forms of microcrystalline GB1. The carbonyl region is on the *right*, and the methyl region is on the *left*. Note that spectra of forms A, D, and E have similarities (labeled in each spectrum), but they are distinctly different and represent unique solid forms of GB1. Adapted from Ref. (123).

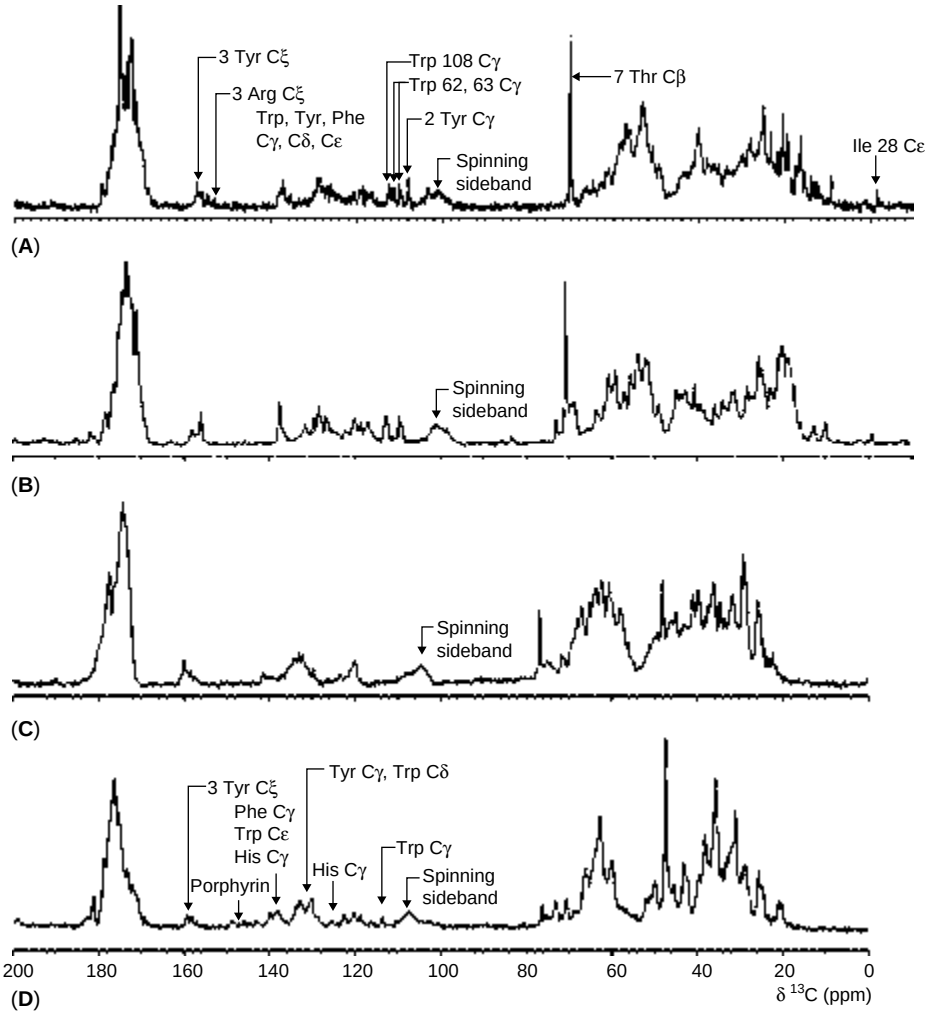

FIGURE 32 ^{13}C CP/MAS spectra of crystalline (**A**) lysozyme, (**B**) streptavidin, (**C**) ribonuclease A, and (**D**) cytochrome *c*. Some possible assignments are labeled. Adapted from Ref. (124).

(T_{CH}), (2) the rotating frame spin-lattice relaxation time for protons ($T_1\rho_H$), and (3) the spin-lattice relaxation time for protons (T_{1H}). The corresponding ^{13}C relaxation times ($T_1\rho_C$ and T_{1C}) usually to not have a significant effect on the observed signal for CP spectra. The T_{CH} determines how rapidly each carbon resonance gets enhanced by ^{1}H polarization transfer. Relatively immobile carbons with directly bonded protons will be polarized most rapidly. The $T_1\rho_H$ determines how rapidly the rotating frame ^{1}H magnetization decreases, and it competes with T_{CH} during the CP process. This means that if $T_1\rho_H$ is rapid, then T_{CH} will not be able to enhance some or all of the ^{13}C resonances sufficiently for CP to be useful. The T_{1H} determines how rapidly the equilibrium magnetization of each proton is re-established, and

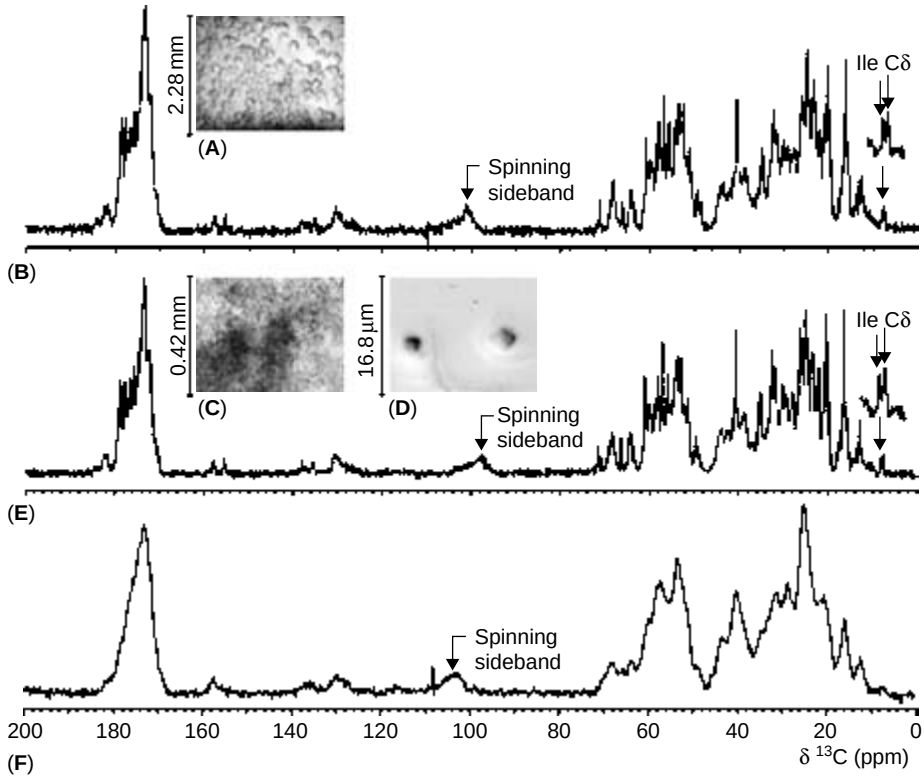

FIGURE 33 ^{13}C CP/MAS spectra of ubiquitin at 18.8 T and 14.5 kHz MAS: (**B**) microcrystalline protein, (**E**) nanocrystalline protein, and (**F**) lyophilized protein. Micrographs of the microcrystalline (**A**) and nanocrystalline (**C** and **D**) proteins are inset: (**A**) 5× magnified light microscope image of microcrystalline protein, (**B**) 225× magnified light microscope image of nanocrystalline protein, and (**C**) 4000× magnified electron microscope image of two larger crystallites in the nanocrystalline protein sample. Adapted from Ref. (124).

therefore, how long one must wait between pulses. Figure 34 shows how the length of the delay between pulses affects the recovery of magnetization. A delay of approximately three times the relevant T_1 value is required for greater than 90% of the magnetization to recover. Because protons are the most prevalent atom in pharmaceutical solids and have strong dipolar coupling, spin polarization will be rapidly distributed over the entire molecule (spin diffusion). Spin diffusion usually results in a single T_{1H} relaxation time for a compound. Even if an internal standard is used, some corrections would be necessary to obtain quantitative data from CP/MAS spectra due to the potential differences in relaxation times.

Direct polarization ^{13}C MAS experiments can be used for quantitative SSNMR analyses, but this requires waiting at least five times the T_{1C} between scans for greater than 99% of the magnetization to recover. Carbon-13 relaxation times can be several to many minutes long, making it impractical to obtain good signal averaging in a reasonable amount of time for many solid materials.

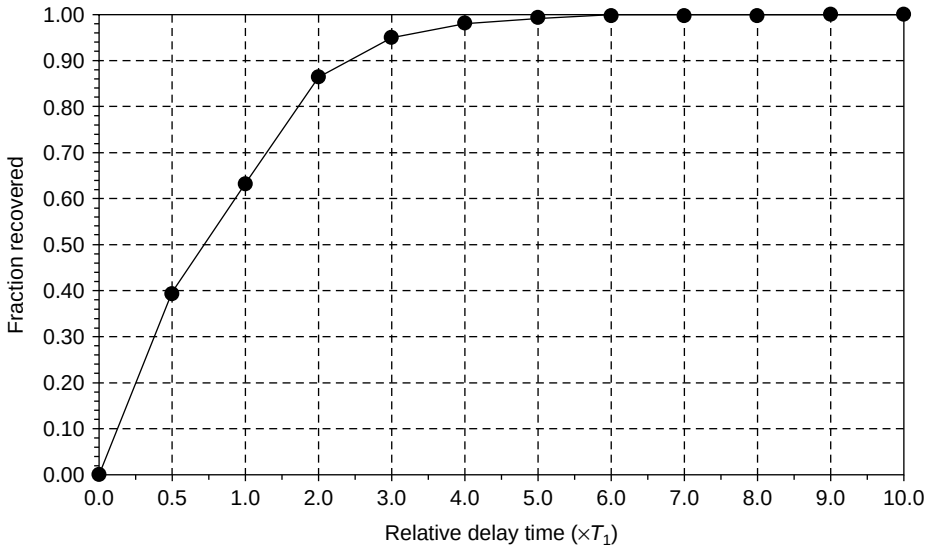

FIGURE 34 Recovery of magnetization (M_z) as a function of the amount of time allowed for relaxation.

Formoterol fumarate dihydrate was quantified at 0.45% in lactose by ^{13}C SSNMR, and the dihydrate to anhydrate ratio could be quantified to 2% in lactose (128). It is typical for quantification of polymorph mixtures to be more difficult than quantification of a single polymorph mixed with excipients because most active pharmaceutical compounds are well resolved from excipients but much less so from a polymorph.

Ziarelli et al. have discussed quantitative ^{13}C and ^{23}Na MAS SSNMR spectroscopy using an unusual external electronic signal (ERETIC™) as a quantification standard (129). They also show that using the center portion of the rotor is necessary to obtain the most accurate results, which has been previously discussed by Campbell et al. (130).

Offerdahl et al. quantified different forms of neotame by ^{13}C CP/MAS SSNMR spectroscopy (131). Their technique requires the determination of T_{CH} and $T_1\rho_H$ of the pure forms, obtaining spectra of mixtures using at least five different contact times that are $>5 \times T_{CH}$, and calculating the $T_1\rho_H$ for each component from a plot of the peak area versus contact time. The resulting graph gives a straight line with the y-intercept equal to the quantity of the particular component in the sample. The authors found a quantification limit of ~1% to 2%, and that both polymorphs contained a significant amount of amorphous material.

Miscellaneous Applications of SSNMR Spectroscopy

SSNMR spectroscopy can be used to analyze essentially any solid with NMR active nuclei. Small organic molecules are the typical compounds used for active pharmaceuticals, although larger proteins are being developed at a rapid rate.

Less commonly used as pharmaceuticals are carbohydrates, lipids, and nucleic acids. Tautomerization, ABMS, solid-state dynamics, hydrogen bonding, and pK_as can also be analyzed by SSNMR. All of these applications have potential uses in characterizing pharmaceutical solids, and some examples of these are discussed in this section.

Paradowska et al. studied seven crystalline methyl glycopyranosides by ^{13}C SSNMR spectroscopy and XRPD (132). Sugars tend to be structurally very similar and potentially difficult to differentiate by spectroscopic techniques. However, the ^{13}C SSNMR spectra were very different for each of the sugars in this study. One of the sugars had two molecules per asymmetric unit, whereas another was apparently contaminated with an unknown sugar that may have two molecules per asymmetric unit. The authors used XRPD and calculated patterns from the single-crystal structure to confirm the results from SSNMR spectroscopy.

Yoshinari et al. studied the effect of water on the β and δ polymorphs of mannitol by DSC, scanning electron microscopy (SEM), XRPD, FT-IR, ^{13}C SSNMR spectroscopy, and water vapor sorption analyses (133). SSNMR spectroscopy was used to confirm the δ polymorph because the crystal structure had not been obtained for it. Upon exposure of the δ polymorph to 97% relative humidity overnight, it completely converted to the β polymorph. The ^{1}H and ^{13}C T_1 relaxation times were obtained for the β and δ polymorphs. The ^{1}H T_1 relaxation time was quite long as is typical for sugars (~4 and ~8 minutes for β and δ, respectively), and the ^{13}C T_1 relaxation times were as much as 15 times longer than the ^{1}H T_1 relaxation times. Surprisingly, the authors used a very short relaxation delay (0.1 second) to obtain the ^{13}C SSNMR spectroscopy. This would require many more scans and more time to obtain useful data given that the relaxation delay was ~0.05% of shortest ^{1}H T_1, and 0.02% of the longest ^{1}H T_1(0). For most pure compounds with long ^{1}H T_1 relaxation times, a ^{13}C CP/MAS with an acceptable signal-to-noise ratio can be obtained using a relaxation delay of 0.5 to 1.0 times the ^{1}H T_1 relaxation time and relatively few scans (≤100). A very useful alternative for obtaining spectra of nuclei with long relaxation times is the flip-back pulse sequence (134).

Colsenet et al. used ^{13}C CST analysis and ^{1}H SSNMR spectroscopy to study hydrogen bonding in malonic acid by lyophilization of solutions at various pH values (135). The δ_{11}, δ_{22}, and δ_{iso} chemical shift tensor values had significant changes with pH, whereas the δ_{33} value did not change very much. The authors also calculated the pK_as of the carboxylate groups with ^{13}C SSNMR spectroscopy determinations of the acid to base ratios in the solid samples.

Mirmehrabi et al. used X-ray diffraction, ^{13}C SSNMR, FT-IR, scanning electron microscopy, and thermal analysis to study tautomerization in two forms of ranitidine hydrochloride (136). Tautomers undergo a configurational change in bonding to give a different isomer of the molecule, and these isomers exist in an equilibrium state among the various configurations depending on the conditions. This is in contrast to the more common conformational changes without bond breaking that lead to polymorphism. A change in protonation state is the most common tautomeric process because it requires less energy to break and reform bonds with electronegative atoms such as oxygen and nitrogen. The authors performed the ^{13}C SSNMR spectroscopy at 9.4 T with a 3.2 mm rotor and relatively fast MAS at 20 kHz. Both forms I and II appeared to have one molecule per asymmetric unit. The spectrum of form II showed significant peak broadening especially in the aliphatic region, which is consistent with a disordered crystalline solid. The single-crystal X-ray structure

confirmed the disorder in form II, but no crystal structure was obtained for form I because only small crystals (1–10 μm) could be grown. The higher degree of order in form I was obvious from the ^{13}C SSNMR spectra, although this was not confirmed by another technique in their study. The highest frequency carbon resonance (C15) was noticeably broader than the other resonances (particularly for form I) because C15 was bonded to two nitrogens. There was no asymmetrical splitting for this carbon resonance because the field strength was high enough to reduce the coupling with the ^{14}N quadrupole.

Novoa de Armas et al. studied two polymorphs of ranitidine base with XRPD, hot-stage microscopy, DSC, thermogravimetry, FT-IR spectroscopy, and ^{13}C SSNMR spectroscopy (137). The XRPD data was used to determine the crystal structure of forms I and II. The SSNMR spectra easily showed the differences between the solid forms, and that there was no indication of a mixture of tautomers as previously observed for the hydrochloride salt (136). The authors state that only X-ray crystallography can determine which tautomer is present, but SSNMR spectroscopy could also be used to do this, although it would probably be much more difficult. SSNMR analysis of the tautomers might require ^{15}N labeling for ^{15}N CP/MAS or REDOR analysis (102,103).

Barich et al. studied peak widths of ibuprofen in various formulations by ^{13}C SSNMR spectroscopy, XRPD, and SEM (138). The authors note that they could not make an amorphous form of ibuprofen, and it has no known polymorphs. The effect of ABMS was tested by mixing ibuprofen with materials that had different ABMS such as talc, hydroxypropyl methyl cellulose, and croscarmellose sodium (139,140). The concentration of the material and its particle size both affected the observed SSNMR peak widths of ibuprofen. The authors note that peak broadening observed after tableting may be due to reduction in the particle size or elimination of air from the voids. This is because air has much lower magnetic susceptibility than the surrounding solid. The authors also note that SSNMR spectroscopy can be used to study crystalline domain size, although they did not have any specific examples of this important issue in their report. The domain size of nanocrystalline materials is important for differentiating them from amorphous or disordered solids, such as solid dispersion formulations. The distance-dependent properties of NMR spectroscopy are particularly useful for studying domain sizes in solids, but this topic is outside the scope of this chapter.

Adam-Berret et al. used ^{13}C SSNMR spectroscopy to analyze the metastable α and stable β polymorphs of five triacylglycerols important in the food industry (141). The ^{1}H T_1 and T_2 relaxation times were determined a 9.4 T, whereas variable-temperature low-resolution time-domain NMR spectroscopy at 0.47 T was also used to measure the dipolar second moments of the polymorphs. They were able to distinguish the different triacyglycerol polymorphs by their different relaxation times (due to mobility differences) as well as by the chemical shift differences.

SSNMR spectroscopy can be a powerful analytical tool for partially ordered systems. Crowley et al. studied mesophases resulting from solid–solid transformations of lipids using variable-temperature ^{13}C SSNMR spectroscopy and T_1 relaxation times (142). They found that α-oleic acid and both forms of propranolol oleate were conformationally disordered crystalline phases.

Hughes and Harris used ^{13}C SSNMR spectroscopy to monitor crystallization of the α and γ polymorphs of ^{13}C-labeled glycine from H_2O and D_2O solutions (143). Both H_2O and D_2O show nucleation of α-glycine, but this converts to

γ-glycine for the D_2O solution (>80% within ~6 hours). The greater CP efficiency of α-glycine (~3-fold) was not a significant factor in observing the transformation, although the quantification would be unreliable without specifically accounting for the differences.

Xu and Harris monitored the dehydration of sodium acetate trihydrate during ^{13}C SSNMR spectroscopic analyses at several spinning rates, and confirmed the resulting solid form by XRPD (144). Their dehydration process produced form I from the trihydrate when all other studies had shown that the β form results from dehydration. A mixture of forms I and β are observed at lower spinning speed (3 kHz), and the ratio of form I increased at higher spinning speed (7 kHz). The final product after about five days was a mixture of forms I and β. Form I had previously been obtained by vacuum drying of the β form. However, the authors demonstrated with ^{13}C SSNMR spectroscopy that both form I and β are simultaneously produced during the drying process rather than an initial transformation of the trihydrate to the β form followed by dehydration to form I. Pure form β, obtained by dehydration, was also rotated at 3 and 7 kHz and did not convert to form I, which demonstrates that a transformation of form β to form I was not occurring.

SUMMARY

SSNMR spectroscopy is a versatile analytical technique for characterizing a wide variety of solid materials. Differentiating polymorphs is only one potential application, but it is critical to pharmaceutical development. SSNMR spectroscopy particularly stands out for mixture analysis, studying dynamic processes, and conformational analysis. It should be used routinely as one of the analytical techniques for characterizing pharmaceuticals as part of regulatory submissions. SSNMR spectroscopy is particularly suitable for patent applications of formulated pharmaceuticals because of its high specificity compared to XRPD or vibrational spectroscopy.

REFERENCES

1. Ripmeester JA. Application of solid state ^{13}C NMR to the Study of polymorphs, clathrates and complexes. Chem Phys Lett 1980; 74: 536–8.
2. Harris RK. NMR studies of organic polymorphs and solvates. Analyst 2006; 131: 351–73.
3. Medek A. Solid-state nuclear magnetic resonance spectrometry, Chapter 11 in Spectroscopy of Pharmaceutical Solids. In: Brittain HG, ed. New York: Taylor and Francis, 2006: 413–557.
4. Tishmack PA, Bugay DE, Byrn SR. Solid-state nuclear magnetic resonance spectroscopy — pharmaceutical applications. J Pharm Sci 2003; 92: 441–74.
5. Harris RK. Applications of solid-state NMR to pharmaceutical polymorphism and Related Matters. J Pharm Pharmacol 2007; 59: 225–39.
6. Berendt RT, Sperger DM, Isbester PK, et al. Solid-state NMR spectroscopy in pharmaceutical research and analysis. TRAC 2006; 25: 977–84.
7. Offerdahl TJ. Solid-state nuclear magnetic resonance spectroscopy for analyzing polymorphic drug forms and formulations. Pharm Tech 2006: 30: S25–S42.
8. U.S. Government. Q6A Specifications: Test Procedures and Acceptance Criteria for new drug substances and new drug products: chemical substances. Federal Register 1997; 62: 227, 62890–910.
9. Baldus M. Solid-state NMR spectroscopy: molecular structure and organization at the atomic level. Angew Chem Int Ed 2006; 45: 1186–8.

10. Reichert D. Solid-state NMR Spectroscopy and its application in analytical chemistry. Anal Bioanal Chem 2003; 376: 308–10.
11. Laws DD, Bitter H-ML, Jerschow A. Solid-state NMR spectroscopic methods in chemistry. Angew Chem Int Ed 2002; 41: 3096–139.
12. Duer MJ. Solid-State NMR Spectroscopy Principles and Applications. London: Blackwell Science Ltd, 2002.
13. Stejskal EO, Memory JD. High Resolution NMR in the Solid State. Fundamentals of CP/MAS. Oxford, U.K: Oxford University Press, 1994.
14. Jelinski LW, Melchior MT. High-Resolution NMR of Solids. In NMR Spectroscopy Techniques, 2nd edition. In: Bruch MD, ed. 1996: 417–85.
15. Friebolin H. Basic One- and Two-Dimensional NMR Spectroscopy, 4th edition. Wiley-VCH, 2005.
16. Chandrakumar N, Subramanian S. Modern Techniques in High-Resolution FT-NMR. New York: Springer Verlag, 1987.
17. Harris RK. Nuclear Magnetic Resonance Spectroscopy, A Physicochemical View. Essex, England: Longman Scientific and Technical, 1986.
18. Becker ED. High Resolution NMR, Theory and Chemical Applications, 3rd edition. San Diego: Academic Press, 2000.
19. Traficante DD. NMR concepts, in NMR Spectroscopy Techniques, 2nd edition, Chapter 1. In: Bruch MD, ed. New York: Marcel Dekker, 1996: 1–60.
20. Carrington AC, McLachlan AD. Introduction to Magnetic Resonance with Applications to Chemistry and Chemical Physics. New York: Harper and Row, 1967.
21. Slichter CP. Principles of Magnetic Resonance with Examples from Solid State Physics. New York: Harper and Row, 1963.
22. Abragam A. Principles of Nuclear Magnetism, International Series of Monographs on Physics, 32. Oxford, England: Oxford University Press, 1983.
23. Grant DM, Harris RK. Encyclopedia of Nuclear Magnetic Resonance. Hoboken, New Jersey: John Wiley & Sons, 1996 (updated 2002).
24. Fundamental Physical Constants – Complete Listing, from: http://physics.nist.gov/constants
25. Frye JS. Comparison of inversion-recovery methods for measuring longitudinal Relaxation rates. Concepts Magn Reson 1989; 1: 27–33.
26. Andrew ER, Bradbury A, Eades RG. Removal of dipolar broadening of nuclear magnetic resonance spectra of solids by specimen rotation. Nature 1959; 183: 1802–3.
27. Andrew ER. Magic angle spinning in solid state N.M.R. spectroscopy. Phil Trans R Soc Lond A 1981; 299: 505–20.
28. Dixon WT. Spinning-sideband-free and spinning-sideband-only NMR spectra in spinning samples. J Chem Phys 1982; 77: 1800–9.
29. Raleigh DP, Olejniczak ET, Griffin RG. Multiple-pulse NMR in inhomogeneously broadened rotating solids: theory of sideband suppression experiments. J Chem Phys 1988; 89: 1333–50.
30. Geen H, Bodenhausen G. Complete sideband suppression in magic angle spinning Solid-state suclear magnetic resonance for arbitrary chemical shift anisotropies. J Am Chem Soc 1993; 115: 1579–80.
31. Antzutkin ON, Song Z, Feng X, et al. Suppression of sidebands in magic-angle-spinning nuclear magnetic resonance: general principles and analytical solutions. J Chem Phys 1994; 100: 130–40.
32. Rienstra CM, Vega S, Griffin RG. Centerband intensity in sideband-suppressed magic-angle-spinning spectra. J Magn Reson 1996; A119: 256–9.
33. Antzutkin ON. Spinning manipulation in magic-angle-spinning nuclear magnetic resonance. Prog Nucl Magn Reson Spectr 1999; 35: 203–66.
34. Pines A, Gibby MG, Waugh JS. Proton-enhanced NMR of dilute spins in solids. J Chem Phys 1973; 59: 569–90.

35. Stejskal EO, Schaefer J. Magic-angle spinning and polarization transfer in proton-enhanced NMR. J Magn Reson 1977; 28: 105–12.
36. Schaefer J, Stejskal EO. Carbon-13 nuclear magnetic resonance of polymers spinning at the magic angle. J Am Chem Soc 1976; 98: 1031–2.
37. Bryce DL, Bernard GM, Gee M, et al. Practical aspects of modern routine solid-state multinuclear magnetic resonance spectroscopy: one dimensional experiments. Can J Anal Sci Spectr 2001; 46: 46–82.
38. Potrzebowski MJ, Tekely P, Dusausoy Y. Comment to 13C-NMR studies of α and γ polymorphs of glycine. Solid State Nucl Magn Reson 1998; 11: 253–7.
39. Taylor RE. Setting up 13C CP/MAS experiments. Concepts Magn Reson 2004; 22A: 37–49.
40. Taylor RE. 13C CP/MAS: application to glycine. Concepts Magn Reson A 2004; 22A: 78–89.
41. Metz G, Ziliox M, Smith SO. Towards quantitative CP-MAS NMR. Solid State Nucl Magn Reson 1996; 7: 155–60.
42. Metz G, Wu X, Smith SO. Ramped-amplitude cross polarization in magic-angle-spinning NMR. J Magn Reson A 1994; 110: 219–27.
43. Peersen OB, Wu X, Smith SO. Enhancement of CP-MAS signals by variable-amplitude cross polarization. Compensation for inhomogeneous B1 fields. J Magn Reson A 1994; 106: 127–31.
44. Peersen OB, Wu X, Kustanovich I, et al. Variable-amplitude cross-polarization MAS NMR. J Magn Reson A 1993; 104: 334–9.
45. Hediger S, Signer P, Tomaselli M, et al. A combination of slow and fast RF field modulation for improved cross polarization in solid-state MAS NMR. J Magn Reson 1997; 125: 291–301.
46. Fu R, Pelupessy P, Bodenhausen G. Freqency-modulated cross-polarization for fast magic angle spinning NMR at high fields: relaxing the hartmann-hahn condition. Chem Phys Lett 1997; 264: 63–9.
47. Baldus M, Geurts DG, Hediger S, et al. Efficient ^{15}N-^{13}C polarization transfer by adiabatic-passage hartmann-hahn cross polarization. J Magn Reson A 1996; 118: 140–4.
48. Hediger S, Meier BH, Ernst RR. Rotor-synchronized amplitude-modulated magnetic resonance spin-lock sequences for improved cross polarization under fast fagic angle sample spinning. J Chem Phys 1995; 102: 4000–11.
49. Ernst M, Samoson A, Meier GH. Low-power XiX decoupling in MAS NMR experiments. J Magn Reson 2003; 163: 332–9.
50. Detken A, Hardy EH, Ernst M, et al. Simple and efficient decoupling in magic-angle spinning solid-state NMR: the XiX scheme. Chem Phys Lett 2002; 356: 298–304.
51. De Paëpe G, Lesage A, Emsley L. The performance of phase modulated heteronuclear dipolar decoupling schemes in fast magic-angle-spinning nuclear magnetic resonance experiments. J Chem Phys 2003; 119: 4833–41.
52. De Paëpe G, Hodgkinson P, Emsley L. Improved heteronuclear decoupling schemes for solid-state magic angle spinning NMR by direct spectral optimization. Chem Phys Lett 2003; 376: 259–67.
53. Khitrin AK, Fujiwara T, Akutsu H. Phase-modulated heteronuclear decoupling in NMR of solids. J Magn Reson 2003; 162: 46–53.
54. Takegoshi K, Mizokami J, Terao T. 1H decoupling with third averaging in solid NMR. Chem Phys Lett 2001; 341: 540–4.
55. Bräuniger T, Wormald P, Hodgkinson P. Improved proton decoupling in NMR spectroscopy of crystalline solids using the SPINAL-64 sequence. Monat Chem 2002; 133: 1549–54.
56. Khitrin A, Fung BM. Design of heteronuclear decoupling sequence for solids. J Chem Phys 2000; 112: 2392–8.
57. Fung BM, Khitrin AK, Ermolaev K. An improved broadband decoupling sequence for liquid crystals and solids. J Magn Reson 2000; 142: 97–101.

58. Gan Z, Ernst RR. Frequency- and Phase-modulated heteronuclear decoupling in rotating solids. Solid State Nucl Magn Reson 1997; 8: 153–9.
59. Bennett A, Rienstra CM, Auger M, et al. Heteronuclear decoupling in rotating solids. J Chem Phys 1995; 103: 6951–8.
60. Frye JS, Maciel GE. Setting the magic angle using a quadrupolar nuclide. J Magn Reson 1982; 48: 125–31.
61. Antonijevic S, Bodenhausen G. High-resolution NMR spectroscopy by truly magic-angle spinning. Angew Chem Int Ed 2005; 44: 2935–8.
62. Barich DH, Gorman EM, Zell MT, et al. 3-methylgutaric acid as a 13C solid-state NMR standard. Solid State NMR 2006; 30: 125–9.
63. Wooten EW, Mueller KT, Pines A. New angles in nuclear magnetic resonance sample spinning. Acc Chem Res 1992; 25: 209–15.
64. Bernstein J. Conformational Polymorphism in Organic Solid State Chemistry. In: Desiraju GR. ed. Amsterdam: Elsevier, 1987: 471–518.
65. Nangia A. Conformational polymorphism in organic crystals. Acc Chem Res 2008; 41: 595–604.
66. Griesser UJ, Jetti RKR, Haddow MF, et al. Conformational polymorphism in oxybuprocaine hydrochloride. Cryst Growth Des 2008; 8: 44–56.
67. Vogt FG, Katrincic LM, Long ST, et al. Enantiotropically-related polymorphs of {4-(4-chloro-3-fluorophenyl)-2-[4-(methyloxy)phenyl]-1,3-thiazol-5-yl} acetic Acid: crystal structures and multinuclear solid-state NMR. J Pharm Sci 2008; 97: 4756–82.
68. Burger A, Ramberger R. On the polymorphism of pharmaceuticals and other molecular crystals. I. Theory of thermodynamic rules. Mikrochim Acta [Wien] 1979; II: 259–71.
69. Burger A, Ramberger R. On the polymorphism of pharmaceuticals and other molecular crystals. II. Applicability of thermodynamic rules. Mikrochim Acta [Wien] 1979; II: 273–316.
70. Maccaroni E, Alberti E, Malpezzi L, et al. Polymorphism of linezolid: a combined single-crystal, powder diffraction and NMR study. Int J Pharm 2008; 351: 144–51.
71. Naito A, Ganapathy S, McDowell CA. High resolution solid state ^{13}C NMR spectra of carbons bonded to nitrogen in a sample spinning at the sagic angle. J Chem Phys 1981; 74: 5393–7.
72. Zumbulyadis N, Henrichs PM, Young RH. Quadrupole effects in the magic-angle-spinning spectra of spin-1/2. Nuclei J Chem Phys 1981; 75: 1603–11.
73. Olivieri AC, Frydman L, Grasselli et al LE. Analysis of ^{13}C, ^{14}N residual dipolar decoupling in the ^{13}C CP/MAS NMR spectra of ribonucleosides. Magn Reson Chem 1988; 26: 281–6.
74. Ebrahimi M, Rossi P, Rogers C, et al. Dependence of ^{13}C NMR chemical shifts on conformations of RNA nucleosides and Nucleotides. J Magn Reson 2001; 150: 1–9.
75. Mooibroek S, Wasylishen RE. A carbon-13 nuclear magnetic resonance study of solid tetracyclines. Can J Chem 1987; 65: 357–62.
76. Zilm KW. Spectral editing techniques: hydrocarbon solids. In Encyclopedia of Nuclear Magnetic Resonance. In: Grant DM, Harris RK, eds. New York: John Wiley and Sons, 1996; 7: 4498–504.
77. Sheikhzadeh M, Rohani, S, Jutan A, et al. Quantitative and molecular analysis of buspirone hydrochloride polymorphs. J Pharm Sci 2007; 96: 569–83.
78. Vrbinc M, Jordan-Kotar B, Smrkolj J, et al. Characterization of physical forms of donepezil hydrochloride. Acta Chim Slov 2007; 54: 254–67.
79. Masuda K, Tabata S, Kono H, et al. Solid-state ^{13}C NMR of indomethacin polymorphism. Int J Pharm 2006; 318: 146–53.
80. Apperley DC, Forster AH, Fournier R, et al. Characterisation of indomethacin and nifedipine using variable-temperature solid-state NMR. Magn Reson Chem 2005; 43: 881–92.
81. Schmidt AC, Schwarz I, Mereiter K. Polymorphism and pseudopolymorphism of silicaine hydrochloride crystal polymorphism of local anaesthetic drugs, part V. J Pharm Sci 2006; 95: 1097–113.

82. Schmidt AC. Solid-state characterization of falicaine hydrochloride and isomorphic dyclonine hydrochloride part IV. crystal polymorphism of local anaesthetic drugs. Eur J Pharm Sci 2005; 25: 407–16.
83. Schmidt AC. Structural characteristics and crystal polymorphism of three local anaesthetic bases. crystal polymorphism of local anaesthetic drugs: part VII. Int J Pharm 2005; 298: 186–97.
84. Schmidt AC, Schwarz I. Solid state characterization of hydroxyprocaine hydrochloride. Crystal polymorphism of local anaesthetic drugs: part VIII. Int. J Mol Struct 2005; 748: 153–60.
85. Schmidt AC, Schwarz I. Solid-state characterization of non-stoichiometric hydrates of ester-type local anaesthetics. part XI. Crystal polymorphism of local anaesthetic drugs. Int J Pharm 2006; 320: 4–13.
86. Rubin-Preminger JM, Bernstein J, Harris RK, et al. [R,S]-ethambutol dihydrochloride: variable-temperature studies of a dimorphic system with very similar packing. J Pharm Sci 2004; 93: 2810–19.
87. Rubin-Preminger JM, Bernstein J, Harris RK, et al. Variable temperature studies of a polymorphic system comprising two pairs of enantiotropically related forms: [S,S]-ethambutol dihydrochloride. Cryst Growth Des 2004; 4: 431–9.
88. Moynihan HA, O'Hare IP. Spectroscopic characterization of the monoclinic and orthorhombic forms of paracetamol. Int J Pharm 2002; 247: 179–85.
89. Shaibat MA, Casablanca LB, Wickramasinghe NP, et al. Characterization of polymorphs and solid-state reactions for paramagnetic systems by ^{13}C solid-state NMR and ab initio Calculations. J Am Chem Soc 2007; 129: 10968–9.
90. Enright GD, Terskikh VV, Brouwer DH, et al. The structure of two anhydrous polymorphs of caffeine from single-crystal diffraction and ultrahigh-field solid-state ^{13}C NMR spectroscopy. Cryst Growth Des 2007; 7: 1406–10.
91. Sheth AR, Lubach JW, Munson EJ, et al. Mechanochromism of piroxicam accompanied by intermolecular proton transfer probed by spectroscopic methods and solid-phase changes. J Am Chem Soc 2005; 127: 6641–51.
92. Bates S, Zografi G, Engers D, et al. Analysis of amorphous and nanocrystalline solids from their X-ray diffraction patterns. J Pharm Res 2006; 23: 2333–49.
93. Harris RK, Ghi PY, Puschmann H, et al. Structural studies of the polymorphs of carbamazepine, its dihydrate, and two solvates. Org Proc Res Dev 2005; 9: 902–10.
94. Portieri A, Harris RK, Fletton RA, et al. Effects of polymorphic differences for sulfanilamide, as seen through ^{13}C and ^{15}N solid-state NMR, together with shielding calculations. Magn Reson Chem 2004; 42: 313–20.
95. Torchia DA. The measurement of proton-enhanced carbon-13 T1 values by a method which suppresses artifacts. J Magn Reson 1978, 30, 613–16.
96. Lee GSH, Taylor RC, Dawson M, et al. High-resolution solid state ^{13}C nuclear magnetic resonance spectra of 3,4-methylenedioxyamphetamine hydrochloride and related compounds and their mixtures with lactose. Solid State NMR 2000; 16: 225–37.
97. Reutzel-Edens SM, Kleemann RL, Lewellen PL, et al. Crystal forms of LY334370 HCl: isolation, solid-state characterization, and physicochemical properties. J Pharm Sci 2003; 92: 1196–205.
98. Antonioli G, Hodgkinson P. Resolution of ^{13}C-19F interactions in the ^{13}C NMR of spinning solids and liquid crystals. J Magn Reson 2004; 168: 124–31.
99. Wang Y, Wenslow RM, McCauley JA, et al. Polymorphic behavior of an NK1 receptor antagonist. Int J Pharm 2002; 243: 147–59.
100. Booy K-J, Weigerinck P, Vader J, et al. The use of 13C labeling to enhance the sensitivity of ^{13}C solid-state CPMAS NMR to study polymorphism in low dose solid formulations. J Pharm Sci 2005; 94: 458–63.
101. Olejniczak S, Mikula-Pacholczyk J, Hughes CE, et al. ^{15}N and ^{13}C high-resolution solid-state NMR study of the polymorphism of the L-enantiomer of N-benzoylphenylalanine. J Phys Chem B 2008; 112: 1586–93.

102. Jaroniec CP, Tounge BA, Rienstra CM, et al. Measurement of ^{13}C–^{15}N distances in uniformly ^{13}C labeled biomolecules: J-decoupled REDOR. J Am Chem Soc 1999; 121: 1023–8.
103. Schmidt-Rohr K, Hong M. Measurements of carbon to Amide-proton distances by C–H Dipolar recoupling with ^{15}N NMR detection. J Am Chem Soc 2003; 125: 5648–9.
104. Zhou J, Kye Y-S, Harbison GS. Isotopomeric polymorphism. J Am Chem Soc 2004; 126: 8392–3.
105. Othman A, Evans JSO, Evans IR, et al. Structural study of polymorphs and solvates of finasteride. J Pharm Sci 2007; 96: 1380–97.
106. Apperley DC, Basford PA, Dallman CI, et al. Nuclear magnetic resonance investigation of the interaction of water vapor with sildenafil citrate in the solid state. J Pharm Sci 2005; 94: 516–23.
107. Rafilovich M, Bernstein J, Harris RK, et al. Groth's original concomitant polymorphs revisited. Cryst Growth Des 2005; 5: 2197–209.
108. Dong Z, Padden BE, Salsbury JSW, et al. Neotame anhydrate polymorphs I: preparation and characterization. Pharm Res 2002; 19: 330–6.
109. Brown SP, Lesage A, Elena B, et al. Probing proton-proton proximities in the solid state: high-resolution two-dimensional 1H–1H double-quantum CRAMPS NMR spectroscopy. J Am Chem Soc 2004; 126: 13230–1.
110. Griffin JM, Martin DR, Brown SP. Distinguishing anhydrous and hydrous forms of an active pharmaceutical ingredient in a tablet formulation using solid-state NMR spectroscopy. Angew Chem Int Ed 2007; 46: 8036–8.
111. Zhou DH, Rienstra CM. Rapid analysis of organic compounds by proton-detected heteronuclear correlation NMR spectroscopy with 40 kHz magic-angle spinning. Angew Chem Int Ed 2008; 47: 7328–31.
112. Harris RK, Hodgkinson P, Larsson T, et al. Characterization of polymorphs and solvates of terbutaline sulfate. Cryst Growth Des 2008; 8: 80–90.
113. Martin-Islán AP, Cruzado MC, Asensio R, et al. Crystalline polymorphism and molecular structure of sodium pravastatin. J Phys Chem B 2006; 110: 26148–59.
114. Maurin MB, Vickery RD, Rabel SR, et al. Polymorphism of roxifiban. J Pharm Sci 2002; 91: 2599–604.
115. Blinc R, Seliger J, Zidanšek A, et al. ^{14}N nuclear quadrupole resonance of some sulfa drugs. Solid State Nucl Magn Reson 2006; 30: 61–8.
116. Pérez SC, Cerioni LL, Wolfenson AE, et al. Utilization of pure nuclear quadrupole resonance spectroscopy for the study of pharmaceutical crystal forms. Int J Pharm 2005; 298: 143–52.
117. Harper JK, Strohmeier M, Grant DM. Pursuing structure in microcrystalline solids with independent molecules in the unit cell using ^{1}H-^{13}C correlation data. J Magn Reson 2007; 189: 20–31.
118. Harris RK, Cadars S, Emsley L, et al. NMR crystallography of oxybuprocaine hydrochloride, modification II°. Phys Chem Chem Phys 2007; 9: 360–8.
119. Harper JK, Barich DH, Heider EM, et al. A Combined Solid-State NMR and X-ray Powder Diffraction Study of a Stable Polymorph of Paclitaxel. Cryst Growth Des 2005; 5: 1737–42.
120. Harris RK, Joyce SA, Pickard CJ, et al. Assigning carbon-13 NMR spectra to crystal structures by the INADEQUATE pulse sequence and first principles computation: a case study of two forms of testosterone. Phys Chem Chem Phys 2006; 8: 137–43.
121. Mifsud N, Elena B, Pickard CJ, et al. Assigning powders to crystal structures by high-resolution ^{1}H-^{1}H double quantum and ^{1}H-^{13}C J-INEPT solid-state NMR spectroscopy and first principles computation. A case study of penicillin. G Phys Chem Chem Phys 2006; 8: 3418–22.
122. Jen A, Merkle HP. Diamonds in the rough: protein crystals from aformulation perspective Pharm Res 2001; 18: 1483–8.

123. Frericks Schmidt HL, Sperling LJ, Gao YG, et al. Crystal polymorphism of protein GB1 examined by solid-state NMR spectroscopy and X-ray diffraction. J Phys Chem B 2007; 111: 14362–9.
124. Martin RW, Zilm KW. Preparation of protein nanocyrstals and their characterization by solid state NMR. J Magn Reson 2003; 165: 162–74.
125. Harris RK. Quantitative aspects of high-resolution solid-state nuclear magnetic resonance spectroscopy. Analyst 1985; 110: 649–55.
126. Stephenson GA, Forbes RA, Reutzel-Edens SM. Characterization of the solid state: quantitative issues. Adv Drug Delivery Rev 2001; 48: 67–90.
127. Kolodziejski W, Klinowski J. Kinetics of cross-polarization in solid-state NMR: a guide for chemists. Chem Rev 2002; 102: 613–28.
128. Apperley DC, Harris RK, Larrson T, et al. Quantitative nuclear magnetic resonance analysis of solid formoterol fumarate and Its dihydrate. J Pharm Sci 2003; 92: 2496–503.
129. Ziarelli F, Viel S, Sanchez S, et al. Precision and sensitivity optimization of quantitative measurements in solid state NMR. J Magn Reson 2007; 188: 260–6.
130. Campbell GC, Galya G, Beeler AJ, et al. Effect of RF inhomogeneity upon quantitative solid-state NMR measurements. J Magn Reson A 1995; 112: 225–8.
131. Offerdahl TJ, Salsbury JS, Dong Z, et al. Quantitation of crystalline and amorphous forms of anhydrous neotame using ^{13}C CPMAS NMR spectroscopy. J Pharm Sci 2005; 94: 2591–605.
132. Paradowska K, Gubica T, Termeriusz A, et al. 13C CP MAS NMR and crystal structure of methyl glycopyranosides. Carb RM,es 2008; 343: 2299–307.
133. Yoshinari T, Forbes RT, York P, et al. Moisture induced polymorphic transition of mannitol and Its morphological transformation. Int J Pharm 2002; 247: 69–77.
134. Tegenfeldt J, Haeberlen U. Cross polarization in solids with flip-back of I-spin magnetization. J Magn Reson 1979; 36: 453–7.
135. Colsenet R, Gardiennet C, Henry B, et al. A straightforward detection of deprotonated conformers of malonic acid by solid-state 13C NMR spectroscopy. Angew Chem Int Ed 2002; 41: 4743–5.
136. Mirmehrabi M, Rohani S, Murthy KSK, et al. Characterization of tautomeric forms of ranitidine hydrochloride: thermal analysis, solid-state NMR, X-ray. J Cryst Growth 2004; 260: 517–26.
137. Novoa de Armas H, Peeters OM, Blaton N, et al. Solid state characterization and crystal structure from X-ray powder diffraction of two polymorphic forms of ranitidine base. J Pharm Sci 2008; 98: 146–58.
138. Barich DH, Davis JM, Schieber LJ, et al. Investigation of solid-state NMR line widths of ibuprofen drug formulations. J Pharm Sci 2006; 95: 1586–94.
139. VanderHart DL. Magnetic susceptibility and high resolution NMR of liquids and solids, in Encyclopedia of NMR. In: Grant D, Harris R, eds. New York: John Wiley & Sons, 1996: 2938–46.
140. Samoson A, Tuherm T, Gan Z. High-Field high-speed MAS resolution enhancement in ^{1}H NMR spectroscopy of solids. Solid State NMR 2001; 20: 130–6.
141. Adam-Berret M, Rondeau-Mouro C, Riaublanc A, et al. Study of triacylglycerol polymorphs by nuclear magnetic resonance: effects of temperature and chain length on relaxation parameters. Magn Reson Chem 2008; 46: 550–7.
142. Crowley KJ, Forbes RT, York P, et al. Characterization of oleic acid and propranolol oleate mesomorphism using ^{13}C solid-state nuclear magnetic resonance spectroscopy (SSNMR). J Pharm Sci 2000; 89: 1286–95.
143. Hughes CE, Harris KDM. A technique for in situ monitoring of crystallization from solution by solid-state ^{13}C CPMAS NMR spectroscopy. J Phys Chem A 2008; 112: 6808–10.
144. Xu M, Harris KDM. Altering the polymorphic product distribution in a solid-state dehydration process by rapid sample rotation in solid-state NMR Probe. J Am Chem Soc 2005; 127: 10832–3.

12 Effects of Polymorphism and Solid-State Solvation on Solubility and Dissolution Rate

Harry G. Brittain
Center for Pharmaceutical Physics, Milford, New Jersey, U.S.A.

David J. R. Grant
College of Pharmacy, University of Minnesota, Minneapolis, Minnesota, U.S.A.

Paul B. Myrdal
College of Pharmacy, University of Arizona, Tucson, Arizona, U.S.A.

INTRODUCTION

It has now been amply demonstrated that the different lattice energies (and entropies) associated with different polymorphs or solvates give rise to measurable differences in the physical properties (density, color, hardness, refractive index, conductivity, melting point, enthalpy of fusion, vapor pressure, etc.). Even the explosive power of cyclotetramethylene-tetranitramine depends on which of its four polymorphs is being used (1). We have seen in previous chapters that the different lattice energies of polymorphs or solvates give rise to different solubilities and dissolution rates. If the solubilities of the various solid forms are sufficiently different, they can be very important during the processing of drug substances into drug products (2), and may have implications for the adsorption of the active drug from its dosage form (3). These concerns have led to an increased regulatory interest in the solid-state physics of drug substances, and in their characterization (4–10).

That the crystal structure can have a direct effect on the solubility of a solid can be understood using a simple model. For a solid to dissolve, the forces of attraction between solute and solvent molecules must overcome the attractive forces holding the solid intact and the solvent aggregates together. In other words, the solvation free energy released upon dissolution must exceed the lattice free energy of the solid plus the free energy of cavity formation in the solvent for the process to proceed spontaneously. The balance of the attractive and disruptive forces will determine the equilibrium solubility of the solid in question (which is an exponential function of the free energy change of the system). The enthalpy change and the increase in disorder of the system (i.e., the entropy change) determine the Ostwald free energy change. Because different lattice energies (and enthalpies) characterize different crystal structures, the solubility of different crystal polymorphs (or solvate species) must differ as well. Finally, the act of dissolution may be endothermic or exothermic in nature, so that measurements of solution calorimetry can be used to provide important information on the substance under study. The most common solvent media used in the characterization of polymorphs or solvates are liquids or liquid mixtures that give rise to liquid solutions of the solute (11) and that constitute the focus of this chapter.

The effect of polymorphism becomes especially critical on solubility because the rate of compound dissolution must also be dictated by the balance of attractive and

disruptive forces existing at the crystal–solvent interface. A solid having a higher lattice free energy (i.e., a less stable polymorph) will tend to dissolve faster, because the release of a higher amount of stored lattice free energy will increase the solubility and hence the driving force for dissolution. At the same time, each species would liberate (or consume) the same amount of solvation energy, because all dissolved species (of the same chemical identity) must be thermodynamically equivalent. The varying dissolution rates possible for different structures of the same drug entity can, in turn, lead to varying degrees of bioavailability for different polymorphs or solvates. To achieve bioequivalence for a given drug compound usually requires equivalent crystal structures in the drug substance, although exceptions are known to exist.

The dissolution rate and solubility in a solvent medium are one of the most important characteristics of a drug substance, because these quantities determine the bioavailability of the drug for its intended therapeutic use. Solubility is defined as the equilibrium concentration of the dissolved solid (the solute) in the solvent medium, and is ordinarily a function of temperature and pressure.

EQUILIBRIUM SOLUBILITY

The capacity of any system to form solutions has limits imposed by the phase rule of Gibbs:

$$F + P = C + 2 \tag{1}$$

where F is the number of degrees of freedom in a system consisting of C components with P phases. For a system of two components and two phases (e.g., solid and liquid) under the pressure of their own vapor and at constant temperature, F equals zero. If one of the phases consists solely of one component (a pure substance), the equilibrium solubility at constant temperature and pressure is a fixed quantity that is given as the amount of solute contained in the saturated solution in a unit amount of the solvent or solution.

For any case in which F is zero, a definite reproducible solubility equilibrium can be reached. Complete representation of the solubility relations is accomplished in the phase diagram, which gives the number, composition, and relative amounts of each phase present at any temperature in a sample containing the components in any specified proportion. Solubilities may therefore be expressed in any appropriate units of concentration, such as the quality of the solute dissolved (defined mass, number of moles) divided by the quantity either of the solvent (defined mass, volume, or number of moles) or of the solution (defined mass, volume, or number of moles). Jacques et al. have provided a compilation of the expressions for concentration and solubility (12).

Determination of Equilibrium Solubility

Methods for the determination of solubility have been thoroughly reviewed (11,13–15), especially with respect to the characterization of pharmaceutical solids (16). Solubility is normally highly dependent on temperature, so the temperature must be recorded for each solubility measurement in addition to the precise nature of the solvent and the solid phase at equilibrium. Plots of solubility against temperature are commonly used for characterizing pharmaceutical solids, and have been extensively discussed (11,17,18). Frequently (especially over a relatively

narrow temperature range), a linear relationship may be given either by a van't Hoff plot:

$$\ln X_2^{\text{sat}} = (-a/RT) + c' \tag{2}$$

or by a Hildebrand plot:

$$\ln X_2^{\text{sat}} = (b/R)\ln T + c'' \tag{3}$$

In equations (2) and (3), X_2^{sat} is the mole fraction solubility of the solid solute at an absolute temperature T, a is the apparent molar enthalpy of solution, b is the apparent molar entropy of solution, and c' and c'' are constants. The combined equation, attributed to Valentiner, has been used by Grant et al. (17) in the form:

$$\ln X_2^{\text{sat}} = (-a/RT) + (b/R)\ln T + c''' \tag{4}$$

This three-parameter equation enables solubility to be simulated and correlated quite accurately over a wide temperature range (e.g., 60°C).

As implied in the previous paragraph, the validity of the afore-mentioned equations requires that each crystal phase is stable with respect to the absence of any phase conversion during the determination of equilibrium solubility. Quite different methods of analysis must be considered if the substance under study is known to undergo a solution-mediated phase transformation.

Two general methods, the analytical method and the synthetic method (16), are available for determining solubility. In the analytical method, the temperature of equilibration is fixed, whereas the concentration of the solute in a saturated solution is determined at equilibrium by a suitable analytical procedure. The analytical method can be either the traditional, common batch agitation method, or the more recent flow column method. In the synthetic method, the composition of the solute–solvent system is fixed by appropriate addition and mixing of the solute and solvent, then the temperature at which the solid solute just dissolves or just crystallizes is carefully bracketed.

Another technique that has recently gained attention is that of the potentiometric titration method (19–21). The results of this technique have been favorably compared to that of the analytical shake flask method (20). In order to utilize this method a compound must be ionizable with some appreciable solubility. If compound solubility is too low, then cosolvents may be utilized; however, this complicates and can confound analysis. Fioritto et al. investigated the pH-metric method for determining the solubility and conversion of eight polymorphic compounds (22). Llinas et al. have used a potentiometric method referred to as the "chasing equilibrium" method (23) to determine the inter-conversion and solubility properties of hydrate polymorphs of sparfloxacin (24).

It is usually not difficult to determine the solubility of solids that are moderately soluble (greater than 1 mg/mL), but the direct determination of solubilities much less than 1 mg/mL is not straightforward. Problems such as slow equilibrium resulting from a low rate of dissolution, the influence of impurities, the apparent heterogeneity in the energy content of the crystalline solid (25), and analytical variability, can lead to large discrepancies in reported values. For example, reported values of the aqueous solubility of cholesterol range from 0.25 to 2600 mg/mL (26).

Metastable Solubility

Because only one member of a family of polymorphs or solvates can be the most thermodynamically stable form under a given set of environmental conditions defined by the phase rule, one frequently finds that one form spontaneously converts to another form during the time required to establish equilibrium solubility. The existence of an unexpected metastable solubility can lead to important (and possible undesirable) consequences. For digoxin, unexpectedly high solubility values and abnormally high dissolution rates have resulted in the overdosing of patients before the phenomenon of its solid-state phase conversion was properly understood and controlled (27). This phenomenon was caused by higher energy crystals resulting from a greater density of crystal defects rather than by polymorphism.

Any metastable phase will have a higher free energy than would a thermodynamically more stable phase, and will undergo a phase transformation to the more stable phase once the activation energy barrier is overcome. Often the barrier to phase transformation is merely the improbability of a suitable nucleation step. Hence, only fortuitously unfavorable kinetics permitted a determination of the equilibrium solubility of the various higher energy phases discussed in the preceding section.

Conversions of a metastable phase into a more stable phase may include the transformation of one polymorphic phase into another, the solvation of an anhydrous phase, the desolvation of a solvate phase, the transformation of an amorphous phase into a crystalline anhydrate or solvate phase, the degradation of a crystalline anhydrate or solvate phase to an amorphous phase, or in the case of digoxin, the conversion of imperfect (less crystalline, more amorphous) crystals with a high density of defects into more perfect (more crystalline) crystals with a lower density of defects. Although it is straightforward to determine the equilibrium solubility of a phase that stablizes with respect to conversion, the measurement of solubilities of metastable phases that are susceptible to conversion is not a trivial matter.

Because determinations of the solubility of solid materials are often made by suspending an excess of the compound in question in the chosen solvent or other dissolution medium, the application of this equilibrium method to a metastable phase will result in a determination of the solubility of the stable phase. One of the attempts to measure the solubility of a metastable polymorph was made by Milosovich, who developed a method based on the measurement of the intrinsic dissolution rates (IDR) and used it to deduce the relative solubilities of sulfathiazole Forms I and II (28). This method assumes that the IDR is proportional to the solubility, the proportionality constant being the transport rate constant that is constant under constant hydrodynamic conditions in a transport-controlled dissolution process. Nogami et al. have also used intrinsic dissolution rate models for characterizing compounds that have metastable states with relatively fast conversion times (29,30).

Ghosh and Grant have developed an extrapolation technique to determine the solubility of a crystalline solid that undergoes a phase change upon contact with a solvent medium (31). They proposed a thermodynamic cycle analogous to Hess's law, but based on free energies, and used this cycle to predict the theoretical solubility of solvates in water. In the model systems to which the technique was applied, good agreement was obtained between the solubility values measured

by equilibration (and derived from an extrapolation method in a mixed solvent system), and those derived from the extrapolation method and calculated by means of the thermodynamic cycle.

A light-scattering method has recently been described for the determination of the solubility of drugs, and its application to solubility evaluations of metastable phases has also been demonstrated (32). Using this technique to deduce solubility data for theophylline anhydrate (metastable with respect to the monohydrate phase in bulk water at room temperature), agreement with the most reliable literature data was excellent. The light-scattering method appears to be most useful in the determination of solubility data for metastable crystal phases in dissolution media in which they spontaneously and rapidly convert into a more stable crystal phase.

Because the solubility determination of metastable polymorphs is often challenging due to conversion kinetics, it is useful to pursue theoretical calculations based on pure component properties (e.g., transition temperatures, entropy, and enthalpy of melting). Indeed, the rigorous derivation of polymorph ideal solubility from first principals can be considered and is detailed elsewhere (18,33,34). A practical consideration when using the ideal solubility equation is to assume that polymorphs have similar heat capacity terms, and that the change in the heat capacity from the solid to the liquid state is negligible. Using these heat capacity assumptions, Mao et al. (34) have shown that for a monotropic polymorph system, the relationship between the solubility of polymorph 1 (X_1) and polymorph 2 (X_2) is,

$$\log \frac{X_1^{(i)}}{X_2^{(i)}} \approx \frac{\Delta H_{m2} - \Delta H_{m1}}{RT} + \frac{\Delta S_{m2} - \Delta S_{m1}}{R} \tag{5}$$

where ΔH_m and ΔS_m are the enthalpy and entropy of melting, respectively.

For the enantiotropic systems, the difference in solubility between two forms is

$$\ln \frac{X_1^{(i)}}{X_2^{(i)}} \approx \frac{\Delta S_t (T_t - T)}{RT} \tag{6}$$

where T_t is the transition temperature and ΔS_t is the entropy of transition.

Mao et al. found that the calculated solubility ratios based on good thermal data were in good agreement for representative enantiotropic and monotropic experimental data. From their work they provided a guide for calculating polymorph solubility ratios based on differential scanning calorimetry (DSC) thermal observations. A modified guide is given in Table 1.

Apparent Solubilities of Polymorphic Systems

The thermodynamic relationships examined in involving polymorphism and solubility has been applied to the methylprednisolone system (35). The solubilities of the two polymorphs of this steroid were determined at various temperatures in water, decyl alcohol, and dodecyl alcohol. Because the chemical potential and thermodynamic activity of the drug in the solid state and in each saturated solution is constant, the solubility ratios for the two forms (which may be found in Table 2) were found to be independent of the solvent. The enthalpy, entropy, and temperature

TABLE 1 Decision Scheme for Choosing a Solubility Ratio Equation Based on Different DSC Thermal Observations

Observations				Methodology		
Transition observed?	**Melting point**	**Heat of event[a]**	**Solubility**	**Relationship[b]**	**Transition temperature[a]**	**Equation[c]**
No	$T_2 > T_1$	$\Delta H_{m2} > \Delta H_{m1}$	$S_1 > S_2$	Monotropic	n.a.	Mono (M)
Yes	No T_1 T_2 seen	$\Delta H'_t$ seen No ΔH_{m1} ΔH_{m2} seen	$S_1 > S_2$	Enantiotropic	$T_t \leq T'_t$ $T_t < T$	Enant (E)
Yes	No T_1 T_2 seen	$\Delta H'_t$ seen No ΔH_{m1} ΔH_{m2} seen	$S_2 > S_1$	Enantiotropic	$T_t \leq T'_t$ $T < T_t$	Enant (E)
No	$T_2 > T_1$	$\Delta H_{m1} > \Delta H_{m2}$	$S_2 > S_1$	Enantiotropic	$T_t > T$	Mono (M)
No	$T_2 > T_1$	$\Delta H_{m1} > \Delta H_{m2}$	$S_1 > S_2$	Enantiotropic	$T_t < T$	Mono (M)

Adapted from Ref. (34).
[a]T_t is the equilibrium transition temperature and T'_t is the solid–solid transition temperature observed by DSC ($\Delta H'_t$ is the heat at T'_t).
[b]Relationship represents the actual thermodynamic relationship between the polymorphs.
[c]Equation refers to the equation that can be used in practice to estimate the solubility ratio based on the data observed.

TABLE 2 Equilibrium Solubility and Solubility Ratios of the Polymorphs of Methylprednisolone in Different Solvent Systems (35)

Temperature (°C)	Solubility (mg/mL)		
	Form I	**Form II**	**Solubility ratio (II/I)**
In Water			
30	0.09	0.15	1.67
39	0.12	0.20	1.67
49	0.16	0.26	1.63
60	0.21	0.33	1.57
72	0.30	0.43	1.43
84	0.43	0.55	1.28
In Decyl Alcohol			
30	2.9	4.8	1.66
39	3.5	5.7	1.63
49	4.3	6.9	1.60
60	5.5	8.6	1.56
72	8.3	11.9	1.43
84	–	–	–

of transition calculated from the data were 1600 cal/mol, 4.1 cal/K·mol, and 118°C, respectively.

Solubility determinations were used to characterize the polymorphism of 3-(((3-(2-(7-chloro-2-quinolinyl)-(*E*)-ethenyl)-phenyl)-((3-dimethylamino-3-oxopropyl)-thio)-methyl)-thio)-propanoic acid (36). The solubility of Form II was

TABLE 3 Equilibrium Solubility of Phenylbutazone Polymorphs, at Ambient Temperature in Different Solvent Systems (37)

Solvent system	Solubility (mg/mL)				
	I	II	IV	V	III
pH 7.5 Phosphate buffer	4.80	5.10	5.15	5.35	5.9
Above buffer with 0.05% Tween 80	4.50	4.85	4.95	5.10	5.52
Above buffer with 2.25% PEG 300	3.52	5.77	5.85	6.15	6.72

Note: The polymorphs are listed in order of increasing free energy at ambient temperature.

found to be higher than that of Form I in both isopropyl alcohol (IPA, solubility ratio approximately 1.7 from 5°C to 55°C) and in methyl ethyl ketone (MEK, solubility ratio approximately 1.9 from 5°C to 55°C), indicating that Form I is the thermodynamically stable form in the range of 5°C to 55°C. An analysis of the entropy contributions to the free energy of solution from the solubility results implied that the saturated IPA solutions were more disordered than were the corresponding MEK solutions, in turn, indicating the existence of stronger solute–solvent interactions in the MEK solution. This finding corroborated results determined for the enthalpy with respect to the relative idealities of the saturated solutions.

Phenylbutazone has been found capable of existing in five different polymorphic structures, characterized by different X-ray powder diffraction patterns and melting points (37). The equilibrium solubilities of all five polymorphs in three different solvent systems are summarized in Table 3. Form I exhibits the highest melting point (suggesting the least energetic structure at the elevated temperature), whereas its solubility is the lowest in each of the three solvent systems studied (actually demonstrating the lowest free energy). These findings indicate that Form I is the thermodynamically most stable polymorph both at room temperature and at the melting point (105°C). However, identification of the sequence of stability for the other forms at any particular temperature was not straightforward. Following one common convention, the polymorphs were numbered in the order of decreasing melting points, but the solubility data does not follow this order. This finding implies that the order of stability at room temperature is not the same as that at 100°C, and emphasizes that only measurements of solubility can predict the stability order at room temperature. If different polymorphs are not discovered in the same study, they are ordinarily numbered according to the order of discovery to avoid re-numbering those discovered earlier. Ostwald's rule of stages, discussed in Chapter 1, explains why metastable forms are often discovered first.

Gepirone hydrochloride was found to exist in at least three polymorphic forms, whose melting points were 180°C (Form I), 212°C (Form II), and 200°C (Form III) (38). Forms I and II, and Forms I and III, were deduced to be enantiotropic pairs in the sense that their G versus T curves crossed. Form III was found to be monotropic with respect to Form II, because the G versus T curves did not cross below their melting points, and because there was no temperature at which Form III was the most stable polymorph. The solubility data illustrated in Figure 1 were used to estimate a transition temperature of 74°C for the enantiotropic Forms I and II, whereas the reported enthalpy difference was 4.5 kcal/mot at 74°C and 2.54 kcal/mot at 25°C.

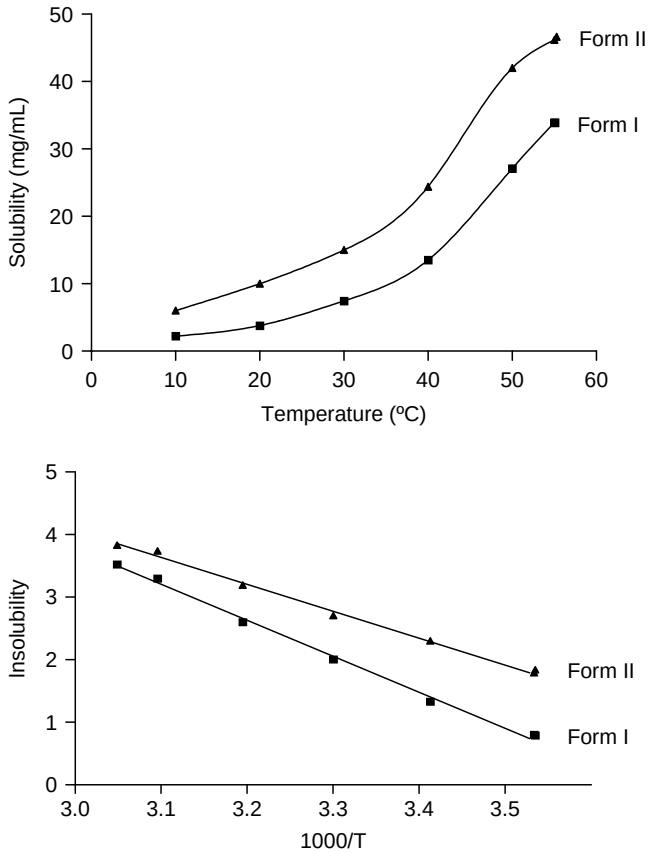

FIGURE 1 Temperature dependence of the equilibrium solubilities of two polymorphic forms of gepirone hydrochloride (38).

The most stable polymorph below 74°C was Form I, whereas Form II was the most stable above 74°C.

The effect of solvent composition on the solubility of polymorphs was investigated with cimetidine (39). Both forms exhibited almost identical melting points, but Form B was found to be less soluble than Form A, identifying it as the most stable polymorph at room temperature. The two forms were more soluble in mixed water–isopropanol solvents than in either of the pure solvents, reflecting the balance between the solvation of the molecules by water and isopropanol in determining the activity coefficient of the solute, and hence, the solubility. At constant temperature, the difference in the Gibbs free energy and the solubility ratio were constant, independent of the solvent system.

The equilibrium solubilities of two polymorphs of an experimental anti-viral compound were used to verify the results of solubility ratio predictions made on the basis of melting point and beat of fusion data (40). Even though the solubilities of Forms I and III were almost equal in three different solvent systems, the theoretically

calculated solubility ratio agreed excellently with the experimentally derived ratios in all of the solvent systems studied. The highest melting form (Form I) was found to be more soluble at room temperature, indicating that an enantiotropic relationship existed between Forms I and III.

It is well established that the temperature range of thermodynamic stability (and certain other quantities) can be determined from measurements of the equilibrium solubilities of the individual polymorphs (41). In one such study, the two polymorphic forms of 2-[[4-[[2-(1*H*-tetrazol-5-ylmethyl)-phenyl]-methoxy]-phenoxy] methyl]-quinoline were found to exhibit an enantiotropic relationship, because their *G* versus *T* curves intersected with Form I melting at a lower temperature than did Form II (42). Form I was determined to be the more thermodynamically stable form at room temperature, although the solubility of the two forms was fairly similar. The temperature dependence of the solubility ratio of the two polymorphs afforded the enthalpy of transition (Form II to Form I) as +0.9 kcal/mol, whereas the free energy change of this transition was –0.15 kcal/mol.

Aqueous suspensions of tolbutamide were reported to thicken to a non-pourable state after several weeks of occasional shaking, whereas samples of the same suspensions that were not shaken showed excellent stability after years of storage at ambient and elevated temperature (43). Examination by microscopy revealed that the thickening was due to partial conversion of the original plate-like tolbutamide crystals to very fine needle-shaped crystals. The new crystals were identified as a different polymorphic form, and did not correspond either to a solvate species or to crystals of a different habit. The crystalline conversion was observed to take place in a variety of solvents, the rate of conversion being faster in solvents where the drug exhibited appreciable solubility. Because the conversion rate in 1-octanol was relatively slow, use of this solvent permitted an accurate solubility ratio of 1.22 to be obtained (Form I being more soluble than Form III).

The polymorphism and phase interconversion of sulfamethoxydiazine (sulfameter) have been studied in detail (44). This compound can be obtained in three distinct crystalline polymorphs, with the metastable Form II being suggested for use in solid dosage forms on the basis of its greater solubility and bioavailability (45). However, the formulation of Form II in aqueous suspensions was judged inappropriate because of the fairly rapid rate of transformation to Form III. This behavior is illustrated in Figure 2, which shows that seeding of a Form II suspension with Form III crystals greatly accelerates the phase conversion. It was subsequently learned that phase conversion could be retarded by prior addition of various formulation additives, possibly permitting the development of a suspension containing the metastable Form II (46). Although there are many examples of the conversion of a metastable polymorph to a stable polymorph during the dissolution process, some of them seminal (47,48), the use of tailor-made additives to inhibit the crystallization of a more stable polymorph is relatively recent (49–52).

Table 4 provides a practical perspective of the differences in solubility that may be observed for compounds that exhibit different polymorphic states. The experimental data in Table 4 is a non-exhaustive list of solubility ratios (solubility of metastable/solubility of stable form) for 30 compounds abstracted from the scientific literature. When many of the reports offer solubilities at multiple equilibration temperatures, representative values nearest to 25–37°C are presented. Acemetacin, acetohexamide, cyclopenthiazide, and oxyclozamide on this list are the only compounds that show solubility ratios of greater than 3.0. Most metastable phases have

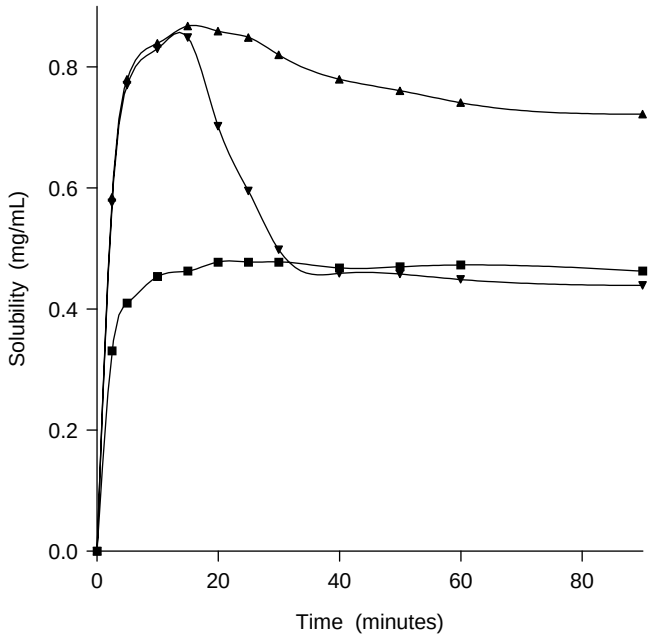

FIGURE 2 Effect on the solubility of sulfamethoxydiazine Form II by seeding with crystals of Form III. Shown are the dissolution profiles of Form II (-▲-), Form III (-■-), and Form II seeded with Form III after 20 minutes elapsed time (-▼-) (46).

apparent solubilities that are 25% to 100% greater than the polymorph with the lowest solubility. This results in a free energy of transition (ΔG_{tr}) of 132–410 cal/mol. As can be seen in the case of buspirone hydrochloride, the magnitudes of the solubilities vary considerably by solvent; however, because of the independence of the solubility ratio from the solvent identity, the ratio is virtually constant.

Pudipeddi and Serajuddin (81) have compiled 81 solubility ratios for 55 different drugs having polymorphic crystal forms, and their results are seen to parallel those of Table 4. Figure 3 combines the data from Table 4 with those of Pudipeddi and Serajuddin to offer a more comprehensive evaluation of observed solubility ratios. The 128 compounds utilized in Figure 3 are presented in order of increasing solubility ratios. Eighty-one percent of the polymorphs have solubility ratios between 1 and 2, whereas 9% of them have ratios greater than 3.5. Although these relative increases in solubility may be characterized as modest, for water-insoluble drugs exhibiting dissolution rate-limited absorption, this difference can be important for therapeutic activity.

Apparent Solubilities of Systems Having Solvate Phases

When the hydrates or solvates of a given compound are stable with respect to phase conversion in a solvent, the equilibrium solubility of these species can be used to characterize these systems. For instance, the equilibrium solubility of the trihydrate phase of ampicillin at 50°C is approximately 1.3 times that of the more stable

TABLE 4 Representative Examples of Solubility Differences Between Polymorphs

Drug	Solvent/Temp.	Solubilities	Ratio	Ref.
Acetohexamide	Distilled water 37°C	I 27 μg/mL II 32 μg/mL	II/I = 1.2	53
	0.1 N HCl 30°C	V 31.4 μg/mL IV 16.3 μg/mL III 10.4 μg/mL I 8.4 μg/mL	V/I = 3.7 IV/I = 1.9 III/I = 1.2	54
Acemetacin	Butanol 20°C	I 9.18 mM II 15.33 mM IV 19.00 mM V 25.65 mM III 43.44 mM	II/I = 1.7 IV/I = 2.1 V/I = 2.8 III/I = 4.7	55
Acetazolamide	pH 7 Phosphate buffer 25°C	A 2.04 mg/mL B 2.28 mg/mL	B/A = 1.1	56
Auranofin	25% aq. PEG 200 37°C	A 0.55 mg/mL B 1.35 mg/mL	B/A = 2.5	57
Benoxaprofen	pH 7 Phosphate buffer 25°C	I 230 μg/mL II 150 μg/mL	I/II = 1.5	58
Buspirone HCl	Distilled water 20°C	I 101.1 g/100 g II 190.0 g/100 g	II/I = 1.9	59
	Isopropanol 20°C	I 0.43 g/100 g II 0.80 g/100 g	II/I = 1.9	
	60:40 Water:isopropanol 20°C	I 84.93 g/100 g II 133.02 g/100 g	II/I = 1.6	
Carbamazepine	2-Propanol 26°C	I 11.16 mg/mL II 9.27 mg/mL	I/II = 1.2	60
{4-(4-Chloro-3-fluorophenyl)-2-[4-(methyloxy)phenyl]-1,3-thiazol-5-yl} acetic acid	Acetonitrile 8.9°C	I 10.6 mg/mL II 13.3 mg/mL	II/I = 1.2	61
	Acetonitrile 43.1°C	I 20.0 mg/mL II 16.0 mg/mL	I/II = 1.2	
Cyclopenthiazide	Distilled water 37°C	I 34.7 μg/mL II 61.8 μg/mL III 17.2 μg/mL	I/III = 2.0 II/III = 3.6	62
Difenoxin HCl	1% aq. tartaric acid 37°C	I 4.5 mg/100 mL II 3.1 mg/100 mL	I/II = 1.5	63
Famotidine	Methanol 37°C	B 11 mg/mL A 6 mg/mL	B/A = 1.8	64
Frusemide	pH 5 Acetate buffer 37°C	II 57.1 mg/100 mL I 35.2 mg/100 mL	II/I = 1.6	65
Gepirone HCl	*n*-Pentyl alcohol 20°C	II 10.01 mg/mL I 3.79 mg/mL	II/I = 2.6	38
Glibenclamide	Distilled water 37°C	II 1.06 mg/100 mL I 0.66 mg/100 mL	II/I = 1.6	66
Glycine	Distilled water 25°C	α 226.8 $g \cdot kg^{-1}$ γ 202.1 $g \cdot kg^{-1}$	α/γ = 1.2	67
Indomethacin	Distilled water 35°C	α 0.87 mg/100 mL γ 0.69 mg/100 mL	α/γ = 1.3	68

(*Continued*)

TABLE 4 Representative Examples of Solubility Differences Between Polymorphs (*Continued*)

Drug	Solvent/Temp.	Solubilities	Ratio	Ref.
Mefloquine HCl	Distilled water 37°C	E 5.1 mg/mL D 4.3 mg/mL	E/D = 1.2	69
Meprobamate	Distilled water 25°C	II 6.2 mg/mL I 3.3 mg/mL	II/I = 1.9	70
MK571	Isopropyl alcohol 25°C	II 0.390 mg/mL I 0.228 mg/mL	II/I = 1.7	36
	Methyl ethyl ketone 25°C	II 2.40 mg/mL I 1.24 mg/mL	II/I = 1.9	
Nateglinide	pH 6.8 Phosphate buffered saline 25°C	H 1663.6 ug/mL B 1192.5 ug/mL S 1553.6 ug/mL	H/B = 1.4 S/B = 1.3	71
Nimodipine	Distilled water 25°C	I 0.036 mg/100 mL II 0.018 mg/100 mL	I/II = 2.0	72
5-Nor-Me	Ethanol 27.8°C	R 2.83 mg/mL O 3.06 mg/mL	O/R = 1.1	73
Oxyclozamide	0.1% aq. tween 80 25°C	III 109 ppm I 73 ppm I 28 ppm	III/I = 3.9 II/I = 2.6	74
Phenylbutazone	pH 7 Phosphate buffer 36°C	I 288.7 mg/100 mL II 279.9 mg/100 mL III 233.6 mg/100 mL IV 213.0 mg/100 mL	I/IV = 1.4 II/IV = 1.3 III/IV = 1.1	75
Phenobarbital	Distilled water 25°C	II-Ba 1.39 mg/mL II 1.28 mg/mL III-Cy 1.17 mg/mL	II-Ba/III = 1.2 II/III = 1.1	76
Piretanide	pH 1.2 37°C	B 13.3 mg/100 mL A 8.3 mg/100 mL	B/A = 1.6	77
Retinoic acid	30:70 Water:methanol 37°C	I 0.097 mg/100 mL II 0.129 mg/100 mL	II/I = 1.3	78
Seratrodast	pH 8 Phosphate buffer 25°C	I 0.543 mg/mL II 0.817 mg/mL	II/I = 1.5	56
Sulfanilamide	Ethanol 39–40°C	Ortho 21.4 g/1000 g Mono 14.0 g/1000 g	O/M = 1.5	79
Tolbutamide	Distilled water 37°C	I 14.61 mg/100 mL III 13.03 mg/100 mL	I/III = 1.1	80
	Octanol 30°C	I 23.54 mg/mL III 19.33 mg/mL	I/III = 1.2	

anhydrate phase at room temperature (82). However, below the transition temperature of 42°C, the anhydrate phase is more soluble and is therefore less stable. These relationships are illustrated in Figure 4.

Amiloride hydrochloride can be obtained in two polymorphic dihydrate forms, A and B (83). However, each solvate dehydrates around 115°C to 120°C, and the resulting anhydrous solids melt at the same temperature. However, form B was found to be slightly less soluble than form A between 5°C and 45°C, indicating that it is the thermodynamically stable form at room temperature. The temperature

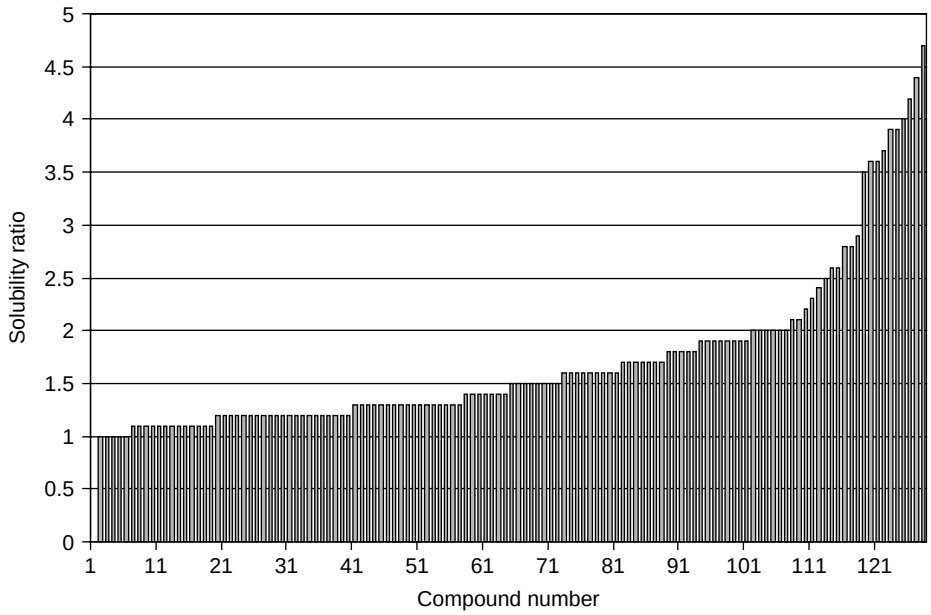

FIGURE 3 One hundred twenty-eight literature solubility ratios (metastable form/stable form) for polymorphic systems.

dependencies of the solubility data were processed by the van't Hoff equation to yield the apparent enthalpies of solution of the two polymorphic dihydrates.

The solubility of polymorphic solids derived from the anhydrate and monohydrate phases of tranilast crystals were evaluated, as were materials processed from them to enhance in vitro availability and micromeritic properties (84). Agglomerates of monohydrate phases I, II, or III were produced using different crystallization solvents and procedures. Monohydrate Form I transformed directly to the stable α-form upon dehydration, whereas Forms II and III dehydrated to the amorphous and β phases, respectively. The apparent equilibrium solubilities of monohydrate Form II and the amorphous form were much higher than those of the α and β forms due to their high surface energies. The solubilities of tranilast hydrate phases exceeded those of the anhydrate phases, which runs counter to the commonly observed trend and suggests that the anhydrate/hydrate transition temperatures are below the temperature of measurement. An analogous situation applies to the anhydrate and trihydrate phases of ampicillin (82) discussed above. The trihydrate phase is more soluble than the anhydrate phase at 50°C, because the transition temperature (42°C) is lower.

Carbamazepine is known to exist in both an anhydrate and a dihydrate form, with the anhydrate spontaneously transforming to the dihydrate upon contact with bulk liquid water (85). The anhydrous phase is reported to be practically insoluble in water, but this observation is difficult to confirm owing to its rapid transition to the dihydrate phase. The rates associated with the phase transformation process have been studied, and appear to follow first-order kinetics (86). Interestingly, the only difference in pharmacokinetics between the two forms was a slightly higher

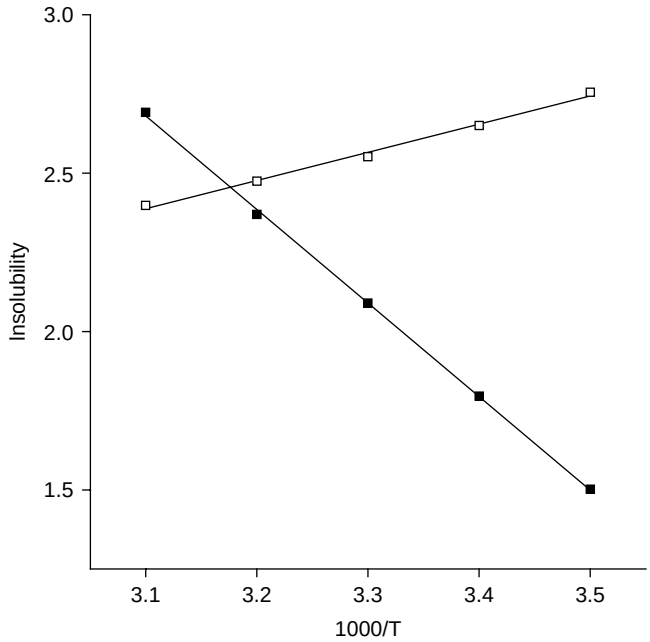

FIGURE 4 The van't Hoff plot for the anhydrate (-□-), and trihydrate (-■-) phases of ampicillin in water (82).

absorption rate for the dihydrate (87). The slower absorption of anhydrous carbamazepine was attributed to the rapid transformation to the dihydrate, accompanied by a fast growth in particle size. Comparison of the bioavailabilities of different polymorphs of a given drug suggest that significant differences are found only when the polymorphs differ significantly in Gibbs free energy deduced from the ratio of solubilities or intrinsic dissolution rates, as in the case of chloramphenicol palmitate.

A monohydrate phase of metronidazole benzoate exhibited solubility properties different from those of the commercially available anhydrous form (88). The monohydrate was found to be the thermodynamically stable form in water below 38°C. The enthalpy and entropy changes of transition for the conversion of the anhydrate to the monohydrate were determined to be –1200 cal/mol and –3.7 cal/K·mol, respectively. This transition was accompanied by a drastic increase in particle size, and caused physical instability of oral suspension formulations. These findings were taken to imply that any difference in bioavailability between the two forms could be attributed to changes in particle size distribution, and not to an inherent difference in the in vivo activity at body temperature.

Recognizing that the hydration state of a hydrate depends on the water activity, in the crystallization medium, Zhu and Grant investigated the influence of solution media on the physical stability of the anhydrate, trihydrate, and amorphous forms of ampicillin (89). The crystalline anhydrate was found to be kinetically stable in the sense that no change was detected by powder X-ray diffraction for at least five days in methanol/water solutions over the whole range of water activity ($a_v = 0$ for pure

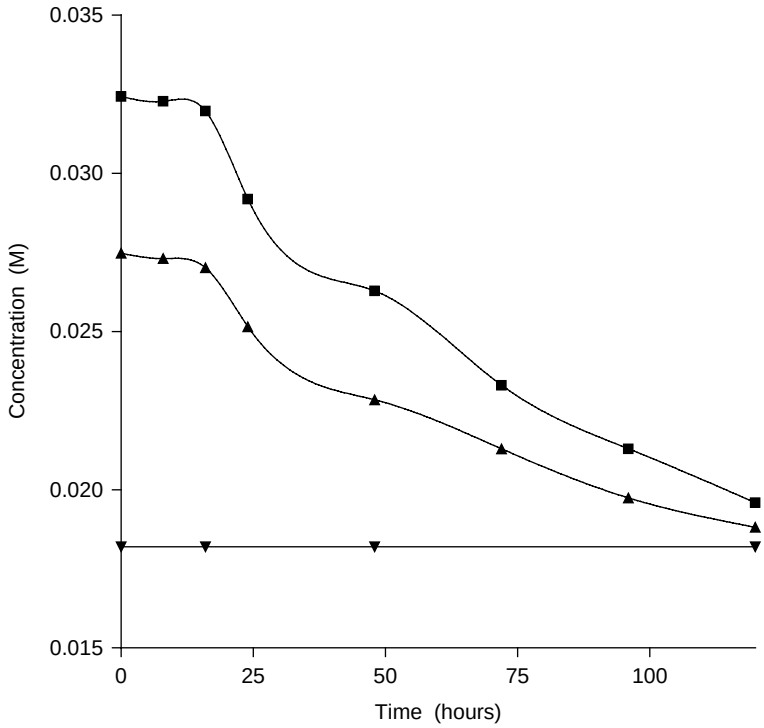

FIGURE 5 Conversion of ampicillin anhydrate to the trihydrate phase at various water activities after seeding with the trihydrate. Shown are the concentration–time data at a_w = 1.0 (-■-), a_w = 0.862 (-▲-), and a_w = 0.338 (-▼-). The curves were adapted from data originally presented in Ref. (89).

methanol to a_v = 1 for pure liquid water). However, addition of trihydrate seeds to ampicillin anhydrate suspended in methanol/water solutions at $a_v \geq 0.381$ resulted in the conversion of the anhydrate to the thermodynamically stable trihydrate. The trihydrate converted to the amorphous form at $a_w \leq 0.338$ in the absence of anhydrate seeds, but converted to the anhydrate phase at $a_w \leq 0.338$ when the suspension was seeded with the anhydrate. These trends are illustrated in Figure 5. The metastable amorphous form took up water progressively with increasing a_w from 0.000 to 0.338 in the methanol/water mixtures. The most significant finding of this work was that water activity was the major thermodynamic factor determining the nature of the solid phase of ampicillin, which crystallized from methanol/water mixtures.

Perhaps the most studied example of phase conversion in the presence of water concerns the anhydrate to monohydrate transition of theophylline. It had been noted in a very early work that the anhydrous phase would convert to the monohydrate phase within seconds of exposure of the former to bulk water (90). The conversion to the monohydrate phase was also demonstrated to take place during wet granulation (91), and could even occur in processed tablets stored under elevated humidity conditions (92). The difficulty in determining the equilibrium solubility of theophylline anhydrate is evident in the literature, which reports a wide range of values (93–95). Better success has been obtained in mixed solvent

TABLE 5 Representative Examples of Solubility Differences Between Solvated Systems

Drug	Solvent/Temp.	Crystal forms and solubilities	Ratio	Ref.
Ampicillin	Water Not given	Anhydrate 10.1 mg/mL Trihydrate 7.6 mg/mL	A/T = 1.3	99
Calcium gluceptate	Distilled water 22°C	Anhydrate 1.3 molal I (3.5 hydrate) 0.07 molal	A/I = 18.6	100
DMHP	Distilled water 25°C	DMHP anhydrate 0.109 M DMHP formate 0.894 M	F/A = 8.2	31
Formoterol fumarate	Water RT	A (anhydrate A) 4.7 mM B (anhydrate B) 3.5 mM C (anhydrate C) 7.5 mM D (dihydrate) 1.5 mM	A/D = 3.1 B/D = 2.3 C/D = 5.0	101
Furosemide	Water* 37°C	Dioxane solvate (X) 25.9 μg/mL DMF solvate (D) 24.7 μg/mL Form I anhydrate 19.8 μg/mL	X/A = 1.3 D/A = 1.2	102
GK-128	pH 4.0 acetate buffer 25°C	Anhydrate I 16.4 mg/mL Hemihydrate 9.3 mg/mL Monohydrate 7.6 mg/mL	A/M = 2.2 H/M = 1.2	103
Glibenclamide	Distilled water 37°C	Pentanol solvate 33.7 mg/100 mL Toluene solvate 2.5 mg/100 mL Form II nonsolvate 1.06 mg/100 m	P/II = 31.8 T/II = 2.4	66
Lamivudine	Distilled water 25°C Ethanol 25°C	I (0.2 hydrate) 84.9 mg/mL II (anhydrate) 98.1 mg/mL I (0.2 hydrate) 18.5 mg/mL II (anhydrate) 11.4 mg/mL	II/I = 1.2 I/II = 1.6	104
Mebendazole	Water Not given	DMA solvate (X) 5.82 μg/mL DMF solvate (D) 4.86 μg/mL Anhydrate 3.16 μg/mL	X/A = 1.8 D/A = 1.5	105
Paroxetine HCl	Distilled water 20°C	I (hemihydrate) 4.9 mg/mL II (anhydrate) 8.2 mg/mL	II/I = 1.7	106
Piroxicam	0.1 N HCl 25°C 0.1 N HCl 30°C	A (anhydrate) 11.90 mg/L B (monohydrate) 12.30 mg/L A (anhydrate) 10.58 mg/L B (monohydrate) 14.64 mg/L	B/A = 1.0 B/A = 1.4	107
Sulfamethoxazole	0.1 N HCl 25°C	A (anhydrate) 119.3 mg/100 mL B (monohydrate) 97.5 mg/100 mL	A/B = 1.2	108
Sparfloxacin	0.15 M KCl 25°C	A (anhydrate) 5600 μg/mL B (trihydrate) 167 μg/mL	A/B = 33.5	24
Theophylline	pH 6 phosphate buffer, 25°C	Anhydrate 12 mg/mL Monohydrate 6 mg/mL	A/M = 2.0	109

systems, as in the work of Zhu and Grant (97), analogous to the experiments with ampicillin (89). However, the data obtained in water-rich solutions was distorted by the formation of the monohydrate phase (96,97,98).

Table 5 provides literature solubility data for some representative solvated systems. The experimental data in Table 5 is a non-exhaustive list of solubility

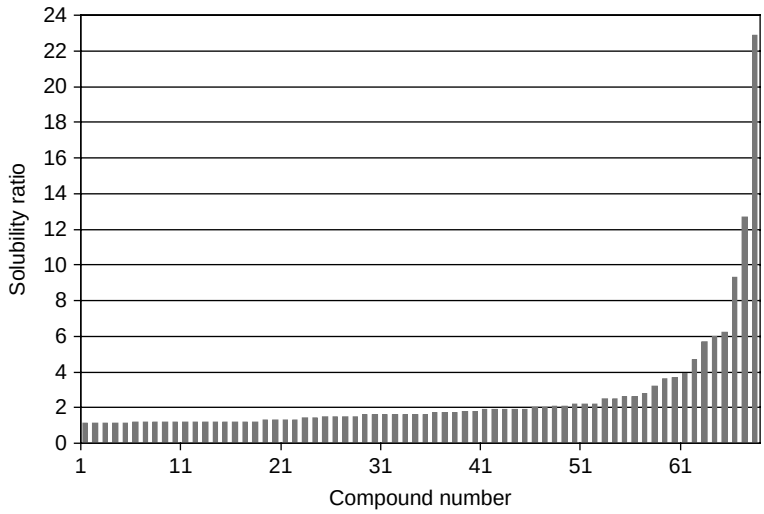

FIGURE 6 Sixty-eight literature solubility ratios (metastable form/stable form) for metastable solvated systems.

ratios (solubility of metastable/solubility of stable form) for 14 different compounds. In general, the solubility ratios for the solvated systems are greater than those of the polymorphic systems. In the case of glibenclamide and sparfloxacin, metastable solids have a 30-fold increase in solubility. Figure 6 combines the data from Table 5 and additional solvated system identified by Pudipeddi and Serajuddin (81). The 68 data points, representing 34 different compounds in Figure 6 are presented in order of increasing solubility ratios. Sixty-nine percent of the polymorphs have solubility ratios between 1 and 2, whereas 15% have ratios greater than 3.5.

SOLUTION CALORIMETRY

The practice of thermochemistry involves measurement of the heat absorbed or evolved when a chemical or physical reaction occurs. Such work entails the determination of the amount of heat, q, in the First Law of Thermodynamics:

$$dE = \delta q - \delta w \tag{7}$$

$$dH = \delta q + V dP \tag{8}$$

The usual practice for solution calorimetry is to conduct the studies at constant pressure, so that the enthalpy change equals either the heat evolved (for an exothermic change) or the heat absorbed (for an endothermic change). The principal chemical requirement for calorimetry is that the measured heat change must be assignable to a definite process, such as the dissolution of a solute in a solvent medium.

Enthalpies of Solution

When a solute is dissolved in a solvent to form a solution, there is almost always absorption or evolution of beat. According to the principle of Le Chatelier, substances that absorb heat as they dissolve must show an increase in solubility with an increase in temperature. Those that evolve heat upon dissolution must become less soluble at higher temperatures.

The heat change per mole of solute dissolved varies with the concentration, c, of the solution that is formed. It is useful to plot the total enthalpy change, ΔH, at constant temperature against the final molar concentration. This type of curve increases rapidly at low solute concentrations, but levels off at the point when the solution is saturated at the temperature of the experiment. The magnitude of the enthalpy change at a given concentration of solute divided by the corresponding number of moles of that solute dissolved represents the increase in enthalpy per mole of solute when it dissolves to form a solution of a particular concentration. This quantity is called the *molar integral heat of solution* at the given concentration. The integral heat of solution is approximately constant in dilute solution, but decreases as the final dissolved solute concentration increases.

For hydrated salts and salts that do not form stable hydrates, the integral heat of solution is ordinarily positive, meaning that heat is absorbed when these substances dissolve. When the anhydrous form of a salt capable of existing in a hydrated form dissolves, there is usually liberation of heat energy. This difference in behavior between hydrated and anhydrous forms of a given salt is attributed to the usual negative change in enthalpy (evolution of heat) associated with the hydration reaction.

Because the heat of solution of a solute varies with its final concentration, there must be a change of enthalpy when a solution is diluted by the addition of solvent. The *molar integral heat of dilution* is the change in enthalpy resulting when a solution containing one mole of a solute is diluted from one concentration to another. According to Hess's law, this change in enthalpy is equal to the difference between the integral heats of solution at the two concentrations.

The increase of enthalpy that takes place when one mole of solute is dissolved in a sufficiently large volume of solution (which has a particular composition), such that there is no appreciable change in the concentration, is the *molar differential heat of solution*. When stating a value for this quantity, the specified concentration and temperature must also be quoted. Because the differential heat of solution is almost constant in very dilute solutions, the molar differential and integral heats of solution are equal at infinite dilution. At higher concentrations, the differential heat of solution generally decreases as the concentration increases.

The *molar differential heat of dilution* may be defined as the heat change when one mole of solvent is added to a large volume of the solution at the specified concentration. The difference between the integral heats of solution at two different concentrations corresponds to the heat of dilution between these two concentrations. The heat of dilution at a specified concentration is normally obtained by plotting the molar heat of solution at various concentrations against the number of moles of solvent associated with a definite quantity of solute, and finding the slope of the curve at the point corresponding to that particular concentration. Because of the approximate constancy of the molar integral heat of solution at small concentrations, such a curve flattens out at high dilutions, and the differential heat of dilution then approaches zero.

The molar differential heats of solution and dilution are examples of partial molar properties, which are important thermodynamic quantities that must be used whenever systems of variable composition, such as solutions, are involved.

Principles Underlying Partial Molar Quantities

A solution that is deduced to be ideal of the chemical potential (μ_i) of every component is a linear function of the logarithm of its mole fraction (X_i), according to the relation:

$$\mu_i = \mu_i^* + RT \ln X_i \tag{9}$$

where μ_i^* is the (hypothetical or actual) value of μ_i when X_i equals unity, and is a function of temperature and pressure. A solution is termed ideal only if equation (9) applies to every component in a given range of composition (usually corresponding to dilute solutions), but it is not necessary that the relation apply to the whole range of composition. Any solution that is approximately ideal over the entire composition range is termed perfect solutions, although there are relatively few such solutions known. However, because a given solution may approach ideality over a limited composition range, it is worthwhile to develop the equations further.

When substance *i* is present both as a pure solid and as a component of an ideal solution, the condition of equilibrium may be stated as:

$$\mu_i^s = \mu_i^* + RT \ln X_i \tag{10}$$

where μ_i^s is the chemical potential of the pure solid, and X_i is the mole fraction in the solution. Rearranging, one finds:

$$\ln X_i = (\mu_i^s/RT) - (\mu_i^*/RT) \tag{11}$$

According to the phase rule, this two-component, two-phase, system is characterized by two degrees of freedom. One concludes that both the temperature and pressure of the solution can be varied independently. Because the pressure on the system is normally held fixed as that of the atmosphere during solubility studies, integration of equation (11) yields:

$$(\delta \ln X_i/\delta T)_P = (H_i - H_i^s)/RT^2 \tag{12}$$

H_i is the partial molar enthalpy of the component in the ideal solution, and H_i^s is its enthalpy per mole as the pure solid. The equation may therefore be rewritten as:

$$(\delta \ln X_i/\delta T)_P = \Delta H_i/RT^2 \tag{13}$$

where ΔH_i is the heat absorbed (at constant temperature and pressure) when one mole of the component dissolves in the ideal solution. As stated above this quantity is the differential heat of solution, and is given by:

$$\Delta H_i = H_i - H_i^s \tag{14}$$

Provided that the solution remains ideal up to $X_i = 1$, and because H_i is independent of composition in the region of ideality, H_i is the same as the enthalpy per mole of the pure liquid component. ΔH_i is equal to its molar heat of fusion, which was formerly termed the molar latent heat of fusion. It is noted, however, that these quantities refer to the temperature at which the solution having mole fraction X_i is in equilibrium with the pure solid.

If one now assumes that ΔH_i is independent of temperature over a narrow temperature range, then equation (13) can be integrated at constant pressure to yield:

$$\ln(X_1/X_2) = (\Delta H_i/R)\{(1/T_2) - (1/T_1)\} \tag{15}$$

where X_1 and X_2 refer to the solubilities (expressed as mole fractions) of the solute at temperatures T_1 and T_2, respectively. If equation (15) remains approximately valid up to a mole fraction of unity, this situation corresponds to that where pure liquid solute is in equilibrium with its own solid at the melting point. In that case, equation (15) yields:

$$\ln X = (\Delta H_i/R)\{(1/T_m) - (1/T)\} \tag{16}$$

where X is the solubility at temperature T, and T_m is the melting point of the solute. ΔH_i is the heat of solution, but by the nature of the assumptions that have been made is also equal to the latent heat of fusion (ΔH^f) of the pure solute.

Because the number of energy levels available to take up thermal energy is greater in the liquid state than in the solid state, the heat capacity of a liquid frequently exceeds that of the same substance in the solid state. As a result, ΔH^f must be assumed to be a function of temperature. If one assumes the change in heat capacity to be constant over the temperature range of interest, then one can use the relation:

$$\Delta H_i = \Delta H_R + \Delta C_p(T_i - T_R) \tag{17}$$

where ΔH_R is the heat of solution at some reference temperature, T_R. This situation has been treated by Grant and coworkers (17), who have provided the highly useful equation (8) for the treatment of solubility data over a wide range of temperature values. Equation (8) was originally derived by Valentiner by substituting the expression for ΔH_i [equation (17)] into the differential form of the van't Hoff [equation (13)], and integrating. In equation (8), a is equal to ΔH_R when T_R equals 0 K, while b is equal to ΔC_p.

The determination of solubility data over a defined temperature range can therefore be used to calculate the differential heat of solution of a given material. For instance, the data illustrated in the bottom half of Figure 1 indicate that equation (16) can be used to deduce a value for the molar differential heat of solution of gepirone. In addition, the fact that Forms I and II yield lines of different slopes indicates the existence of unique values of the molar differential heats of solution for the two polymorphs. One can subtract the differential heats of solution obtained for the two polymorphs to deduce the heat of transition (ΔH_T) between the two forms:

$$\Delta H_T = \Delta H_S{}^B - \Delta H_S{}^A \tag{18}$$

where ΔH_S^A and ΔH_S^B denote the differential heats of solution for polymorphs A and B, respectively.

The validity of the assumption regarding constancy in the heats of solution for a given substance with respect to temperature can be made by determining the enthalpy of fusion (ΔH_F) for the two forms, and then taking the difference between these:

$$\Delta H'_T = \Delta H_F^B - \Delta H_F^A \tag{19}$$

where $\Delta H'_T$ represents the heat of transition between forms A and B at the melting point. The extent of agreement between ΔH_T and $\Delta H'_T$ can be used to estimate the validity of the assumptions made.

For example, the heats of fusion and solution have been reported for the polymorphs of auranofin (57), and these are summarized in Table 6. The similarity of the heats of transition deduced in 95% ethanol (2.90 kcal/mol) and dimethylformamide (2.85 kcal/mol) with the heat of transition calculated at the melting point (3.20 kcal/mol) provides a fair estimation of the thermodynamics associated with this polymorphic system.

Because of the temperature dependence of the various phenomena under discussion, and because of the important role played by entropy, discussions based purely on enthalpy changes are necessarily incomplete. One can rearrange equation (9) to read:

$$\mu_i^* - \mu_i^s = -RT \ln X_i \tag{20}$$

where the left-hand side of the equation represents the difference in chemical potential between the chemical potential of i in its pure solid and the chemical potential of this species in the solution at a defined temperature and pressure. This difference in chemical potential is by definition the molar Gibbs free energy change associated with the dissolution of compound i, so one can write:

$$\Delta G_s = -RT \ln X_i \tag{21}$$

TABLE 6 Heats of Solution and Fusion Measured for the Polymorphs of Auranofin (57)

	Heat of solution, 95% ethanol (kcal/mol)	Heat of solution, dimethylformamide (kcal/mol)
Form A	12.42	5.57
Form B	9.52	2.72
Differential heat of solution	2.90	2.85
	Heat of fusion (kcal/mol)	
Form A	9.04	
Form B	5.85	
Differential heat of formation	3.20	

where ΔG_s is the molar Gibbs free energy of solution. By analogy with equation (12), the molar Gibbs free energy associated with the transformation of polymorph A to B is given by:

$$\Delta G_T = \Delta G_S^{\ B} - \Delta G_S^{\ A} \tag{22}$$

$$= RT \ln(X_A/X_B) \tag{23}$$

where X_A and X_B are the equilibrium solubilities of polymorphs A and B, respectively, expressed in units of mole fraction.

Finally, the entropy of solubility (ΔS_s) is obtained from the relation:

$$\Delta S_s = \{\Delta H_s - \Delta G_s\}/T \tag{24}$$

For basic thermodynamic understanding of the solubility behavior of a given substance, ΔG_s, ΔH_s, and ΔS_s must be determined. Similarly, a basic thermodynamic understanding of a polymorphic transition requires an evaluation of the quantities ΔG_T, ΔH_T, and ΔS_T associated with the phase transition.

To illustrate the importance of free energy changes, consider the solvate system formed by paroxetine hydrochloride, which can exist as a non-hygroscopic hemihydrate or as a hygroscopic anhydrate (106). The heat of transition between these two forms was evaluated both by DSC ($\Delta H'_T$ = 0.0 kJ/mol) and by solution calorimetry (ΔH_T = 0.1 kJ/mol), which would indicates that both forms are isoenthalpic. However, the free energy of transition (–1.25 kJ/mol) favors conversion of the anhydrate to the hemihydrate, and such phase conversion can be initiated by crystal compression or by seeding techniques. Because the two forms are essentially isoenthalpic, the entropy increase that accompanies the phase transformation is responsible for the decrease in free energy and may therefore be viewed as the driving force for the transition.

Methodology for Solution Calorimetry

Any calorimeter with a suitable mixing device and designed for use with liquids can be applied to determine heats of solution, dilution, or mixing. To obtain good precision in the determination of heats of solution requires careful attention to detail in the construction of the calorimeter. The dissolution of a solid may sometimes be a relatively slow process and requires efficient and uniform stirring. Substantial experimental precautions are ordinarily made to ensure that heat input from the stirrer mechanism is minimized.

Most solution calorimeters operate in the batch mode, and descriptions of such systems are readily found in the literature (110,111). The common practice is to use the batch solution calorimetric approach, in which mixing of the solute and the solvent is affected in a single step. Mixing can be accomplished either by breaking a bulb containing the pure solute, allowing the reactants to mix by displacing the seal separating the two reactants in the calorimeter reaction vessel, or by rotating the reaction vessel and allowing the reactants to mix (111). Although the batch calorimetric approach simplifies the data analysis, there are design problems associated with mixing of the reactants. Guillory and coworkers have described the use of a stainless steel ampoule whose design greatly facilitates batch solution calorimetric

analyses (112). This device was validated by measurement of the enthalpy of solution of potassium chloride in water, and the reproducibility of the method was demonstrated by determination of the enthalpy of solution of the two common polymorphic forms of chloramphenicol palmitate in 95% ethanol.

Applications of Solution Calorimetry

Solution calorimetric investigations may be classified into studies that focus entirely on enthalpic processes and studies that seek to understand the contribution of the enthalpy change to the free energy change of the system. Although the former can prove to be quite informative, only the latter permit the deduction of unequivocal thermodynamic conclusions about relative stability.

Although heats of solution data are frequently used to establish differences in enthalpy within a polymorphic system, they cannot be used to deduce accurately the relative phase stability. According to equation (12), the difference between the differential heats of solution of two polymorphs is a measure of the heat of transition (ΔH_T) between the two forms. Because enthalpy is a state function (Hess's Law), this difference must necessarily be independent of the solvent system used. However, conducting calorimetric measurements of the heats of solution of the polymorphs in more than one solvent provides an empirical verification of the assumptions made. For instance, ΔH_T values of two losartan polymorphs were found to be 1.72 kcal/mol in water and 1.76 kcal/mol in dimethylformamide (113). In a similar study with moricizine hydrochloride polymorphs, ΔH_T values of 1.0 and 0.9 kcal/mol were obtained from their dissolution in water and dimethylformamide, respectively (114). These two systems, which show good agreement, may be contrasted with that of enalapril maleate, where ΔH_T was determined to be 0.51 kcal/mol in methanol and 0.69 kcal/mol in acetone (115). Disagreements of this order (about 30%) suggest that some process, in addition to dissolution, is taking place in one or both solvents.

In systems characterized by the existence of more than one polymorph, the heats of solution have been used to deduce the order of stability. As explained above, the order of stability cannot be deduced from enthalpy changes but only from free energy changes. If the enthalpy change reflects the stability, then the polymorphic change is not driven by an increase in entropy, but by a decrease in enthalpy. The heat of solution measured for cyclopenthiazide Form III (3.58 kcal/mol) was significantly greater than the analogous values obtained for Form I (1.41 kcal/mol) or Form II (1.47 kcal/mol), identifying Form III as the polymorph with the greater enthalpy, but not necessarily the most stable polymorph at ambient temperature (62).

In the case of the anhydrate and hydrate phases of norfloxacin (116), the dihydrate phase was found to exhibit a relatively large endothermic heat of solution relative to either the anhydrate or the sesquihydrate. Both urapidil (117) and dehydroepiandrosterone (118) were found to exhibit complex polymorphic/solvate systems, but the relative enthalpy of these could be deduced through the use of solution calorimetry. As an example, the data reported for urapidil (117), which have been collected into Table 7, show that the form with the lowest heat of solution implies the highest enthalpy content, which would therefore be the least stable form. These deductions have merit because the rank order of enthalpy changes corresponded to that of the free energy changes.

It is invariably found that the amorphous form of a compound is less stable than its crystalline modification, in the sense that the amorphous form tends to

TABLE 7 Heats of Solution for the Various Polymorphs and Solvates of Urapidil (117)

Crystalline form	Heat of solution (kJ/mol)
Form I	21.96
Form II	24.26
Form III	22.98 (estimated)
Monohydrate	44.28
Trihydrate	53.50
Pentahydrate	69.16
Methanol solvate	48.39

crystallize spontaneously, indicating that the amorphous form has the greater Gibbs free energy. As discussed in Chapter 1, the amorphous form is more disordered, and must therefore have a greater entropy than does the crystalline form. Hence, the enthalpy of the amorphous form is also greater. The heat of solution of amorphous piretanide in water was found to be 12.7 kJ/mol, whereas the heat of solution associated with Form C was determined to be 32.8 kJ/mol (119). The authors calculated the heat of transformation associated with the amorphous-to-crystalline transition to be –20.1 kJ/mol. Any facile transformation of the two phases was obstructed by the significant activation energy (145.5 kJ/mol).

As emphasized above, a basic thermodynamic understanding of a polymorphic system requires a determination of the free energy difference between the various forms. The two polymorphs of 3-amino-1-(*m*-trifluoromethlyphenyl)-6-methyl-1*H*-pyridazin-4-one have been characterized by a variety of methods, among which solubility studies were used to evaluate the thermodynamics of the transition from Form I to Form II (120). At a temperature of 30°C, the enthalpy change for the phase transformation was determined to be –5.64 kJ/mol. From the solubility ratio of the two polymorphs, the free energy change was then calculated as –3.67 kJ/mol, which implies that the entropy change accompanying the transformation was –6.48 cal/K·mol. In this system, one encounters a phase change that is favored by the enthalpy term, but not favored by the entropy term. However, because the overall free energy change (ΔG_T) is negative, the process takes place spontaneously, provided that the molecules can overcome the activation energy barrier at a significant rate.

A similar situation has been described for the two polymorphic forms of 2-[[4-[[2-(1*H*-tetrazol-5-ylmethyl)phenyl]-methoxy]phenoxy]methyl]quinoline (42). The appreciable enthalpic driving force for the transformation of Form II to Form I (–0.91 kcal/mol) was found to be partially offset by the entropy of transformation (–2.6 cal/K·mol), resulting in a modest free energy difference between the two forms (–0.14 kcal/mol).

In other instances, an unfavorable enthalpy term was found to be compensated by a favorable entropy term, thus rendering negative the free energy change associated with a particular phase transformation. Latnivudine can be obtained in two forms, one of which is a 0.2-hydrate obtained from water or from methanol that contains water, and the other which is non-solvated and is obtained from many non-aqueous solvents (104). Form II was determined to be thermodynamically favored in the solid state. Solubility studies of both forms as a function of solvent

TABLE 8 Thermodynamic Parameters for Lamivudine in Various Solvents (104)

	Form I	Form II
Solvent = Water		
ΔG_{SOL} (cal/mol)	2990	2950
ΔH_{SOL}(cal/mol)	5720	5430
ΔS_{SOL}(cal/deg·mol)	9.2	8.3
Solvent = Ethanol		
ΔG_{SOL} (cal/mol)	3180	3460
ΔH_{SOL}(cal/mol)	5270	4740
ΔS_{SOL}(cal/deg·mol)	7.0	4.3
Solvent = *n*-Propanol		
ΔG_{SOL} (cal/mol)	3120	3610
ΔH_{SOL}(cal/mol)	5350	5000
ΔS_{SOL}(cal/deg·mol)	7.5	4.7

and temperature were used to determine whether entropy of enthalpy was the driving force for solubility. Solution calorimetric data indicated that Form I would be favored in all solvents studied on the basis of enthalpy alone (Table 8). In higher alcohols and other organic solvents, Form I exhibited a larger entropy of solution than did Form II, compensating for the unfavorable enthalpic factors and yielding an overall negative free energy for the phase change.

Shefter and Higuchi considered the thermodynamics associated with the anhydrate/hydrate equilibrium of theophylline and glutethimide (90). For both compounds, the free energy change for the transformation from the anhydrate to the hydrate was negative (hence, indicating a spontaneous process), the favorable enthalpy changes being mitigated by the unfavorable entropy changes. In this work, the free energy was calculated from the solubilities of the anhydrate and hydrate forms, whereas the enthalpy of solution was calculated from the temperature dependence of the solubility ratio using the van't Hoff equation. The entropy of solution was evaluated using equation (24).

A similar conclusion was reached regarding the relative stability of the monohydrate and anhydrate phases of metronidazole benzoate (88). The enthalpy term (–1.20 kcal/mol) favored conversion to the monohydrate, but the strong entropy term (–3.7 cal/K·mol) essentially offset this enthalpy change. At 25°C, the overall ΔG_T of the transition was still negative, favoring the monohydrates, but only barely so (–0.049 kcal/mol). This difference was judged to be too small to result in any detectable bioavailability differences.

KINETICS OF SOLUBILITY: DISSOLUTION RATES

Evaluation of the dissolution rates of drug substances from their dosage forms is extremely important in the development, formulation, and quality control of pharmaceutical agents (16,121–123). Such evaluation is especially important in the characterization of polymorphic systems owing to the possibility of bioavailability differences that may arise from differences in dissolution rate that may themselves arise from differences in solubility (4). The wide variety of methods for determining

the dissolution rates of solids may be categorized either as batch methods or as continuous-flow methods, for which detailed experimental protocols have been provided (124).

Factors Affecting Dissolution Rates

The dissolution rate of a solid may be defined as dm/dt, where m is the mass of solid dissolved at time t. To obtain dm/dt, the following equation, which defines concentration, must be differentiated:

$$m = Vc_b \tag{25}$$

In a batch dissolution method the analyzed concentration (c_b) of a well-stirred solution is representative of the entire volume (V) of the dissolution medium, so that:

$$dm/dt = V(dc_b/dt) \tag{26}$$

In a dissolution study, c_b will increase from its initial zero value until a limiting concentration is attained. Depending on the initial amount of solute presented for dissolution, the limiting concentration will be at the saturation level, or less than this.

Batch dissolution methods are simple to set up and to operate, are widely used, and may be carefully and reproducibly standardized. Nevertheless, they suffer from several disadvantages (16). The hydrodynamics are usually poorly characterized, a small change in dissolution rate will often create an undetectable and immeasurable perturbation in the dissolution time curve, and the solute concentration may not be uniform throughout the solution volume.

In a continuous flow method, the volume flow rate over the surface of the solid is given by dV/dt, so that differentiation of equation (25) leads to:

$$dm/dt = c_b(dV/dt) \tag{27}$$

where c_b is the concentration of drug dissolved in the solvent that has just passed over the surface of the solid drug.

Continuous-flow methods have the advantages that sink conditions may be easily achieved, and that a change in dissolution rate is reflected in a change in c_b (16). At the same time, they require a significant flow rate that may require relatively large volumes of dissolution medium. Should the solid be characterized by a low solubility and a slow dissolution rate, c_b will be small and a very sensitive analytical method would be required.

The diffusion layer theory is the most useful and best known model for transport-controlled dissolution, and satisfactorily accounts for the dissolution rates of most pharmaceutical solids. In this model, the dissolution rate is controlled by the rate of diffusion of solute molecules across a thin diffusion layer. With increasing distance from the surface of the solid, the solute concentration decreases in a non-linear manner across the diffusion layer. The dissolution process at steady state is described by the Noyes–Whitney equation:

$$dm/dt = k_D A(c_s - c) \tag{28}$$

where dm/dt is the dissolution rate, A is the surface area of the dissolving solid, c_s is the saturation solubility of the solid, and c is the concentration of solute in the bulk solution. The dissolution rate constant, k_D, is given by D/h, where D is the diffusion constant. The hydrodynamics of the dissolution process have been fully discussed by Levich (125).

It has been shown (16) that the dissolution rates of solids are determined or influenced by a number of factors, which may be summarized as follows:

1. Solubility of the solid, and the temperature.
2. Concentration in the bulk solution, if not under sink conditions.
3. Volume of the dissolution medium in a batch-type apparatus, or the volume flow rate in a continuous flow apparatus.
4. Wetted surface area, which consequently is normalized in measurements of intrinsic dissolution rate.
5. Conditions in the dissolution medium that, together with the nature of the dissolving solid, determine the dissolution mechanism.

The conditions in the dissolution medium that may influence the dissolution rate can be summarized as:

1. The rate of agitation, stirring, or flow of solvent, if the dissolution is transport-controlled, but not when the dissolution is reaction-controlled.
2. The diffusivity of the dissolved solute, if the dissolution is transport-controlled. The dissolution rate of a reaction-controlled system will be independent of the diffusivity.
3. The viscosity and density influence the dissolution rate if the dissolution is transport-controlled, but not if the dissolution is reaction-controlled.
4. The pH and buffer concentration (if the dissolving solid is acidic or basic), and the pKa values of the dissolving solid and of the buffer.
5. Complexation between the dissolving solute and an interactive ligand, or solubilization of the dissolving solute by a surface-active agent in solution. Each of these phenomena tends to increase the dissolution rate.

Applications of Dissolution Rate Studies to Polymorphs and Hydrates

Historically, batch-type dissolution rate studies of loose powders and compressed disks have played a major role in the characterization of essentially every polymorphic or solid-state solvated system (35,82,90). Stagner and Guillory used these two methods of dissolution to study the two polymorphs and the amorphous phase of iopanoic acid (126). As evident in the loose powder dissolution data illustrated in the *upper half* of Figure 7, the two polymorphs were found to be stable with respect to phase conversion, but the amorphous form rapidly converted to Form I under the dissolution conditions. In the powder dissolution studies, the initial solubilities of the different forms followed the same rank order as did their respective intrinsic dissolution rates, but the subsequent phase conversion of the amorphous form to the stable Form I appeared to change the order. The amorphous form demonstrated a 10-fold greater intrinsic dissolution rate relative to Form I, whereas the intrinsic dissolution rate of Form II was 1.5 times greater than that of Form I.

The nature of the dissolution medium can profoundly affect the shape of a dissolution profile. The relative rates of dissolution and the solubilities of the two polymorphs of 3-(3-hydroxy-3-methylbutylamino)-5-methyl-*as* triazino-[5,6-*b*]-indole

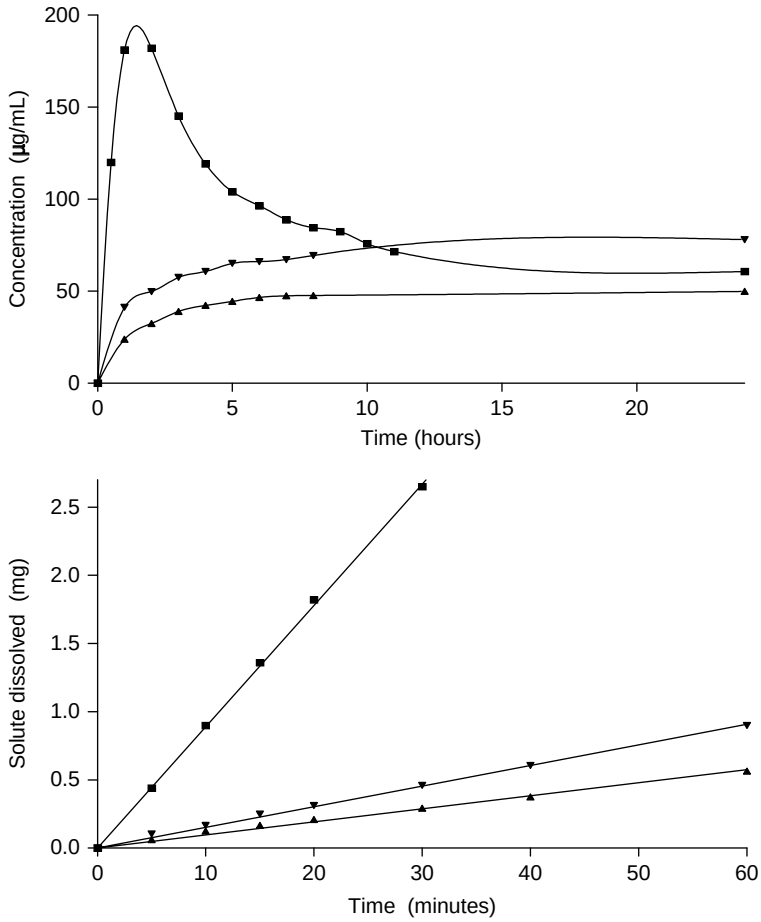

FIGURE 7 Loose powder dissolution (*upper set of traces*) and intrinsic dissolution (*lower set of traces*) profiles of iopanoic acid. Shown are the profiles of Form I (-▲-), Form II (-▼-), and the amorphous form (-■-). The plots were adapted from data originally presented in Ref. (126).

were determined in artificial gastric fluid, water, and 50% ethanol solution (127). In USP artificial gastric fluid, both polymorphic forms exhibited essentially identical dissolution rates. This behavior has been contrasted in Figure 8 with that observed in 50% aqueous ethanol, where Form II has a significantly more rapid dissolution rate than Form I. If the dissolution rate of a solid phase is determined by its solubility, as predicted by the Noyes–Whitney equation, the ratio of dissolution rates would equal the ratio of solubilities. Because this type of behavior was not observed for this triazinoindole drug, the different effects of the dissolution medium on the transport rate constant may be suspected.

The solubilities of the two polymorphs of difenoxin hydrochloride have been studied, as well as the solubility of tablets formed from mixtures of these

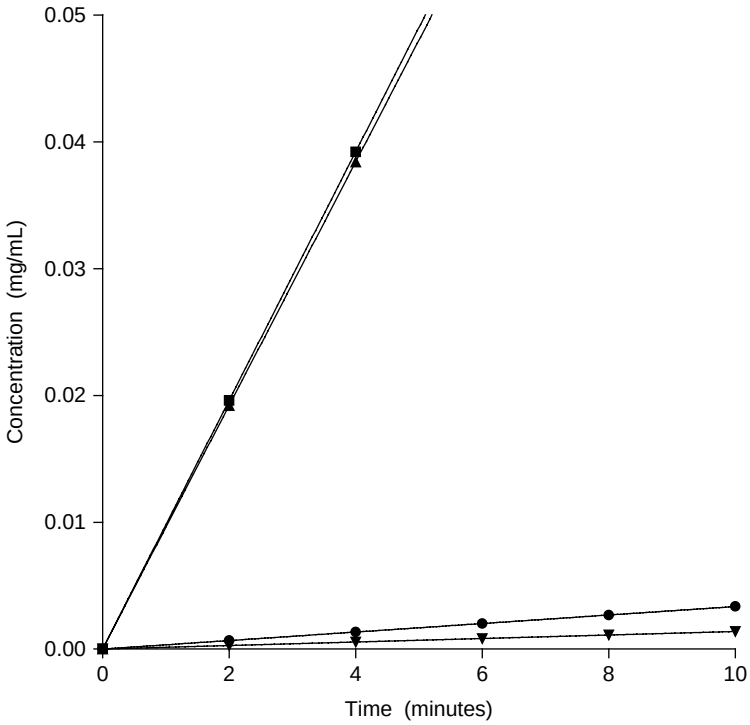

FIGURE 8 Initial stages of the dissolution of the two polymorphs of 3-(3-hydroxy-3-methylbutylamino)-5-methyl-*as* triazino-[5,6-*b*]-indole in different media. Shown are the profiles obtained for Form I (-■-) and Form II (-▲-) in simulated gastric fluid, as well as the profiles of Form I (-●-) and Form II (-▼-) in 50% aqueous ethanol. The traces were adapted from data originally presented in Ref. (127).

polymorphs (63). Form I was found to be more soluble than was Form II, and the solubilities of materials containing known proportions of Forms I and II reflected the differences in the solubilities of the pure forms. Likewise, the dissolution rate of difenoxin hydrochloride from tablets was determined by the ratio of Form I to Form II. In these studies, no solid-state transformation of the more soluble form to the less soluble form was observed. In addition, micronization proved to be a successful method for improving the dissolution of tablets prepared from the less soluble polymorph.

Stoltz and coworkers have conducted extensive studies on the dissolution properties of the hydrates and solvates of oxyphenbutazone (128,129). They compared the dissolution properties of the benzene and cyclohexane solvates with those of the monohydrate, hemihydrate, and anhydrate forms, and then compared their findings with results reported in the literature. The powder dissolution rates of the solvates proved to be comparable to those of the hemihydrate and the anhydrate, but superior to that of the monohydrate. This trend is illustrated in Figure 9, which confirms the usual observation that increasing degrees of hydration results in slower dissolution

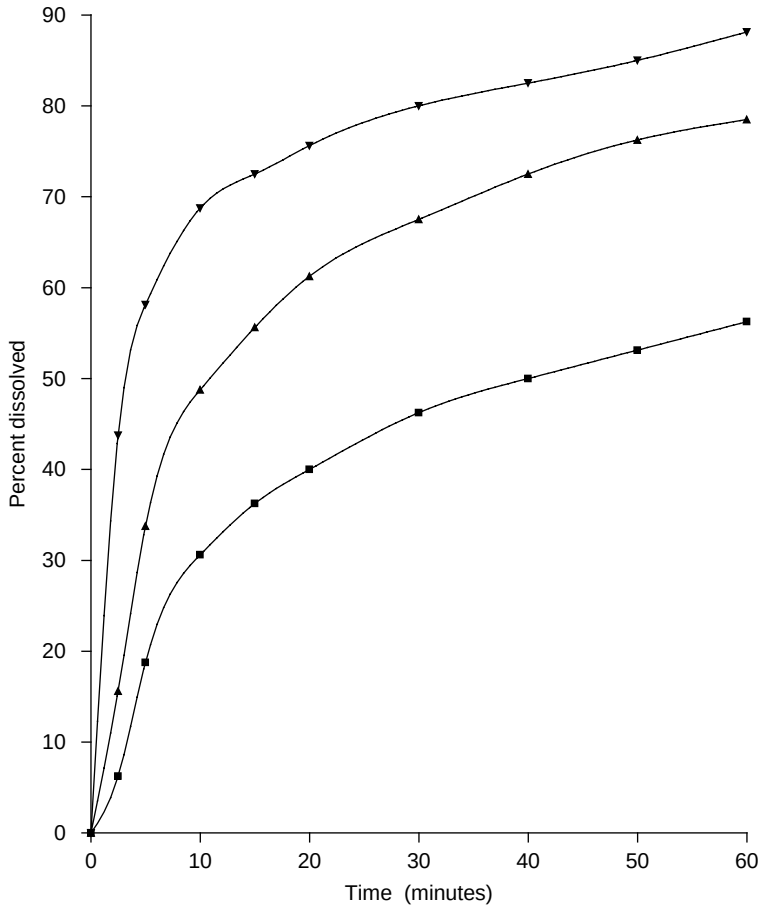

FIGURE 9 Powder dissolution profiles obtained for oxyphenbutazone anhydrate (-▼-), hemihydrate (-▲-), and monohydrate (-■-). The curves were adapted from data originally presented in Ref. (128).

rates. This observation differed from that previously reported by Matsuda and Kawaguchi, who reported powder dissolution rates in simulated intestinal fluid that were in the sequence hemihydrate > monohydrate > anhydrate (130). The reversed order in the dissolution rates of the former work (128) was attributed to the presence of a surfactant in the dissolution medium, which apparently overcame the hydrophobicity of the crystal surfaces of the anhydrate form. In terms of the Noyes–Whitney equation these results may be explained by the influence of the surface active agent in increasing either the wetted surface area, or the transport rate constant, or both quantities.

It has been noted from the earliest dissolution work (90) that, for many substances, the dissolution rate of an anhydrous phase usually exceeds that of any corresponding hydrate phase. These observations were explained by thermodynamics, where it was reasoned that the hydrates possessed less activity and

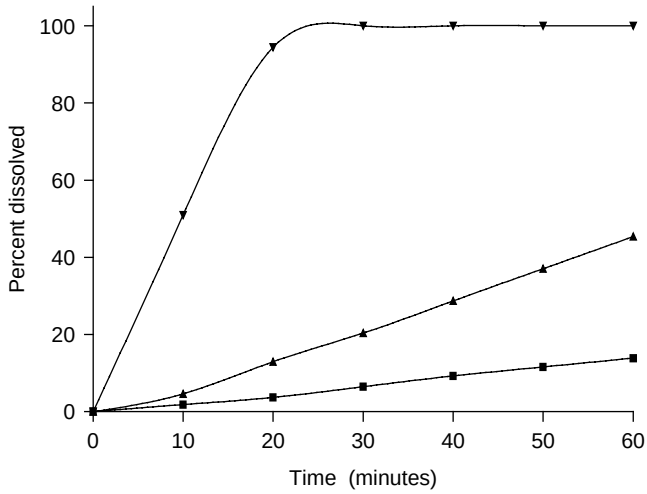

FIGURE 10 Dissolution profiles of erythromycin anhydrate (-■-), monohydrate (-▲-), and dihydrate (-▼-). The plots were adapted from data originally presented in Ref. (133).

would be in a more stable state relative to their anhydrous forms (131). This general rule was found to hold for the previously discussed anhydrate/hydrate phases of theophylline (93,95,97), ampicillin (89), metronidazone benzoate (88), carbamazepine (85,87), glutethimide (132), and oxyphenbutazone (129), as well as for many other systems not mentioned here. In addition, among the hydrates of urapidil, the solubility decreases with increasing crystal hydration (117).

Since the mid-1970s, a number of exceptions to the general rule have been found. For example, Figure 10 shows that the hydrate phases of erythromycin exhibit a reverse order of solubility where the dihydrate phase exhibits the fastest dissolution rate and highest equilibrium solubility (133). More recent examples include the magnesium, zinc, and calcium salts of nedocromil, for which the intrinsic dissolution rate increases with increasing water stoichiometry of their hydrates (134). The explanation for this behavior is that the transition temperatures between the hydrates are below the temperature of the dissolution measurements and decrease with increasing water stoichiometry of the hydrates. Consequently, the solubilities, and hence the intrinsic dissolution rates, increase with increasing stoichiometry of water in the hydrates. Acyclovir was recently found to be capable of forming a 3:2 drug/water hydrate phase, which exhibited an almost instantaneous dissolution relative to the more slowly dissolving anhydrous form (135). This latter finding implies a substantial difference in Gibbs free energy between the two forms.

Intrinsic Dissolution Rates

It should be recognized that the final concentration measured using the loose powder dissolution method is the equilibrium solubility, and that the initial stages of this dissolution are strongly affected by the particle size and surface area of the dissolving solids. For this reaction, many workers have chosen to study the dissolution

of compacted materials, where the particle size and surface area are regulated by the process of forming the compact.

In the disk method for conducting intrinsic dissolution studies, the powder is compressed in a die to produce a compact. One face of the disk is exposed to the dissolution medium, and rotated at a constant speed without wobble. The dissolution rate is determined as for a batch method, whereas the wetted surface area is simply the area of the disk exposed to the dissolution medium.

It is good practice to compare the powder X-ray diffraction patterns of the compacted solid and of the residual solid after the dissolution experiment with that of the original powder sample. In this manner, one may test for possible phase changes during compaction or dissolution.

The dissolution rate of a solid from a rotating disc is governed by the controlled hydrodynamics of the system, and has been treated theoretically by Levich (125). In this system, the intrinsic dissolution rate (J) may be calculated using either of the following relations:

$$J = 0.620D^{2/3}\nu^{-1/6}(c_s - c_b)\,\omega^{1/2} \tag{29}$$

or

$$J = 1.555D^{2/3}\nu^{-1/6}(c_s - c_b)W^{1/2} \tag{30}$$

where D is the diffusivity of the dissolved solute, ω is the angular velocity of the disc in radians per second, ν is the kinematic viscosity of the fluid, c_b is the concentration of solute at time t during the dissolution study, and c_s is the equilibrium solubility of the solute. The dependence of J on $\omega^{1/2}$ has been verified experimentally (136).

Equations (29) or (30) enable the diffusivity of a solute to be measured. These relations assume the dissolution of only one diffusing species, but because most small organic molecules exhibit a similar diffusivity (of the order 10^{-5} cm^2/sec in water at 25°C), it follows that J depends on the 2/3 power of D. Consequently, the errors arising from several diffusing species only become significant if one or more species exhibit abnormal diffusivities. In fact, diffusivity is only weakly dependent on the molecular weight, so it is useful to estimate the diffusivity of a solute from that of a suitable standard of known diffusivity under the same conditions. In most cases, the diffusivity predictions agree quite well with those obtained experimentally (137).

Intrinsic Dissolution Rate Studies of Polymorphic and Hydrate Systems

Under constant hydrodynamic conditions, the intrinsic dissolution rate is usually proportional to the solubility of the dissolving solid. Consequently, in a polymorphic system, the most stable form will ordinarily exhibit the slowest intrinsic dissolution rate. For example, a variety of high-energy modifications of frusemide were produced, but the commercially available form was found to exhibit the longest dissolution times (138). Similar conclusions were reached regarding the four polymorphs of tegafur (139) and (*R*)-*N*-[3-[5-(4-fluorophenoxy)-2-furanyl]-1-methyl-2-propynyl]-*N*-hydroxyurea (140). However, it is possible that one of the less stable polymorphs of a compound can exhibit the slowest dissolution rate, as was noted in the case of diflunisal (141).

TABLE 9 Intrinsic Dissolution Rates for the Various Polymorphs of Aprazolam at Different Spindle Speeds (142)

Crystalline form	IDR, 50 RPM (μg/min/cm²)	IDR, 75 RPM (μg/min/cm²)
Form I	15.8	21.8
Form II	18.4	21.9
Form V	20.7	27.3

Intrinsic dissolution rate studies proved useful during the characterization of the two anhydrous polymorphs and one hydrate modification of alprazolam (142). The equilibrium solubility of the hydrate phase was invariably less than that of either anhydrate phase, although the actual values obtained were found to be strongly affected by pH. Interestingly, the intrinsic dissolution rate of the hydrate phase was higher than that of either anhydrate phase, with the anhydrous phases exhibiting equivalent dissolution rates. The IDR data of Table 9 reveal an interesting phenomenon, where discrimination between some polymorphs was noted at slower spindle speeds, but not at higher rates. Thus, if one is to use IDR rates as a means to determine the relative rates of solubilization of different rates, the effect of stirring speed must be investigated before the conclusions can be judged genuine.

Intrinsic dissolution rate investigations can become complicated when one or more of the studied polymorphs interconverts to another during the time of measurement. Sulfathiazole has been found to crystallize in three distinct polymorphic forms, two of which are unstable in contact with water (143) but which convert only slowly to the stable form (i.e., are kinetically stable) in the solid state. As may be seen in Figure 11, the initial intrinsic dissolution rates of these are all different, but as Forms I and II convert into Form III, the dissolved concentrations converge. Only the dissolution rate of Form III remains constant, which suggests that it is the thermodynamically stable form at room temperature. Aqueous suspensions of Forms I or II each converted into Form III over time, supporting the conclusions of the dissolution studies.

Suitable manipulation of the dissolution medium can sometimes inhibit the conversion of one polymorph to another during the dissolution process, thus permitting the measurement of otherwise unobtainable information. In studies on the polymorphs of sulfathiazole and methylprednisolone, Higuchi, who used various alcohols and additives in the dissolution medium to inhibit phase transformations, first employed this approach (144). Aguiar and Zeliner were able to thermodynamically characterize the polymorphs formed by chloramphenicol palmitate and mefenamic acid through the use of dissolution modifiers (145). Furthermore, the use of an aqueous ethanol medium containing 55.4% v/v ethanol yielded adequate solubility and integrity of the dissolving disc during studies conducted on digoxin (146).

One area of concern associated with intrinsic dissolution measurements is associated with the preparation of the solid disc by compaction of the drug particles. If a phase transformation is induced by compression, one might unintentionally measure the dissolution rate of a polymorph different from the intended one. This situation was encountered with phenylbutazone, where Form III was transformed to the most stable modification (Form IV) during the initial compression step (75).

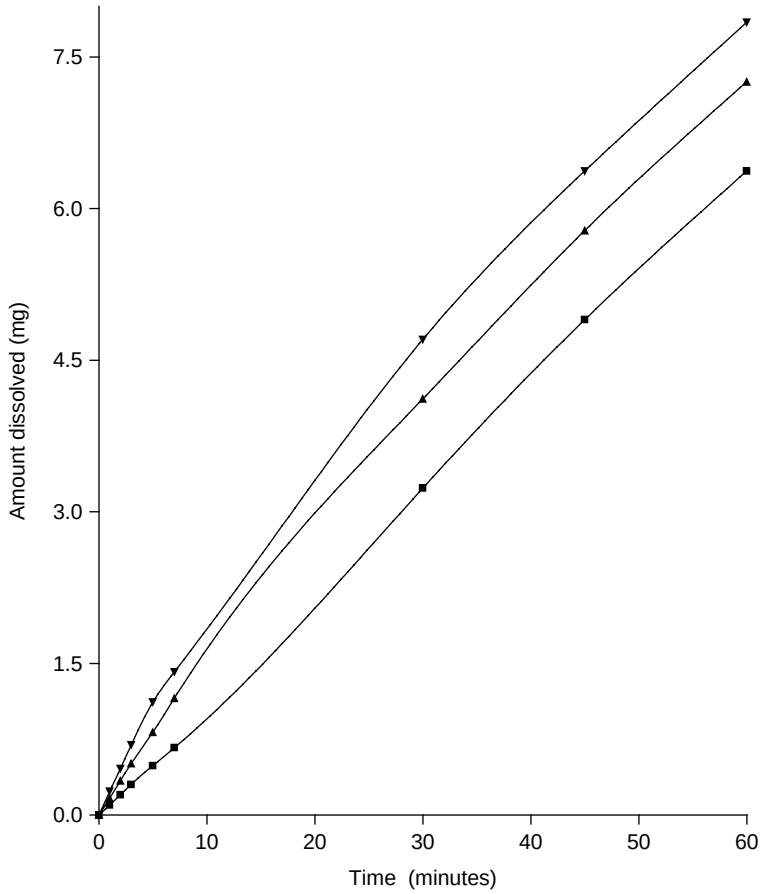

FIGURE 11 Dissolution profiles obtained for sulfathiazole Form I (-▲-), Form II (-▼-), and Form III (-■-) in water at 37°C. The figure has been adapted from data originally presented in Ref. (143).

One interesting note concerns the aqueous dissolution rates of solvate forms, where the solvent bound in the crystal lattice is not water. As noted earlier, the dissolution rate of an anhydrous phase normally exceeds that of any corresponding hydrate phase, but this relation is not usually applicable to other solvate species. It has been reported that the methanol solvate of urapidil exhibits a heat of solution approximately twice that of any of the anhydrate phases, and that it also exhibits the most rapid dissolution rate (147). Similarly, the pentanol and toluene solvates of glibenclainide exhibit significantly higher aqueous dissolution rates and aqueous equilibrium solubility values when compared to either of the two anhydrous polymorphs (66). The acetone and chloroform solvates of sulindac yielded intrinsic dissolution rates that were double those of the two anhydrate phases (148). These trends would imply that a non-aqueous solvate phase could be considered as being a high-energy form of the solid with respect to dissolution in water.

The most usual explanation of these phenomena is that the negative Gibbs free energy of mixing of the organic solvent, released during the dissolution of the solvate, contributes to the Gibbs free energy of solution, increasing the thermodynamic driving force for the dissolution process (90). This explanation, due to Shefter and Higuchi, was originally derived from observations on the higher dissolution rate of the pentanol solvate of succinylsulfathiazole than of the anhydrate (90). Prior addition of increasing concentrations of pentanol to the aqueous dissolution medium reduced the initial dissolution rate of the pentanol solvate. This reduction was attributed to a less favorable (less negative) Gibbs free energy of mixing of the released pentanol in the solution that already contained pentanol. In this way, the Gibbs free energy of solution was rendered less favorable (less negative), reducing the thermodynamic driving force for dissolution of the solvate. Thermodynamic characterization of the various steps in the dissolution of solvates and evaluation of their respective Gibbs free energies (and enthalpies) has been carried out by Ghosh and Grant (31).

CONSEQUENCES OF POLYMORPHISM AND SOLVATE FORMATION ON THE BIOAVAILABILITY OF DRUG SUBSTANCES

In those specific instances where the absorption rate of the active ingredient in a solid dosage form depends upon the rate of drug dissolution, the use of different polymorphs would be expected to affect the bioavailability. One can imagine the situation in which the use of a metastable polymorph would yield higher levels of a therapeutically active substance after administration owing to its higher solubility. This situation may be either advantageous or disadvantageous depending on whether the higher bioavailability is desirable or not. On the other hand, unrecognized polymorphism may result in unacceptable dose-to-dose variations in drug bioavailability, and certainly represents a drug formulation not under control.

The trihydrate/anhydrate system presented by ampicillin has received extensive attention, with conflicting conclusions from several investigations. In one early study, Poole and co-workers reported that the aqueous solubility of the anhydrate phase was 20% higher than that of the trihydrate form at 37°C (149). They also found that the time for 50% of the drug to dissolve in vitro was 7.5 and 45 minutes for the anhydrate and trihydrate forms, respectively (150). Using dogs and human subjects, these workers then determined in vivo blood levels, following separate administration of the two forms of the drug in oral suspensions or in capsules. The anhydrous form produced a higher maximum concentration of ampicillin (C_{max}) and an earlier time to reach maximum concentration (T_{max}) in the blood serum relative to the trihydrate form. This behavior was more pronounced in the suspension formulations. In addition, the area under the curve (AUC) was found to be greater with the anhydrous form, implying that the anhydrous form was more efficiently absorbed.

Since the early works just discussed, an interesting discussion on the comparative absorption of ampicillin has arisen. Some workers have concluded that suspensions and capsules containing ampicillin anhydrate exhibit superior bioavailabilities than analogous formulations made from the trihydrate (151,152). For instance, in a particularly well-controlled study, Ali and Farouk (152) obtained the clear-cut distinction between the anhydrate and the trihydrate, which is illustrated in Figure 12. However, others have found that capsules containing either form of

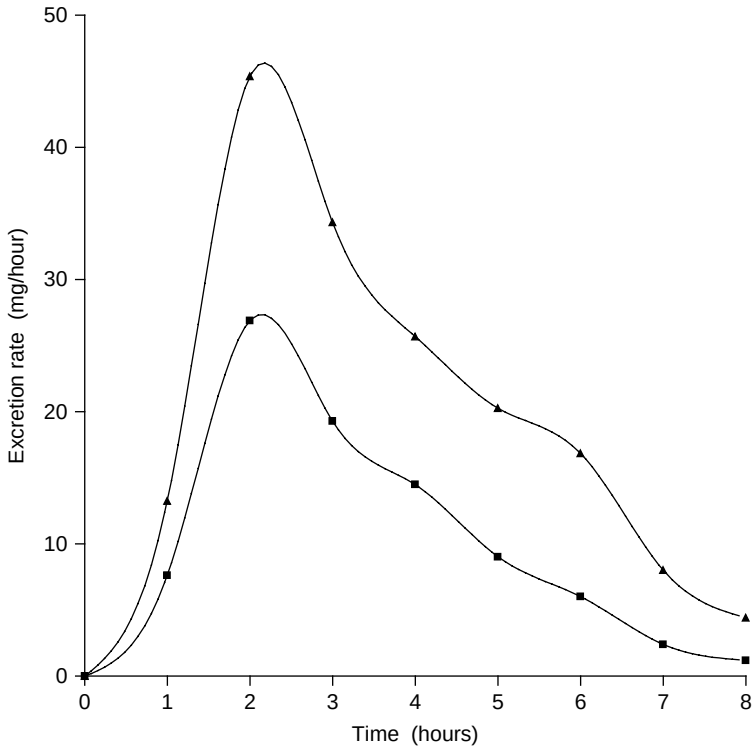

FIGURE 12 Ampicillin urinary excretion rates at various times after separate administration of the two forms. Shown are the profiles obtained for the anhydrate (-▲-) and trihydrate phases (-■-). The figure has been adapted from data provided in Ref. (152).

ampicillin yielded an essentially identical bioavailability (153–155). These conflicting observations indicate that the problem is strongly affected by the nature of the formulation used, and that the effects of compounding can overshadow the effects attributed to the crystalline state.

Chloramphenicol palmitate has been shown to exist in four crystal modifications, and the effect of two of these on the degree of drug absorption has been compared (156). After oral ingestion of Forms A and B, the highest mean blood levels were obtained with suspensions containing only Form B. In mixed dosage forms, the blood levels of the drug were found to bear an inverse relationship with the fraction of Form A. This finding explained the previous report, which noted that a particular suspension formulation of chloramphenicol palmitate exhibited an unsatisfactory therapeutic effect (157). A study of various commercial products indicated that the polymorphic state of the drug in this formulation was uncontrolled, consisting of mixtures of the active polymorph B and the inactive polymorph A.

Sulfamethoxydiazine has been shown to exist in a number of polymorphic forms, which exhibit different equilibrium solubilities and dissolution rates (158). Form II, the polymorph with the greater thermodynamic activity, was found to

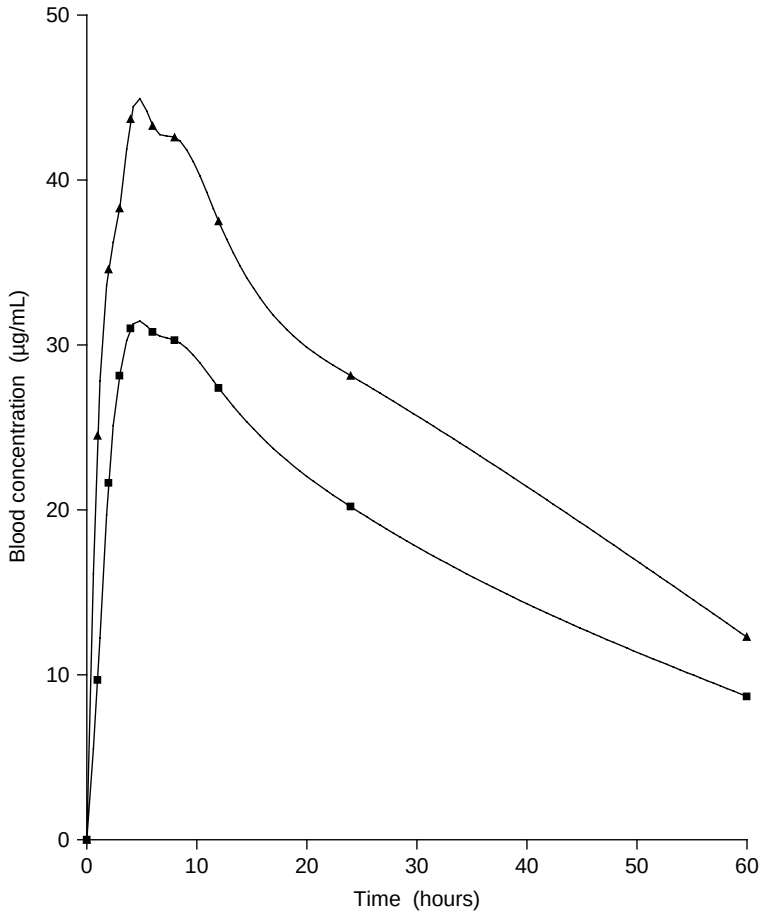

FIGURE 13 Mean concentrations of sulfamethoxydiazine in blood as influenced by the polymorphic state of the drug substance. Shown are the profiles of Form II (-▲-) and Form III (-■-). The figure has been adapted from data provided in Ref. (159).

yield higher blood concentration than those of Form III, which is stable in water (159). This relationship has been illustrated in Figure 13. Although the urinary excretion rates during the absorption phase confirmed the different drug absorption of the two forms as previously observed, the extent of absorption (as indicated by 72-hour excretion data) of the two forms was ultimately shown to be equivalent (160).

Fluprednisolone has been shown to exist in seven different solid phases, of which six were crystalline and one was amorphous (161). Of the crystalline phases, three were anhydrous, two were monohydrates, and one was a *tert*-butylamine solvate. The in vitro dissolution rates of the six crystalline phases of fluprednisolone were determined and compared with in vivo dissolution rates derived from pellet implants in rats (162). The agreement between the in vitro and in vivo dissolution

rates was found to be quite good, but the correlation with animal weight loss and adrenal gland atrophy was only fair. These results can be interpreted to indicate that, for fluprednisolone, differences in dissolution rates of the drug did not lead to measurable biological differences.

Erythromycin base is reported to exist in a number of structural forms, including an anhydrate, a dihydrate, and an amorphous form (163,164). The commercially available product appears to be a partially crystalline material, containing a significant amount of amorphous drug (165). From studies conducted in healthy volunteers, it was learned that the anhydrate and dihydrate phases were absorbed faster and more completely than was either the amorphous form or the commercially available form (166). These observations were reflected in two pharmaco-kinetic parameters (C_{max} and AUC).

Azlocillin sodium can be obtained either as a crystalline form or as an amorphous form, depending on the solvent and method used for its isolation (167). The antibacterial activity of this agent was tested against a large number of reference strains, and in most cases, the crystalline form exhibited less antibacterial activity than did the amorphous form. Interestingly, several of the tested microorganisms also proved to be resistant to the crystalline form.

Whether the different polymorphs or solvates of a given drug substance will lead to the existence of observable differences in the adsorption, metabolism, distribution, or elimination of the compound clearly cannot be predicted a priori at the present time. It is certainly likely that different crystal forms of highly soluble substances should be roughly bioequivalent, owing to the similarity of their dissolution rates. An effect associated with polymorphism that leads to a difference in bioavailability would be anticipated only for those drug substances whose absorption is determined by the dissolution rate. However, the literature indicates that, even in such cases, the situation is not completely clear. Consequently, when the existence of two or more polymorphs or solvates is demonstrated during the drug development process, wise investigators will determine those effects that could be associated with the drug crystal form and will modify their formulations accordingly.

REFERENCES

1. McCrone WC. Fusion Methods in Chemical Microscopy. New York: Interscience, 1957: 133.
2. Haleblian JK, McCrone WC. Pharmaceutical applications of polymorphism. J Pharm Sci 1969; 58: 911–29.
3. Higuchi WI, Lau PK, Higuchi T, et al. Polymorphism and drug availability. Solubility relationships in the methylprednisolone system. J Pharm Sci 1963; 52: 150–3.
4. Byrn S, Pfeiffer R, Ganey M, et al. Pharmaceutical solids: a strategic approach to regulatory considerations. Pharm Res 1995; 12: 945.
5. Q6A International Conference on Harmonization; Guidance on Q6A Specifications: Test Procedures and Acceptance Criteria for New Drug Substances. Federal Register 2000; 65: 83041–63.
6. Yu LX, Furness MS, Raw A, et al. Scientific considerations of pharmaceutical solid polymorphism in abbreviated new drug applications. Pharm Res 2003; 20: 531.
7. Snider DA, Addicks W, Owens W. Polymorphism in generic drug product development. Adv Drug Del Rev 2004; 56: 391–5.

8. Raw AS, Furness MS, Gill DS, et al. Regulatory considerations of pharmaceutical solid polymorphism in abbreviated new drug applications (ANDAs). Adv Drug Del Rev 2004; 56: 397–414.
9. Miller SPF, Raw AS, Andre S, et al. Scientific considerations of pharmaceutical solid polymorphism in regulatory applications, chapter 15 in Polymorphism in the Pharmaceutical Industry. In: Hilfiker R, ed. Wiley-VCH, 2006: 385–403.
10. Yu LX. Pharmaceutical quality by design: product and process development, understanding, and control. Pharm Res 2008; 25: 781–91.
11. Grant DJW, Higuchi T. Solubility Behavior of Organic Compounds, Vol. 21, Techniques of Chemistry. New York: John Wiley and Sons, 1990.
12. Jacques J, Collet A, Wilen SH. Enantiomers, Racemates and Resolutions. New York: Wiley, 1981: 168.
13. Mader WJ, Vold RD, Vold MJ. In Physical Methods of Organic Chemistry, 3rd ed. Vol. 1, Part I. In: Weissberger A, ed. New York: Interscience Publishers, 1959: 655–88.
14. Yalkowsky SH and Banerjee S. Aqueous Solubility Methods of Estimation for Organic Compounds. New York: Marcel Dekker, 1992: 149–54.
15. Brittain HG. Solubility methods for the characterization of new crystal forms, chapter 3.7 in Preformulation in Solid Dosage Form Development. In: Adeyeye MC, Brittain HG, eds. New York: Informa Healthcare, 2008: 323–46.
16. Grant DJW, Brittain HG. Solubility of pharmaceutical solids, chapter 11 in Physical Characterization of Pharmaceutical Solids. In: Brittain HG, ed. New York: Marcel Dekker, 1995: 321–86.
17. Grant DJW, Mehdizadeh M, Chow AH-L, et al. Non-linear van't Hoff solubility-temperature plots and their pharmaceutical interpretation. Int J Pharm 1984; 18: 25–38.
18. Bennema P, van Eupen J, van der Wolf BMA, et al. Solubility of molecular crystals: polymorphism in the light of solubility theory. Int J Pharm 2008; 351: 74–91.
19. Avdeef A, Berger CM, Brownell C. pH-metric solubility. 2: correlation between the acid-base titration and the saturation shake-flask solubility-pH methods. Pharm Res 2000; 17: 85–9.
20. Avdeef A, Berger CM. pH-metric solubility. 3. Dissolution titration template method for solubility determination. Eur J Pharm Sci 2001; 14: 281–91.
21. Avdeef A, Voloboy D, Foreman A. Comp Med Chem II 2006; 5: 399.
22. Fioritto AF, Bhattachar SN, Wesley JA. Solubility measurement of polymorphic compounds via the pH-metric titration technique. Int J Pharm 2007; 330: 105–13.
23. Stuart M, Box K. Chasing equilibrium: measuring the intrinsic solubility of weak acids and bases. Anal Chem 2005; 77: 983–90.
24. Llinás A, Burley JC, Prior TJ, et al. Concomitant hydrate polymorphism in the precipitation of sparfloxacin from aqueous solution. Cryst Growth Des 2008; 8: 114–18.
25. Higuchi T, Shih F-ML, Kimura T, et al. Solubility determination of barely aqueous-soluble organic solids. J Pharm Sci 1979; 68: 1267–72.
26. Bagley EB, Scigliano JM. Polymer solutions, chapter 16 in Solutions and Solubilities. Part II, Techniques of Chemistry, Vol. VIII. In: Dack MRJ, ed. New York: John Wiley, 1976: 437–85.
27. Chiou WL, Kyle LE. Differential thermal, solubility, and aging studies on various sources of digoxin and digitoxin powder: biopharmaceutical implications. J Pharm Sci 1979; 68: 1224–9.
28. Milosovich G. Determination of solubility of a metastable polymorph. J Pharm Sci 1964; 53: 484–7.
29. Nogami H, Nagai T, Suzuki A. Studies on powdered preparations. XVII. dissolution rate of sulfonamides by rotating disk method. Chem Pharm Bull 1966; 14: 329–38.
30. Nogami H, Nagai T, Yotsuyanagi T. Dissolution phenomena of organic medicinals involving simultaneous phase changes. Chem Pharm Bull 1969; 17: 499–509.

31. Ghosh S, Grant DJW. Determination of the solubilities of crystalline solids in solvent media that induce phase changes: solubilities of 1,2-dialkyl-3-hydroxy-4-pyridones and their formic acid solvates in formic acid and water. Int J Pharm 1995; 114: 185–96.
32. Brittain HG. A method for the determination of solubility of metastable crystal phases based on total light scattering. Langmuir 1996; 12: 601–4.
33. Gu C-H, Grant JW. Estimating the relative stability of polymorphs and hydrates from heats of solution and solubility data. J Pharm Sci 2001; 90: 1277–87.
34. Mao C, Pinal R, Morris KR. A quantitative model to evaluate solubility relationship of polymorphs from their thermal properties. Pharm Res 2005; 22: 1149.
35. Higuchi WI, Lau PK, Higuchi T, et al. Polymorphism and drug availability: solubility relationships in the methylprednisolone system. J Pharm Sci 1963; 52: 150–3.
36. Ghodbane S, McCauley JA. Study of the polymorphism of 3-(((3-(2-(7-chloro-2-quinolinyl)-(E)-ethenyl)phenyl) ((3-(dimethylamino-3-oxopropyl) thio) methyl)-thio) propanoic acid (MK571) by DSC, TG, XRPD and solubility measurements. Int J Pharm 1990; 59: 281–6.
37. Tuladhar MD, Carless JE, Summers MP. Thermal behavior and dissolution properties of phenylbutazone polymorphs. J Pharm Pharmacol 1983; 35: 208.
38. Behme RJ, Brooke D, Farney RF, et al. Characterization of polymorphism of gepirone hydrochloride. J Pharm Sci 1985; 74: 1041–6.
39. Sudo S, Sato K, Harano Y. J Chem Eng Japan 1991; 24: 237.
40. Rocco WL, Swanson JR. Win 63843 polymorphs: prediction of enantiotropy. Int J Pharm 1995; 117: 231–6.
41. Aguiar AJ, Zelmer JE. Dissolution behavior of polymorphs of chloramphenicol palmitate and mefenamic acid. J Pharm Sci 1969; 58: 983–7.
42. Carlton RA, Difeo TJ, Powner TH, et al. Preparation and characterization of polymorphs for an LTD4 antagonist, RG 12525. J Pharm Sci 1996; 85: 461–7.
43. Chiou EL, Anderson BD. Thermodynamic studies of tolbutamide polymorphs. J Pharm Sci 1984; 73: 1673–5.
44. Moustafa MA, Ebian AR, Khalil SA et al. Sulfamethoxydiazine crystal forms. J Pharm Pharmacol 1971; 23: 868.
45. Moustafa MA, Khalil SA, Ebian AR et al. Kinetics of interconversion of sulfamethoxydiazine crystal forms. J Pharm Pharmacol 1972; 24: 921.
46. Ebian AR, Moustafa MA, Khalil SA et al. Effect of additives on the kinetics of interconversion of sulfamethoxydiazine crystal forms. J Pharm Pharmacol 1973; 25: 13.
47. Levy G, Procknal JA. Dissolution rate studies on methylprednisolone polymorphs. J Pharm Sci 1964; 53: 656–8; Wurster DE, Taylor PW. Dissolution kinetics of certain crystalline forms of prednisolone. J Pharm Sci 1965; 54: 670–6.
48. Higuchi WI, Bernardo PD, Mehta SC. Polymorphism and drug availability II. Dissolution rate behavior of the polymorphic forms of sulfathiazole and methylprednisolone. J Pharm Sci 1967; 56: 200–7.
49. Addadi L, Berkovitch-Yellin Z, Weissbuch I, et al. Growth and dissolution of organic crystals with tailor-made inhibitors: implications in stereochemistry and materials science. Angew Chem Int Ed 1985; 24: 466–85.
50. Hulliger J. Chemistry and Crystal Growth. Angew Chem Int ed 1994; 33: 143–62.
51. Qu H, Louhi-Kultanen M, Kallas J. Additive effects on the solvent-mediated anhydrate/hydrate phase transformation in a mixed solvent. Cryst Growth Des 2007; 7: 724–9.
52. Skrdla PJ. Physicochemically relevant modeling of nucleation-and-growth kinetics: investigation of additive effects on the solvent-mediated phase transformation of carbamazepine. Cryst Growth Des 2008; 8: 4185–9.
53. Kuroda K, Yokoyama T, Umeda T, et al. Studies on drug nonequivalence. VI. Physicochemical studies on polymorphism of acetohexamide. Chem Pharm Bull 1978; 26: 2565–8.
54. Graf E, Beyer C, Abdallah O. Pharm Ind 1984; 46: 955.

55. Bruger A, Lettenbichler A. Pharmazie 1993; 48: 262.
56. Urakami K. Current Pharm Biotech 2005; 6: 193.
57. Lindenbaum S, Rattie ES, Zuber GE, et al. Polymorphism of auranofin. Int J Pharm 1985; 26: 123–32.
58. Umeda T, Matsuzawa A, Ohnishi N, et al. Physico-chemical properties and bioavailability of benoxaprofen polymorphs. Chem Pharm Bull 1984; 32: 1637–40.
59. Sheikhzadeh M, Rohani S, Taffish M, et al. Solubility analysis of buspirone hydrochloride polymorphs: measurements and prediction. Int J Pharm 2007; 338: 55–63.
60. Behme RJ, Brooke D. Heat of fusion measurement of a low melting polymorph of carbamazepine that undergoes multiple-phase changes during differential scanning calorimetry analysis. J Pharm Sci 1991; 80: 986–90.
61. Katrincic LM, Sun YT, Carlton RA, et al. Characterization, selection, and development of an orally dosed drug polymorph from an enantiotropically related system. Int J Pharm 2009; 366: 1–13.
62. Gerber JJ, van der Watt JG, Lötter AP. Physical characterization of solid forms of cyclopenthiazide. Int J Pharm 1991; 73: 137–45.
63. Walkling WD, Almond H, Paragamian V, et al. Difenoxin hydrochloride polymorphism. Int J Pharm 1979; 4: 39–46.
64. Lu J, Wang X-J, Yang X, et al. Polymorphism and crystallization of famotidine. Cryst Growth Des 2007; 7: 1590–8.
65. Doherty C, York P. Fresemide crystal forms; solid state and physicochemical analyses. Int J Pharm 1988; 47: 141–55.
66. Suleiman MS, Najib NM. Isolation and physicochemical characterization of solid forms of glibenclamide. Int J Pharm 1989; 50: 103–9.
67. Yang X, Wang X, Ching CB. Solubility of form α and form γ of glycine in aqueous solutions. J Chem Eng Data 2008; 53: 1133.
68. Kaneniwa N, Otsuka M, Hayashi T. Physicochemical characterization of indomethacin polymorphs and the transformation kinetics in ethanol. Chem Pharm Bull 1985; 33: 3447–5.
69. Kitamura S, Chang L-C, Guillory JK. Polymorphism of mefloquine hydrochloride. Int J Pharm 1994; 101: 127–44.
70. Clements JA, Popli SD. Can J Pharm Sci 1973; 8: 88.
71. Li Gang G, Xu Q-W, Li R, et al. Acta Chimica Sinica 2007; 65: 2817.
72. Gronenberg A, Keil B, Henck J-O. Processing effects on crystallinity of cephalexin: characterization by vacuum microbalance. Int J Pharm 1995; 118: 11–21.
73. Li H, Stowell JG, Borchardt TB, et al. Synthesis, conformational polymorphism, and construction of a G–T diagram of 2-[(2-Nitrophenyl)amino]-3-thiophenecarbonitrile. Cryst Growth Des 2006; 6: 11,2469.
74. Pearson JT, Varney G. The anomalous behavior of some oxyclozanide polymorphs. J Pharm Pharmacol 1973; 25: 62P.
75. Ibrahim HG, Pisano F, Bruno A. Polymorphism of phenylbutazone: properties and compressional behavior of crystals. J Pharm Sci 1977; 66: 669–73.
76. Kato Y, Okamoto Y, Nagasawa S, et al. New polymorphic forms of phenobarbital. Chem Pharm Bull 1984; 32: 4170–4.
77. Chikarishi Y, Sano A, Tsujiyama T, et al. Preparation of piretanide polymorphs and their physicochemical properties and dissolution behaviors. Chem Pharm Bull 1994; 42: 1123–8.
78. Caviglioli G, Pani M, Gatti P, et al. Study of retinoic acid polymorphism. J Pharm Sci 2006; 95: 2207–21.
79. Carstensen JT. Pharmaceutical principles of solid dosage forms. Lancaster, PA: Technomic Publishing Co, Inc, 1993: 133–149.
80. Rowe EL, Anderson BD. Thermodynamic studies of tolbutamide polymorphs. J Pharm Sci 1984; 73: 1673–5.

81. Pudipeddi M, Serajuddin ATM. Trends in solubility of polymorphs. J Pharm Sci 2005; 94: 929–39.
82. Poole JW, Bahal CK. Dissolution behavior and solubility of anhydrous and trihydrate forms of ampicillin. J Pharm Sci 1968; 57: 1945–8.
83. Jozwiakowski MJ, Williams SO, Hathaway RD. Relative physical stability of the solid forms of amiloride HCl. Int J Pharm 1993; 91: 195–207.
84. Kawashima Y, Niwa T, Takeuchi H, et al. Characterization of polymorphs of tranilast anhydrate and tranilast monohydrate when crystallized by two solvent change spherical crystallization techniques. J Pharm Sci 1991; 80: 472–8.
85. Laine E, Tuominen V, Ilvessalo P, et al. Formation of dihydrate from carbamazepine anhydrate in aqueous conditions. Int J Pharm 1984; 20: 307–14.
86. Young WWL, Suryanarayanan R. Kinetics of transition of anhydrous carbamazepine to carbamazepine dihydrate in aqueous suspensions. J Pharm Sci 1991; 80: 496–500.
87. Kahela P, Aaltonen R, Lewing E, et al. Pharmacokinetics and dissolution of two crystalline forms of carbamazepine. Int J Pharm 1983; 14: 103–12.
88. Annie Hoelgaard, Niels Moller. Hydrate formation of metronidazole benzoate in aqueous suspensions. Int J Pharm 1983; 15: 213–21.
89. Zhu H, Grant DJW. Influence of water activity in organic solvent + water mixtures on the nature of the crystallizing drug phase. 2. Ampicillin. Int J Pharm 1996; 139: 33–43.
90. Shefter E, Higuchi T. Dissolution behavior of crystalline solvated and nonsolvated forms of some pharmaceuticals. J Pharm Sci 1963; 52: 781–91.
91. Herman J, Remon JP, Visavarungroj N, et al. Formation of theophylline monohydrate during the pelletization of microcrystalline cellulose-anhydrous theophylline blends. Int J Pharm 1988; 42: 15–18.
92. Ando H, Ishii M, Kayano M, et al. Effect of moisture on crystallization of theophylline in tablets. Drug Dev Indust Pharm 1992; 18: 453–67.
93. Fokkens JG, van Amelsfoort JGM, de Blaey CJ, et al. A thermodynamic study of the solubility of theophylline and its hydrate. Int J Pharm 1983; 14: 79–93.
94. Bogardus JB. Crystalline anhydrous-hydrate phase changes of caffeine and theophylline in solvent-water mixtures. J Pharm Sci 1983; 72: 837–8.
95. de Smidt JH, Fokkens JG, Grijseels H, et al. Dissolution of theophylline monohydrate and anhydrous theophylline in buffer solutions. J Pharm Sci 1986; 75: 497–501.
96. Gould PL, Howard JR, Oldershaw GA. The effect of hydrate formation on the solubility of theophylline in binary aqueous cosolvent systems. Int J Pharm 1989; 51: 195–202.
97. Zhu H, Yuen C, Grant DJW. Influence of water activity in organic solvent + water mixtures on the nature of the crystallizing drug phase. 1. Theophylline. Int J Pharm 1996; 135: 151–60.
98. Otsuka N, Kaneniwa N, Otsuka K, et al. Effect of geometric factors on hydration kinetics of theophylline anhydrate tablets. J Pharm Sci 1992; 81: 1189–93.
99. Wells JI. Pharmaceutical preformulation: the physicochemical properties of drug substances. Chichester, United Kingdom: Ellis Horwood Ltd, 1988: 94–5.
100. Suryanarayanan R, Mitchell AG. Phase transitions of calcium gluceptate. Int J Pharm 1986; 32: 213–21.
101. Jarring K, Larsson T, Stensland B, et al. Thermodynamic stability and crystal structures for polymorphs and solvates of formoterol fumarate. J Pharm Sci 2006; 95: 1144–61.
102. Matsuda Y, Tatsumi E. J Pharmacobio-Dyn 1989; 12: s-38.
103. Ito S, Nishimura M, Kobayashi Y, et al. Characterization of polymorphs and hydrates of GK-128, a serotonin receptor antagonist. Int J Pharm 1997; 151: 133–43.
104. Jozwiakowski MJ, Nguyen NAT, Sisco JM, et al. Solubility behavior of lamivudine crystal forms in recrystallization solvents. J Pharm Sci 1996; 85: 193–9.
105. Kumar S, Chawla G, Sobhia ME, et al. Characterization of solid-state forms of mebendazole. Pharmazie 2008; 63: 136.
106. Buxton PC, Lynch IR, Roe JA. Solid-state forms of paroxetine hydrochloride. Int J Pharm 1988; 42: 135–43.

107. Kozjek F, Golic L, Zupet P, et al. Acta Pharm Jugosl 1985; 35: 275.
108. Abdallah O, El-Fattah SA. Pharm Ind 1984; 46: 970.
109. Rodriguez-Hornedo N, Lechuga-Ballesteros D, Wu H-J. Phase transition and heterogeneous/epitaxial nucleation of hydrated and anhydrous theophylline crystals. Int J Pharm 1992; 85: 149–62.
110. Sturtevant JM. Calorimetry, chapter 14 in Physical Methods of Organic Chemistry, 2nd edn. In: Weisssberger A, ed. New York: Interscience Pub, 1949: 817–27.
111. Hansen LD, Lewis EA, Eatough DJ. In Analytical Solution Calorimetry. In: Grime JK, ed. New York: John Wiley & Sons, 1985.
112. Winnike RA, Wurster DE, Guillory JK. A solid sampling device for use in batch solution calorimetry. Thermochim Acta 1988; 124: 99–108.
113. Wu L-S, Gerard C, Hussain MA. Thermal analysis and solution calorimetry studies on losartan polymorphs. Pharm Res 1993; 10: 1793–5.
114. Wu L-S, Torosian G, Sigvardson K, et al. Investigation of moricizine hydrochloride polymorphs. J Pharm Sci 1994; 83: 1404–6.
115. Ip DP, Brenner GS, Stevenson JM, et al. High resolution spectroscopic evidence and solution calorimetry studies on the polymorphs of enalapril maleate. Int J Pharm 1986; 28: 183–91.
116. Katdare AV, Ryan JA, Bavitz JF, et al. Characterization of hydrates of norfloxacin. Mikrochim. Acta 1986; III: 1.
117. Botha SA, Caira MR, Guillory JK, et al. Physical characterization of the hydrates of urapidil. J Pharm Sci 1988; 77: 444–51.
118. Chang L-C, Caira MR, Guillory JK. Solid state characterization of dehydroepiandrosterone. J Pharm Sci 1995; 84: 1169–79.
119. Chikaraishi Y, Otsuka M, Matsuda Y. Dissolution phenomenon of the piretanide amorphous form involving phase change. Chem Pharm Bull 1996; 44: 2111–15.
120. Chauvet A, Masse J, Ribet J-P, et al. Characterization of polymorphs and solvates of 3-amino-1-(m-trifluoro-methylphenyl)-6-methyl-1H-pyridazin-4-one. J Pharm Sci 1992; 81: 836–41.
121. Leeson LJ, Carstensen JT. Dissolution Technology. Washington DC: American Pharmaceutical Association, 1974.
122. Hanson R, Gray V. Handbook of Dissolution Testing, 3rd edn. Hockessin, Delaware: Dissolution Technologies, Inc, 2004.
123. Abdou HM. Dissolution, Bioavailability and Bioequivalence. Easton PA: Mack, 1989.
124. Dissolution, General Test <711>, United States Pharmacopoeia 32, volume 1. Rockville MD: United States Pharmacopoeial Convention, Inc, 2009: 263–71.
125. Levich VG. Physicochemical Hydrodynamics. Englewood Cliffs NJ: Prentice-Hall, 1962.
126. Stagner WC, Guillory JK. Physical characterization of solid iopanoic acid forms. J Pharm Sci 1979; 68: 1005–9.
127. Ravin LJ, Shami EG, Rattie E. Physical-chemical evaluation of 3-(3-hydroxy-3-methylbutylamino)-5-methyl-as, triazino [5,6-b] indole (SK&F 30097). J Pharm Sci 1970; 59: 1290–5.
128. Stoltz M, Lötter AP, van der Watt JG. Physical characterization of two oxyphenbutazone pseudopolymorphs. J Pharm Sci 1988; 77: 1047–9.
129. Stoltz M, Caira MR, Lötter AP, et al. Physical and structural comparison of oxyphenbutazone monohydrate and anhydrate. J Pharm Sci 1989; 78: 758–63.
130. Matsuda Y, Kawaguchi S. Physicochemical characterization of oxyphenbutazone and solid-state stability of its amorphous form under various temperature and humidity conditions. Chem Pharm Bull 1986; 34: 1289–98.
131. Yalkowsky SH. Techniques of Solubilization of Drugs. New York: Marcel Dekker, 1981: 160–80.
132. Khankari RK, Grant DJW. Pharmaceutical hydrates. Thermochim Acta 1995; 248: 61–79.

133. Allen PV, Rahn PD, Sarapu AC, et al. Physical characterization of erythromycin: anhydrate, monohydrate, and dihydrate crystalline solids. J Pharm Sci 1978; 67: 1087–93.
134. Zhu H, Khankari RK, Padden BE, et al. Physicochemical characterization of nedocromil bivalent metal salt hydrates. 1. Nedocromil magnesium. J Pharm Sci 1996; 85: 1026–34; Zhu H, Padden BE, Munson EJ, et al. Physicochemical characterization of nedocromil bivalent metal salt hydrates. 2. Nedocromil zinc. J Pharm Sci 1997; 86: 418–29; Zhu H, Halfen JA, Young VG, et al. Physicochemical characterization of nedocromil bivalent metal salt hydrates. 3. Nedocromil calcium. J Pharm Sci 1997; 86: 1439–47.
135. Kristl A, Srcic S, Vrecer F, et al. Polymorphism and pseudopolymorphism: influencing the dissolution properties of the guanine derivative acyclovir. Int J Pharm 1996; 139: 231–5.
136. Mooney KG, Mintun MA, Himmelstein KJ, et al. Dissolution kinetics of carboxylic acids I: effect of pH under unbuffered conditions. J Pharm Sci 1981; 70: 13–22.
137. Higuchi T, Dayal S, Pitman IH. Effects of solute – solvent complexation reactions on dissolution kinetics: testing of a model by using a concentration jump technique. J Pharm Sci 1972; 61: 695–700.
138. Doherty C, York P. Fresemide crystal forms; solid state and physicochemical analyses. Int J Pharm 1988; 47: 141–55.
139. Uchida T, Yonemochi E, Oguchi T, et al. Polymorphism of Tegafur: physico-chemical properties of four polymorphs. Chem Pharm Bull 1993; 41: 1632–5.
140. Li R, Mayer PT, Trivedi JS, et al. Polymorphism and crystallization behavior of abbott-79175, a second-generation 5-lipoxygenase inhibitor. J Pharm Sci 1996; 85: 773–80.
141. Martínez-Ohárriz MC, Martín C, Goñi MM, et al. Polymorphism of diflunisal: isolation and solid-state characteristics of a new crystal form. J Pharm Sci 1994; 83: 174–7.
142. Laihanen N, Muttonen E, Laaksonen M. Solubility and intrinsic dissolution rate of alprazolam crystal modifications. Pharm Dev Tech 1996; 1: 373–80.
143. Lagas M, Lerk CF. The polymorphism of sulphathiazole. Int J Pharm 1981; 8: 11–24.
144. Higuchi WI, Bernardo PD, Mehta SC. Polymorphism and drug availability II. Dissolution rate behavior of the polymorphic forms of sulfathiazole and methylprednisolone. J Pharm Sci 1967; 56: 200–7.
145. Aguiar AJ, Zelmer JE. Dissolution behavior of polymorphs of chloramphenicol palmitate and mefenamic acid. J Pharm Sci 1969; 58: 983–7.
146. Botha SA, Flanagan DR. Non-thermal methods in characterization of anhydrous digoxin and two digoxin hydrates. Int J Pharm 1992; 82: 195–204.
147. Botha SA, Caira MR, Guillory JK, et al. Physical characterization of the methanol solvate of urapidil. J Pharm Sci 1989; 78: 28–34.
148. Tros de Ilarduya MC, Martín C, Goñi MM, et al. Dissolution rate of polymorphs and two new pseudopolymorphs of sulindac. Drug Dev Indust Pharm 1997; 23: 1095–8.
149. Poole JW, Owen G, Silverio J, et al. Current Therap Res 1968; 10: 292.
150. Poole JW, Bahal CK. Dissolution behavior and solubility of anhydrous and trihydrate forms of ampicillin. J Pharm Sci 1968; 57: 1945–8.
151. MacLeod C, Rabin H, Ruedy J, et al. Can Med Assoc J 1972; 107: 203.
152. Ali AA, Farouk A. Comparative studies on the bioavailability of ampicillin anhydrate and trihydrate. Int J Pharm 1981; 9: 239–43.
153. Cabana BE, Willhite LE, Bierwagen ME. Antimicrob. Agents Chemotherap 1969; 9: 35.
154. Mayersohn M, Endrenyi L. Can Med Assoc J 1973; 109: 989.
155. Hill SA, Jones KH, Seager H, et al. Dissolution and bioavailability of the anhydrate and trihydrate forms of ampicillin. J Pharm Pharmacol 1975; 27: 594.
156. Aguiar AJ, Krc J, Kinkel AW, et al. Effect of polymorphism on the absorption of chloramphenicol from chloramphenicol palmitate. J Pharm Sci 1967; 56: 847–53.
157. Anderson CM. Aust J Pharm 1966; 47: S44.
158. Moustafa MA, Ebian AR, Khalil SA, et al. Sulfamethoxydiazine crystal forms. J Pharm Pharmacol 1971; 23: 868.

159. Khalil SA, Moustafa MA, Ebian AR, et al. GI absorption of two crystal forms of sulfameter in man. J Pharm Sci 1972; 61: 1615–17.
160. Khalafallah N, Khalil SA, Moustafa MA. Bioavailability determination of two crystal forms of sulfameter in humans from urinary excretion data. J Pharm Sci 1974; 63: 861–4.
161. Haleblian JK, Koda RT, Biles JA. Isolation and characterization of some solid phases of fluprednisolone. J Pharm Sci 1971; 60: 1485–8.
162. Haleblian JK, Koda RT, Biles JA. Comparison of dissolution rates of different crystalline phases of fluprednisolone by in vitro and in vivo methods. J Pharm Sci 1971; 60: 1488–91.
163. Allen PV, Rahn PD, Sarapu AC, et al. Physical characterization of erythromycin: anhydrate, monohydrate, and dihydrate crystalline solids. J Pharm Sci 1978; 67: 1087–93.
164. Fukumori Y, Fukuda T, Yamamoto Y, et al. Physical characterization of erythromycin dihydrate, anhydrate and amorphous solid and their dissolution properties. Chem Pharm Bull 1983; 31: 4029–39.
165. Murthy KS, Turner NA, Nesbitt RU, et al. Characterization of commercial lots of erythromycin base. Drug Dev Ind Pharm 1986; 12: 665–90.
166. Laine E, Kahela P, Rajala R, et al. Crystal forms and bioavailability of erythromycin. Int J Pharm 1987; 38: 33–8.
167. Kalinkova GN, Stoeva SV. Polymorphism of azlocillin sodium. Int J Pharm 1996; 135: 111–14.